CHARLES UNIVERSITY IN PRAGUE

Faculty of Science

Dissertation

Regulation of Mast Cell Activation at the Level of the High-affinity Receptor for IgE and STIM1

Author: Mgr. Viktor Bugajev

Supervisor: RNDr. Petr Dráber, DrSc.

Study program: Immunology

This thesis was prepared at the Institute of Molecular Genetics, Academy of Sciences of the Czech Republic, Laboratory of Signal Transduction. Experimental data were compiled into four articles (three original and one review with original data). One of the articles is submitted for publication in Journal of Immunological Methods.

I hereby declare that I have elaborated this thesis independently, and all the resources employed as well as co-authors are indicated. I further declare that I did not submit this thesis, or an essential part of it, to obtain other, or the same university degree.

Prague, 29 April, 2013 Viktor Bugajev

I would like to thank my supervisor Petr Dráber for giving me the opportunity to perform these studies. Without his encouragment and guidance this work could not have been accomplished.

I appreciated very much the collaborations and/or useful discussions with my former and current colleagues from the “lab No. 22“, namely with (in alphabetical order) Monika Bambousková, Romana Budovičová, Peter Dráber, Helena Dráberová, Lubica Dráberová, Jiří Eitler, Filip Franko, Ivana Hálová, Petr Heneberg, Lukáš Kocanda, Martin Machyna, Hana Mrázová, Anna Koffer, Pavel Lebduška, Dana Lorenčíková, Tomáš Paulenda, Iva Polakovičová, Gouse Mohidin Shaik, Daniel Smrž, Lucie Stegurová, Magda Tůmová, Petra Volná, Šárka Šilhánková, Michal Šimíček and Pavol Uťekal. I appreciated very much collaboration with "lab No. 26", namely with (in alphabetical order) Eduarda Dráberová, Pavel Dráber, Zuzana Hájková, Stanislav Vinopal. Collaboratrion with Jiří Janáček from Department of Biomathematics, Institute of Physiology, Czech Academy of Sciences and with Petr Matoušek and Petr Wagner from department of Clinical Biochemistry, Regional Hospital Liberec is also highly appreciated.

Last but not least, I would like to thank my parents and family for the endless support.

INDEX

ABSTRACT (EN)

This thesis is focused on two important gate-keepers of mast cell signaling. The first is the complex of the high-affinity receptor for immunoglobulin E (IgE) (FcεRI) associated with Lck/Yes-related novel tyrosine kinase (Lyn), which is involved in acquired immune responses and the second is the stromal interaction molecule (STIM)1, which senses calcium levels in endoplasmic reticulum (ER) and upon depletion of ER Ca^{2+} stores participates in opening of the plasma membrane Ca^{2+} release-activated Ca^{2+} (CRAC) channels.

Although the structure of FcεRI is known for many years and numerous molecules associated with the receptor have been described, the exact molecular mechanism of initiation and termination of the FcεRI signaling is elusive. Therefore, we evaluated the current knowledge on the molecular mechanisms of FcεRI phosphorylation with emphasis on the newly described model according to which cross-talk between protein tyrosine phosphatases (PTPs) and protein tyrosine kinases (PTKs) sets the threshold for FcεRI tyrosine phosphorylation (PTK-PTP interplay model). Furthermore, we extended the knowledge about topography of active phosphatases which are prone to oxidation within the clusters of transmembrane adaptor proteins non-T cell activation linker (NTAL) and linker for activation of T cells (LAT) upon FcεRI triggering.

Using bone marrow-derived mast cells BMMCs as a model, we obtained new data on colocalization of STIM1 with microtubule filaments and movement of STIM1 in microtubule-dependent manner that reflected direct communication between STIM1 and microtubule plus-end tracking protein EB1. To determine whether STIM1 regulates EB1 movement and microtubules organization in calcium dependent manner we prepared BMMCs with reduced expression of STIM1. We found, as expected, that STIM1-deficient cells exhibited impaired calcium signaling upon activation and that this resulted in inhibition of de-novo reorganization of microtubules. Unexpectedly, treatment of BMMCs with the inhibitor of microtubules polymerization (nocodazole) failed to impaire translocation of STIM1 to ER/plasma membrane junctions and CRAC channels function. The cross-talk between microtubules and STIM1 was analyzed in detail by recording changes in reorganization of microtubules in BMMCs attached on fibronectin-coated slides after their activation with different stimuli (antigen, thapsigargin or pervanadate). BMMCs activated by all activators employed showed formation of distinct microtubule protrusions. This hitherto unknown mast cell function required co-stimulatory signaling from integrins. STIM1 was localized in the plasma membrane protrusions suggesting that local calcium signaling plays a role in formation of such protrusions.

Significant effort was also directed towards production of new monoclonal and polyclonal antibodies toward STIM1 and development of new real-time polymerase chain reaction (PCR) master mixes suitable for amplification of DNA fragments from whole blood and/or GC-rich templates. Outputs from these projects are either commercially available products (anti-STIM1 monoclonal antibody) or are in the processing for commercial use [new quantitative PCR (qPCR) master mixes].

ABSTRACT (CZ)

Tato disertační práce je zaměřena na dva důležité regulátory signalizace žírných buněk. Prvním z nich je komplex vysoce afinního receptoru pro imunoglobulin E (IgE) (FcεRI), který se podílí na získaných (adaptivních) imunitních odpovědí a druhý je stromální interakční molekula 1 (STIM1), která monitoruje hladiny vápníku v endoplasmickém retikulu (ER) a po uvolnění Ca^{2+} z ER se podílí na otevření vápníkovým uvolněním aktivovaných vápníkových (CRAC) kanálů.

I když je struktura FcεRI známá již mnoho let a byla popsána řada molekul asociovaných s tímto receptorem, přesný molekulární mechanismus zahájení a ukončení FcεRI signalizace zůstává nejasný. V této studii jsme vyhodnotili dosavadní poznatky o molekulárních mechanismech iniciace fosforylace FcεRI s důrazem na nově popsaný model, podle kterého vzájemné interakce mezi protein tyrosin fosfatázami (PTPs) a protein tyrosin kinázami (PTKs) nastaví práh tyrosinové fosforylace FcεRI (PTK-PTP interakční model). Dále jsme rozšířili poznatky týkající se topografie fosfatáz citlivých k oxidaci po stimulaci FcεRI v rámci klastrů transmembrálních adaptorových proteinů: T buňky neaktivující „linker“ (NTAL) a „linker“ aktivovaných T lymfocytů (LAT).

Žírné buňky původem z kostní dřeně (BMMC) jsme použili jako modelový systém pro získání nových poznatků o vzájemné lokalizaci STIM1 s mikrotubulovými filamenty a pohybu STIM1 závislém na pohybu mikrotubulů, který reflektoval přímou komunikaci mezi STIM1 a proteinem sledujícím plus-konce mikrotubulů, EB1. Abychom určili, zda STIM1 reguluje organizaci mikrotubulů v závislosti na vápníku připravili jsme BMMCs se sníženou expresí STIM1. V souladu s očekáváním jsme zjistili, že buňky se sníženou expresí STIM1 mají po aktivaci narušenou vápníkovou signalizaci, a že de-novo reorganizace mikrotubulů byla inhibovaná. Překvapivě, v buňkách ovlivněných inhibitorem polymerace mikrotubulů (nocodazolem) nebyla narušena translokace STIM1 do oblastí přiblížení ER/plazmatické membrány a aktivace CRAC kanálů nebyla narušena. Vzájemná interakce mezi mikrotubuly a STIM1 byla detailně analyzována sledováním změn v reorganizaci mikrotubulů BMMCs po jejich aktivaci různými podněty (antigenem, thapsigarginem nebo pervanadátem). Aktivace buněk přisedlých přes fibronektin na podložní sklíčka vedla k tvorbě mikrotubulových výčnělků. Tento doposud neznámý fenotyp žírných buněk vyžadoval integrínovou kostimulaci. Přítomnost STIM1 ve výčnělcích naznačuje, že lokální vápníková signalizace může hrát roli při tvorbě mikrotubulových výběžků.

Významné úsilí bylo také zaměřeno na přípravu nových monoklonálních a polyklonálních protilátek proti STIM1 a vývoji nových polymerázových řetězových reakčních (PCR) směsí vhodných pro amplifikaci DNA fragmentů z krve anebo GC-bohatých templátů. Výstupy z těchto projektů jsou buď komerčně dostupné produkty (anti-STIM1 monoklonální protilátka), nebo jsou v procesu přípravy pro komerční využití (nové kvantitativní PCR směsi).

ABBREVIATIONS

AA	Arachidonic acid
BaP	Basophil progenitor
BCR	B cell receptor
BMCP	Bipotent basophil/mast cell progenitor
BMMCs	Bone marrow-derived mast cells
BSA	Bovine serum albumin
BSS	Buffered saline solution
Btk	Bruton tyrosine kinase
CAD	CRAC-activation domain
CCL	Chemokine (C-C motif) ligand
CD	Cluster of differentiation
C/EBP α	CCAAT/enhancer-binding protein α
CMP	Common myeloid progenitors
CNS	Central nervous system
CRAC	Ca^{2+} release-activated Ca^{2+}
CRACM	CRAC modulator
CRACR2A	CRAC regulator 2A
Cpa3	Carboxypeptidase 3A
CTMCs	Connective tissue mast cells
Csk	C-terminal Src kinase
DAG	Diacylglycerol
DNA	Deoxyribonucleic acid
DNP	2,4-Dinitrophenyl
DLN	Draining lymphoid node
DRM	Detergent resistant membranes
EAE	Experimental autoimmune encephalomyelitis
EB1	End binding 1
ECFP	Enhanced cyan fluorescent protein
EGFP	Enhanced green fluorescent protein
ER	Endoplasmic reticulum
Erk	Extracellular-signal regulated kinase
esRNA	Exosomal shuttle ribonucleic acid
EYFP	Enhanced yellow fluorescent protein
FcεRI	High-affinity receptor for IgE (Type I receptor for IgE)
FcεRII	Low-affinity receptor for IgE

FcγRI	Fc-gamma receptor I
FcγRIII	Low affinity IgG receptor
FcR	Fc receptor
FcR α	α subunit of FcεRI receptor
FcR β	β subunit of FcεRI receptor
FcR γ	γ subunit of FcεRI receptor
FRET	Fluorescence resonance energy transfer
Gab-2	Grb2-associated binder 2
GMP	Granulocyte-macrophage progenitor
GPI	Glycosylphosphatidylinositol
GPI-AP	Glycosylphosphatidylinositol-anchored protein
Grb2	Growth factor receptor-bound protein 2
ICAM-1	Intercellular adhesion molecule 1
I_{CRAC}	Ca^{2+}-selective calcium-release activated calcium current
IgE	Immunoblobulin E
IgG	Immunoglobulin G
IL	Interleukin
IFN- γ	Interferon γ
IP3	Inositol 1,4,5-trisphosphate
IP3R	Inositol trisphosphate receptor
ITAM	Immunoreceptor tyrosine-based activation motif
JNK	Jun N-terminal kinase
kDa	Kilodalton
LAT	Linker for activation of T-cells
5-LO	5-lipoxygenase
LT	Leukotrien
Lyn	Lck/Yes-related novel tyrosine kinase
MCP	Mast cell progenitor
Mcpt	Mast cell protease
MHC	Major histocompatibility complex
MMC	Mucosal mast cell
mMCP	Mouse mast cell protease
MLCK	Myosin light chain kinase
MPP	Multipotential cell progenitor
mRNA	Messenger ribonucleic acid
NFAT	Nuclear factor of activated T-cells
NF-κB	Nuclear factor kappa-light-chain-enhancer of activated B cells
NTAL	Non-T cell activation linker

OASF	Orai1 activating small fragment
PAG	Phosphoprotein associated with glycosphingolipid-enriched microdomains
PAMPs	Pathogen–associated molecular patterns
PBS	Phosphate buffered saline
PCR	Polymerase chain reaction
PI3K	Phosphatidylinositol 3-kinase
PIP2	Phosphatidylinositol 4,5,-bisphosphate
PIP3	Phosphatidylinositol 3,4,5,-trisphosphate
PLCγ	Phospholipase Cγ
PTK	Protein tyrosine kinase
PTP	Protein tyrosine phosphatase
qPCR	Quantitative polymerase chain reaction
RBL	Rat basophilic leukemia
ROS	Reactive oxygene specious
RNAi	RNA interference
SAM	Single sterile alpha-motif
SARAF	SOCE-associated regulatory factor
SCF	Stem cell factor
SDS	Sodium dodecyl sulfate
SDS-PAGE	Sodium dodecyl sulfate polyacrylamide gel electrophoresis
SH	Src homology
SHP	SH2-domain containing phosphatase
SHIP-1	SH2-domain containing inositol polyphosphate 5-phosphatase 1
shRNA	Short hairpin ribonucleic acid
SOAR	STIM1-Orai1 activating region
SOC	Store-operated channel
SOCE	Store operated calcium entry
SP	Signal-peptide
Surf4	Surfeit locus protein 4
STIM1	Stromal interaction molecule 1
Syk	Spleen tyrosine kinase
TCR	T cell receptor
TGF-β	Transforming growth factor β
Th	T helper
+TIPs	Microtubule plus-end tracking proteins
TNFα	Tumor necrosis factor α
TNP	2,4,6-trinitrophenol
TRPC	Transient receptor potential canonical

TRAP	Transmembrane adaptor protein
ZAP-70	ζ –associated protein of 70 kDa

INTRODUCTION

Mast cells and basophils – from history to the present

Paul Ehrlich in his thesis (1878) described tissue-resident granular cell type based on staining with toluidine blue and other cationic aniline dyes. He called them in German "Mastzellen" (mast cells) and misleadingly hypothesized that their granules could nourish the surrounding tissue. In his other work, he described also eosinophiles, neutrophiles and blood mast cells, now known as basophils. From the current point of view mast cells and basophiles are critical effector cells in immunoglobulin E (IgE)-associated immune responses to pathogens (parasites and some bacteria) as well as in allergic disorders, such as eczema, asthma, hay fever and anaphylaxis. Furthermore, mast cells are present at the sites of autoimmune inflammation and are able to modulate adaptive immune system [1].

Mast cells and basophils belongs to the innate immune system and share a lot of common features, among them the most prominent is rapid release of preformed proinflammatory mediators to antigen challenge, presence of the FcεRI and c-Kit receptor for stem cell factor (SCF), and similar but not identical production of proinflammatory mediators. On the other hand, some morphological and physiological features are different: mature mast cells are long-lived (weeks to months) cells resident in almost all tissues including central nervous system (CNS) or testes; in contrast, short-lived (days) basophiles form a minority fraction of blood leukocytes and to the sites of inflammation are recruited [1].

Mast cells are derived from cluster of differentiation (CD)34+ hematopoetic stem cells residing in bone marrow [2]. Recent works slightly lifted the fog over the basophile and mast cells relationship and several models have been proposed (Figure 1). Mast cell progenitor (MCP) derived from multipotential cell progenitors (MPP) was isolated from adult mouse bone marrow (Figure 1A) [3]. Arinobu et al. identified a bipotent basophil/mast cell progenitors (BMCPs) in mouse spleen. These progenitors are derived probably from common myeloid progenitors (CMP) or granulocyte-macrophage progenitors (GMP). BMCPs are characterized by expression of non-specific transcription factors GATA-1 (globin transcription factor 1), PU.1 and MITF1 (microphthalmia-associated transcription factor) and low level of CCAAT/enhancer-binding protein α (C/EBP α; Figure 1B). The up-regulation of C/EBP α plays a critical role in basophile lineage development. Overexpression of C/EBPα in mast cells leads to reprogramming them into basophils lineage whereas engraftment of mice lacking mast cells (Kit^{W/W^v}) with BMCPs leads to repopulation of the spleens and stomachs with mast cells. In this work, authors also isolated another mast cell progenitor from intestine and basophil progenitor residing in bone marrow [4]. It is obvious that mast cells rais from progenitors of a common hematopoetic origin and that the environmental milieu of the tissue influences their development.

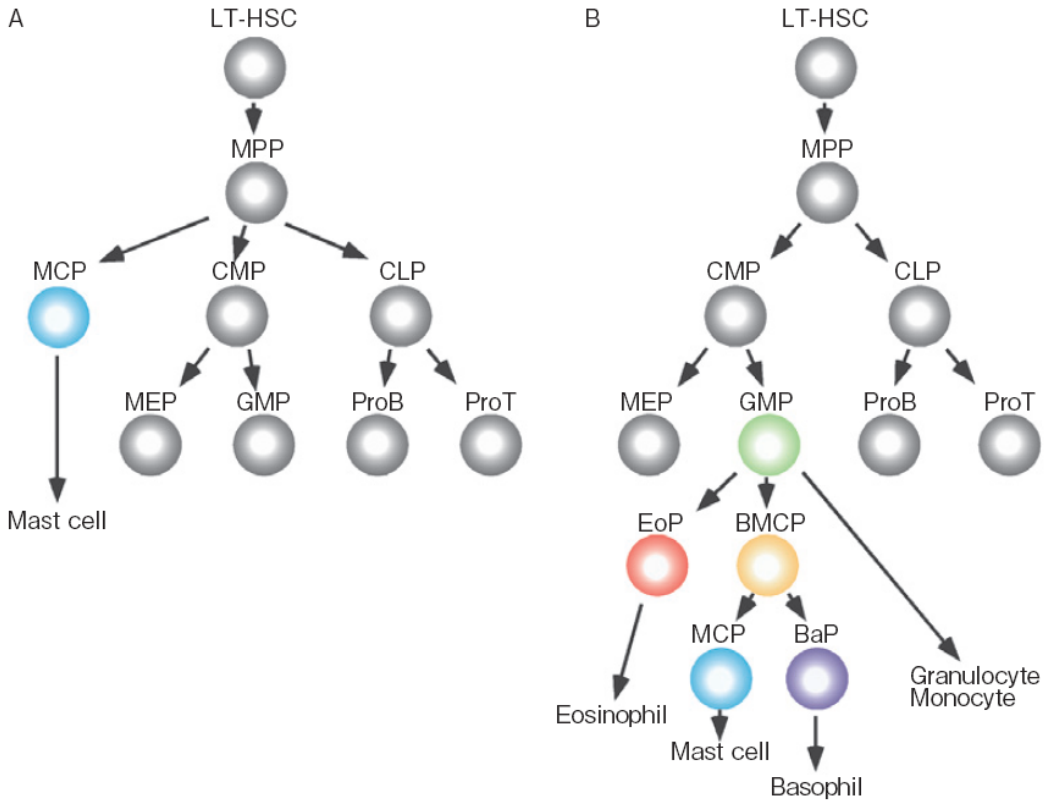

Figure 1. Two current models decribing the development of mast cells in the context of development of other hematopoetic lineages. (A) According to Chen et al. mast cells progenitors (MCP; denoted in blue) are derived from multipotential cell progenitors (MPP). (B) In contrast, Arinobu et al. found a basophil/mast cell progenitors (BMCP; orange sphere) in mouse spleens. BMCP are derived from granulocyte-macrophage progenitors (GMP; green sphere) and give rise to both MCP and basophil progenitors (BaP; violet sphere; Arinobu et al., 2009).

Mast cells subpopulations

Rodent mast cells can be distinguished by histochemical staining on two main populations, safranin positive connective tissue mast cells (CTMCs) and safranin negative mucosal mast cells (MMCs). These two distinct populations differ both qualitatively and quantitatively in composition of mast cell granules, which depend on the local humoral microenvironment [5]. CTMCs are readily stained with safranin because of heparin presence; reside in skin, joints and in rodents also in peritoneal cavity. The MMCs convert arachidonic acid (AA) mainly to leukotriens (LT) via 5-lipoxygenase (5-LO) dependent pathway [6], while CTMCs preferentially exhibit cyclooxygenase activity leading to prostaglandins production [7]. Interestingly, *in vitro* differentiated BMMCs, which is a widely used research model cell strain, resemble some attributes of interleukin (IL)-3 dependent MMCs of jejunum [8]. It has been shown, that tumor growth factor β (TGF-β) induces in BMMCs expression of MMCs specific chymase: mouse mast cell protease (mMCP)1 [9].

Mast cells responses to stimuli

FcεRI-induced response to antigen/pathogen is a multistep process which can be divided according to the timing of responses to the following step: 1) an immediate response leading to exocytotic release of secretory compartments 2) initiation of AA metabolism 3) *de novo* synthesis of cytokines, growth factors and chemokines 4) long-term homeostatic regulation after mast cells activation (Figure 2).

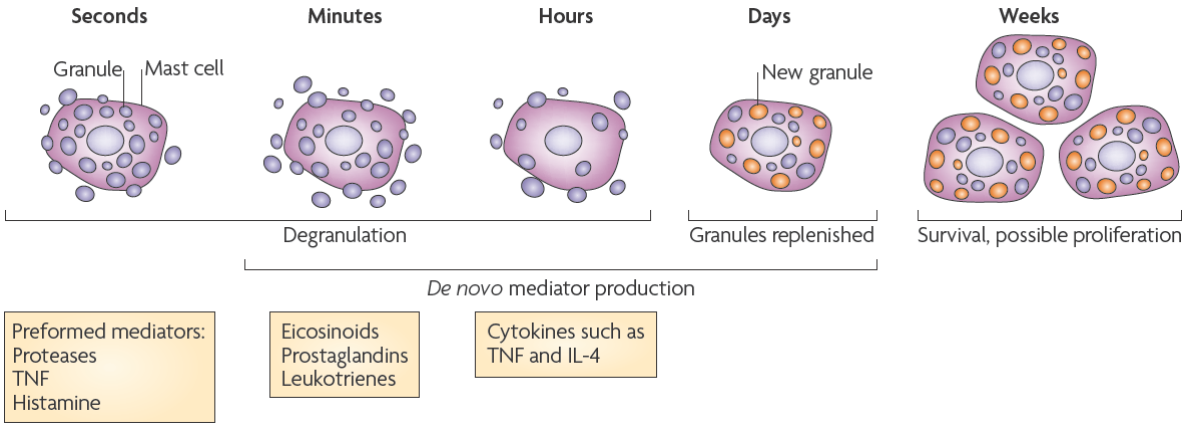

Figure 2. The IgE-mediated effector functions of mast cells can be grouped according to the timing of responses to immediate responses: releasing of preformed proinflammatory mediators dependent on Fyn-Gab2 (Grb2-associated binder 2)-RhoA signaling axis and calcium mobilization; delayed immediate responses: production of eicosanoids in calcium dependent manner; late responses: activation of transcription factors [e.g. nuclear factor of activated T-cells (NFAT) and nuclear factor kappa-light-chain-enhancer of activated B cells (NF-κB)] induces *de novo* synthesis of cytokines, chemokines or growth factors; delayed homeostatic responses: mast cells restore the secretory lysosomes, initiate the pro-survival pathways, and despite being terminally differentiated, they can proliferate in response to appropriate signals (Abraham and St. John, 2010).

1) Mast cells degranulation

Degranulation is a Ca^{2+}-depended process initiated with pathogen or allergen challenge. Relevancy of mast cells in host defense against pathogens highlights the fact that degranulation of heparine/tryptase complexes is an evolutionary conserved immune response first described in mast-cell-like cells in lowly urochordates [10]. Mast cell granules are compartments of endocytic origin with dual function – secretory and degradative therefore are referred as secretory lysosomes. Many synthesized products targeted to secretion [at least 15 serine proteases, serotonin, histamine, tumor necrosis factor α (TNFα), cathepsin D or cathelin-related antimicrobial peptide] are stored in secretory lysosomes together with lysosomal enzymes such as β-glucuronidase, β-hexosaminidase, arylsulfatase and carboxypeptidases [5;11;12] . At the molecular level, two functionally distinct secretory lysosomes have been described. Secretory lysosomes bearing vesicle resident fusion v-SNARE (vesicle SNAP receptor) isoform VAMP-8 (vesicle-associated membrane protein 8) comprise histamine and TNFα but are devoid of serotonin and cathepsin D [13]. According to ultrastructural electron microscopy, granules can be distinguished into three types of compartments (I-III). Type I is characterized with internal

vesicles, type II are organelles with electron-dense core enriched in serotonin surrounded by vesicles and type III elecron-dense serotonin rich granules [12] .

Internal vesicles, also called exosomes, are spherical particles (30-100 nm in diameter) formed by inward budding of the late endosome membranes. Such compartments are known as multivesicular bodies which can fuse with membranes and are released as membrane exosomes into cell environment [14]. It has been shown that 30% of mast cells and almost all basophils contain on the surface of exosomes major histocompatibility complex (MHC) clas II in the orientation enabling antigen presentation. MHC class II can be also exposed on the surface of basophils [12;15-17] and in some cases also on the surface of mast cells [12;16-18]. The exosomes play an important role in cell-cell communication [19]. It has been shown, that mast cells-derived exosomes contain also functional messenger ribonucleic acids (mRNAs) and microRNAs, which are transferable to other mast cells. This mRNA referred as exosomal shuttle RNA (esRNA) can be translated in the recipients cells [20]. Thus, a new mechanism of cell-cell communication mediated by esRNA was proposed. Recently, it has been shown that mouse mast cells exposed to oxidative stress have different composition of mRNA exosomes content in contrast to control cells. Subsequently, the exosomes have been capable of inducing protection against oxidative stress in recipient cells [21].

Electron-dense granules contain negatively charged serglycin proteoglycans heparin and/or chondroitin sulfate that serve as an electrostatic scaffold for a range of proteases, serotonin and TNFα [5;12;22]. This macro-molecular complexes are released from mast cells as approximately 0.9 μm large spherical particles composed of many smaller ~60nm spheres and potentially are endocytosed by fibroblasts, macrophages or eosinophiles [5;22]. These mast cells-derived sub-micrometer particles comprising heparin bound TNFα can also enter lymphatic vessels and thus explain fast accumulation of unstable TNFα in draining lymphoid nodes (DLN) without dilution to ineffective concentration or degradation during the way from the site of inflammation [22]. Mast cell-like heparin-chymosan particles loaded with TNFα were successfully used as potent adjuvants during mice immunization. On the other hand, artificial particles with encapsulated IL-12 promoted Th1 response. Thus, this newly described phenomena triggered by mast cell activation seem to be promising in clinical modulation of adaptive immune system because of the capacity to transfer the biological message to remote distances from the site of application [23].

2) Arachidonic acid derived mediators

Eicosanoid synthetic pathways initiate cytosolic phospholipase A2 which yields AA from membrane phospholipids including nuclear envelope phospholipids. AA is a substrate for cyclooxygenases, which catalyze conversion to prostanoids including prostaglandins and thromboxanes, and lipoxygenases, which converse AA into leukotriens and lipoxins [24]. 5-LO converts AA into unstable intermediator LTA4 which is further metabolized to LTB4 by LTA4 hydrolase in nucleus and cytoplasm or by endoplasmic reticulum (ER) transmembrane protein LTC4 synthase to LTC4 in cytoplasm [25].

3) Production of cytokines, growth factors and chemokines

A broad spectrum of stimuli induces expression of genes coding cytokines, growth factors and chemokines. The plethora of products is reviewed in Gali et al. [26], the expression of some of them is species and tissue dependent. Shortly, mouse BMMCs mostly express IL-3, IL-4, IL-6, IL-13 and TNFα cytokines; chemokine (C-C motif) ligand (CCL)2, CCL3, CCL5 and CCL8 chemokines and NGF (nerve growth factor), VEGF (vascular endothelial growth factor) and GM-CSF (granulocyte/macrophage colony stimulating factor) growth factors [26].

4) Homeostatic events following mast cell degranulation

In comparison to some other cell types of the innate immune system, mast cells are able to survive activation, replenish granules and even further proliferate in the local tissues [23;26]. Crosslinking of FcεRI or aggregation of glycosylphosphatidylinositol-anchored proteins (GPI-APs) is accompanied by transient massive externalization of phosphatidylserine on the outer cytoplasmic membrane leaflet which is not recognized as an apoptotic signal [27]. Similarly, mast cells are resistant to Fas-mediated cell death in antigen-activated mast cells which increasingly express Fas receptor on the surface [28]. The most critical activation-induced survival factors upon FcεRI crosslinking depend on up-regulation of anti-apoptotic Bcl-2 (B-cell lymphoma 2) family member A1 or a human homolog Bfl-1 [29;30]. Interestingly, antigen-mediated expression of A1 is associated only with CTMCs which explains prolonged survival of this subpopulation in contrast to MMCs [31].

Mast cells in immunological network

Mast cell responses to pathogens

Mast cells are located mostly at the body interface with external environment, surrounding both blood and lymphatic vessels, and periferal nerves; in gastrointestinal and respiratory tract are in the close association with smooth muscles and mucus-producing glands; under physiological conditions reside in CNS mainly in the vicinity of meninges venules [26;32;33]. The positioning of mast cells in the blood venules vicinity is important for the IgE capturing from circulation because mast cells can dynamically surmount the venule walls with extended processes outstanding into the vascular compartment [34]. Tissue resident macrophages, dendritic cells and mast cells together with epithelial cells can recognize among the first invasive pathogens and inform the host immune system of a potential threat [35]. The expression of the innate immune-associated receptors enables mast cells to respond to pathogen–associated molecular patterns (PAMPs) and a tissue injury evoked damage-associated molecular patterns [35;36]. Proteases released by mast cells [carboxypeptidase 3A (Cpa3) and mast cell protease 4 (Mcpt4)] play a central protective role to snakes, honeybea, Gila monster lizard or scorpions envenomation [37;38]. The exocytosis of stored histamine and TNFα rapidly enhances vascular permeability and the resulting edema is a physiological process accompanied with the local tissue enrichment in fluid and plasma proteins followed by appearance of blood leukocytes in the site of inflammation [39]. Changes in vascular permeability are further potentiated by cysteinyl LTs (LTC4,

LTD4 and LTE4) [40]. Histamine, LTC4 and LTD4 induce also releasing of the vascular endothelial cells specific granules known as Weibel-Palade bodies compraising among others preformed P-selectin. The externalization of P-selectin on the vascular endothelial cells contributes to the leukocytes rolling and their extravasation from the blood stream [41;42]. TNFα induces the expression of others molecules involved in leukocytes tissue-directed migration: intercellular adhesion molecule 1 (ICAM-1) and E-selectin on the endothelial cells. These effects can be synergistically enhanced by histamine [43] and are important for a recruitment of dendritic cells into the tissues infected with bacteria [44]. Mast cell-derived TNFα is also important in early recruitment of neutrophils to the CNS in experimental autoimmune encephalomyelitis (EAE). Neutrophils presence in CNS subsequently disturbs the integrity of blood brain barrier [33]. Cysteinyl LTs are responsible for bronchoconstriction [45;46] and potently contribute to the IgE-mediated pathophysiology to allergens. Recently, it has been shown that intact parasympathetic system and mast cells-derived serotonin are important for bronchoconstriction [47]. Mast cells ability to induce contraction of mucosal smooth muscle is behind their involvement in the expulsion of parasites from intestine [48;49]. Engrafment of mast cells into mast cell-deficient Ws/ws rats and $kit^{Wsh/Wsh}$ mice revealed that mast cells play a role in the primery response to hookworm parasite (*Nippostrongylus brasiliensis*) but the second wave was mediated by basophils independently of Th2 cells and mast cells [49]. This mast cells – basophils interplay seems to be important in immunity against blood-feeding ectoparasite *Haemaphysalis longicornis*. The IgE-mediated acquired immunity to a secondary challenge with ticks is crucially dependent on basophiles as has been shown in mice lacking this cell type [50]. Furthermore, TNFα of mast cell origin preclude the onset of malaria in mice infected with *Plasmodium berghei* [51]. The list of parasites inducing mast cell-dependent defense includes also nematode *Trichinella spiralis* [52] or protozoa *Leishmania major* [53]. The numbers of mast cells enhance in DLN of mice infested with *L. major* [54] and $kit^{W/W-v}$ mice infected with *L. major* developed larger skin lesions with more parasites than control mice [53].

Mast cells defence against bacteria could be divided on direct or indirect response. Direct response to *Streptococcus pyogenes* includes formation of mast cells extracellular traps; the mechanism of these phenomena was firstly recognized in neutrophils defence towards pathogens [55]. The extracellular traps are nets composing of a cell material bound to DNA released during specific type of cell death which depend on elastase and myeloperoxidase activity [56]. Because of presence of tryptases or cathelicidin antimicrobial peptide, the entraped bacterias *S. pyogenes* are effectively killed [55]. Phagocytosis is another direct mechanism of mast cells-mediated defence against bacteria. BMMCs recognize and phagocytose the type 1 fimbrated enterobacteria *Escherichia coli*, *Enterobacter cloacae* and *Klebsiella pneumonia* [57]. Human cord blood-derived mast cells can also bind and internalize different gram-negative and gram-positive bacteria [58]. On the other hand, the ability of *Staphylococcus aureus* to escape killing promoted by cellular machinery enables to *S. aureus* simultaneously survive a potent extracellular antimicrobial activity developed by mast cells, thus, long-lived mast cells can serve as a refuge of *S. aureus* latent infection [59]. The interaction between mast cell and bacteria is followed by TNFα secretion [57-59]. This cytokine response indirectly recruits neutrophils to the sites of inflammation and is crucial for mice survival as was proved in studies of

experimentally induced peritonities in mice lacking mast cells [60;61]. The recruitment of neutrophils into peritonal cavity during peritonitis is also dependent on other mast cells derived mediators, such leukotrienes [62], mMCP-6 protease which promotes endothelial cells to induce IL-8-mediated long-lasting attraction of neutrophils [63] and mast cells-derived IL-6 which enhances neutrophils-mediated killing of *K. pneumonie* during intraperitoneal infection [64]. Mouse mast cells express cathelicidin peptide called cathelin-related antimicrobial peptide and human skin mast cells cathelicidin LL-37. Mice mast cells lacking cathelin-related antimicrobial peptide are not capable of efficient *Streptococcus* eradication comparing to mast cells derived from control littermates [65].

Mast cells promotion of the antiviral activity is less understood. Convincing data link dengue virus to degranulation of human, monkey and rodent mast cells and induction of anti-viral immunity genes transcription. Mice deficient in mast cells reveal impaired clearance of dengue virus because of diminished recruitment of naturel killer and natural killer T cells to the sites infested with dengue viruses [66].

IgE-mediated immune responses

Mast cells are central effector cells in IgE-associated acquired immune responses which can be protective (anti-parasitic immunity) or deleterious (allergic disorders). In other words, the T helper (Th)2 cells-dependent immune responses are targeted against physiological antigens (parasites) or environmental antigens (allergens). IgE involvement in parasite clearance was well documented in mice infected with a nematode *Trichinella spiralis*, which is accompanied in humans and mice with the augmented production of IgE and a mastocytosis in the mucosa of the small intestine [67;68]. Infection of IgE-deficient mice with *T. spiralis* exhibit a similar mastocytosis and eosinophilia in jejunum comparing to wild type cells but spleen mast cells hyperplasia and serum levels of mMCP-1 (MCPT-1) were lowered in IgE-deficient mice. The expulsion of the nematode from the gut was slowly delayed in IgE-deficient mice [69]. This data are in corcordance with the study on mice mMCP1-deficient mice which exhibit a significant delay in *T. spiralis* expulsion from intestine (Knight 192:1849). Moreover, in IgE-deficient mice the numbers of larval encystment in the tongue muscle was enumerated more than twice comparing to the control mice and the necrosis of larvae was in IgE-deficient mice diminished. In the control mice, IgE was associated with encysted larvae, thus, IgE is involved in immune responses to different development stages of *T. spiralis* [69].

IgE-mediated deleterious immune responses could be divided on immediate, late and delayed phases which develop in minutes, hours and days, respectively [70]. Persisting or repetitive exposure to allergen could mediate chronic allergy disorders such as asthma, allergic rhinitis and atopic dermatis which are accompanied with tissue remodelling and altered function of affected organs [71]. It has been shown that almost all IgE-dependent immediate and late hypersensitivity responses are directly dependent on mast cells humoral activity and that the basophils are responsible for some of the systemic anaphylaxis responses as well as delayed phases of IgE-mediated allergic inflammation. The later immune responses are promoted by the effector activity of other lymphocytes recruited into the sites of

inflammation [70;72]. Using mice lacking the expression of FcεRI or a low-affinity receptor for IgE (FcεRII) it has been shown that FcεRI is crucial for developing of the immediate, late and delayed phase of IgE-mediated immune responses and that FcεRII is dispensable [70]. Recently, it has been demonstrated, that the passive cutaneous and systemic anaphylaxis was completely abolished in a new model of mast cell-deficient mice. The expression of Cre recombinase from the mast cell specific carboxypeptidase A locus (Cre-Master mice) led to a selective depletion of MMCs and CTMCs lineages. Cre-Master mice exhibit no spontaneous onset of immune responses and thus seem to be a more suitable model for study of mast cells because previous models of mast cells deficiency relied on mutation of c-kit or its ligand, which influnced a wide scale of hematopoetic cell types. However, because basophils express low levels of Cpa3, their numbers in the spleens of Cre-Master mice were decreased about 40% [73].

The involvement of distinct cell types in IgE-associated immune responses was studied in transgenic mice expressing 2,4,6-trinitrophenol-(TNP)-specific IgE. Single intradermal challenge with TNP-ovalbumin elicited a triphasic ear swelling response, which corresponded to the IgE-mediated immune responses. The authors referred to the third phase of ear swelling as an IgE-mediated chronic allergic inflammation accompanied with eosinophiles and neutrophils infiltration. Interestingly, they revealed that basophils infiltration is indispensable for developing of the third phase of ear swallowing and that this process is surprisingly based on basophils while independent of mast cells and other lymphocytes [70].

Mast cells in autoimmune diseases

Mast cells contribution to autoimmune diseases remains controversial because of contradictory data obtained on different animal models. Rheumatoid arthritis and multiple sclerosis are two examples of serious human autoimmune diseases promoted by autoantibody-directed immune responses which are studied on animal models induced by immunization to elicit autoimmune response. Mast cells deficient mice are those with mutation in Kitlg, gene encoding c-kit ligand SCF or in c-Kit receptor ($Kit^{W/Wv}$ or $Kit^{Wsh/Wsh}$). It has been shown that administration of K/BxNserum elicits experimental arthritis in animal models. However, $Kit^{W/Wv}$ mice are resistant to develop the experimental arthritis. $Kit^{W/Wv}$ mice reconstituted with BMMCs from wild type C57Bl/6 mouse reverts the susceptibility to arthritis. Interestingly, BMMCs from IL-1α-deficient mice failed to develop arthritis and IL-1α administration together with arthritogenic K/BxN serum to mast cells deficient $Kit^{W/Wv}$ reestablished the susceptibility to arthritis [74]. Similarly, involvement of mast cells in EAE has been documented by restoration of susceptibility to EAE in $Kit^{W/Wv}$ mice immunized with myelin glycoprotein and complete Freund adjuvans after their engraftment with wild type BMMCs. EAE is accompanied with increase in blood-brain barrier permeability and infiltration of CNS with Th1 and Th17 cells. Moreover, EAE development was reverted in $Kit^{W/Wv}$ engrafted with mast cells lacking TNFα. The authors suggest that mast cells-derived TNFα dependent recruitment of neutrophils in the early stages of the EAE is crucial for blood-brain barrier disruption and acceleration of CNS damage after immunization with myelin

glycoprotein [33]. The key role of neutrophils in EAE was corroborated by Carlsson and colleagues who suppressed EAE by genetic silencing or blockade of a chemokine receptor CXCR2 [chemokine C-X-C) motif receptor 2] which is important for polymorphonuclears to be recruited into the sites of inflammation [75].

In contrast to these data, studies on $Kit^{Wsh/Wsh}$ mice failed to report impaired susceptibility to immunization-mediated arthritis [76] or even in the case of EAE the manifestations of disease exacerbate in these mice after administration of myelin [77]. As was mentioned in the previous chapter recently was established the Cre-Master mice model with eradicated mast cells and partially decreased numbers of basophiles [73]. Cre-Master mice after injection with K/BxN serum were fully susceptible to the disease but $Kit^{W/Wv}$ mice were resistant, thus the authors proposed that unrecognized Kit signaling event, independent of mast cells, is responsible for susceptibility to arthritis [73]. Current animal models suffer from unnatural eliciting of autoimmune diseases which could mask the subtle contributory role of distinct cell types in the early stages of autoimmune diseases. Thus, further studies on more natural animal models which tend to develop autoimmune responses are desirable to reveal the role of mast cells in autoimmune diseases.

Mast cell as a partner in immune interactions

Mast cells are potent modulators of adaptive immune system. They are capable of inducing dendritic cells migration towards the sites of inflammation and into the lymph nodes. There is strong evidence that mast cells influence other cell types by humoral activity, releasing of exosomes and cell-cell interactions. Direct interactions of mast cells with dendritic cells have been observed [19]. The central role in this immunological synapses plays FcεRI and the transfer of mast cells-internalized material to dendritic cells has been documented [19]. Moreover, artificially immobilized antigen and even mobile monovalent antigen in lipid bilayers induce formation of signaling competent IgE-FcεRI synapses which resemble synapses triggered by T-cell receptor (TCR) and B-cell receptor (BCR) signaling [78].

Immunological synapses are formed also between T cells and mast cells. Co-incubation of human mast cell line 1 or BMMCs with activated T cells led to β-hexosaminidase and histamine release. This effect was not observed when transwell cell culture chambers were used indicating that direct contact of T-cells with mast cells is crucial for mast cells degranulation [79]. These data were extended by Inamura et al. who found out that antibody-mediated blocking of intercellular heterotypic aggregation based on leukocyte function-associated antigen-1 and ICAM-1 abolished in mast cells co-cultured with T lymphocytes degranulation [80]. Finally, synapse formation has been shown between effector CD4+ T helper cells and isolated peritoneal mast cells or peritoneal cell-derived mast cells primed with interferon γ (IFN- γ) and IL-4 which induced surface expression of MHC class II and CD86 costimulatory molecule on mast cells. These T cells-mast cells synapses were enriched in TCR/CD3/Lck (lymphocyte-specific protein tyrosine kinase) signaling complexes and the treshold for activation of mast cells cultivated with T helper lymphocytes was lowered [18].

Humoral activity of mast cells modulates dendritic cells function; mast cells-derived histamine and TNFα play a central role in dendritic cells recruitment to the sites of inflammation, maturation and mobilization to DLN. Histamine alone induces chemokine production and transient expression of co-stimulatory molecules on human immature dendritic cells isolated from peripheral blood [81]. As was mentioned before, mast cells-derived TNFα elicited by bacterial infection induced endothelial surface E-selectin expression-dependent migration of dendritic cells to the sites of inflammation. Furthermore, mast cells-derived TNFα enhances DLNs-mediated production of a key chemokine CCL21 responsible for dendritic cells migration and therefore mobilize dendritic cells to the DLNs [44]. It has been shown that supernatant from activated MC/9 mast cell line exhibit a co-stimulatory effect to CCL21 induced dendritic cells chemotaxis [82]. As was discussed above, mast cells-derived TNFα is delivered to DLNs from the local tissue inflammation via lymphatic vessels as a large cargo [22]. Injection of mast cell-derived particles originated from $TNF\alpha^{-/-}$ mice revealed that TNFα is responsible for lymph nodes hypertrophy [22]. Two studies using new mice models of mast cells-deficiency reported that mast cells trigger irritant contact dermatitis which is a delayed type hypersensitivity response. In both studies the emigration of dendritic cells was impaired in the absence of mast cells and contact hypersensitivity was attenuated [83;84]. There is an evidence that mast cells degranulation *in vivo* can modulate balance between Th cells. Immunization of mice with simultaneous mast cells activation lowered the capacity of dendritic cells to develop Th1 response in favor of Th2 response as was measured by the shift in IL-4/IFN-γ ratio [85]. Other group found that activated mast cells influence dendritic cells capacity to induce significant Th2 polarization in the presence of pro-inflammatory cytokine milieu. The authors proposed that such conditions *in vivo* could up-regulate allergic responses. In line with this hypothesis, skin with lesions of atopic dermatitis obtained by biopsy revealed anatomical apposition of mast cells to dendritic cells [86]. Contrary to these data, Dudeck et al. showed that peritoneal cultured mast cells-driven maturation of dendritic cells polarize the immune responses to Th1 and Th17 as was determined by measuring the levels of released IFN-γ and IL-17. $Kit^{W\text{-}sh}$ mice infested with *L. major* exhibit suppression of IFN-γ and IL-17 cytokines to the benefit of IL-4 and IL-10 cytokines. The authors speculate that the contradictory results could be explained by mast cells preactivation with strong proinflammatory stimuli (liposacharide) in previous studies [87].

Maturation of dendritic cells can be forced by exosomes released from activated mast cells as was detected by up-regulation of MHC class II and co-stimulatory molecules on the surface of dendritic cells [88]. Mast cell exosomes containing MHC class II and CD86 can also activate B- and T-cells [89] and T-cell derived exosomes can stimulate mast cells [90]. Although the presence of MHC class II on mast cells exosomes is well documented [12;89;91], the convincing biological evidence of antigen presenting by mast cells-derived exosomes is still missing.

In spite of mast cells ability to locally express mature MHC class II and costimulatory molecule CD86 on the cell surface under IFN-γ and IL-4 cytokine pressure [18], three independent studies on the mice models determined basophils as the central professional antigen presenting cells inducing *in vivo* and *in vitro* Th2 responses by surface expression of mature MHC class II [15-17]. However, human

basophils failed to express on the surface MHC class II even in antigen-activated cells, moreover human basophils were unable to induce Th2 polarization [89].

Mast cell signaling at the molecular level - associated receptors

There is a plenty of receptors expressed by mast cells which enable them to respond to environmental stimuli as well as to respond to autocrine and paracrine signals [1]. Most of the receptors are expressed on the mast cells surface; the most prominent receptor is FcεRI capable of triggering all three main effector functions (degranulation, eicosanoids synthesis and gene expression) but also other receptors can elicit the release of pro-inflammatory mediators on their own [FcγRI (Fc-gamma receptor I), c-Kit, PAMP associated receptors, complement receptor CA_3R, or CCR1 receptor for chemokine MIP-1α (macrophage inflammatory protein 1α)]. In the figure 3 are depicted synergistic effects of distinct receptors enhancing the outcome of FcεRI signaling.

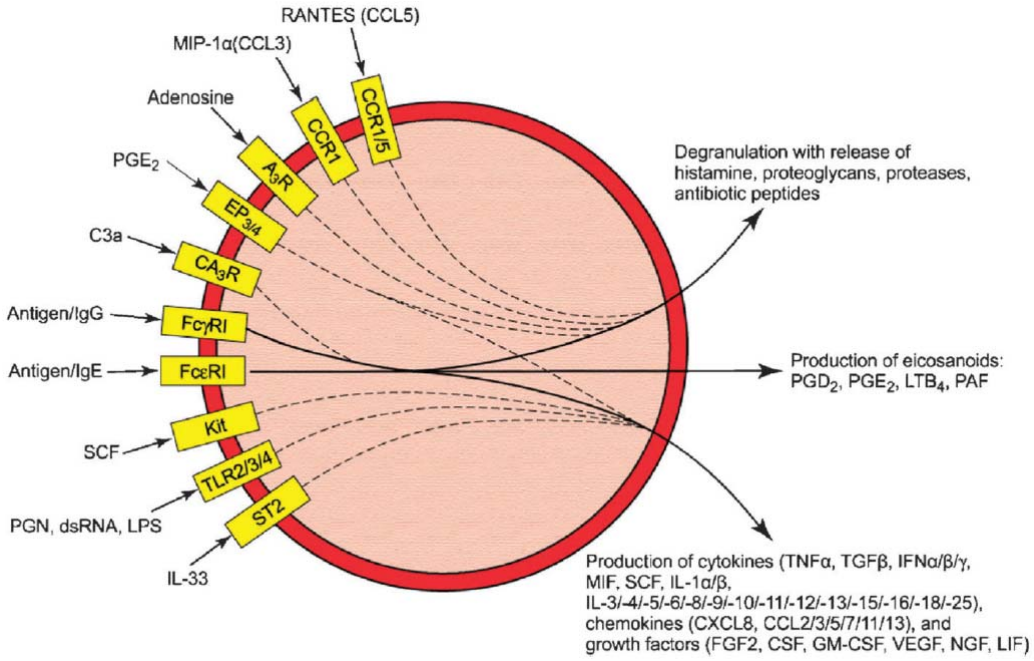

Figure 3. The examples of costimulatory effects on responses to antigen either through FcεRI or, in the case of complement C3a, through FcγRI. Some of these costimulations enhance mainly degranulation while others enhance primarily cytokine production. Yellow boxes denote receptors to specific ligands, solid lines denote the responses to IgE and IgG antigen *via* FcεRI or FcγRI, respectively, and dashed lines indicate the potentiation to these responses. (Beaven, 2009).

FcεRI

Although mast cells also express FcεRII, FcεRI is an indispensable receptor for IgE-mediated immune responses [70]. Along with BCR and TCR, FcεRI belongs to the multichain immune recognition receptor family. In 1989 was proposed a model which described rodent FcεRI as a tetrameric receptor composed of one IgE-binding α subunit, one β subunit and a dimer of disulphide-

linked γ subunits [92] A few years later the structure of the antibody-binding portion of the human IgE receptor was determined by crystalography [93]. Expression of the FcεRI differs in humans and rodent in compositions and cellular distribution. The tetrameric structure αβγγ is confined to human and rodent mast cells and basophils, while in mice is expressed also on non-T and non-B cells, in humans could be expressed also in eosinophiles and platelets. The trimeric αγγ form is expressed in human monocytes, Langerhans cells, and dendritic cells [94-96]. Surprisingly, functional tetrameric FcεRI was found at the protein level in murine superior cervical ganglion neurons. IgE-sensitized neurons activated by corresponding antigen induced strong calcium response which was successfully propagated to the neighboring cell bodies and neurites [97].

The α subunit (FcRα) belongs to the immunoglobulin superfamily, contains two extracellular immunoglobulin-related domains capturing IgE, one transmembrane helix, and a short intracellular tail [95]. Extracellular part is heavily glycosylated to prevent misfolding and retention of α chain in the ER [98]. The crystal structure of dimeric IgE-Fc molecule with extracellular domains of the FcRα chain reveals that one dimeric IgE-Fc molecule is bound to one receptor asymmetrically through interactions at two sites, each involving one Cε3 domain of the IgE-Fc and thus IgE molecule is bent. This IgE-Fc-FcεRI complex blocks the binding of a second receptor to bound IgE [99]. Moreover, the deletion of Cε2 domain from IgE Fc fragment lowered the binding affinity of FcεRI to IgE, because Cε2 domain stabilise the FcεRI-IgE complex [100]. The human FcRα chain was expressed on transfected cell line COS 7 (no expression of FcεRI) only if rat β and γ chains were co-expressed or in the presence of the γ chain alone [101] It has been thought that rodent FcRα subunit is expressed on surface only in the tetrameric form [95]; surprisingly, presence of the trimeric αγγ form of FcεRI was found also in rat eosinophiles and macrophages [102]. Later it has been shown, that FcRα chain comprises a dilysine ER retention motif which is hidden after assembly with the γ subunit [103].

The β chain (FcRβ) is a common component of FcεRI and the low affinity IgG receptor (FcγRIII). It consists of four transmembrane domains and both N- and C-terminal tails faces into the cytoplasm [95]; as a non-obligatory component of FcεRI it is capable of amplifying the magnitude of calcium mobilization and spleen tyrosine kinase (Syk) phosphorylation 5- to 7-fold in cells expressing αβγγ complex in contrast to signaling triggered by αγγ FcεRI [104]. FcRβ contains one non-canonical immunoreceptor tyrosine-based activation motif (ITAM), which after phosphorylation, serves as a docking site for signaling molecules containing Src homology (SH)2 domain [95]. The FcRβ ITAM motif differs from a canonical ITAM because of a shorter spacing between the canonical tyrosine residues and it possesses a third tyrosine between the canonical tyrosines [105].

The γ chain (FcRγ) is a member of the γζη family of immunoreceptors subunits consisting of a transmembrane domain and a cytoplasmic tail. This family forms homo- or heterodimeric forms in many receptors, as FcγRIII, FcεRI, FcαR (Fc fragment of immunoglobulin A receptor), and the TCR depending on the cellular context. In FcεRI signaling, the dimer of disulfide-linked *γ* subunits, functions as an autonomous activation module because each *γ* chain contains the canonical ITAM motif [95;104].

Reconstitution of FcRγ chain with or without functional mutation in ITAM in mice lacking FcRγ subunit revealed that FcRγ ITAM motif is essential for degranulation, cytokine production, and prostaglandins synthesis as well as for passive systemic anaphylaxis [106].

The study on rat basophilic leukemia (RBL) cell line has shown that FcεRI is regulated by IgE serum levels. IgE bound to FcεRI has an effect on prolonged FcεRI surface survival and the numbers of FcεRI on the plasma membrane increase. Also the FcεRI-bound IgE has an extended half-time when compared with free IgE [107]. This work was extended in the study describing IgE-regulatory role *in vitro and in vivo*. Peritoneal mast cells lacking IgE exhibit robust down-regulation of FcεRI expression and IgE enhances markedly FcεRI expression on mouse peritoneal mast cells and BMMCs in a time- and dose-dependent manner. IgE-induced enhancement of mouse BMMCs FcεRI expression facilitates the cytokines and serotonin release in response to the specific antigen [108]. Mutation of tyrosines in the FcRγ-resident ITAM motif decreased IgE-mediated survival of mast cell but IgE-dependent up-regulation of surface FcεRI expression was maintained [106].

FcεRI signalosome

Cross-linking of IgE-FcεRI complex with multivalent antigen initiates a series of biochemical events starting with the Src family protein tyrosine kinase Lyn-dependent phosphorylation of the adjacent β nad γ chains associated ITAM motives within the aggregate [109]. Phosphorylated ITAM motives serve as a docking sites for proteins comprising SH2 domain, mainly additional Lyn molecules and Syk, a PTK of the Syk/ZAP-70 (ζ –associated protein of 70 kDa) family [95;110]. These activated kinases further propagate the signal through phosphorylation of many down-stream signaling targets: phospholipases C γ (PLC γ)1 and PLC γ 2, phosphoinositide 3-kinase (PI3K), VAV or transmembrane adaptor proteins (TRAPs). These events lead to activation of MAPK (mitogen-activated protein kinase kinases) [ERK (extracellular-signal regulated kinase), JNK (Jun N-terminal kinase), and p38], exocytosis of granules, and generation of LTs and cytokines [94-96].

Src family kinases involved in early FcεRI signaling

Src family tyrosine kinases share the common structure comprising the variable N-terminal tail, SH3 and SH2 domains, the kinase domain, and the C-terminal regulatory tail. Intramolecular interactions mediated by phosphorylation of the conserved tyrosines switch on/off their enzymatic activity. The N-terminal domain of Src family kinases involved in early FcεRI signaling (Lyn, Fyn, Hck and Fgr) contains signals for myristoylation and palmitoylation, both of which are responsible for the membrane association of the Src family kinases [111]. Negative regulation of Src family kinases is mediated by C-src tyrosine kinase (Csk) dependent phosphorylation of highly conserved tyrosine residues close to their carboxyl termini [112].

Lck/Yes-related novel tyrosine (Lyn) kinase is the most abundant Src family kinase in mast cells and exists as two alternatively spliced variants, Lyn A and Lyn B of 53 and 56 kDa, respectively.

Unlike Lyn B, Lyn A comprises in the unique N-terminal domain a 21-aa insert [113]. Both Lyn isoforms ($p53/56^{lyn}$) have been coimmunoprecipitated with FcεRI and at least 3-4% of the non-aggregated FcεRI was found to be directly associated with Lyn [114]. Restoration of distinct isoforms in $Lyn^{-/-}$ BMMCs revealed that Lyn A was more potent inducer of degranulation, inositol 1,4,5-triphosphate (IP3) production and calcium mobilization whereas Lyn B more readily bound phosphorylated proteins, including SH2-containing Inositol 5′-Phosphatase 1 (SHIP-1) [115]. Mutation in the myristoylation, palmitoylation, or both acylation sites revealed that myristoylation is crucial for Lyn association with plasma membrane while palmitoylation for localization in membrane rafts [116]. The concept of the lipid raft membrane microdomains assumes that biological membranes possess microdomains having a lipidic structure with properties of lipid order phase surrounded by membranes with lipid structure resembling lipid disorder phase possessing phosphatidylinositols and a majority of the transmembrane proteins. The lipid raft membrane microdomains are rich in cholesterol and sphingomyelin, and comprise a specific set of proteins, including those anchored to the membrane via acyl groups (e.g. palmitoyl or myristoyl) or glycolipids [e.g. glycosylphosphatidylinositol (GPI)], and also some acylated proteins with transmembrane domain (e.g. some of the TRAPs) [117]. Studies on BMMCs isolated from $Lyn^{-/-}$ mice yielded at first sight controversial results because FcεRI-mediated degranulation, accompanied by severally reduced tyrosine phosphorylation of the FcRβ and FcRγ chains was impaired [118], without changes [119], or increased [120-122]. These discrepancies could be explained by distinct genetic backrounds of cells derived from different mouse strains. The deficiency of the Lyn increased degranulation in 129/Sv BMMCs but impaired this response in BMMCs of C57BL/6 origin [123]. The second explanation is based on the fact that Lyn mediated both positive and negative regulation depending on the intensity of stimuli (e.g. valency of antigen) [124].

Src family kinase Fyn has been found in coimmunoprecipitates with FcRβ subunits and in spite of the lower expression in comparison with Lyn kinase, $Fyn^{-/-}$ BMMCs exhibited approximately 80% reduced degranulation [122]. In $Fyn^{-/-}$ BMMCs phosphorylation of FcRβ and Syk is normal, thus, it seems that FcεRI also utilizes a Fyn-mediated pathway leading to mast cell degranulation independent of Lyn kinase activity. Fyn kinase phosphorylates Grb2-associated binder 2 (Gab2) and subsequent activation of PI3K is strongly impaired in $Fyn^{-/-}$ BMMCs [122]. These data are in conflict with Yu et al who showed that in $Fyn^{-/-}$ BMMCs phosphorylation of Syk kinase is reduced and that Gab2 phosphorylation is Syk dependent [125]. Fyn/Gab2/RhoA signaling axis has been found as a central player in calcium-independent microtubule-dependent granule translocation to the plasma membrane which explain the impaired degranulation in $Fyn^{-/-}$ BMMCs whereas calcium responses are normal [126]. It has been shown that BMMCs deficient in Lyn exhibit the enhanced kinase activity of Fyn even in non-stimulated cells [120] and that the overexpression of Fyn in $C57BL/6Lyn^{-/-}$ BMMCs massively enhanced the impaired hexosaminidase release [123].

Other src family kinase, $p56/p59^{hck}$, has been studied in BMMCs. The combined amount of these two isoforms is similar to the amount of Fyn [127]. Surprisingly, Hck deficiency leads to enhanced Lyn activity and enhanced Lyn phosphorylation targets (e.g. FcRβ and FcRγ subunits or LAT) but phosphorylation of Syk, Btk (Bruton´s tyrosine kinase), pp38 and Akt (protein kinase B) was

reduced. In summary, the histamine release in $Hck^{-/-}$ BMMCs is reduced when BMMCs are stimulated with high concentration of antigen which reflect the decreased Gab2 phosphorylation and impaired microtubule formation while calcium mobilization is unchanged [127]. Thus, Lyn activity is inhibited by Hck.

Recently, association of Fgr src family kinase with FcεRI has been described. BMMCs or RBL-2H3 cells with reduced Fgr levels exhibit decreased phosphorylation of Syk, Syk-dependent signals, degranulation, TNFα production and LTC4 synthesis after FcεRI aggregation. Moreover, knock-down of Fgr decreased association of Syk with FcRγ subunit as well as the phosphorylation of FcRγ ITAM [128].

In the mouse mast cell line PT-18 the association of $p62^{c\text{-}yes}$ with FcεRI has been documented, but there are no other studies extending this subject [129].

TRAPs

In mast cells, TRAPs organizes macromolecular complexes associated with aggregated FcεRI by docking various molecules involved in the signal propagation to the plasma membrane. Five members of TRAPs family are expressed in mast cells: phosphoprotein associated with glycosphingolipid-enriched membrane microdomains (PAG), NTAL, LAT, LAX (linker for activation of X cells) and GAPT [growth factor receptor-bound protein2 (Grb2)-binding adaptor protein, transmembrane]. General characteristic of these proteins is a short extracellular N-terminal part, transmembrane domain and an intracellular tail with various tyrosine-based binding motives [130]. Presence of CxxC palmitoylation site determines LAT, NTAL, and PAG for their interactions with lipids and localization in lipid-ordered regions [131;132]. Although we found that these protein are associated with detergent resistant membranes (DRM) fractiones isolated from BMMCs this DRMs are rather artificial because fine topography revealed the distinct sub-membrane compartmentalization of LAT and NTAL in quiescent and activated cells [132].

The LAT adaptor has been recognized as a secondary signaling domains organizer in RBL cells activated via FcεRI [133]. Fine topography of NTAL and LAT revealed that in resting cells both TRAPs, NTAL and LAT, were found in small clusters independently of FcεRI whereas aggregation of FcεRI induced formation of large distinct clusters of NTAL and LAT in the close neighborhood of aggregated receptors [132]. Tyrosine-based motives of both proteins, LAT and NTAL, are rapidly phosphorylated by Syk and Lyn after FcεRI aggregation. The proteins anchored to these adaptors can be common (e.g. adaptor protein Grb2 and SHIP1) or LAT specific (PLCγ1 and adaptor protein Gads). Grb2 and Gads are cytoplasmic adaptor proteins involved in shaping the signaling pathways [130].

Experiments *in vivo* showed that mice deficient in LAT exhibited impaired passive systematic anaphylaxis; this implies that LAT has a positive regulatory role in mast cells signaling [134]. This conclusion was confirmed by *in vitro* studies comparing the properties of antigen-activated BMMCs derived from LAT-deficient or WT mice. $LAT^{-/-}$ BMMCs exhibited decreased phosphorylation of PLCγ1, PLCγ2, SLP-76, calcium mobilization, degranulation, cytokines production, and kinase activity

of Erk and JNK1 whereas phosphorylation of FcRβ, FcRγ, Syk or Vav was intact [134]. Moreover, LAT was found indispensable for peritoneal cultured mast cells [135]. The molecular dissection of LAT tyrosine motives showed that BMMCs require all four distal tyrosines to promote IgE- and IgG-induced signaling whereas Y136 is apparently sufficient in peritoneal cultured mast cells [135].

In contrast to LAT, NTAL was found to be a negative regulator of IgE-mediated passive systemic anaphylaxis and BMMCs effector functions. NTAL-deficient BMMCs exhibited augmented phosphorylation of LAT, PLCγ1, PLCγ2 and Erk, enzymatic activity of PI3K, calcium mobilization, cytokines production, and degranulation [132;136]. NTAL could function also as a positive regulator of BMMCs signaling, as was demonstrated in $NTAL^{-/-}/LAT^{-/-}$ BMMCs which exhibit more impaired phenotype than BMMC deficient only in LAT [132;136]. Volná et al. proposed that the distinct clusters of NTAL and LAT compete for Syk in activated mast cells. This hypothesis could explain the increased phosphorylation of LAT in $NTAL^{-/-}$ BMMCs and Ca^{2+} responses initiated by enhanced anchoring of PLCγ1 and PLCγ2 via LAT to plasma membrane. Although human mast cells with NTAL knock-downs exhibited decrease in β-hexosaminidase release [137], these contradictory data were not confirmed in the RBL cells and BMMCs with reduced NTAL levels which provided similar results to thus obtained in $NTAL^{-/-}$ BMMCs ([138], Polakovičová in preparation). NTAL was surprisingly linked to calcium responses initiated with the blocker of SERCA (sarco/endoplasmic reticulum Ca^{2+} ATPase) pumps, thapsigargin. The magnitude of Ca^{2+} mobilization and $^{45}Ca^{2+}$ uptake in RBL cells stimulated with thapsigargin corresponds to increased or decreased expression levels of NTAL independently of NTAL or LAT phosphorylation. Thus, it was proposed that NTAL could be involved in the direct or indirect regulation of CRAC channels [138].

PAG serves as a substrate for Lck, Fyn and probably Hck but not for ZAP70 and/or Syk [127;131]. Two proline-rich sequences of PAG serve as docking sites for proteins containing SH3 domains; moreover phosphorylated YSSV tyrosine motif of PAG anchor Csk to the plasma membrane thus negatively regulating the activity of Src family kinases [131;139]. FcεRI aggregation induced rapid phosphorylation of PAG in RBL cells which was followed by recruitment of Csk to the plasma membrane. In line with these data, overexpression of PAG let to reduction of IgE-mediated degranulation, Ca^{2+} mobilization and phosphorylation of FcRβ and FcRγ subunits. Thus, enhanced recruitment of Csk to the plasma membrane in RBL cells with increased PAG expression levels inhibited the src family kinases-dependent FcεRI signaling [140].

Store operated calcium entry

As was mentioned above, phosphorylated LAT recruits PLCγ1, which yields diacylglycerol (DAG) and IP3. IP3 diffuses through the cytosol to bind to IP3 receptors (IP3R), particular Ca^{2+} channels in the ER membranes allowing the leak of Ca^{2+} from ER into the cytosol [141]. The concept of a capacitative regulation of Ca^{2+} release and Ca^{2+} entry was formulated by James Putney in 1986 but molecular mechanism remained almost 20 years elusive. This phenomena is now known as capacitative Ca^{2+} entry or store operated calcium entry (SOCE) [142]. In RBL cells was found a Ca^{2+}-selective

calcium-release activated calcium current (I_{CRAC}), this implied the existence of the CRAC channel [143]. A few hypotheses have been proposed to explain molecular mechanism of SOCE including a production of an elusive calcium influx factor upon depletion of ER Ca^{2+} stores but all these models were misleading [142].

Stromal interaction molecule 1

Breakthrough occurred in 2005, when two independent RNA interference (RNAi) screens targeted on proteins potentially relevant to calcium signaling identified STIM1 and STIM2 in HeLa cells or their homologue, dStim, in Drosophila S2 cells [144;145]. It should be noted that although the role of STIM1 in SOCE was discovered 8 years ago, a great number of publications have been drawn since this time. According to PubMed database it has been published to date 673 publications containing keyword STIM1.

STIM1, STIM2 and dStim proteins were already known as proteins with a conserved genomic organization, implicating that the vertebrate family of two STIMs genes most probably arose from a single ancestral gene, but the function of STIM1 was not associated with SOCE but rather with tumor suppression. STIMs are characterized as a single spanning ER-membrane proteins which contain at the C-terminal part a single sterile alpha-motif (SAM) domain and conserved coiled-coil domains whereas at the N-terminal tail an unpaired EF-hand [146]. It has been shown that thapsigargin-mediated Ca^{2+} depletion from ER stores induces STIM1 aggregation to the distinct puncta near the plasma membrane because STIM1 senses ER Ca^{2+} depletion with its luminal EF-hand domain. The HeLa cells transfected with EF-hand mutant STIM1 (D76A) exhibited persistant STIM1 aggregates and constitutive active SOCE even in non-stimulated cells [144]. The reduction of I_{CRAC} was documented by Roos et al. also in Jurkat T cells and HEK293 cells with STIM1 knock-downs; this suggested that STIM1 is a crucial regulator of CRAC channels across cell types and organisms [145].

Moreover, mutations in EF hand motif or thapsigargin activation induced STIM1 translocation to the plasma membrane [147]. The presence of STIM1 on the plasma membrane of activated cells was controversial until it has been found that fluorescent tag on the N-terminus prevented cells to expose STIM1 on the surface [148]. This surface exposition of STIM1 is calcium dependent and is probably involved in sensing of extracellular calcium levels and in inactivation of SOCE by extracellular Ca^{2+}-dependent manner because antibody corresponding to the exposed EF-hand domain (25-139aa) blocked the inactivation of SOCE [149]. In spite of these studies, it is now generally accepted that ER-bound STIM1 is translocated to the ER-plasma membrane junctions after Ca^{2+} store depletion where induces the opening of plasma membrane CRAC channel via *trans*-interaction (Figure 4). This model was first proposed by Luik et al. who found that the regions of CRAC-mediated Ca^{2+} influx overlap with STIM1 puncta and that STIM1 and CRAC channel subunit Orai1 (see below) form closely apposed clusters in the ER/plasma membrane junctions (Figure 4). The distance between ER and plasma membranes was estimated on 10-25nm [150].

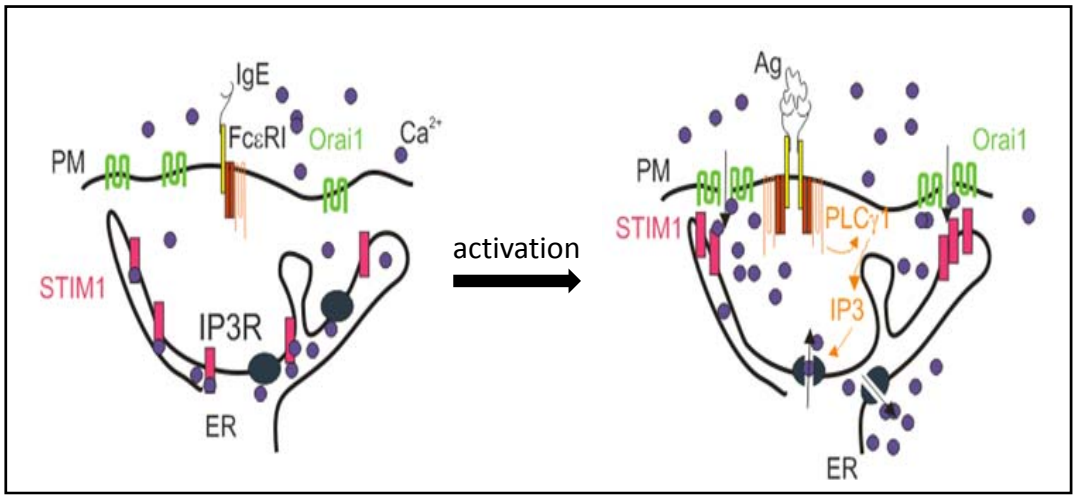

Figure 4. Aggregation of FcεRI on the surface of mast cells triggers activation of Src kinase Lyn (not depicted) and initiates signaling cascades which include activation of PLCγ and subsequent generation of IP3 and DAG. IP3 binds to IP3R (black dot) and mediates ER Ca^{2+} (magenta dot) store depletion. The levels of Ca^{2+} are sensed with ER-luminal EF-hand domain of STIM1 (purple box). In resting cells STIM1 is distributed evenly in ER but upon ER Ca^{2+} store depletion STIM1 forms clusters close to the plasma membrane where directly interacts with the CRAC channels subunits (Orai1; green) and calcium can enter into the cells

Orai1

Drosophila Orai1, dOrai, known also as CRAC modulator (CRACM)1 or olf186-F was identified as a pore-forming subunit of the CRAC channel by three independent genome wide RNAi screens in Drosophila S2 cells. This plasma membrane protein comprises four transmembrane domains and both tails face into the cytosol [151-153]. Orai1 was also recognized by a genome-wide single nucleotide particles array screen as a genetic cause of a specific hereditary severe combined immunodeficiency disease in patients from two different families [151]. Vig et al. identified Drosophila CRACM2 (dOrai2) and a human ortholog of CRACM1, a protein encoded by gene FLJ14466 mapped in 12q24, as well as CRACM2 (Orai2) and CRACM3 (Orai3) [152;154]. The efficacies of this mamalian homologs of Orai1 to induce SOCE was in the order Orai1>Orai2>Orai3 [155]. Moreover, it has been shown that overexpression of dOrai in S2 cells increased the average I_{CRAC} density 3-fold and although dStim by itself did not alter current density, co-transfection of dStim with dOrai exhibited a remarkable 8-fold gain [147]. Similarly, in HEK293 cells co-transfection of STIM1 with Orai1 resulted in ~20-fold enhancement in SOCE and I_{CRAC} [155]. It has been shown that Orai1 forms homomultimers as well as heteromultimers with Orai2 and Orai3 [156] and that in resting cells Orai1, like Orai3 was found dimeric and mainly tetrameric when activated with truncated C-terminal part of STIM1 [157].

STIM-Orai1 interaction

The close association of STIM1 with Orai1 was confirmed by immunoprecipitation [158] or by fluorescence resonance energy transfer (FRET) studies [159;160]) and the intensity of this interaction reflected the Ca^{2+} store depletion. It has been shown that a soluble fragment of STIM1 cytosolic part, which contains a coiled coil domain 2, constitutively induced SOCE [159;161;162]. Various names denote this domain as three independent groups of researchers identified this region: CRAC-activation domain (CAD), STIM1-Orai activating region (SOAR) or Orai1 activating small fragment (OASF). This CAD/SOAR/OASF region with basic amino acid residues directly binds to Orai1 and activates SOCE [159;161;162]. Moreover, when the whole part of cytosolic STIM1 was co-expressed with Orai1, no interaction was detected. Thus, this data indicate that conformational changes in STIM1 result in allosteric activation of Orai1 channels [161]. Indeed, this scenario was extended in further studies and a current model of STIM1 activation was proposed [159;163]: in resting cells STIM1 preferentially forms dimer; depletion of ER Ca^{2+} store induces aggregation of STIM1 into clusters. This clustering is accompanied with an intra-molecular transition into stretching conformations which is accessible to Orai1.

The role of STIM2 is different from STIM1 because STIM2 is more sensitive to even small decreases in ER Ca^{2+} levels compared to STIM1. STIM2 moves to ER-plasma membrane junctions upon small changes in ER Ca^{2+} stores and subsequently regulates Orai1 to maintain the basal Ca^{2+} levels in narrow limits. Thus, it was proposed that STIM2 is the important regulator of basal Ca^{2+} [164].

The regulation of SOCE by cellular machinery

There is no doubt that the macromolecular complex of STIM1 and Orai1 is controlled and modulated at many levels, including phosphorylation, Orai1 internalization and/or interaction with other proteins. These proteins are involved in regulation of STIM1 aggregation, stabilizing the STIM1-Orai1 complex or in the termination of SOCE. The most prominent positive regulator is CRAC regulator 2A (CRACR2A) [165]; negative regulators associated with SOCE complexes involve: stanniocalcin 2 [166], calmodulin [167], surfeit locus protein 4 (Surf4) [168] and SOCE-associated regulatory factor (SARAF) [169]; junctate was described in Jurkat T-cells as both negative and positive regulator [170].

CRACR2A seems to be the crucial regulator of STIM1-Orai1 interactions because in cells with reduced CRACR2A levels the SOCE is impaired and the clustering of STIM1 with Orai1 in subplasmalemmal region was abolished. CRACR2A is a cytosolic protein which comprise EF-hand motif. When STIM1 aggregates and forms complexes with Orai1, CRACR2A probably stabilizes this complex. Increasing of Ca^{2+} concentrations leads to binding of Ca^{2+} by EF-hand domain, thus CRACR2A dissociates complex which is subsequently prone to disaggregation [165].

On the other hand, the dissociation of CRAC channels is Ca^{2+} dependent and two modes of negative feedback were described. Fast inactivation depends mainly on calmodulin binding to STIM1 and Orai1. Calmodulin binds in a Ca^{2+}-dependent manner to N-terminal domain of Orai1 and induces a Ca^{2+}-dependent inactivation of SOCE. The mutation of Orai1 which blocks calmodulin binding also prevents SOCE inactivation [167]. The slow Ca^{2+}-dependent dissociation of STIM1 and STIM2 clusters

is based on a single-spanning ER membrane protein SARAF which responds to the cytosolic elevation of Ca^{2+} after ER Ca^{2+} refilling by the dismantling of STIM1 and STIM2 aggregates via direct interaction to efficiently turn off SOCE. Moreover, it has been shown that basal Ca^{2+} levels in ER and cytosol are changed when SARAF expression is enhanced or reduced. It was suggested that SARAF plays a similar role as STIM2 in homeostasis of Ca^{2+} levels in intracellular stores [169].

Deletion of Surf4 exhibits an enhancement of SOCE and facilitates STIM1 clustering upon store-depletion [168;170]. Junctate was found in rodent sperm as a component of a macromolecular complex comprising IP3R and some of the transient receptor potential canonical (TRPC) channels [171]. Interestingly, junctate deletion plays a role in inhibition of SOCE but mutation of junctate ER-luminal EF-hand domain facilitates aggregation of STIM1 independently of Ca^{2+} store depletion and partially activates SOCE [170].

Recently, cAMP (cyclic adenosine 3',5'-monophosphate) has been unravelled as an inducer of STIM1 aggregation at the subplasmalemmal region independently of Orai1 clustering and SOCE. Apparently, other factors in addition to formation of STIM1 puncta are important for the clustering of Orai1 channels and activation of SOCE [172].

Phosphorylation of the SOCE components is important to link the depletion of ER stores to I_{CRAC} activation as well as deactivation. Interestingly, activation of B lymphocytes DT40 cell line genetically manipulated to suppress the expression of Lyn, Syk or both kinases Lyn and Syk, with thapsigargin or through IP3 exhibits impaired SOCE and I_{CRAC} only in double deficient Lyn/$Syk^{-/-}$ cells. This means that release of ER Ca^{2+} stores is not sufficient to provoke SOCE and that some undefined processes are dependent on the simultaneous activity of Lyn and Syk in DT40 cell line. Thapsigargin stimulation bypasses the receptor-mediated phosphorylation of Syk and Lyn and the process of SOCE regulation is at least at the Lyn level associated with the plasma membrane [173]. In platelets the additional role of Src/Abl subfamily of the Src family kinases in tyrosine phosphorylation of STIM1 was defined. Interestingly, the maximal tyrosine phosphorylation of STIM1 occurred 2.5s after activation of platelets with thapsigargin [174]. It has been shown that ERK1/2 phosphorylates STIM1 *in vitro* and *in vivo*. Mutation of the ERK1/2 sites which were identified using mass spectrometry reduced significantly calcium mobilization [175].

Both cell types of divisions, meiosis and mitosis, exhibit strongly suppressed SOCE because Ca^{2+} depletion is uncoupled from the activation of Ca^{2+} influx [176;177]. Smyth et al. identified Ser-486 and Ser-668 as mitosis-specific phosphorylation sites. Mutation of these sites significantly rescued mitotic SOCE [176]. During meiosis, interaction between STIM1-STIM1 is inhibited and Orai1 internalized into an intracellular vesicular compartment. Interestingly, both serines described in mitosis study are not involved in SOCE deactivation during meiosis. The mechanism of abrogation of STIM1-STIM1 interaction was not found and is probably independent of phosphorylation [177]. In this context we should mention the study in which ML-9 inhibitor of myosin light chain kinase (MLCK) prevented formation of STIM1 clusters and melted the thapsigargin induced puncta as well as puncta of constitutively active STIM1 (with mutation in EF-hand D76N/D78N). These effects seem to be independent of MLCK because cells with reduced levels in MLCK lacked the STIM1 puncta dissolving

[178]. PKC (Protein kinase C) was linked also to SOCE inactivation by phosphorylation of Ser-27 and Ser-30 [179].

The regulation of SOCE by STIM1

As already mentioned, CRAC channels are composed of Orai family proteins and generate I_{CRAC} when activated through STIM1. Of note, STIM1 is able to regulate various TRPC channels to form the store-operated channels (SOCs). SOCs in contrast to highly selective CRAC channels are non-selective, Ca^{2+} permeable channels. Various TRPC channels can interact with STIM1 and the STIM1-mediated regulation modulates TRPC in response as SOCs channels [180]. TRPC1 can associate with other TRPCs and thus generate SOCs with different properties. The ternary complex composed of TRPC1/STIM1/Orai1 was also described [181]. Although the STIM1 CAD/SOAR/OASF region is responsible for binding of STIM1 to both types of channels, Orai and TRPC, CAD/SOAR/OASF region is sufficient to open the Orai but the STIM1 polylysine region mediates opening of the TRPC channels [182]. The direct interaction was also found between STIM1 and the L-type voltage-gated Ca^{2+} channel CaV1.2. The region CAD/SOAR/OASF directly suppressed depolarization-induced opening of CaV1.2. STIM1 without CAD/SOAR/OASF region failed to inactivate CaV1.2 [183]. Furthermore, it has been shown that STIM1 exposed on the plasma membrane can regulate AA-regulated Ca^{2+}-selective channels [184].

STIM1-Orai1 complex in the context of plasma membrane organization

The combine data indicate that STIM1 and Orai1 form dynamic macromolecular complexes that are linked to the molecules involved in the proximal signaling (Lyn and Syk) and that even in resting state is STIM1 associated with some signaling proteins because its phosphorylation is detected in the first seconds upon stimulation with thapsigargin. The presence and function of STIM1 exposed on the plasma membrane has already been mentioned in subchapter STIM1.

The inhibition of PI3K activity reduced formation of STIM1 puncta. This effect was dependent on the presence of phosphatidylinositol 4,5-bisphosphate (PIP2) and phosphatidylinositol 3,4,5-trisphosphate (PIP3) [185]. The study made in mast cells proved that in ER-plasma membrane junctions, STIM1 binds first to PIP2 in the liquid ordered domains in the plasma membrane, followed by the redistribution of Orai1 from the liquid disordered regions of the plasma membrane to its association with STIM1 in the liquid ordered lipid domains [186]. Enzymatic activity of inositol 5-phosphatase L10-Inp54p resident in lipids ordered domains reduced PIP2 in DRM, resembling the lipid ordered regions, and blocked the STIM1-Orai1 association in RBL cell line, while 5-phosphatase S15-Inp54p resident in disordered lipids domains reduced PIP2 in these regions and enhances STIM1-Orai1 interaction.

The STIM1-Orai1 macromolecular complex was found in the immunological synapse between primary human T cells and autologous dendritic cells measured by its colocalization with CD3.

Detection of Ca^{2+} influx in living cells was found to be most prominent in the area of immunological synapse [187].

STIM1 in mast cell signaling

Both, STIM1 and Orai1, are ubiquitously expressed proteins and play a major role in Ca^{2+} entry pathway in the non-excitable cells including mast cells (Figure 4). Calcium is a second messenger that triggered many of signaling pathways therefore the tight regulation of calcium entry is of importance. The resting Ca^{2+} levels in cytosol are low (0.1 μM) but after FcεRI triggering the cytosolic concentration increases to > 1.0 μM [143].

Mice lacking STIM1 or Orai1 exhibit increased perinatal lethality and surviving mice suffered from marked growth retardation. *In vivo* studies in mice $STIM1^{+/-}$ or $Orai1^{-/-}$ indicate that passive cutaneous anaphylaxis is strongly inhibited in these mice. Mast cells derived from these knock-out mice showed defective degranulation, cytokine secretion, LTC4 production and calcium mobilization [188;189]. Some of these data were corroborated by our study on BMMCs with STIM1 reduced levels [190]. Interestingly, T cells isolated form $Orai1^{-/-}$ mice exhibit no changes in SOCE but reduced cytokines production [189]. In $STIM^{-/-}$ fetal liver mast cells the phosphorylation of FcεRI proximal molecules was unaffected, but the translocation of NF-κB and NFAT into the cell nucleus was impaired.

The cross-talk of STIM1 with cytoskeleton

Inhibitors of actin polymerization, cytochalasin D and latrunculin A, induced coalescence of STIM1 and Orai1 puncta into larger aggregates in the subplasmalemmal region of Jurkat T cells whereas I_{CRAC} and SOCE were unchanged [150]. It has been found that treatment with cytochalasin D reduced I_{CRAC} and SOCE in platelets or pancreatic acinar cells but not in RBL, smooth muscles, and corneal epithelial cells [191]. On the other hand, depolymerization of microtubules by nocodazole reduced the Ca^{2+} influx in RBL and BMMCs indicating that microtubules play a facilitive role in formation of STIM1 puncta [190;192].

In some tissues (mainly skeletal muscles or CNS) was identified the actin binding splice variant of STIM1 (90 kDa), STIM1L (115 kDa), that forms permanent clusters colocalizing with Orai1 in ER-PM junctions even in resting cells. This constitutive association of STIM1L and Orai1 enables them to activate SOCE almost immediately and generate repetitive Ca^{2+} signals within seconds. Disruption of actin fibers led to the uncoupling of STIM1L from Orai1, and SOCE was delayed [192;193].

Baba et al. were the first who drew attention to the fact that STIM1 is dynamically moved in microtubule-dependent manner but treatment of B-cells with nocodazole failed to exhibit reduced SOCE [192;194]. Indeed, in resting HEK293 cells STIM1 exactly matched the microtubules filament as was determined by confocal microscopy. In these cells SOCE was impaired after treatment with nocodazole [195]. It has been found that STIM1 interacts with protein end binding 1 (EB1) [member of microtubule plus-end tracking proteins (+TIP)] and tracks its comet-like behavior. However, depletion

of EB1 or the inhibition of microtubule dynamics by taxol had no significant influence on SOCE in HeLa cells [196] but STIM1 mRNA silencing prevented changes in microtubule dynamics in thapsigargin-activated mast cells [190]. Later it has been shown that STIM1 comprises a newly described short polypeptide motif, Ser-x-Ile-Pro which is responsible for EB1 binding [197].

AIMS

This thesis is focused on two separate but related questions. First, to understand early signaling pathways (events) induced by FcεRI aggregation and second, to comprehend the biological significance of STIM1-microtubules cross-talk in mast cells. Experimental data leading to development of improved PCR, which was used in this study, are also included. Specific aims of this thesis are:

1. **To analyze the current models of initial stages of FcεRI phosphorylation and to propose a new model, which includes current knowledge about fine topography of signaling molecules and the role of oxidized PTPs involved in the FcεRI signaling.**

2. **To contribute to elucidation of STIM1-directed microtubules reorganization in activated mast cells, with the following sub-aims.**

2.1 To produce monoclonal and polyclonal antibodies specific for STIM1.

2.2 To prepare mCherry-STIM1 construct for expression in mast cells.

2.3 To induce knock-down of STIM1 by transducing BMMCs by distinct lentivirus-based vectors comprising short hairpin RNA (shRNA) constructs.

2.4 To determine degranulation and calcium response in BMMCs with down-regulated expression of STIM1.

2.5 To determine relationship between formation of microtubules protrusions and mast cells degranulation.

2.6 To reconstitute the microtubule formation and Ca^{2+} mobilization by nucleofection of hSTIM1 into BMMCs with STIM1 knock-down.

2.7 To determine degranulation in cells pretreated with a microtubule depolymerization agent nocodazole.

3. **To develop new PCR master mixes for amplification of templates which are difficult to amplify.**

METHODS

To fulfil the particular aims of this work, the following biochemical, immunochemical and molecular biology methods were used. All these methods are described in detail in the corresponding papers/manuscript in the Results section with exception of FRET assay and detection of mast cell spreading, which are described here.

BMMCs isolation and cultivation

Bone marrow cells were isolated form femurs and tibias of 6-8 weeks old mice. The cells were then kept in suspension culture for 4-8 weeks in complete medium IMDM supplemented with 15% fetal calf serum in the presence of IL-3 (20 or 36 ng/ml) and SCF (36 or 40 ng/ml).

Degranulation assay – detection of β-glucuronidase activity

BMMCs (6×10^6/ml) were sensitized with anti-2,4-dinitrophenyl (DNP) IgE (1 μg/ml) at 37°C in culture medium supplemented with 10% FCS, but devoid of SCF and IL-3. After 4 hours, the cells were washed in buffered saline solution (BSS), supplemented with 0.1% BSA (bovine serum albumin), and challenged with various concentrations of antigen (DNP-albumin; 30–40mol of DNP per mole of albumin) or thapsigargin. 20 μl aliquots of the supernatant were mixed with 50 μl of 40 μM 4-methylumbelliferyl β-D-glucuronide as a substrate. After 1h incubation at 37°C, the reaction was terminated by addition of 200 μl cold glycine buffer (pH 10), and amount of fluorescent product was assessed by reading the plate with Infinite 200M instrument at excitation and emission wavelength 355 nm and 460 nm, respectively. Effect of nocodazole on degranulation was tested in BMMCs exposed to nocodazole (10 mM) for 30 min and then exposed to thapsigargin (2 μM) or BSS-BSA alone.

Flow cytometry

Flow cytometry was used for detection of surface expression of FcεRI on BMMCs. Cells were probed by incubation for 30 min at 4°C with IgE diluted in PBS followed by washing and subsequent incubation with secondary antibody conjugated to fluorescein isothiocyanate. Flow cytometry was also used for detection of calcium mobilization and FRET (see below).

Transfection of BMMCs

BMMCs are difficult to transfect, therefore nucleofection by AMAXA was used. The nucleofection was carried out *according* to the *manufacturer's instructions using specific* mouse macrophage cell line nucleofector kit and program Y-001.

Preparing of monoclonal and polyclonal antibodies

To prepare monoclonal antibodies specifc for STIM1, BALB/c mice were immunized with 29-aa oligopeptide corresponding to the C-terminal sequence of STIM1. The oligopeptide was covalently coupled to the carrier proteins, maleimide-activated keyhole limpet hemocyanin via cystein added at the N terminus of the oligopeptide. Sera from immunized mice were monitored for antibody activity by ELISA on the corresponding oligopeptide-BSA conjugate. Splenocytes were fused with mouse myeloma cells Sp2/0 and screening by ELISA was used for selection of positive clones. The detection of antibody class was done using IsoStrip Isotyping kit. Two selected hybridoma cell lines ST-01 produced specific antibodies of the IgG1 class. Ascitic fluids were produced in BALB/c mice. Polyclonal antibodies specific for STIM1 were obtained from rabbits immunized with the same oligopeptide-BSA conjugate as described above. Serum from immunized rabbits was tested by immunoblotting. To gain the required specificity, the crude serum was affinity purified on immobilized STIM1 oligopeptide.

Western blotting and protein immunodetection on nitrocellulose membrane

Whole-cell extracts were prepared by washing the cells in cold phosphate buffered saline (PBS), solubilizing them in hot sodium dodecyl sulfate (SDS)-sample buffer, and boiling for 5 min. For size fractionation 7.5% acrylamide gel was used for sodium dodecyl sulfate polyacrylamide gel electrophoresis (SDS-PAGE). After electrophoretic separation the proteins were than electrophoretically transfered onto nitrocellulose. Antibodies against STIM1 and actin (Sigma-Aldrich) were diluted 1:2000 and 1:3000, respectively. Bound primary antibodies were detected after incubation of the blots with horseradish peroxidase-conjugated secondary antibodies diluted 1:10.000.

Generation of lentiviral particles and cells transduction

To generate lentiviral particles for stable and effective BMMCs transduction, cells of the production cell line HEK-293 FT were transfected with pLKO.1 vector alone or with a set of five murine STIM1 shRNA constructs cloned into the pLKO.1 vector. Aliquots of 1.4 ml Opti-MEM medium were mixed with 21 μl ViraPower Lentiviral Packaging Mix (Invitrogen), 14 μg STIM1 shRNA constructs, and 82 μl Lipofectamine 2000. This mixture was added to semiconfluent HEK-293FT packaging cells in 150 cm^2 culture flask. After 3 days, viruses in culture supernatants were concentrated by centrifugation at 25,000 rpm (JA-25.50 rotor) for 2 h. Supernatant was discarded and viral particles were resuspended in 1 ml of culture medium. BMMCs (5×10^7/ml) were then transduced in complete medium without antibiotics and cells were incubated for 2 days. Medium was then replaced with complete medium supplemented with puromycin (5 μg/ml) and transduced cells were selected for 1 weak. The stable transductants were regularly passaged with complete medium containing puromycin (3 μg/ml).

Calcium assays

Cultivation and sensitization procedure of BMMCs before experiment was described in degranulation assay (see above). Cells were washed with BSS-BSA and resuspended in BSS-BSA supplemented with 2.5 mM probenecid and 1 μg/ml Fluo3 as a reporter; final concentration of the cells was 6×10^6/ml. After 30 min incubation at 37°C, the cells were washed and resuspended in BSS-BSA containing probenecid and cooled on ice for 10 min. The cells (5×10^5) were subsequently centrifuged, resuspended in 200 μl BSS-BSA, and preincubated for 4 min at 37°C. Cells were activated by exposure to 100 ng/ml DNP-BSA or 2 μM thapsigargin. Calcium mobilization was determined in the FL1 channel of a FACSCalibur Flow Cytometer. In the rescue experiments, enhanced yellow fluorescent protein (EYFP) alone or EYFP-STIM1 were transfected into BMMC using AMAXA (see above). Calcium responses were measured 48 hours after nucleofection. The experimental procedure was similar to that described above with some differences. Cells were loaded with the calcium reporter Fura Red (5 μg/ml), and changes in fluorescence intensity were monitored on an LSRII flow cytometer. EYFP positive cells were gated based on fluorescence in the FL1 channel. Fura Red was excited with 406- and 488-nm lasers, and data were collected separately using 675/45 BP and 675/20 BP filters, respectively.

FRET

The kinetics of the Orai1-STIM1 interactions was measured by flow cytometry based FRET in living HEK293 FT cells during activation with thapsigagin. This method described by Banning et al. [198] was modified. The standard FRET pair (enhanced cyan fluorescent protein) ECFP/EYFP under cytomegalovirus (CMV) promoter was used and EYFP fluorescence was measured after 488 nm excitation; emission was taken with a 529/24 filter by LSRII flow cytometer. To measure ECFP and FRET, cells were excited with a 405 nm laser and fluorescence was collected in the ECFP channel with a standard 450/40 filter, while the FRET-signal was measured with a 529/24 filter. Cells expressing pEYFP/ECFP and non-ligated pEYFP with pECFP were used to set the threshold for analysis of FRET. The interaction between STIM1 and Orai1 was detected in HEK293 cells coexpressing STIM1-EYFP with Orai1-ECFP in time.

Vector construction

The signal-peptide (SP) region (1–23 aa) of human STIM1 (hSTIM1) was amplified by PCR and this PCR fragment was inserted into pmCherry_N1 upstream of mCherry, using EcoRI and AgeI restriction sites that were involved in primers. The remaining part of hSTIM1 was also amplified by PCR and cloned downstream of mCherry into the BsrGI site (restriction site for BsrGI was in forward and reverse primers). The correct orientation of the remaining part of hSTIM1 after insertion into SP-mCherry was detected directly from bacterial colonies (JM109) using PCR. All constructs were sequenced to prove correct insertions.

Bacterial transformation, plasmid production

Competent *Escherichia coli* cells (JM109) were transformed by electroporation with different plasmids (pLP1, pLP2, VSVG, pLKO.1, pEYFP-hSTIM1, SP-mCherry and SP-mCherry-STIM1). A set of five shRNA STIM1 specific constructs in pLKO.1 vector was purchased as bacterial glycerol stocks. Plasmids were isolated from bacteria using commercial DNA Lego kit (Top-Bio) according to manufacturer's protocol or by separation on CsCl gradient.

PCR and DNA mobility assay

Different PCRs were performed using PCR mixes supplemented with various additives, including various concentrations of 1,2-propanediol and trehalose . DNA mobility assay was done with PCR mixes supplemented with 1,2-propanediol and 0.2 M trehalose or without these additives. Mix of DNA fragments was used to analyze the changes in mobility of DNA by fractionation on agarose gel in the presence of various additives at different temperatures.

Mast cell spreading

Eight-well multitest slides (ICN Biomedicals, OH, USA) were coated overnight at 4^{o}C with 20 μL of the solution containing 50 μg/ml fibronectin in PBS. Coated wells were washed with BSS-BSA and cells was added per well. Cells were allowed to attach for 1 h at 37^{o}C, washed and then activated with antigen, thapsigargin or with combination of both activators. After 30 min, the cells were fixed for 15 min at room temperature with 3% paraformaldehyde in PBS. For F-actin staining, cells were washed with 50 mM glycine in glutamate/EGTA buffer (137 mM K-glutamate, 2 mM $MgCl_2$, 3 mM EGTA and 20 mM NaOH-PIPES, pH 6.8) and then exposed to phalloidin conjugated with Alexa Fluor 488 diluted 1:250 in PBS supplemented with L-α-lysophosphatidylcholine (120 μg/mL). After 30 min, cells were washed, mounted with MOWIOL and examined with Olympus ScanR system. Cell area was determined and normalized to non-activated cells and the statistic was calculated from ~500 cells in each experiments.

PUBLICATIONS

List of publications

1) **Bugajev V**., Bambousková M., Dráberová L. And Dráber P.: What precedes the initial tyrosine phosphorylation of the high affinity IgE receptor in antigen-activated mast cell?. FEBS Lett. 2010 Dec 15;584(24):4949-55. $IF_{(2010)}$ = 3.601

2) Hájková Z., **Bugajev V**., Dráberová E., Vinopal S., Dráberová L., Janáček J., Dráber P. and Dráber P.: STIM1-directed reorganization of microtubules in activated mast cells. J. Immunol. 2011 Jan 15;186(2):913-23. $IF_{(2011)}$ = 5.788

3) Horáková H., Polakovičová I., Shaik G.M., Eitler J., **Bugajev** V., Dráberová L., Dráber P.: 1,2-propanediol-trehalose mixture as a potent quantitative real-time PCR enhancer. BMC Biotechnol. 2011 Apr 18;11:41. doi: 10.1186/1472-6750-11-41. $IF_{(2011)}$ = 2.349

4) Kocanda L., Matoušek P., Wagner P., Utekal P., **Bugajev V**. and Dráber P.: Real-time PCR-based genotyping from whole blood using Taq DNA polymerase and a buffer supplemented with 1,2-propanediol and trehalose. J. Immunol. Meth. (submitted)

What precedes the initial tyrosine phosphorylation of the high affinity IgE receptor in antigen-activated mast cell?

FEBS Lett. 2010 Dec 15;584(24):4949-55

FEBS Letters 584 (2010) 4949–4955

journal homepage: www.FEBSLetters.org

Review

What precedes the initial tyrosine phosphorylation of the high affinity IgE receptor in antigen-activated mast cell?

Viktor Bugajev, Monika Bambousková, Lubica Dráberová, Petr Dráber *

Laboratory of Signal Transduction, Institute of Molecular Genetics, Academy of Sciences of the Czech Republic, CZ-142 20 Prague 4, Czech Republic

ARTICLE INFO

Article history:
Received 21 July 2010
Revised 23 August 2010
Accepted 31 August 2010
Available online 7 September 2010

Edited by Israel Pecht

Keywords:
Mast cell
Immunoreceptor
Cell signaling
Protein tyrosine kinase
Protein tyrosine phosphatase
Plasma membrane

ABSTRACT

An interaction of multivalent antigen with its IgE bound to the high-affinity IgE receptor (FcεRI) on the surface of mast cells or basophils initiates a series of signaling events leading to degranulation and release of inflammatory mediators. Earlier studies showed that the first biochemically defined step in this signaling cascade is tyrosine phosphorylation of the FcεRI β subunit by Src family kinase Lyn. However, the processes affecting this step remained elusive. In this review we critically evaluate three current models (transphosphorylation, lipid raft, and our preferential protein tyrosine kinase–protein tyrosine phosphatase interplay model) substantiating three different mechanisms of FcεRI phosphorylation.

1. Introduction

Activation of mast cells and basophils through the high-affinity IgE receptor (FcεRI) leads to the release of pro-inflammatory mediators involved in inflammation and allergy disorders [1]. FcεRI, which belongs to the multichain immune recognition receptor (MIRR) family is a tetrameric complex formed by an IgE-binding α-subunit, a signal-amplifying β-subunit, and a homodimer of disulphide-linked γ-subunits. Each FcεRI β- and γ-subunit contains one immunoreceptor tyrosine-based activation motif (ITAM) which, after tyrosine phosphorylation, serves as a docking site for other signaling molecules such as Src homology 2 (SH2) domain-containing Src family kinase Lyn or Syk/Zap family kinase Syk [1]. Several models have been proposed to explain mechanistically how the FcεRI becomes phosphorylated by protein tyrosine kinase (PTK) Lyn. The models differ in their perception of the spatiotemporal relationship between Lyn kinase and FcεRI, and of the role of protein tyrosine phosphatases (PTPs) at initial tyrosine phosphorylation of the receptor.

2. Models of FcεRI phosphorylation

2.1. Transphosphorylation model

This model assumes that FcεRI in quiescent cells is non-covalently associated through its non-phosphorylated β subunit with Lyn kinase which is unable to phosphorylate its carrier receptor (Fig. 1). Aggregation of the IgE–FcεRI complexes with multivalent antigen initiates Lyn-dependent phosphorylation of the neighboring receptors within the aggregate [2]. This process is known as transphosphorylation and was suggested to play a role in the signal transduction in several other systems [3]. It is corroborated by several experimental findings. First, when biochemically crosslinked, at least 3–4% of the non-aggregated FcεRI was found to be directly associated with Lyn [4]. Second, Vonakis et al. [5] showed that Lyn binds through its unique domain to β subunit of FcεRI, irrespective of phosphorylation of the ITAM. This binding does not involve Lyn SH2 domain which interacts with phosphorylated ITAM, serving to amplify the initial activation signal. Third, transfection of Lyn unique domain into rat basophilic leukemia (RBL) cells inhibited antigen-induced phosphorylation of FcεRI β and γ subunit; this

Abbreviations: FcεRI, high-affinity IgE receptor; MIRR, multichain immune recognition receptor; ITAM, immunoreceptor tyrosine-based activation motif; SH2, Src homology 2; PTK, protein tyrosine kinase; PTP, protein tyrosine phosphatase; RBL, rat basophilic leukemia; EGFP, enhanced green fluorescent protein; DRM, detergent-resistant membrane; MBCD, methyl-β-cyclodextrin; ROS, reactive oxygen species; NADPH, nicotinamide adenine dinucleotide phosphate; BMMC, bone marrow-derived mast cell; LAT, linker of activated T cell; PLC, phospholipase; NTAL, non-T cell activation linker

* Corresponding author. Address: Laboratory of Signal Transduction, Institute of Molecular Genetics, Academy of Sciences of the Czech Republic, Vídeňská 1083, Prague 4, CZ 142 20, Czech Republic. Fax: +420 241062214.
E-mail address: draberpe@img.cas.cz (P. Dráber).

0014-5793/$36.00 © 2010 Federation of European Biochemical Societies. Published by Elsevier B.V. All rights reserved.
doi:10.1016/j.febslet.2010.08.045

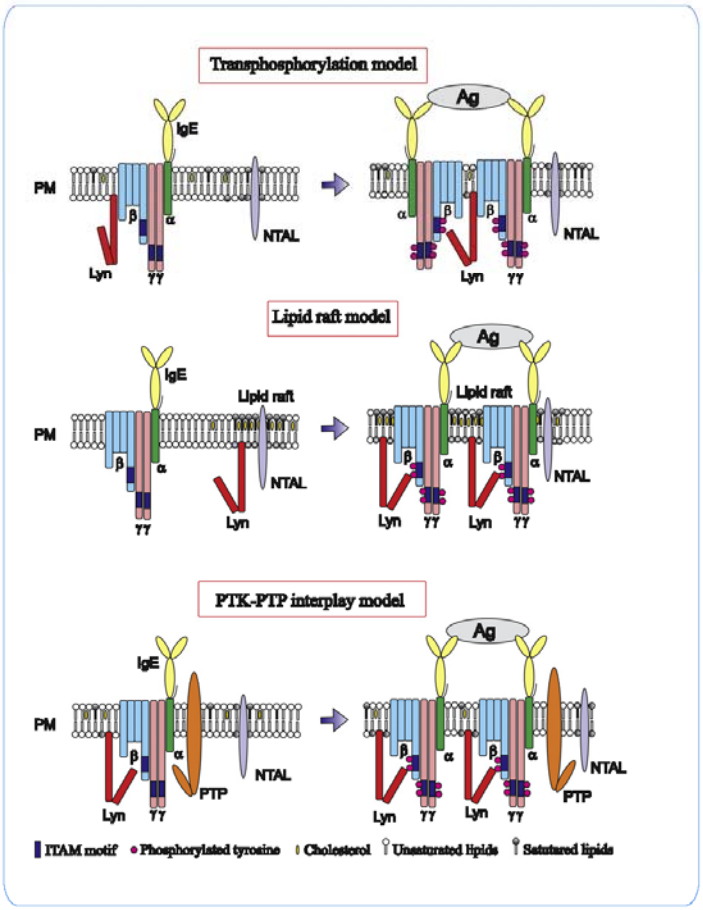

Fig. 1. Models of FcεRI phosphorylation. Transphosphorylation model presumes that active Lyn is constitutively associated with non-phosphorylated FcεRI; upon FcεRI aggregation, Lyn phosphorylates adjacent receptors in the aggregate. Lipid raft model postulates that FcεRI and Lyn are localized in different plasma membrane microdomains; after aggregation FcεRI is translocated to lipid rafts where it is phosphorylated by lipid raft-associated Lyn kinase. PTK–PTP interplay model assumes that PTPs set the threshold of FcεRI tyrosine phosphorylation; after FcεRI triggering there is a shift in the PTK–PTP steady state in favor of PTKs.

suggests a competition for FcεRI as a substrate between endogenous Lyn and the transfected Lyn unique domain [6]. Fourth, studies with Chinese hamster ovary fibroblasts expressing FcεRI and various amounts of Lyn showed a direct correlation between amount of Lyn and tyrosine phosphorylation of the FcεRI. Detailed mathematic analysis demonstrated that one Lyn molecule is capable of phosphorylating numerous adjacent FcεRIs [7]. Fifth, Lyn was found to colocalize with FcεRI as detected by transmission electron microscopy on plasma membrane sheets isolated from RBL cells. In non-stimulated cells about 25% of randomly dispersed FcεRI was associated with one or a few Lyn molecules [8]. Sixth, Lyn kinase in quiescent mast cells is enzymatically active and its activity is not further enhanced after FcεRI triggering [9]. A mutation of the C terminal tyrosine, responsible for inhibition of Lyn kinase activity, led to a weak constitutive tyrosine phosphorylation of several substrates including β and γ subunits of FcεRI and Syk kinase in non-stimulated cells [9]. Seventh, aggregation of FcεRI with trivalent ligands bound in defined distance to a symmetric DNA scaffold, resulted in phosphorylation of the FcεRI β and γ subunits depending on the length of DNA spacer; more potent trivalent ligands were those with shorter spacer [10]. Similarly, it has been suggested that dominant factor affecting signaling capacity of various anti-FcεRI monoclonal antibodies is the orientational element [11]. Eight, simultaneous observation of FcεRI marked with various quantum dot-labeled IgE revealed that aggregates of at least three crosslinked FcεRI remained mobile, showed prolonged diffusion and exhibited phosphorylation of the FcεRI β subunit and β-glucuronidase release [12]. Finally, fluorescence correlation spectroscopy of Lyn-enhanced green fluorescent protein (EGFP) and fluorescently labeled IgE bound to FcεRI confirmed that a small fraction of FcεRI in non-activated cells colocalized with Lyn [13]. Taken together, the results from the studies applying different methods provide a strong support for the hypothesis that a fraction of Lyn binds to unphosphorylated FcεRI, and strengthen the notion that transphosphorylation could be the first step in FcεRI signaling. However, some data are in conflict with this hypothesis. For exam-

ple, aggregated FcεRI becomes tyrosine phosphorylated even in the absence of β subunit [14]. Furthermore, chimeric receptors containing only the γ cytoplasmic tail become tyrosine phosphorylated upon their aggregation [15]. Alternative models had been therefore proposed.

2.2. Lipid raft model

Lipid raft membrane microdomains were conceived as a mechanism for intracellular trafficking of lipids and lipid-anchored proteins. The model assumes that biological membranes possess microdomains having a lipidic structure with properties of lipid order phase. These domains are rich in cholesterol and sphingomyelin, and possess a limited set of proteins, including those anchored to the membrane via glycolipids (e.g. glycophosphatidylinositol) or acyl groups (e.g. palmitoyl or myristoyl), and also some acylated proteins with transmembrane domain. They are surrounded by membranes with lipid structure resembling lipid disorder phase possessing phosphatidylinositols and a majority of the transmembrane proteins [16]. Cholesterol plays a crucial role in the formation of lipid rafts, and cholesterol-depletion experiments have been used in lipid raft function studies. Membrane domains with properties of lipid rafts are often isolated as membranes resistant to solubilization with non-ionic detergents, such as Triton X-100 at low temperature. Thus, the lipid raft hypothesis is in part based on studies presuming that detergent-resistant membranes (DRMs) correspond to lipid rafts, an assumption which is probably incorrect [16]. On the other hand, the lipid raft model is supported by experiments showing that aggregation of FcεRI and some other membrane proteins leads to a decreased detergent solubility as can be documented by density gradient ultracentrifugation. From the FcεRI perspective, lipid raft model postulates that in quiescent cells FcεRI is physically separated from active Lyn residing in lipid raft domains [17]. After aggregation, FcεRI is translocated into these domains and is phosphorylated there by Lyn (Fig. 1). Decreased detergent solubility was observed not just in extensively aggregated FcεRI, but even upon FcεRI dimerization, although the activation was delayed and more sustained [18]. Furthermore, it has been shown that cholesterol depletion with methyl-β-cyclodextrin (MBCD) reduced phosphorylation of the FcεRI subunits as well as other proteins. The tyrosine phosphorylation of FcεRI was rescued when cholesterol was added [19]. These data were taken as evidence that FcεRI cannot be phosphorylated in the cells in which lipid rafts are destroyed. Removal of cholesterol with MBCD, however, led to a decreased expression of FcεRI and had some other effects on mast cell physiology [20]; therefore, these experiments cannot simply be interpreted as supporting the role of lipid rafts in FcεRI signaling.

Recent studies based on advanced microscopy methods revealed that membrane domains in quiescent cells are highly dynamic and small in size (less than 10 nm). They can transiently coalesce after ligand-induced aggregation of membrane proteins and form larger domains [21]. In antigen-stimulated mast cells, transient increase of FcεRI in specialized cholesterol-rich domains, peaking at 5 min after receptor aggregation has been described [22]. However, it remains to be determined whether these changes reflect either an association of FcεRI with cholesterol-enriched lipid rafts possessing sequestered Lyn, or rather changes leading to removal of aggregated FcεRI. In fact, experiments with N-palmitoylation-site deficient Lyn show that anchor of the Lyn to the plasma membrane but not to DRMs is important for proper tyrosine phosphorylation of the FcεRI [23]. Furthermore, Lyn-EGFP mobility within the plasma membrane decreased upon FcεRI triggering, and association of the kinase with FcεRI was increased. However, no change in association of aggregated FcεRI with EGFP anchored to the plasma membrane through Lyn acylation site was observed [13]. Thus, lipid raft localization of Lyn is not sufficient for its interaction with aggregated FcεRI.

2.3. PTK–PTP interplay model

The key player in the transphosphorylation and lipid raft models in antigen-activated mast cells is the PTK Lyn utilizing FcεRI ITAM as a substrate. However, the extent of phosphorylation of the immunoreceptors and other substrates depends not only on enzymatic activity of the PTKs, but, at least partly, also on the activity of PTPs. As an attempt to explain some conflicting experimental data which were inconsistent with lipid raft model, the PTK–PTP interplay model was coined (Fig. 1). Initially, the model was elaborated in studies of immunoreceptor signaling in B cells. Reth and co-workers [24] showed that the B cell receptor, belonging to the MIRR family, forms a complex with PTKs and PTPs; this complex is indispensable for reactive oxygen species (ROS)-induced phosphorylation. Also, ROS encompassing superoxide or hydrogen peroxide are known inhibitors of PTPs and are capable of initiating early FcεRI-induced signaling events in mast cells. Despite a growing list of confirmed PTPs present in mast cells, their contribution to cell signaling regulation is still poorly understood [25,26]. One possible way of regulation of the PTP activity is reversible oxidation of Cys residue in a conserved signature motif (I/

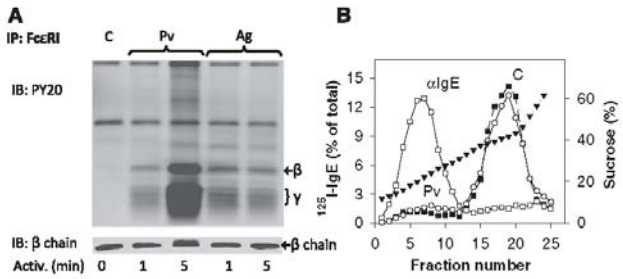

Fig. 2. Phosphorylation of FcεRI does not require its translocation into lipid rafts. (A) IgE-senzitized BMMCs were non-activated (C, 0 min) or activated for 1 or 5 min with pervanadate (Pv) or antigen (Ag). The cells were solubilized and the FcεRI complexes were immunoprecipitated (IP) and analyzed by immunoblotting (IB) with antibodies specific for phosphotyrosine (PY20) or FcεRI β chain (loading control). Positions of FcεRI β and γ chains are indicated. (B) Density gradient fractionation of cell lysates. The cells were sensitized with ^{125}I-IgE and then left non-activated (C; filled squares) or activated with pervanadate (Pv; open circles) or anti-IgE (αIgE; open squares). After 5 min the cells were solubilized and fractionated by sucrose density gradient ultracentrifugation. Radioactivity in individual fractions was determined and expressed as percentage of the total radioactivity recovered. Percentage of sucrose in individual fractions is also shown (filled triangles). Methodological details can be found elsewhere [32].

V)HCxxGxxR(S/T) in the catalytic domain. The proximity of Arg in the signature motif makes it possible for an invariant Cys to form a thiolate anion at physiological pH (p*Ka* <6.0) that can act in nucleophilic attack on the phosphate group. However, the same Cys residue can be oxidized by ROS to catalytically inactive Cys-sulphenic acid, a mechanism that is fully reversible by action of glutathione or other thiols [27]. ROS are produced under physiological conditions by the activity of specialized enzymes such as nicotinamide adenine dinucleotide phosphate (NADPH)-oxidase [28,29]. Strong oxidants like pervanadate (a mixture of vanadate and H_2O_2) irreversibly inactivate PTPs by the formation of Cys-sulphonic acid residues [30]. Exposure of mast cells to pervanadate leads to activation events which resemble those induced by physiological activators [31,32].

The PTK–PTP interplay model is supported by several lines of evidence. First, exposure of RBL or bone marrow-derived mast cells (BMMCs) to pervanadate or H_2O_2 induced robust tyrosine phosphorylation of the FcεRI subunits in the absence of receptor migration into DRMs, as determined by solubilization of the cells in Triton X-100 followed by sucrose density gradient ultracentrifugation. This was in sharp contrast to antigen- or anti-IgE antibody-induced activation which led to the movement of FcεRI into DRMs (Fig. 2). Such data indicate that association of FcεRI with DRMs is not required for receptor phosphorylation. Second, electron microscopy studies on isolated plasma membrane sheets showed that FcεRI in pervanadate-activated cells was distributed in the same way as the receptor in non-activated cells. Thus, enhanced receptor clustering is not required for tyrosine phosphorylation

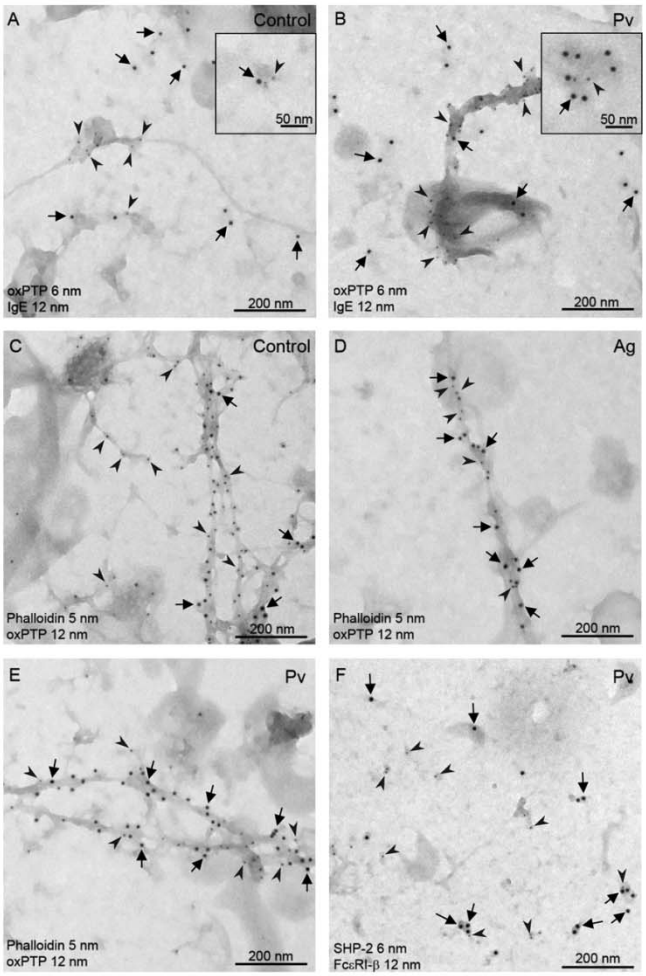

Fig. 3. Membrane topography of phosphatases, actin and FcεRI. Plasma membrane sheets were prepared from non-activated (Control; A and C), pervanadate-activated (Pv; B, E, and F) or antigen-activated (Ag; D) BMMCs and after two-step labeling procedure were analyzed by electron microscopy. FcεRI was labeled extracellularly using IgE (12 nm gold; A and B) or from cytoplasmic side using anti-FcεRI β chain (12 nm gold; F). Oxidized phosphatases were labeled with oxPTP monoclonal antibody marked with 6 nm (A and B) or 12 nm gold particles (C–E). F-Actin or SHP-2 were labeled with phalloidin (5 nm gold; C–E) or anti-SHP-2 antibody (6 nm gold; F), respectively. Gold particles of 5–6 nm are indicated by arrowheads and those of 12 nm by arrows. Inlets in A and B show higher magnification. Experimental procedure details have been described [32].

of FcεRI [32]. Third, using a monoclonal antibody (oxPTP) recognizing oxidized Cys residue in catalytic domain of PTPs, enzymatically inactive PTPs were detectable in a time- and dose-dependent manner in cells activated with pervanadate, H_2O_2 or antigen [32]. Fourth, most of PTK substrates are not phosphorylated if pervanadate is added to cell lysates instead of intact cells [24]. Similarly, lysates prepared from non-activated mast cells and treated with H_2O_2 or pervanadate exhibited a lower amount of oxidized PTPs than lysates prepared from cells activated with H_2O_2 or pervanadate before lysis [32]. These data suggest that solubilization of the cells with detergents destroys preformed signaling assemblies containing PTKs, PTPs, and their substrates. Fifth, pretreatment of activated cells with saponine, leading to cell permeabilization and release of the majority of free cytoplasmic components, resulted in association of the majority of oxidized PTPs with cellular ghosts [32]. This indicates that oxidized PTPs are not freely moving in cytosol, but rather form large complexes. In fact, FcεRI on plasma membrane sheets isolated from non-activated (Fig. 3A) or activated (Fig. 3B) cells occasionally colocalizes with oxidized PTPs. Interestingly, fraction of oxidized PTPs was associated with membrane-bound actin cytoskeleton, especially after activation (Fig. 3C–E). Finally, activation of the cells with antigen leads to decreased enzymatic activity of HePTP (PTPN7) and some other PTPs, and exposure of the cells to H_2O_2 leads to a substantial decrease in overall phosphatase activity [32].

An important task is the identification of PTPs directly involved in regulating the tyrosine phosphorylation of the receptor. Using a modified immunoprecipitation procedure with oxPTP antibody, followed by mass spectrometry analysis of the immunoprecipitated proteins, we found that several PTPs are oxidized in activated

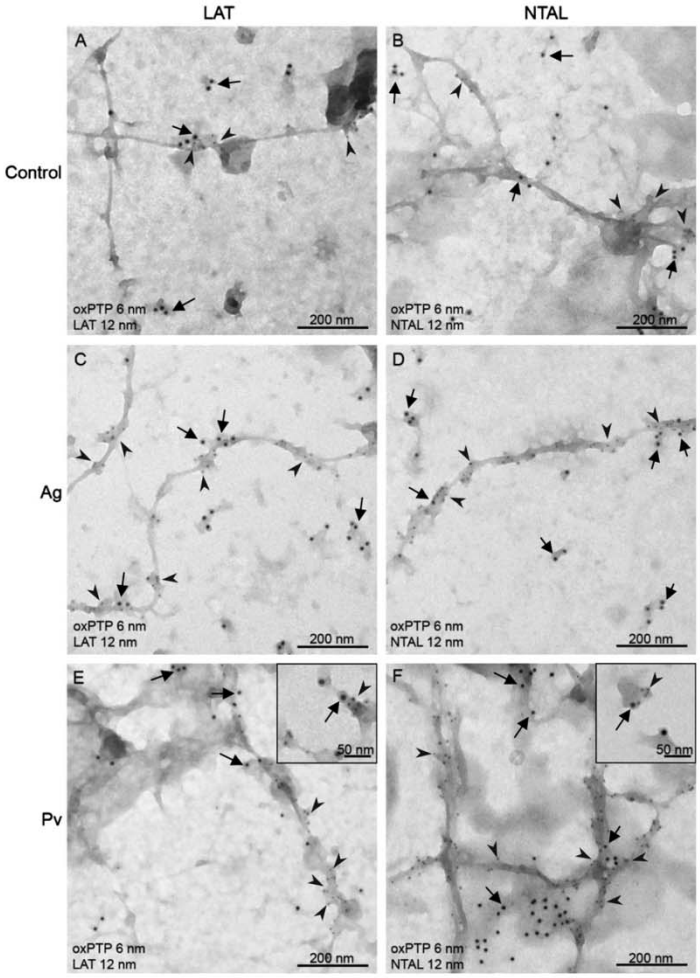

Fig. 4. Topography of oxidized phosphatases and transmembrane adaptor proteins. Plasma membrane sheets were prepared from non-activated (Control; A and B), antigen-activated (Ag; C and D) and pervanadate-activated (Pv; E and F) BMMCs and labeled for oxidized PTPs with 6 nm gold (A–F) or for LAT (A, C, and E) or NTAL (B, D, and F) with 12 nm gold. Gold particles of 6 or 12 nm in size are indicated with arrowheads or arrows, respectively. Inlets in E and F show higher magnification. Experimental procedure details have been described [32,38].

mast cells; they include SHP-1 (PTPN6), SHP-2 (PTPN11), PTP-MEG2 (PTPN9) and HePTP. However, we failed to co-immunoprecipitate the PTPs with FcεRI and we found no binding motifs in FcεRI β and γ subunits for the phosphatases, except for the phosphotyrosine motifs. Interestingly, it has been found that SHP-2 occasionally colocalizes with FcεRI (Fig. 3F), and that FcεRI is pre-associated in non-activated cells with SHP-1 [33]; these phosphatases exhibited enhanced enzymatic activity after FcεRI triggering [32]. The finding that a fraction of these phosphatases was reversibly oxidized in their active sites [32], suggests that there are spatiotemporal differences in enzymatic activity of the phosphatases. It is possible that the enzyme molecules in the vicinity of the receptor in submembraneous region have different enzymatic activity immediately after receptor triggering than the rest of molecules in the cell. Another PTP, the HePTP, also oxidized in activated mast cells, exhibited a decreased enzymatic activity after FcεRI triggering, and could thus contribute to an enhanced phosphorylation in activated cells.

How could the PTPs become inactivated under physiological conditions? Production of ROS either intracellularly [28] or by adjacent macrophages [34] influences mast cell activation. It has been shown that ROS produced by NADPH oxidase is crucial for phosphorylation of many substrates [linker of activated T cells (LAT), phospholipase (PLC)γ1 and (PLC)γ2], but NADPH oxidase alone is dependent on the activity of Src family kinases and PI3-kinase [28]. In one recent study, however, abrogation of FcεRI-dependent ROS production had no effect on degranulation or cytokine production [29]; this would suggest that antigen-induced conformational changes in FcεRI and resulting impaired access of PTPs to their substrates could be more important for enhanced FcεRI β and γ subunits phosphorylation than inhibition of enzymatic activity of the PTPs by ROS. Conformational changes in activated MIRRs have already been described [35,36]. It is possible that a similar change could lead to a shift in PTK–PTP steady state phosphorylation level of FcεRI after mast cells triggering. The combined data suggests, that non-activated mast cells possess preformed signaling assemblies containing immunoreceptors, and PTKs and PTPs which are in steady state. The binding of a multivalent antigen could cause a change in conformation of FcεRI which would be followed by a change in the steady state in favor of PTKs.

3. Topography of signaling molecules

Electron microscopy studies showed that most of the plasma membrane-bound molecules are associated with osmiophilic regions of the membrane [37]. Interestingly, molecules which were expected to be localized in lipid rafts, such as non-T cell activation linker (NTAL) and LAT, were localized individually or in small clusters and were not intermixed [38]. This suggests that lipid rafts, if they exist, are smaller than previously thought, and could be restricted to individual proteins or their clusters and surrounding lipids. Small size of signaling domains was documented in studies in which FcεRI dimers were capable of initiating signaling cascades without any dramatic changes in their redistribution in the plasma membrane [12,18]. Signalosomes of dimerized FcεRI persisted at the membrane longer than large aggregates formed by binding of multivalent antigen to IgE–FcεRI complexes. Thus, formation of large FcεRI aggregates is important for more potent removal of the membrane signalosomes at later stages of signaling.

Interesting data were obtained in studies analyzing the topography of membrane-bound PTPs. Antibody specific for oxidized phosphatases reacted mostly with cytoskeleton-like structures in non-activated mast cells [32]. Enhanced association of oxidized phosphatases with these structures was observed in cells activated by antigen and especially by pervanadate. The same structures were labeled with phalloidin (Fig. 3C–E), indicating that oxidized phosphatases are preferentially associated with actin cytoskeleton. These data suggest that actin cytoskeleton is involved in early signaling events by regulating the topography of phosphatases. Alternatively, actin could play a role in sequestering and/or scavenging irreversibly oxidized PTPs. In this connection it should be mentioned that actin probably plays a role in sequestering Lyn kinase to the periphery of large FcεRI aggregates which are consequently internalized [8].

Further studies showed that PTPs could also play a role in activation-induced tyrosine phosphorylation of the transmembrane adaptor protein NTAL and LAT, which in phosphorylated state serve as docking sites for molecules involved in FcεRI signaling [1]. Although both LAT and NTAL are detergent-resistant proteins, they exhibited enhanced colocalization with oxidized PTPs after FcεRI triggering and even more so after treatment with pervanadate (Fig. 4). Nevertheless, oxidized phosphatases have not been found in DRMs [32]. Similarly, Syk was detected in FcεRI clusters on plasma membrane sheets isolated from activated mast cells [8], in spite of the fact that only FcεRI, was associated with DRMs [39]. Moreover, experiments with disaggregated FcεRI clusters showed that the rate of their dephosphorylation was the same as that of other proteins [39]. These data indicate that proteins in DRMs are not protected from phosphatase activity and that even typical DRM proteins could be phosphorylated as proposed by the PTK–PTP interplay model.

4. Conclusions

We evaluated three models which have been proposed to explain the molecular mechanism whereby aggregation of the FcεRI initiates the first biochemically defined step in the antigen-mediated signaling in mast cells – tyrosine phosphorylation of the FcεRI β subunit by Lyn kinase. Although the transphosphorylation and lipid raft models are supported by numerous studies that are not limited to immunoreceptor signaling, they do not satisfactorily explain all activation events, such as tyrosine phosphorylation by ROS. This necessitated the introduction of PTK–PTP interplay model based on an assumption that PTKs and PTPs are in steady state in quiescent cells and activation disturbs this steady state in favor of kinases. Considering the fact that the turnover rate of active PTPs is 100- to 1000-times higher than that of PTKs [40], one can hypothesize that the PTK–PTP steady state in quiescent cell is set to override PTK, a process that could serve as a threshold of FcεRI signaling. Local ROS production or conformational changes of FcεRI leading to inactivation of the enzymatic activity of PTPs or their inaccessibility to the substrate could precede tyrosine phosphorylation of the FcεRI.

New approaches and methods are required to understand in detail the initiation of FcεRI phosphorylation and spatiotemporal coordination of the FcεRI signalosome formation. Better understanding of these events is expected from the introduction of new real-time methodologies with nanoscale resolution. Promising are approaches analyzing immunoreceptor signaling in cell-free systems with defined composition of lipid bilayers and properly accommodated signaling molecules. Genetic approaches will no doubt play a major role in deciphering signaling events in a complex cellular environment. Detailed analysis of properties of cells with knock-out of selected genes and restored with various mutant forms of the gene (knock-in approach) could still lead to the discovery of new players involved in initial stages of FcεRI signaling. These, in turn, could become targets for new drugs, and thus contribute to new rational approaches to therapy of mast cell mediated diseases.

Acknowledgements

This work was supported by Project 1M6837805001 (Center of Molecular and Cellular Immunology), LC-545, and a stipend to M.B. from Ministry of Education, Youth and Sports of the Czech Republic, Grants 204/05/H023, 301/09/1826 and P302/10/1759 from the Grant Agency of the Czech Republic, and Institutional project AVOZ50520514. M. B. was also supported by a specific Research Project No. 33779266 from Charles University, Prague.

References

[1] Kraft, S. and Kinet, J.P. (2007) New developments in FcεRI regulation, function and inhibition. Nat. Rev. Immunol. 7, 365–378.
[2] Pribluda, V.S., Pribluda, C. and Metzger, H. (1994) Transphosphorylation as the mechanism by which the high-affinity receptor for IgE is phosphorylated upon aggregation. Proc. Natl. Acad. Sci. USA 91, 11246–11250.
[3] Tamir, I. and Cambier, J.C. (1998) Antigen receptor signaling: integration of protein tyrosine kinase functions. Oncogene 17, 1353–1364.
[4] Yamashita, T., Mao, S. Y. and Metzger, H. (1994) Aggregation of the high affinity IgE receptor and enhanced activity of $p53/p56^{lyn}$ protein-tyrosine kinase. Proc. Natl. Acad. Sci. USA 91, 11251–11255.
[5] Vonakis, B.M., Chen, H., Haleem-Smith, H. and Metzger, H. (1997) The unique domain as the site on lyn kinase for its constitutive association with the high affinity receptor for IgE. J. Biol. Chem. 272, 24072–24080.
[6] Vonakis, B.M., Gibbons Jr., S.P., Rotté, M.J., Brothers, E.A., Kim, S.C., Chichester, K. and MacDonald, S.M. (2005) Regulation of rat basophilic leukemia-2H3 mast cell secretion by a constitutive Lyn kinase interaction with the high affinity IgE receptor (FcεRI). J. Immunol. 175, 4543–4554.
[7] Wofsy, C., Vonakis, B.M., Metzger, H. and Goldstein, B. (1999) One lyn molecule is sufficient to initiate phosphorylation of aggregated high-affinity IgE receptors. Proc. Natl. Acad. Sci. USA 96, 8615–8620.
[8] Wilson, B.S., Pfeiffer, J.R. and Oliver, J.M. (2000) Observing FcεRI signaling from the inside of the mast cell membrane. J. Cell Biol. 149, 1131–1142.
[9] Tolar, P., Dráberová, L., Tolarová, H. and Dráber, P. (2004) Positive and negative regulation of Fcε receptor I-mediated signaling events by lyn kinase C-terminal tyrosine phosphorylation. Eur. J. Immunol. 34, 1136–1145.
[10] Sil, D., Lee, J.B., Luo, D., Holowka, D. and Baird, B. (2007) Trivalent ligands with rigid DNA spacers reveal structural requirements for IgE receptor signaling in RBL mast cells. ACS Chem. Biol. 2, 674–684.
[11] Ortega, E., Schweitzer-Stenner, R. and Pecht, I. (1988) Possible orientational constraints determine secretory signals induced by aggregation of IgE receptors on mast cells. EMBO J. 7, 4101–4109.
[12] Andrews, N.L., Pfeiffer, J.R., Martinez, A.M., Haaland, D.M., Davis, R.W., Kawakami, T., Oliver, J.M., Wilson, B.S. and Lidke, D.S. (2009) Small, mobile FcεRI receptor aggregates are signaling competent. Immunity 31, 469–479.
[13] Larson, D.R., Gosse, J.A., Holowka, D.A., Baird, B.A. and Webb, W.W. (2005) Temporally resolved interactions between antigen-stimulated IgE receptors and Lyn kinase on living cells. J. Cell Biol. 171, 527–536.
[14] Lin, S., Cicala, C., Scharenberg, A.M. and Kinet, J.P. (1996) The FcεRIβ subunit functions as an amplifier of FcεRIγ-mediated cell activation signals. Cell 85, 985–995.
[15] Eiseman, E. and Bolen, J.B. (1992) Signal transduction by the cytoplasmic domains of FcεRI-γ and TCR-ζ in rat basophilic leukemia cells. J. Biol. Chem. 267, 21027–21032.
[16] Brown, D.A. (2006) Lipid rafts, detergent-resistant membranes, and raft targeting signals. Physiology 21, 430–439.
[17] Field, K.A., Holowka, D. and Baird, B. (1997) Compartmentalized activation of the high affinity immunoglobulin E receptor within membrane domains. J. Biol. Chem. 272, 4276–4280.
[18] Dráberová, L., Lebduška, P., Hálová, I., Tolar, P., Štokrová, J., Tolarová, H., Korb, J. and Dráber, P. (2004) Signaling assemblies formed in mast cells activated via Fcε receptor I dimers. Eur. J. Immunol. 34, 2209–2219.
[19] Sheets, E.D., Holowka, D. and Baird, B. (1999) Critical role for cholesterol in lyn-mediated tyrosine phosphorylation of FcεRI and their association with detergent-resistant membranes. J. Cell Biol. 145, 877–887.
[20] Surviladze, Z., Dráberová, L., Kovářová, M., Boubelík, M. and Dráber, P. (2001) Differential sensitivity to acute cholesterol lowering of activation mediated via the high-affinity IgE receptor and Thy-1 glycoprotein. Eur. J. Immunol. 31, 1–10.
[21] Kusumi, A. and Suzuki, K. (2005) Toward understanding the dynamics of membrane-raft-based molecular interactions. Biochim. Biophys. Acta 1746, 234–251.
[22] Davey, A.M., Krise, K.M., Sheets, E.D. and Heikal, A.A. (2008) Molecular perspective of antigen-mediated mast cell signaling. J. Biol. Chem. 283, 7117–7127.
[23] Kovářová, M., Tolar, P., Arudchandran, R., Dráberová, L., Rivera, J. and Dráber, P. (2001) Structure-function analysis of Lyn kinase association with lipid rafts and initiation of early signaling events after Fcε receptor I aggregation. Mol. Cell Biol. 21, 8318–8328.
[24] Wienands, J., Larbolette, O. and Reth, M. (1996) Evidence for a preformed transducer complex organized by the B cell antigen receptor. Proc. Natl. Acad. Sci. USA 93, 7865–7870.
[25] Heneberg, P. and Dráber, P. (2002) Nonreceptor protein tyrosine and lipid phosphatases in type I Fcε receptor-mediated activation of mast cells and basophils. Int. Arch. Allergy Immunol. 128, 253–263.
[26] Zhang, J., Mendoza, M., Guiraldelli, M.F., Barbic, E.A. and Siraganian, R.P. (2010) Small interfering RNA screen for phosphatases involved in IgE-mediated mast cell degranulation. J. Immunol. 184, 7178–7185.
[27] Denu, J.M. and Tanner, K.G. (1998) Specific and reversible inactivation of protein tyrosine phosphatases by hydrogen peroxide: evidence for a sulfenic acid intermediate and implications for redox regulation. Biochemistry 37, 5633–5642.
[28] Suzuki, Y., Yoshimaru, T., Matsui, T., Inoue, T., Niide, O., Nunomura, S. and Ra, C. (2003) FcεRI signaling of mast cells activates intracellular production of hydrogen peroxide: role in the regulation of calcium signals. J. Immunol. 171, 6119–6127.
[29] Swindle, E.J., Coleman, J.W., DeLeo, F.R. and Metcalfe, D.D. (2007) FcεRI- and Fcγ receptor-mediated production of reactive oxygen species by mast cells is lipoxygenase- and cyclooxygenase-dependent and NADPH oxidase-independent. J. Immunol. 179, 7059–7071.
[30] Barrett, W.C., DeGnore, J.P., König, S., Fales, H.M., Keng, Y.F., Zhang, Z.Y., Yim, M.B. and Chock, P.B. (1999) Regulation of PTP1B via glutathionylation of the active site cysteine 215. Biochemistry 38, 6699–6705.
[31] Teshima, R., Ikebuchi, H., Nakanishi, M. and Sawada, J. (1994) Stimulatory effect of pervanadate on calcium signals and histamine secretion of RBL 2H3 cells. Biochem. J. 302, 867–874.
[32] Heneberg, P., Dráberová, L., Bambousková, M., Pompach, P. and Dráber, P. (2010) Down-regulation of protein tyrosine phosphatases activates an immune receptor in the absence of its translocation into lipid rafts. J. Biol. Chem. 285, 12787–12802.
[33] Kimura, T., Zhang, J., Sagawa, K., Sakaguchi, K., Appella, E. and Siraganian, R.P. (1997) Syk-independent tyrosine phosphorylation and association of the protein tyrosine phosphatases SHP-1 and SHP-2 with the high affinity IgE receptor. J. Immunol. 159, 4426–4434.
[34] Swindle, E.J., Hunt, J.A. and Coleman, J.W. (2002) A comparison of reactive oxygen species generation by rat peritoneal macrophages and mast cells using the highly sensitive real-time chemiluminescent probe pholasin: inhibition of antigen-induced mast cell degranulation by macrophage-derived hydrogen peroxide. J. Immunol. 169, 5866–5873.
[35] Gil, D., Schamel, W.W., Montoya, M., Sánchez-Madrid, F. and Alarcón, B. (2002) Recruitment of Nck by CD3ε reveals a ligand-induced conformational change essential for T cell receptor signaling and synapse formation. Cell 109, 901–912.
[36] Tolar, P., Hanna, J., Krueger, P.D. and Pierce, S.K. (2009) The constant region of the membrane immunoglobulin mediates B cell-receptor clustering and signaling in response to membrane antigens. Immunity 30, 44–55.
[37] Lillemeier, B.F., Pfeiffer, J.R., Surviladze, Z., Wilson, B.S. and Davis, M.M. (2006) Plasma membrane-associated proteins are clustered into islands attached to the cytoskeleton. Proc. Natl. Acad. Sci. USA 103, 18992–18997.
[38] Volná, P., Lebduška, P., Dráberová, L., Šímová, S., Heneberg, P., Boubelík, M., Bugajev, V., Malissen, B., Wilson, B.S., Hořejší, V., Malissen, M. and Dráber, P. (2004) Negative regulation of mast cell signaling and function by the adaptor LAB/NTAL. J. Exp. Med. 200, 1001–1013.
[39] Peirce, M. and Metzger, H. (2000) Detergent resistant microdomains offer no refuge for proteins phosphorylated by the IgE receptor. J. Biol. Chem. 275, 34976–34982.
[40] Reth, M. (2002) Hydrogen peroxide as second messenger in lymphocyte activation. Nat. Immunol. 3, 1129–1134.

STIM1-directed reorganization of microtubules in activated mast cells

J. Immunol. 2011 Jan 15;186(2):913-23

The Journal of Immunology

STIM1-Directed Reorganization of Microtubules in Activated Mast Cells

Zuzana Hájková,*[,1] Viktor Bugajev,[†,1] Eduarda Dráberová,* Stanislav Vinopal,* Lubica Dráberová,[†] Jiří Janáček,[‡] Petr Dráber,[†] and Pavel Dráber*

Activation of mast cells by aggregation of the high-affinity IgE receptors (FcεRI) initiates signaling events leading to the release of inflammatory and allergic mediators stored in cytoplasmic granules. A key role in this process play changes in concentrations of intracellular Ca^{2+} controlled by store-operated Ca^{2+} entry (SOCE). Although microtubules are also involved in the process leading to degranulation, the molecular mechanisms that control microtubule rearrangement during activation are largely unknown. In this study, we report that activation of bone marrow-derived mast cells (BMMCs) induced by FcεRI aggregation or treatment with pervanadate or thapsigargin results in generation of protrusions containing microtubules (microtubule protrusions). Formation of these protrusions depended on the influx of extracellular Ca^{2+}. Changes in cytosolic Ca^{2+}concentration also affected microtubule plus-end dynamics detected by microtubule plus-end tracking protein EB1. Experiments with knockdown or reexpression of STIM1, the key regulator of SOCE, confirmed the important role of STIM1 in the formation of microtubule protrusions. Although STIM1 in activated cells formed puncta associated with microtubules in protrusions, relocation of STIM1 to a close proximity of cell membrane was independent of growing microtubules. In accordance with the inhibition of Ag-induced Ca^{2+} response and decreased formation of microtubule protrusions in BMMCs with reduced STIM1, the cells also exhibited impaired chemotactic response to Ag. We propose that rearrangement of microtubules in activated mast cells depends on STIM1-induced SOCE, and that Ca^{2+} plays an important role in the formation of microtubule protrusions in BMMCs. *The Journal of Immunology*, 2011, 186: 913–923.

Mast cells play a pivotal role in innate immunity, allergy, and inflammation; they express plasma membrane-associated FcεRIs, the aggregation of which by multivalent Ag–IgE complexes triggers mast cell activation resulting in the degranulation and release of inflammatory mediators such as histamine, proteases, lipid mediators, and cytokines. The first defined step in FcεRI signaling is tyrosine phosphorylation of the FcεRI β and γ subunits by Src family kinase Lyn. This step is followed by enhanced activity of Syk kinase and phosphorylation of transmembrane adaptor linker for activation of T cells. Phosphorylated linker for activation of T cells is an anchor site for phospholipase Cγ. After membrane anchoring and activation, phospholipase Cγ produces inositol 1,4,5,-triphosphate that binds to its receptors in the endoplasmic reticulum (ER). This results in Ca^{2+} efflux from the ER (1). Subsequently, depletion of Ca^{2+} from ER lumen induces Ca^{2+} influx across the plasma membrane through store-operated Ca^{2+} channels (SOCs). The influx leads to enhancement of free cytoplasmic Ca^{2+} concentration, a step that is substantial in further signaling events. The store-operated Ca^{2+} entry (SOCE) is also important for the replenishment of intracellular stores by means of sarcoendoplasmatic reticulum Ca^{2+}-ATPase (SERCA) pumps located in the ER membrane (2, 3).

The stromal interacting molecule 1 (STIM1) is a pivotal component of the SOCE pathway (4, 5). It represents the Ca^{2+} sensor responsible for communicating the depleted state of intracellular Ca^{2+} compartments to SOCs. In quiescent cells with ER filled with Ca^{2+}, STIM1 is distributed homogenously throughout the ER (6), but relocates upon release of Ca^{2+} from ER stores to distinct puncta on the ER in close proximity to the plasma membrane (5). Aggregated STIM1 activates members of the Orai family of SOCs, resulting in the opening of the plasma membrane Ca^{2+} channels and Ca^{2+} influx into the cell (7); in this way STIM1 serves as a major regulator of SOCE.

STIM1 is a microtubule-tracking protein (8, 9) and interacts with the end-binding protein 1 (EB1) that associates with the tips of growing microtubules (10, 11). Although microtubules are necessary for positioning of membrane-enclosed organelles in-

*Department of Biology of Cytoskeleton, Institute of Molecular Genetics, Academy of Sciences of the Czech Republic, 142 20 Prague, Czech Republic; †Department of Signal Transduction, Institute of Molecular Genetics, Academy of Sciences of the Czech Republic, 142 20 Prague, Czech Republic; and ‡Department of Biomathematics, Institute of Physiology, Academy of Sciences of the Czech Republic, 142 20 Prague, Czech Republic

[1]Z.H. and V.B. contributed equally to this work

Received for publication June 25, 2010. Accepted for publication November 13, 2010.

This work was supported in part by Grants 204/09/H084, 204/09/1777, 301/09/1826, and P302/10/1759 from the Grant Agency of the Czech Republic, Grants LC545, LC06063, and 1M6837805001 from the Ministry of Education, Youth and Sports of the Czech Republic, Grants KAN200520701 and M200520901 from the Grant Agency of the Czech Academy of Sciences, Grant 11109 from the Grant Agency of Charles University, and by the Institutional Research Supports (AVOZ 50520514 and 50110509). S.V. was supported in part by the Department of Cell Biology, Faculty of Science, Charles University, Prague, Czech Republic.

Address correspondence and reprint requests to Dr. Pavel Dráber or Dr. Petr Dráber, Department of Biology of Cytoskeleton, Institute of Molecular Genetics, AS CR v.v.i., Vídeňská 1083, 142 20 Prague, Czech Republic (Pavel Dráber), or Department of Signal Transduction, Institute of Molecular Genetics, AS CR v.v.i., Vídeňská 1083, 142 20 Prague, Czech Republic (Petr Dráber). E-mail addresses: paveldra@img.cas.cz (Pavel Dráber) and draberpe@img.cas.cz (Petr Dráber)

The online version of this article contains supplemental material.

Abbreviations used in this article: BMMC, bone marrow-derived mast cell; BMMCL, BMMC line; BSS, buffered saline solution; $[Ca^{2+}]_i$, concentration of free intracellular calcium; EB1, end-binding protein 1; ER, endoplasmic reticulum; KD, knockdown; SCF, stem cell factor; SERCA, sarcoendoplasmatic reticulum Ca^{2+}-ATPase; shRNA, short hairpin RNA; SOC, store-operated Ca^{2+} channels; SOCE, store-operated Ca^{2+} entry; STIM1, stromal interacting molecule 1; Tg, thapsigargin; TIRF, total internal reflection fluorescence; TIRFM, total internal reflection fluorescence microscopy; YFP, yellow fluorescent protein.

www.jimmunol.org/cgi/doi/10.4049/jimmunol.1002074

cluding ER (12), the role of microtubules in regulating SOCE is not fully understood. Whereas inhibition of microtubule dynamics by taxol, a microtubule stabilizer, or by knockdown (KD) of EB1 had no significant effect on SOCE (11), Ca^{2+} influx in different cell types was inhibited by microtubule depolymerizing drug nocodazole (13, 14). It has been suggested that microtubules play a facilitative role in SOCE signaling pathway by optimizing the localization of STIM1 (15).

Microtubules are involved in mast cell degranulation, because the movement of secretory granules depends on intact microtubules (16, 17). This finding is supported by demonstrations that agents inhibiting tubulin polymerization also suppress degranulation (18–20). Importantly, FcεRI aggregation triggers reorganization of microtubules and their concentration in cell periphery (17, 21). It has also been reported that translocation of granules along microtubules to plasma membranes occurred independently of Ca^{2+}, whereas the release of mediators and granule-plasma membrane fusion were dependent on Ca^{2+} (17). Although these data confirm that a microtubule network is required for mast cell degranulation, our understanding of the mechanisms responsible for microtubule formation in bone marrow-derived mast cells (BMMCs) during activation events is still limited.

In this study, we investigated the interplay between Ca^{2+} signaling and changes in microtubule distribution in the course of BMMC activation. Our results indicate that microtubules in activated cells are in protrusions that depend on STIM1 activity and Ca^{2+} influx. Whereas microtubules are not necessary for the relocation of STIM1 to puncta in close proximity to the plasma membrane in activated cells, changes in the concentration of cytoplasmic Ca^{2} affect microtubule plus-end dynamics and result in dramatic modifications in cell physiology documented by chemotactic response. The results support the concept of a tight crosstalk between microtubular network and Ca^{2+} signaling machinery in the course of mast cell activation.

Materials and Methods

Reagents

Fibronectin, nocodazole, thapsigargin, probenecid, DNP-albumin, and DNP-lysine were acquired from Sigma-Aldrich (St. Louis, MO). Src-family selective tyrosine kinase inhibitor PP2 and the negative control, PP3, were obtained from Calbiochem (Darmstadt, Germany). Fluo 3-AM, Fura Red-AM, 4-methylumbelliferyl β-D-glucuronide, and Lipofectamine 2000 were purchased from Invitrogen (Carlsbad, CA), and puromycin was acquired from InvivoGen (San Diego, CA). IL-3 and stem cell factor (SCF) were from PeproTech (Rocky Hill, NJ). Restriction enzymes were bought from New England Biolabs (Ipswich, MA). SuperSignal WestPico Chemiluminescent reagents were bought from Pierce (Rockford, IL).

Abs

Mouse mAb PY-20 (IgG_{2b}) labeled with HRP and anti-STIM1(GOK) mAb (IgG_{2a}) were acquired from BD Biosciences (San Jose, CA). Rabbit Ab to α-tubulin was acquired from GeneTex (Irvine, CA). Rabbit Ab to actin, mAb TUB 2.1 (IgG_1) to β-tubulin labeled with indocarbocyanate (Cy3) and mAb SPE-7 (IgE) specific for DNP were acquired from Sigma-Aldrich. Anti-mouse and anti-rabbit Abs conjugated with HRP were purchased from Promega Biotec (Madison, WI), Alexa Fluor 488-conjugated anti-rabbit IgG Ab was acquired from Invitrogen (Carlsbad, CA), and FITC-conjugated anti-mouse IgG cross-reacting with mouse IgE were acquired from Jackson ImmunoResearch Laboratories (West Grove, PA).

To prepare mouse mAb specific for STIM1, 29-aa oligopeptide DNGSIGEETDSSPGRKKFPLKIFKKPLKK corresponding to the mouse STIM1 sequence 657-685 from the C-terminal end of the molecule (22) was synthesized by Clonestar Peptide Service (Brno, Czech Republic). A cysteine had been added to the N terminus of the peptide to allow oriented covalent coupling to the carrier proteins, maleimide-activated keyhole limpet hemocyanin, or BSA (Imject Activated Immunogen Conjugation Kit, Pierce, Rockford, IL), according to the manufacturer's directions. BALB/c mice were immunized with the peptide-keyhole limpet hemocyanin conjugate, and sera were monitored for Ab activity by ELISA on peptide-BSA conjugate as described (23). Fusion of splenocytes with mouse myeloma cells Sp2/0, screening by ELISA, cloning and production of ascitic fluids in BALB/c mice have been described previously (24). The subclasses of mAbs were identified by ISO1 isotyping kit (Sigma-Aldrich). The selected hybridoma cell line ST-01 produced Ab of the IgG_1 class.

Cell cultures and transfection

Bone marrow cells were isolated from the femurs and tibias of 6–8-wk-old BALB/c mice. All mice were maintained and used in accordance with the Institute of Molecular Genetics guidelines. The cells were differentiated in suspension cultures in freshly prepared culture medium (IMDM supplemented with antibiotics [100 U/ml penicillin, 100 μg/ml streptomycin] 10% FCS, 35 μM 2-ME, IL-3 [36 ng/ml] and SCF [36 ng/ml]). Cells were grown at 37°C in 10% CO_2 in air and passaged every 2–3 d. After 6–8 wk, ~99% of cells were identified as mast cells, expressing FcεRI and c-Kit as detected by flow cytometry. BMMCs isolated from at least three mice were used for each experiment.

Mouse BMMC line (BMMCL) was by M. Hibbs (Ludwig Institute for Cancer Research, Melbourne, Australia). In this study, the cells are denoted as BMMCL and were cultured in freshly prepared culture medium (RPMI 1640 supplemented with 20 mM HEPES, pH 7.5, 100 U/ml penicillin, 100 μg/ml streptomycin, 100 μM MEM nonessential amino acids, 1 mM sodium pyruvate, 10% FCS, and 10% WEHI-3 cell supernatant as a source of IL-3). Cells were grown at 37°C in 5% CO_2 in air and passaged every 2 d.

HEK 293FT packaging cells (Invitrogen) were grown at 37°C in 5% CO_2 in DMEM supplemented with 10% FCS and antibiotics. The cells used for lentivirus production were at passage 4–15.

BMMCL cells were transfected with DNA constructs by nucleofection using Mouse Macrophage Kit and program Y-001 on Amaxa Nucleofector II (Lonza Cologne AG, Cologne, Germany) according to the manufacturer's instructions. After nucleofection, cells were transferred into culture media supplemented with IL-3 and cultured for 24–48 h before analysis.

DNA constructs

Full-length human STIM1 cloned into pDS_XB-YFP vector (pYFP-hSTIM1) was provided by Dr. T. Meyer (5). The signal-peptide region (22), sequence 1–23 aa, of STIM1 was recloned from this vector into pmCherry_N1 from Clontech Laboratories (Mountain View, CA) upstream of mCherry, using *Eco*RI and AgeI restriction sites. The remaining part of STIM1 was recloned downstream of mCherry into the BsrGI site. The construct was verified by DNA sequencing. Expression plasmid coding mouse EB1 fused with GFP (pEB1-GFP) was obtained from Dr. Y. Mimori-Kiyosue (25). Expression plasmid coding human EB3 fused with mRFP1 (26) was obtained from Dr. A. Akhmanova (11).

Lentivirus short hairpin RNAs and virus transduction

A set of five murine STIM1 (GenBank accession number: NM_ 009287) short hairpin RNA (shRNA) constructs cloned into the pLKO.1 vector (TRCN0000175139, TRCN0000175008, TRCN0000193877, TRCN0000193400, and TRCN0000173765) were purchased from Open Biosystems (Huntsville, AL). Aliquots of 1.4 ml Opti-MEM medium (Invitrogen) were mixed with 21 μl ViraPower Lentiviral Packaging Mix (Invitrogen), 14 μg STIM1 shRNA constructs, and 82 μl Lipofectamine 2000. The mixture was incubated for 20 min at room temperature before it was added to semiconfluent HEK-293FT packaging cells in a 150-cm^2 tissue-culture flask. After 3 d, viruses in culture supernatants were concentrated by centrifugation at 25,000 rpm for 2 h using a JA-25.50 rotor (Beckman Coulter, Palo Alto, CA). The pellets were resuspended in 1 ml of culture medium and added to 29 ml of medium, supplemented with 5 μg/ml puromycin containing 5×10^5 BMMCs or BMMCL cells. Stable selection was achieved by culturing cells for 1 wk in the presence of puromycin. Cells were pooled and analyzed for STIM1 expression by immunoblotting. Cells with the highest reduction of STIM1 protein, obtained with TRCN0000175008 (KD1) and TRCN0000193400 (KD2), were selected for additional experiments. Cells transfected with empty pLKO.1 vector were used as negative controls.

Cell activation

Cells at a concentration of 6×10^6 cells/ml were sensitized for 2 h at 37°C in IL-3– and SCF-free culture medium supplemented with DNP-specific IgE mAb (SPE-7; 1 μg/ml). The cells were then washed in buffered saline solution (BSS; 20 mM HEPES, pH 7.4, 135 mM NaCl, 5 mM KCl, 1.8 mM $CaCl_2$, 5.6 mM glucose, 2 mM $MgCl_2$), supplemented with 0.1% BSA (BSS-BSA), and challenged with various concentrations of Ag (DNP-albumin; 30–40 mol of DNP per mole of albumin) or thapsigargin.

For immunofluorescence experiments, cells at a concentration of 6×10^6 cells/ml were sensitized in suspension for 1 h at 37°C with DNP-specific

IgE (1 μg/ml) and diluted to a concentration of 1.5×10^6 cells/ml. The suspension (1 ml) was then overlaid on fibronectin-coated coverslips (immersed for 1 h at 37°C in 50 μg/ml fibronectin in 50 mM $NaHCO_3$ and rinsed in PBS) placed in a 3.5-cm tissue culture dish. Cells were allowed to attach for 1 h at 37°C, washed in BSS-BSA, and challenged for 3–5 min with Ag (DNP-albumin) at a final concentration of 100 ng/ml. To determine the time course of activation, cells were challenged with Ag for 1–10 min. For dose response curve construction, the concentration of Ag ranged from 10 to 1000 ng/ml.

Alternatively, cells were activated by pervanadate or thapsigargin, in which case the sensitization step was omitted. Pervanadate solution was prepared fresh by mixing sodium orthovanadate solution with hydrogen peroxide to get a final concentration (10 mM) of both components. The pervanadate solution was incubated for 15 min at room temperature and then diluted 1:100 in BSS-BSA. Attached cells were incubated with pervanadate solution for 15 min at 37°C. Cells were also incubated for 20 min with BSS-BSA containing 2 μM thapsigargin. To determine the time course of activation, cells were activated with thapsigargin for 5–20 min. Dose response measurements were done at thapsigargin concentrations ranging from 0.01 to 2 μM. In some experiments, $[Ca^{2+}]$-free BSS was used. Trypan blue exclusion test was used to evaluate the effect of pervanadate and thapsigargin on viability of cells.

To depolymerize microtubules, cells were treated for 1 h at 37°C with 10 μM nocodazole and activated with pervanadate or thapsigargin in the presence of nocodazole. To inhibit the activity of Src family kinases, IgE-sensitized cells were pretreated for 60 min with Src family selective tyrosine kinase inhibitor PP2 at a concentration of 10 μM before incubation with DNP-albumin. Cells treated for 60 min with 10 μM PP3 were used as controls.

Flow cytometry analysis of FcεRI

To determine the surface FcεRI expression, cells (5×10^5/ml) were exposed for 30 min on ice to 1 μg/ml anti-DNP IgE followed by 30 min incubation with FITC-conjugated anti-mouse Ab (cross-reacting with mouse IgE). After incubation the cells were washed in ice-cold BSS-BSA. Mean fluorescence intensities were determined in the FL1 channel of FACSCalibur (BD Biosciences, Mountain View, CA).

Degranulation assay

The degree of degranulation was quantified as the release of β-glucuronidase from anti-DNP IgE-sensitized and DNP-albumin or thapsigargin-activated cells, using 4-methylumbelliferyl β-D-glucuronide as a substrate (27). The total content of the enzyme was evaluated in supernatants from cells lysed by 0.1% Triton X-100.

Determination of intracellular Ca^{2+} concentrations and $^{45}Ca^{2+}$ uptake

Concentrations of free intracellular calcium ($[Ca^{2+}]_i$) were determined using Fluo3 as a reporter. Cells were sensitized with anti-DNP IgE (1 μg/ml) at 37°C in culture medium supplemented with 10% FCS, but devoid of SCF and IL-3. After 4 h, the cells were washed and resuspended at a concentration of 1×10^7 cells/ml in the same medium supplemented with Fluo3 and probenecid at final concentrations of 1 μg/ml and 2.5 mM, respectively. After 30 min, the cells were washed in BSS-BSA supplemented with probenecid and put on ice for 10 min. Before measurement, the cells (5×10^5) were briefly centrifuged, resuspended in 200 μl BSS-BSA, and preincubated for 4 min at 37°C. Cells were activated by adding 100 ng/ml DNP-albumin or 2 μM thapsigargin. Calcium mobilization was determined in the FL1 channel of a FACSCalibur Flow Cytometer (BD Biosciences, San Jose, CA) using FlowJo software (Ashland, OR). In the yellow fluorescent protein (YFP)-hSTIM1 rescue experiments, calcium responses were measured 48 h after nucleofection. STIM1 KD cells nucleofected with pYFP alone (Clontech Laboratories, Mountain View, CA) were used as a mock control. The experimental procedure was similar to that described above with some differences. Cells were loaded with the calcium reporter Fura Red (5 μg/ml), and changes in fluorescence intensity were monitored on an LSRII flow cytometer (BD Biosciences). Populations of live cells were selected based on forward and side scatters. In live nucleofected cells, YFP-positive cells were gated based on fluorescence in the FL1 channel. Fura Red was excited with 406- and 488-nm lasers, and data were collected separately using 675/45 BP and 675/20 BP filters, respectively.

Uptake of extracellular calcium was determined as described previously (28). Cells were sensitized with anti-DNP IgE (1 μg/ml) and activated for various time intervals with 100 ng/ml DNP-albumin or 2 μM thapsigargin in the presence of extracellular $^{45}Ca^{2+}$ (1 mM). Cell-bound radioactivity was measured in 10 ml scintillation liquid (EcoLite; ICN Biomedicals, Costa Mesa, CA) using a QuantaSmart TM counter.

Chemotaxis assay

Chemotactic responses of BMMCs were examined using 96-well chemotaxis plates (ChemoTx system; Neuro Probe, Gaithersburg, MD) with 8-μm pore size polycarbonate filters. Chemoatractant (DNP-BSA) at concentrations of 50–250 ng/ml in RPMI 1640 supplemented with 20 mM HEPES and 1% BSA (assay buffer), or assay buffer alone was added in 305 μl to the lower wells, and IgE-sensitized BMMCs (0.15×10^6) in 60-μl assay buffer were added on top of the membrane above each well. After 8 h incubation at 37°C and 5% CO_2 in humidified air, cells on the upper membrane surface were removed with suction, and the plates with membrane frames were centrifuged ($156 \times g$, 4 min). After centrifugation, 200 μl media above the cells was removed and 100 μl of water containing 0.1% Triton X-100 and 10 μM SYTOX Green nucleic acid stain (Invitrogen) was added to the well. Fluorescence was determined at 485-nm excitation and 530-nm emission, using TECAN Infinite M200 fluorescence microplate reader (Grödig, Austria). A linear standard curve with serial dilutions of the cells (400–50,000 cells) was included in each experiment to equate fluorescence intensity with cell number. Four independent experiments were run in triplicates.

Gel electrophoresis and immunoblotting

Whole-cell extracts were prepared by washing the cells in cold PBS, solubilizing them in hot SDS-sample buffer (29), and boiling for 5 min. SDS-PAGE on 7.5% gels, electrophoretic transfer of separated proteins onto nitrocellulose, and details of the immunostaining procedure have been described elsewhere (30). Abs against STIM1 and actin were diluted 1:2000 and 1:3000, respectively. Bound primary Abs were detected after incubation of the blots with HRP-conjugated secondary Ab diluted 1:10,000. Phosphotyrosine was detected by PY-20–HRP conjugate (dilution 1:2000). HRP signal was detected with chemiluminescence reagents in accordance with the manufacturer's directions and quantified using LAS 3000 imaging system (Fujifilm, Tokyo, Japan).

Immunofluorescence microscopy

Immunofluorescence microscopy was performed on fixed cells as described previously (31). Cells attached to fibronectin-coated coverslips were rinsed with microtubule-stabilizing buffer (0.1 M MES, pH 6.9, 2 mM EGTA, 2 mM $MgCl_2$, 4% polyethylene glycol 6000), fixed for 20 min in 3% formaldehyde in microtubule-stabilizing buffer, and extracted for 4 min with 0.5% Triton X-100 in microtubule-stabilizing buffer. TUB 2.1 mAb conjugated with Cy3 and polyclonal Ab to α-tubulin were diluted 1:600 and 1:200, respectively. AlexaFluor 488-conjugated anti-rabbit Ab was diluted 1:300. The preparations were mounted in MOWIOL 4-88 (Merck, Darmstadt, Germany), supplemented with DAPI to label nuclei, and examined with an Olympus A70 Provis microscope equipped with ×60 water-immersion or ×100 oil-immersion objectives. Images were recorded with a SensiCam cooled CCD camera (PCO IMAGING, Kelheim, Germany). Conjugated secondary Ab did not give any detectable staining.

Alternatively, samples were examined with a confocal laser scanning microscope Leica TCS SP5 equipped with an ×63/1.4.N.A. oil-immersion objective. Excitation and emission wavelengths were 561 nm and 566 to 633 nm for Cy3 (diode pumped solid-state laser). Optical sections were acquired in 125-nm steps, and z-series were made from 70 sections. Deconvolution and rotation was performed using Huygens Deconvolution Software (Scientific Volume Imaging, Hilversum, The Netherlands).

To estimate the number of cells that responded to activation events by generation of microtubule protrusions, three independent immunofluorescence experiments were performed. In each experiment usually 500 cells were examined, and cells with five and more microtubule protrusions after activation were counted up. These protrusions were not discernible in nonactivated cells. Statistical comparison of data was conducted with Student *t* test.

Time-lapse imaging by total internal reflection fluorescence microscopy

Control BMMCL cells, BMMCL cells with empty pLKO.1 vector, or cells with STIM1 KD were nucleofected with pEB1-GFP. Alternatively, BMMCL cells were nucleofected with YFP-hSTIM1 or simultaneously with YFP-hSTIM1 and EB3-mRFP1. Twenty-four hours later, 100 μl of cell suspension at concentration 1.5×10^6 cells/ml was overlaid on 35-mm glass-bottom culture dishes (MatTek, Ashland, MA; Cat. No. P35G-1.5-14-C) precoated with fibronectin (see above), and cells were allowed to attach for 1 h at 37°C. Perfusion insert for the 35-mm culture dish was

inserted (Warner Instruments, Hamden, CT; model RC-37F), and cells were washed and subsequently incubated in RPMI medium for live cell imaging (RPMI 1640 without phenol red, riboflavin, folic acid, pyridoxal, $Fe[NO_3]_3$) supplemented with 20 mM HEPES. Cells were imaged on the Leica AM total internal reflection fluorescence (TIRF) MC (Leica Microsystems) at 37°C. Time-lapse sequences of EB1-GFP or YFP-hSTIM1 were acquired in TIRF mode (GFP cube, laser line 488 nm; Ex, 470/40; Em, 525/50; penetration depth, 150 nm) using HCX PL APO ×100/1.46 NA oil-immersion TIRF objective. Images were taken for 3 min at 1-s intervals with 30–40% laser power and exposure times ranging from 500–800 ms. Time-lapse sequences of EB3-mRFP1 in combination with YFP-hSTIM1 were acquired in TIRF mode (laser lines 561 nm or 488 nm, Em: 640/40 or 530/30, respectively; the same penetration depth 150 nm for both channels) using the same objective as above. Individual channels were imaged sequentially. Images were taken for 3 min at 2-s intervals with 50–80% (561 nm) or 30–40% (488 nm) laser power and exposure times ranging from 500–800 ms. Cells were scanned before, during, and after thapsigargin or nocodazole addition to final concentrations of 2 μM and 10 μM, respectively.

Time-lapse sequences were adjusted and analyzed with a particle tracking plug-in written in house. The images were smoothed to remove noise (σ 80 nm). The particles were then enhanced by subtracting the images obtained by Gaussian smoothing (σ 300 nm). The coordinates of particles were detected as centers of mass of maxima of the image intensity found by morphologic reconstruction (32). Regions of pixels with distance less than 3 μm from cell boundary were detected by thresholding the Euclidean distance transform (33) of the cell binary image. Only the particles in the selected region were evaluated. The corresponding particles in subsequent images were detected by pairing the closest particles, and the particle trajectories were constructed by continuation. The speed of the particles was calculated as the ratio of particle trajectory length and trajectory duration. The histogram of the particles speed was calculated from the trajectory speed weighted by the trajectory duration. The algorithms were implemented as plug-in modules of the Ellipse program, version 2.07 (ViDiTo, Systems, Košice Slovakia). Statistical analysis was done in Microsoft Excel.

Results

Reorganization of microtubules during activation of BMMCs

To compare microtubule organization in resting and activated mast cells, BMMCs were attached to fibronectin-coated coverslips and then activated by various means before fixation and immunofluorescence labeling for β-tubulin. Data showed a clear difference between resting and activated cells in microtubule distribution. Quiescent cells were characterized by rounded morphology and microtubules in cell periphery running predominantly alongside the plasma membrane (Fig. 1*A*, *a*, *b*; −Ag). When activated by FcεRI aggregation, many cells had multiple protrusions containing microtubules, in the following text denoted as microtubule protrusions (Fig. 1*A*, *c*, *d*; +Ag). Similarly, activation by pervanadate, a potent protein tyrosine phosphatase inhibitor (34) that mimics in part the stimulatory effect of Ag (35), gave rise to multiple microtubule protrusions (Fig. 1*A*, *e*, *f*; +Pv). Surprisingly, generation of robust microtubule protrusions was also found in cells treated with thapsigargin, a compound that discharges intracellular Ca^{2+} stores by inhibition of the SERCA (36) (Fig. 1*A*, *g*, *h*; +thapsigargin [Tg]). Microtubule protrusions do not reflect only the spreading of cells during activation events, because they are also found on the dorsal side of cells as clearly documented on deconvoluted three-dimensional images from laser scanning confocal microscopy. Although no protrusions were found in resting cells (Fig. 2*A*, 2*B*, –Ag), they were clearly discernible in cells activated by Ag-mediated FcεRI aggregation (Fig. 2*C*, 2*D*, +Ag), pervnadate (Fig. 2*E*, 2*F*, +Pv) or thapsigargin (Fig. 2*G*, 2*H*, +Tg). To determine whether the number of cells with protrusions depends on the mode of activation, BMMCs were evaluated for the presence of protrusions in three independent experiments (each included 500 cells). Activation of the cells with Ag, pervanadate, or thapsigargin resulted in 37 ± 9, 59 ± 8, and 94 ± 3% (mean ± SD; n = 3), respectively, of cells with microtubule protrusions (Fig. 1*B*). To prove that the generation of microtubule protrusion is not restricted only to cells of primary cultures, activations were repeated with an established cell line, BMMCL. In that case the rates of activation with Ag, pervanadate, or thapsigargin were 55 ± 10, 64 ± 3, and 80 ± 5% (mean ± SD; n = 3), respectively. The microtubule protrusions in cells activated by FcεRI aggregation were most prominent ~5 min after crosslinking. In contrast, cells stimulated by pervanadate or thapsigargin reached the maximum after 15 and 20 min, respectively.

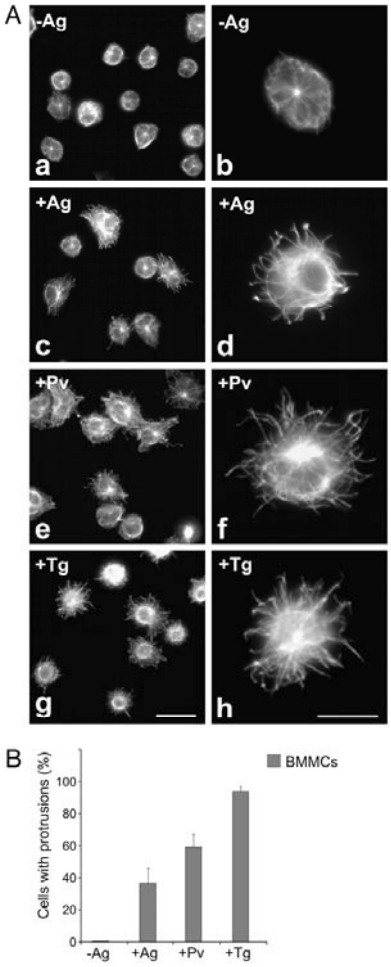

FIGURE 1. Organization of microtubules in resting and activated mast cells. *A*, Resting BMMCs (*a*, *b*; −Ag), the cells activated by FcεRI aggregation (*c*, *d*; +Ag), pervanadate (*e*, *f*; +Pv), or thapsigargin (*g*, *h*; +Tg) were fixed and stained for β-tubulin. The preparations were imaged by fluorescence microscopy. Scale bars, 20 μm (*g*) and 10 μm (*h*). Comparable magnifications are in (*a*, *c*, *e*, *g*) and in (*b*, *d*, *f*, *h*). *B*, Quantitative analysis of the frequency of microtubule protrusions in BMMCs. Resting cells (−Ag), cells activated by FcεRI aggregation (+Ag), pervanadate (+Pv) or thapsigargin (+Tg). Three independent experiments were performed, each involving 500 BMMCs examined for the presence of microtubule protrusions. Values indicate means ± SD (n = 3).

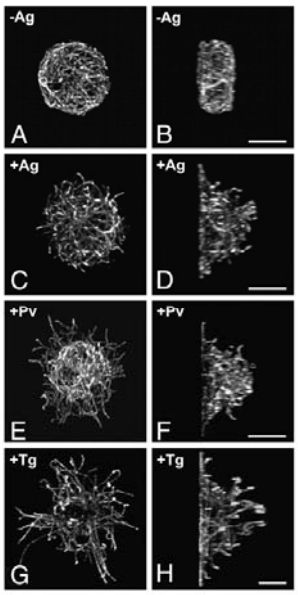

FIGURE 2. Changes in the spatial distribution of microtubules in resting and activated BMMCs. Resting cells (*A*, *B*; −Ag), cells activated by FcεRI aggregation (*C*, *D*; +Ag), pervanadate (*E*, *F*; +Pv), or thapsigargin (*G*, *H*; +Tg) were fixed and stained for β-tubulin. The preparations were imaged by laser scanning confocal microscopy. The stacks of confocal sections were deconvoluted and subjected to three-dimensional reconstruction. Resulting three-dimensional images viewed from top of the cells (*A*, *C*, *E*, *G*) and from the plane perpendicular to the plane of cell adhesion (*B*, *D*, *F*, *H*). Each pair (*A–B*, *C–D*, *E–F*, and *G–H*) represents the same cells. Scale bars, 5 μm.

Dose response curves demonstrating the relations between the formation of microtubule protrusions and the degree of degranulation, quantified as the release of β-glucuronidase, in BMMCL activated by FcεRI aggregation for 5 min and by thapsigargin for 20 min are shown in Supplemental Fig. 1A and 1B, respectively. There were dose response correlations between formation of microtubule protrusions and degranulation. Correlations between the time course of microtubule protrusion formation and the degree of degranulation after activation by FcεRI aggregation at Ag concentration 100 ng/ml and by thapsigargin at concentration 2 μM are shown in Supplemental Fig. 1C and 1D, respectively. Although there was a correlation between morphologic changes and degranulation in case of thapsigargin activation, cells activated by Ag reached the maximum of microtubule protrusions at 5 min, whereas the increase in β-glucuronidase release persisted to 10 min. Activation by either pervanadate or thapsigargin had no effect on viability of the cells (not shown). When the cells were pretreated with microtubule inhibitor nocodazole and activated in its presence, protrusions were not formed (not shown). This implies that microtubules are essential in this process.

Formation of microtubule protrusions in FcεRI-activated cells was substantially reduced if a monovalent hapten causing receptor disengagement (50 μM DNP-lysine) (37) was added together with or 1 min after Ag (not shown). Inhibition of protrusion formations was also observed in IgE-sensitized cells pretreated for 60 min with Src family inhibitor PP2 (10 μM) and then activated by Ag. Pretreatment with PP3 (negative control for PP2) failed to affect protrusion formation (not shown). This finding suggests that the activity of Src family protein tyrosine kinases is essential for this process. Interestingly, when the cells were activated by FcεRI aggregation, pervanadate, or thapsigargin in Ca^{2+}-free media, microtubule protrusions were basically not detectable. A typical example of the effect of extracellular Ca^{2+} on generation of microtubule protrusions in cells after their activation by FcεRI aggregation is shown in Fig. 3*A*. Statistical evaluation of these and other experiments is documented by histogram (Fig. 3*B*). Collectively, these data suggest that dramatic changes in microtubule arrangement during activation of BMMCs by FcεRI aggregation depend on the activity of Src family kinases and are modulated by Ca^{2+} influx.

Changes of microtubule dynamics in activated cells

Microtubule plus-end dynamics in BMMCL cells expressing EB1-GFP was monitored by means of time-lapse imaging using TIRF microscopy (TIRFM). Cells were activated or not by thapsigargin, and the distribution of growing microtubules in cell periphery was evaluated after collecting 180 frames in 1-s intervals for 3 min total time. In activated cells, time-lapse imaging started 13 min after thapsigargin addition. Data from a typical experiment are shown in Fig. 4*A*. A comparison of single-frame or 20-frame projections obtained either from control (Fig. 4*A*, *a*, *b*; –Tg) or thapsigargin-activated (Fig 4A, *c*, *d*; + Tg) cell indicated more growing microtubules in cell periphery of the latter. This finding was confirmed by statistical data evaluation and documented with

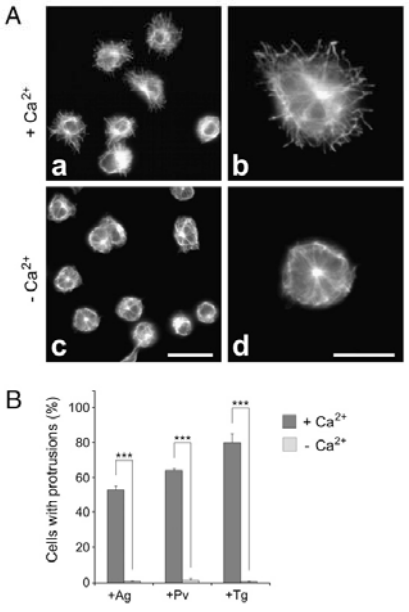

FIGURE 3. Effect of extracellular Ca^{2+} on generation of microtubule protrusions. *A*, BMMCL cells activated by FcεRI aggregation in the presence (*a*, *b*; $+Ca^{2+}$) or absence (*c*, *d*; $–Ca^{2+}$) of extracellular Ca^{2+} (1.8 mM) were fixed and stained for β-tubulin. Scale bars, 20 μm (*c*) and 10 μm (*d*). Comparable magnifications are in (*a*, *c*) and in (*b*, *d*). *B*, Statistical analysis of the frequency of microtubule protrusions in BMMCL cells. Cells activated by FcεRI aggregation (+Ag), pervanadate (+Pv), or thapsigargin (+Tg) in the presence ($+Ca^{2+}$) or absence ($-Ca^{2+}$) of extracellular Ca^{2+}. Three independent experiments were performed, each involving 500 cells, and examined for the presence of microtubule protrusions. Values indicate means ± SD, $n = 3$; $^{***}p < 0.001$.

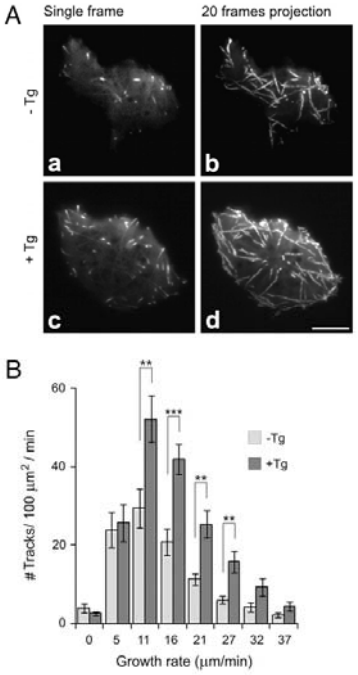

FIGURE 4. Activation of mast cells increases the number of growing microtubules in cell periphery as determined by TIRFM time-lapse imaging. *A*, Time-lapse imaging of resting (*a*, *b*) and thapsigargin-activated (*c*, *d*) BMMCL cells expressing EB1-GFP. Still images of EB1 (*a*, *c*) and tracks of EB1 comets over 20 s created by maximum intensity projection of the 20 consecutive frames (*b*, *d*). Scale bar, 5 µm. *B*, Histogram of microtubule growth rates in cell periphery of resting (−Tg) and thapsigargin-activated (+Tg) cells. A total of 15 different cells were tracked in five independent experiments. Values indicate mean ± SE, $n = 15$; $^{**}p < 0.01$; $^{***}p < 0.001$.

a histogram of the microtubule growth rates (Fig. 4*B*). Typical time-lapse imaging of control (Supplemental Video 1) and activated (Supplemental Video 2) cells are shown in the supplemental material. These data suggest that activation increases the number of growing microtubules in the cell periphery where microtubule protrusions are formed. More growing microtubules at cell periphery, compared with nonactivated cells, were also observed after activation of cells by FcεRI aggregation (Supplemental Fig. 2).

Reduced degranulation, Ca^{2+} influx, and free cytoplasmic Ca^{2+} concentration in cells with reduced level of STIM1

STIM1 represents the key regulator in the SOCE pathway leading to an influx of extracellular Ca^{2+}. To discover whether STIM1 is involved in the generation of microtubule protrusion, we first isolated cells with reduced levels of STIM1 and characterized their properties. STIM1-deficient cells were produced in both BMMCs and BMMCL cells using lentiviral vectors. At the best silencing, the amount of STIM1 in BMMCs and BMMCL cells reached 20 ± 12% and 10 ± 9% (means ± SD; n = 5-8), respectively, when compared with the expression level in control cells with an empty pLKO.1 vector. A typical immunoblotting experiment is shown in Fig. 5*A*, and evaluation of all data obtained is shown in Fig. 5*B*. Cells with the highest STIM1 reduction (denoted KD2) were selected for further experiments. As detected by flow cytometry, the

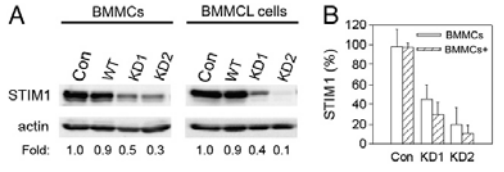

FIGURE 5. Characterization of mast cells with reduced level of STIM1. *A*, Immunoblots of whole cell lysates from BMMCs or BMMCL cells probed with anti-STIM1 and anti-actin (loading control) Abs. Control cells infected with empty pLKO.1 vector (Con), noninfected wild-type cells (WT), cells selected after KD of STIM1 by shRNA1 (KD1), or shRNA2 (KD2). Numbers under the blots indicate relative amounts of STIM1 normalized to control cells (Con) and to the amount of actin in individual samples (Fold). *B*, Comparison of STIM1 expression levels in control and STIM1 KD BMMCs or BMMCL cells. Values indicate means ± SD from independent experiments ($n = 6$ for controls; $n = 3$ for KD1; $n = 5$ for KD2).

expression levels of surface FcεRI were similar in cells with normal and reduced amount of STIM1 (not shown). No substantial changes in the profile of total tyrosine-phosphorylated proteins were detected in STIM1 KD2 cells (not shown).

It is well established that an increase in $[Ca^{2+}]_i$ is a prerequisite for mast cell degranulation (1). To confirm the functional relevance of STIM1 KD, we determined the degree of degranulation by measuring the release of β-glucuronidase in cells activated by FcεRI aggregation or by thapsigargin. As expected, a substantial decrease in degranulation was observed in BMMCs with STIM1 KD compared with control cells. The inhibition of degranulation was observed in cells activated by both FcεRI aggregation (Supplemental Fig. 3*A*) and by thapsigargin (Supplemental Fig. 3*B*). The uptake of $^{45}Ca^{2+}$ after activation by FcεRI aggregation (Supplemental Fig. 3*C*) or by thapsigargin (Supplemental Fig. 3*D*) was also inhibited in STIM1 KD cells. Finally, a substantially lower concentration of free intracellular calcium $[Ca^{2+}]_i$ was detected in STIM1 KD cells, after activation by both FcεRI aggregation (Supplemental Fig. 3*E*) and thapsigargin (Supplemental Fig. 3*F*; thapsigargin). Similar results were obtained with BMMCL cells (not shown). Collectively, these data clearly demonstrate that STIM1 is essential for Ca^{2+} mobilization and degranulation in cells used in this study.

Generation of microtubule protrusions is dependent on STIM1

When BMMCs carrying empty pLKO.1 vector were activated with thapsigargin, the formation of microtubule protrusions was prominent (Fig. 6*A*, *a*, *c*; control + Tg) and essentially the same as in BMMCs without vector (not shown). Alternatively, thapsigargin-induced activation in BMMCs with STIM1 KD failed to generate microtubule protrusions, and the cell shape was spherical (Fig. 6*A*, *b*, *d*; STIM1 KD + Tg). Significant inhibition of protrusion formations in STIM1 KD cells was also found after stimulation with pervanadate or Ag in both BMMCs and BMMCL cells (Fig. 6*B*). No obvious change in microtubule dynamics was detected by time-lapse imaging in BMMCL cells with STIM1 KD after activation by thapsigargin. Data from a typical experiment of time-lapse imaging are shown in Fig. 7*A*. Comparison of still images (single frame or 20 frames projections) from nonactivated (Fig. 7*A*, *a*, *b*; STIM1 KD – Tg) or activated (Fig 7A, *c*, *d*; STIM1 KD + Tg) cells disproved the notion that more microtubules grow in the cell periphery of activated cells. This finding was confirmed by the histogram comparing microtubule growth rates (Fig 7*B*). Although thapsigargin-activated cells exhibited some increase in the number of growing microtubules in the cell periphery, it was insignificant except for the fast-growing group (27 µm/min). In control

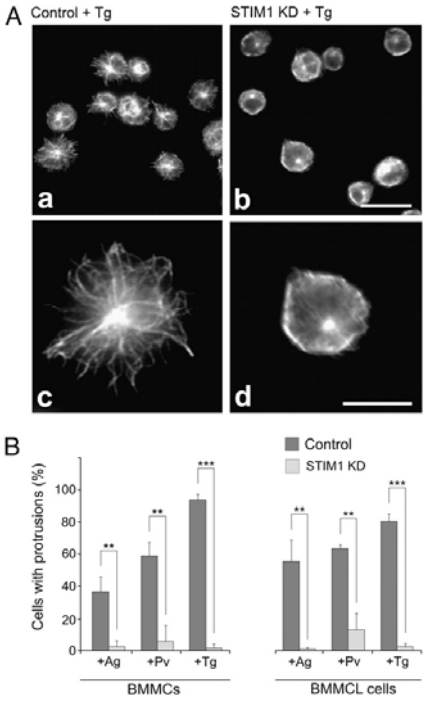

FIGURE 6. Decreased expression of STIM1 inhibits the generation of microtubule protrusions in activated cells. *A*, Control BMMCs, carrying empty pLKO.1 vector (*a*, *c*) or STIM1 KD2 cells (*b*, *d*) were activated by thapsigargin, fixed, and stained for β-tubulin. Scale bars, 20 μm (*a*, *b*) and 10 μm (*c*, *d*). *B*, Statistical analysis of the frequency of microtubule protrusions in control cells (carrying empty pLKO.1 vector) and STIM1 KD2 cells activated by FcεRI aggregation (+Ag), pervanadate (+Pv), or thapsigargin (+Tg). Three independent experiments were performed, each involving 500 BMMCs or BMMCL cells, and examined for the presence of microtubule protrusions. Values indicate means ± SD, $n = 3$; $^{**}p < 0.01$; $^{***}p < 0.001$.

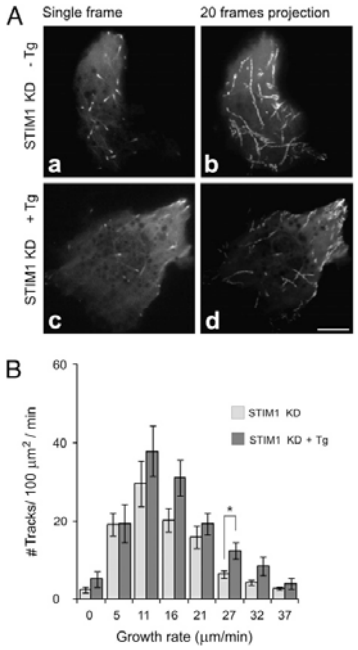

FIGURE 7. KD of STIM1 prevents changes in microtubule dynamics in activated cells as determined by TIRFM time-lapse imaging. STIM1 KD2 cells were nucleofected with EB1-GFP and used for time-lapse imaging. *A*, Resting (*a*, *b*) and thapsigargin-activated (*c*, *d*) STIM1 KD2 cells. Still images of EB1 (*a*, *c*) and tracks of EB1 comets over 20 s created by a maximum intensity projection of 20 consecutive frames (*b*, *d*). Scale bar, 5 μm. *B*, Histogram of microtubule growth rates in the cell periphery of resting (STIM1 KD) and thapsigargin-activated (STIM1 KD +Tg) cells. A total of nine different cells were tracked in three independent experiments. Values indicate means ± SE, $n = 9$; $^{*}p < 0.05$.

BMMCL cells carrying empty pLKO.1 vector, the distribution of growing microtubules in resting and thapsigargin-treated cells was similar as in BMMCL cells (Fig. 4).

To strengthen the evidence of STIM1-dependent formation of microtubule protrusions during activation, a rescue experiment was performed with construct-encoding mCherry-tagged human STIM1. Proper localization of mCherry-hSTIM1 was demonstrated in cells expressing EB1-GFP. It has been shown previously that STIM1 associates with the plus ends of growing microtubules (11); in addition, the mCherry-hSTIM1 localized in quiescent cells both in the ER and in the growing ends of microtubules labeled with EB1 (Fig. 8*A*, *a–c*). When BMMCL cells with STIM1 KD were nucleofected with mCherry-hSTIM1 and activated by thapsigargin, the formation of typical microtubule protrusions was recovered (Fig. 8*B*, *a–c*). Alternatively, no protrusions were generated after activation of cells nucleofected with empty mCherry vector (Fig. 8*B*, *d–f*). Control experiments revealed that no microtubule protrusions were evident in nonactivated BMMCL cells nucleofected either with mCherry-hSTIM1 or mCherry vector alone (not shown). The formation of microtubule protrusions was also recovered when YFP-hSTIM1 was used in rescue experiments as documented by quantitative data (Fig. 8*C*). Nucleofection of YFP-hSTIM1 into STIM1 KD2 cells also restored calcium mobilization upon triggering with thapsigargin (Fig. 8*D*) or aggregation of the FcεRI (not shown). Collectively, these data strongly suggest that STIM1 is essential for the generation of microtubule protrusions during activation of BMMCs.

Microtubules are not essential for STIM1 puncta formation

To address the question of whether microtubules in BMMCs have a role in activating SOCE, we investigated the effect of nocodazole, a microtubule-depolymerizing drug, on the distribution of STIM1 in the absence or presence of thapsigargin. In control cells, a typical comet-like movement was observed in quiescent BMMCs expressing YFP-hSTIM1 (Supplemental Video 3). After activation by thapsigargin, STIM1 formed puncta (Supplemental Video 4) similar to those previously described in other cells (5, 15). The addition of 10 μM nocodazole led to the rapid disappearance of comet-like movement of YFP-hSTIM1 as well as EB3-mRFP1, used as marker of growing microtubules. YFP-hSTIM1 was located only on the ER. When the nocodazole-treated cells were then activated with thapsigargin, YFP- hSTIM1 formed robust puncta (Supplemental Video 5). Staining of parallel samples for tubulin confirmed that most microtubules were disassembled (not shown). This finding suggests that initial STIM1 aggregation does not require intact microtubules. Interestingly, the disruption of microtubules only moderately inhibited the $^{45}Ca^{2+}$ uptake in

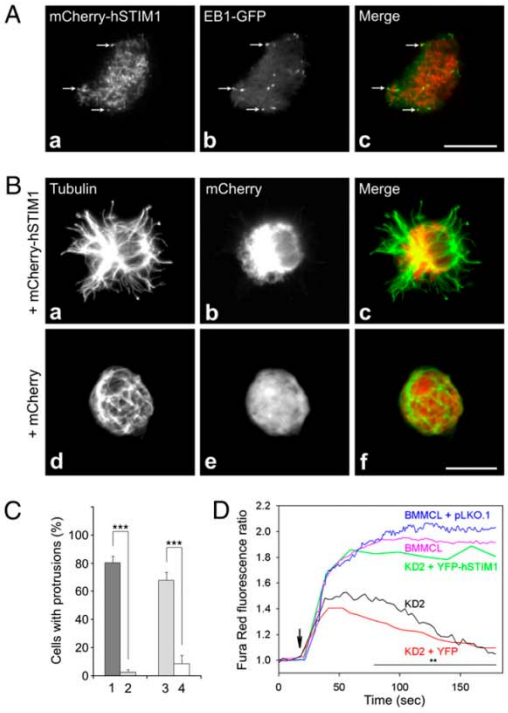

FIGURE 8. Phenotype rescue of STIM1 KD2 BMMCL cells after introduction of human STIM1. *A*, Localization of mCherry-tagged human STIM1 during TIRFM time-lapse imaging of resting cells expressing EB1-GFP. Still images of mCherry-hSTIM1 (*a*) EB1-GFP (*b*) and superposition of images (*c*; mCherry, red; GFP, green). Arrows indicate the same positions. Scale bar, 10 μm. *B*, STIM1 KD2 cells were nucleofected with mCherry-hSTIM1 (*a–c*) or mCherry vector alone (*d–f*; control) and activated by thapsigargin. Microtubules in fixed cells stained with anti-α-tubulin Ab (*a*, *d*). Fluorescence of nucleofected mCherry vectors (*b*, *e*). Superposition of images (*c*, *f*; tubulin, green; mCherry, red). The preparations were imaged by fluorescence microscopy; *a–c* and *d–f* represent the same cells. Scale bar, 10 μm. *C*, Statistical analysis of the frequency of microtubule protrusions in thapsigargin-activated control cells (1), STIM1 KD2 cells (2), STIM1 KD2 cells nucleofected with pYFP-hSTIM1 (3) and STIM1 KD2 cells nucleofected with pYFP empty vector (4). Three independent experiments were performed, each involving 500 (1, 2) or 100 (3, 4) cells examined for the presence of microtubule protrusions. Values indicate means ± SD, $n = 3$; $^{***}p < 0.001$. *D*, Changes in intracellular Ca^{2+} mobilization. KD2 cells were nucleofected with pYFP-hSTIM1 (green line) or with pYFP empty vector (red line). Non-transfected cells (pink line), cells transfected with pLKO.1 (blue line) and STIM1 KD2 cells (black line) served as controls. The arrow indicates activation by 2 μM thapsigargin. The extent of activation is expressed as a ratio of Fura Red fluorescence intensity induced with 406- and 488-nm lasers. Representative curves are plotted against time. The line below the asterisks indicates the time interval of significant differences between STIM1 KD2 cell transfected with pYFP-hSTIM1 or with pYFP empty vector; $^{**}p < 0.01$; $n = 3$.

thapsigargin-activated cells (Fig. 9*A*), but degranulation was substantially reduced (Fig. 9*B*).

STIM1 associates with microtubule protrusions and plays a role in chemotactic response

The movement of YFP-hSTIM1, not associated with growing tips of microtubules, was observable at later stages of activation when microtubule protrusions started to form. Association of YFP-hSTIM1 with microtubule protrusions was evident in thapsigargin-activated BMMCs and was detectable by confocal microscopy on cells stained for β-tubulin (Fig. 10*A*, *a–c*). Similarly, FcεRI aggregation led to partial association of YFP-hSTIM1 with microtubule protrusions (not shown).

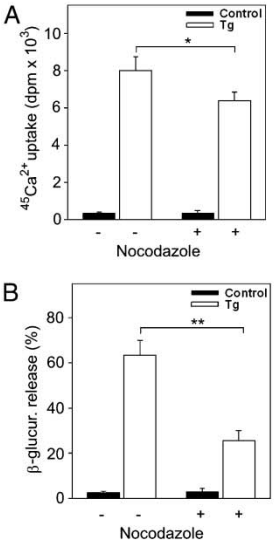

FIGURE 9. Effect of microtubule depolymerization on Ca^{2+} uptake and degranulation. *A*, Effect of nocodazole on Ca^{2+} uptake. BMMCs were treated or not with nocodazole (10 μM) for 30 min and then exposed to thapsigargin (2 μM; Tg) or BSS-BSA alone (Control) for 15 min in the presence of extracellular $^{45}Ca^{2+}$ (1 mM) and nocodazole (10 μM). *B*, Effect of nocodazole on degranulation. BMMCs were treated with nocodazole and exposed to thapsigargin as in *A*, and the release of β-glucuronidase was determined. Data in *A* and *B* represent means ± SD, $n = 6–8$; $^{*}p < 0.05$; $^{**}p < 0.01$.

The observed formation of STIM1-dependent microtubule protrusions could be related to enhanced movement of the activated cells. Therefore, in additional experiments, we investigated the chemotactic response of STIM1-deficient BMMCs. The data presented in Fig. 10*B* indicate that at low concentrations of Ag (25–100 ng/ml), the chemotactic response is contingent on STIM1 in a dose-dependent manner. At a higher concentration (250 ng/ml), the difference disappears mainly because of the high-dose–mediated inhibition of chemotaxis in control cells. This finding demonstrates that STIM1-dependent Ca^{2+} influx promotes chemotaxis.

Discussion

FcεRI stimulation of mast cells leads to rapid cytoskeleton rearrangement that is important for cell activation and degranulation. Accumulating recent data point to an important role of microtubules in these processes (38). Previous studies focused primarily on the role of microtubules in granular transport (13, 16, 17, 20) or on the initial stages of SOCE signaling pathway (13, 15, 39). In this study, we show that microtubule network rearrangement in activated BMMCs and formation of microtubule protrusions is dependent on the activity of Ca^{2+} sensor STIM1. This conclusion is supported by several lines of evidence. First, microtubule protrusions were found in cells stimulated by three types of activators that induced depletion of Ca^{2+} from internal stores (FcεRI aggregation, pervanadate, or thapsigargin treatment). Second, the generation of protrusions was impaired when multivalent Ag-

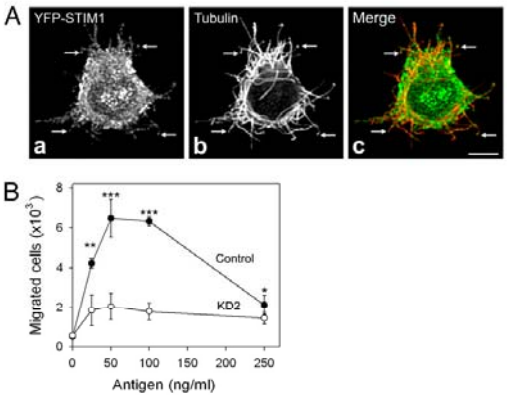

FIGURE 10. STIM1 associates with microtubule protrusions in activated cells and is essential for chemotactic response. *A*, Laser scanning confocal microscopy of BMMCL cells expressing YFP-hSTIM1 after activation by thapsigargin. Cells were fixed and immunostained for β-tubulin, and both STIM1 (*a*) and tubulin (*b*) were visualized in a single confocal section. Superposition of STIM1 and tubulin staining is shown in *c*. Association of YFP-hSTIM1 with microtubule protrusions is depicted (arrows). Scale bar, 5 μm. *B*, Chemotactic response in activated cells. Various concentrations of DNP-BSA (chemoattractant) were added to the lower wells of ChemoTx system plate, and IgE-sensitized BMMCs infected with empty pLKO.1 vector (Control) or STIM1 KD2 cells (KD2) were added on top of the membrane above each well. The numbers of cells migrated to the lower well were determined as described in *Materials and Methods*. Values indicate mean ± SD, $n = 12$; $^{*}p < 0.05$; $^{**}p < 0.01$; $^{***}p < 0.001$.

induced FcεRI aggregation and signaling were inhibited either by monovalent hapten or by Src family specific inhibitor; this implies that early, physiologically relevant signaling events leading to STIM1 aggregation are important for microtubule rearrangement. Third, the formation of protrusions was also inhibited in cells with a decreased level of STIM1 and with correspondingly diminished influx of extracellular Ca^{2+}. Fourth, microtubule protrusions were restored in STIM1 KD cells after the introduction of hSTIM1. Finally, microtubule protrusions were not observed in cells activated in Ca^{2+}-free media. Thus, STIM1-regulated Ca^{2+} influx plays a crucial role in the generation of microtubule protrusions.

We have shown previously that, compared with resting cells, FcεRI- or pervanadate-induced activation of BMMCs attached to poly-L-lysine-coated coverslips resulted in more intense staining of microtubules. However, no obvious microtubule protrusions were detected (21). Similarly, activation and fixation of BMMCs in suspension followed by attachment to glass slides by cytospin intensified the tubulin immunostaining, but microtubule protrusions were not reported (17). In this study, the cells were attached to fibronectin before activation, resembling more closely the natural conditions in connective tissue where mast cells are congregated (40). Although the attachment of BMMCs to fibronectin alone did not generate microtubule protrusions, they were observable after cell triggering. It is known that engagement of integrins by their ligands activates some signaling pathways that modulate signals originating from other receptors (41). It has been reported that, when mast cells were activated simultaneously via both FcεRI and integrins, phosphorylation events were prolonged and intensified (42). Thus, generation of microtubule protrusions could reflect such integrated signals in activated cells.

To discover whether the generation of microtubule protrusions is limited to BMMCs, several other cell types were tested. However, thapsigargin treatment failed to induce formation of protrusions in any other cell type examined, including mouse embryonal fibroblasts 3T3, human osteosarcoma cell line U2OS or human glioblastoma T98G (Z. Hájková, unpublished data). By contrast, in BMMCL cells, which are grown for many years in the absence of SCF, the formation of protrusions was observed after triggering with cell activators (Ag, pervanadate, thapsigargin). The reduction of STIM1 expression both in BMMCs and BMMCL cells had a detrimental impact on the formation of microtubule protrusions. This finding indicates that protrusion formation could be a typical feature of mast cells that are characterized by immediate response to outer stimuli. However, we cannot rule out at present that the generation of microtubule protrusions can also be observable in the other cell types.

Colocalization of ER-embedded STIM1 with microtubules has been described for several cell types, including rat basophilic leukemia RBL-2H3 (8, 9, 15, 43), and comet-like movement of STIM1 was also reported (11). Furthermore, STIM1 contains a short sequence (SxIP) responsible for direct binding to EB1 (44). Thus, STIM1 can associate with growing microtubules, a mechanism that might facilitate the transport of STIM1 to plasma membrane. Using TIRFM we have confirmed the comet-like movement of STIM1 and its association with EB1 in resting BMMCL cells. This movement was substantially reduced after the addition of thapsigargin, which is in agreement with the impaired association of STIM1 with microtubules in Ag-activated RBL-2H3 cells (43). Recent data on FRET imaging of EB1 and STIM1 in HEK293 cells showed that, upon store depletion of Ca^{2+}, STIM1 dissociated from EB1 and associated with SERCA. This process was reversible, because the replenishment of intracellular Ca^{2+} stores also restored the STIM1–EB1 interactions (45). Moreover, no effect on SOCE was observed in HeLa cells with depleted EB1 (11). Taking these findings together, it is likely that the interaction of STIM1 with EB1 on growing microtubules is not essential for the transport of STIM1 to plasma membrane during mast cell activation.

After depletion of intracellular Ca^{2+} stores, STIM1 accumulates into puncta, discrete subregions of ER located in a close proximity (10–25 nm) to the plasma membrane (46). STIM1 puncta are formed several seconds before the opening of calcium channels (47), and one could expect that microtubules are involved in this process. However, our data demonstrate that although microtubule disruption by nocodazole abolished the comet-like movement of STIM1, it had no effect on puncta formation in activated cells. This finding is in line with our observation that the uptake of extracellular Ca^{2+} was only partially inhibited in nocodazole-pretreated and thapsigargin-activated BMMCs. This suggests that STIM1 aggregation beneath the plasma membrane and subsequent opening of Ca^{2+} release-activated Ca^{2+} channels does not require intact microtubules in activated mast cells. Previous studies often reported discordant effects of nocodazole treatment on SOCE or I_{CRAC}, the current most frequently associated with SOCE, in various cell types. Whereas there was no effect of nocodazole treatment observed in NIH 3T3 (48), RBL-1 (15, 39), and DT40 cells (8), an inhibitory effect was demonstrated for other cell types, such as RBL-2H3 cells, BMMCs (13), and HEK 293 (15). It appears that different factors, including cell type, treatment protocol and the way of Ca^{2+} depletion might modify the results of the experiments. It is also possible that microtubules play a supporting role in SOCE signaling by optimizing the location of ER containing STIM1 before cell activation (15).

Nocodazole treatment, in contrast, effectively suppressed degranulation in BMMCs, suggesting that microtubules have a key role in the intracellular transport of granules. This finding is in accordance with previously published data demonstrating

microtubule-dependent movement of secretory vesicles during exocytotic response (16, 17, 20) and studies documenting a dramatic decrease in degranulation, but not in Ca^{2+} response in nocodazole treated cells (49). Our observation that STIM1 puncta are associated with microtubules in protrusions (Fig. 10*A*) indicates that microtubules might be important for translocation of clustered STIM1 as well. This process could possibly be dependent on the movement of ER components to protrusions via microtubule motor proteins; an important role of kinesin and dynein in the distribution of ER has already been reported (14).

Compared with quiescent cells or cells with decreased expression of STIM1, the number of growing microtubules at the periphery of activated BMMCL cells is substantially increased. This finding suggests the stabilization of microtubule plus ends. It is known that an important role in stabilization of growing microtubules is to be assigned to the plus end-tracking proteins whose interactions with microtubules are regulated by phosphorylation (10). Ca^{2+}-dependent kinases (e.g., conventional protein kinases C, calcium-calmodulin–dependent kinases) or phosphatases (e.g., PP2B) might participate in the regulation of microtubule stability in activated BMMCs. It has been reported that calcium-dependent activation of Rac (from the RhoA family of small GTPases) depends on the activity of conventional protein kinase C (50). FcεRI stimulation induced in BMMCs the activation of RhoA (17), which participates in the stabilization of microtubule plus ends through its target mDia (51). It remains to be determined whether stimulated kinases, small GTPases, or both have a stabilizing role in thapsigargin-treated BMMCs.

Nishida et al. (17) reported that FcεRI stimulation of BMMCs triggered the formation of microtubules and the translocation of granules in a manner independent of Ca^{2+}. Alternatively, our results demonstrate Ca^{2+}-dependent formation of microtubule protrusions. This discrepancy could be explained by differences in cell activation (the absence or presence of integrin engagement) and unlike methods of preparation of samples for microscopic evaluation, as discussed above. However, it is also possible that the initial stages of microtubule formation and transport of granules along microtubules are independent of Ca^{2+}, but later stages of activation and formation of microtubule protrusions depend on sustained influx of Ca^{2+}. The presence of aggregated STIM1 in protrusion could help to organize Ca^{2+} release-activated Ca^{2+} channels (46) and open locally these channels to cause SOCE. These interactions could be modulated by Ca^{2+} channel regulators, such as calmodulin (52) and the recently discovered CRACR2A (53). Our finding that STIM1-deficient BMMCs exhibited defective chemotaxis toward Ag is in line with these interpretations, and it supports previous data on the role of Ca^{2+} in chemotaxis (54, 55). We propose that microtubule protrusions might be involved in sensing external chemotactic gradients of Ag or other signals reaching mast cells at inflammatory sites.

In conclusion, our data indicate that the activation of mast cells leads to microtubule rearrangements and formation of microtubule protrusions. This process is dependent on STIM1-induced SOCE and enhanced levels of free cytoplasmic Ca^{2+} concentration, which have an important role in the regulation of microtubule dynamics, degranulation, and chemotactic response. Interference with the microtubular network via STIM1 or other Ca^{2+} regulators could potentially open new rational approaches to the treatment of inflammatory and allergic diseases.

Acknowledgments

We thank Dr. M. Hibbs (Ludwig Institute for Cancer Research, Melbourne, Australia) for BMMCL cells, Dr. T. Meyer (Department of Molecular Pharmacology, Stanford University Medical School, Stanford, CA) for YFP–hSTIM1 construct, Dr. Y. Mimori-Kiyosue (KAN Research Institute, Kyoto, Japan) for EB1-GFP construct, and Dr. A. Akhmanova (Department of Cell Biology, Erasmus Medical Center, Rotterdam, The Netherlands) for EB3-mRFP1.

Disclosures

The authors have no financial conflicts of interest.

References

1. Rivera, J., N. A. Fierro, A. Olivera, and R. Suzuki. 2008. New insights on mast cell activation via the high affinity receptor for IgE. *Adv. Immunol.* 98: 85–120.
2. Parekh, A. B., and J. W. Putney, Jr. 2005. Store-operated calcium channels. *Physiol. Rev.* 85: 757–810.
3. Smyth, J. T., W. I. Dehaven, B. F. Jones, J. C. Mercer, M. Trebak, G. Vazquez, and J. W. Putney, Jr. 2006. Emerging perspectives in store-operated Ca^{2+} entry: roles of Orai, Stim and TRP. *Biochim. Biophys. Acta* 1763: 1147–1160.
4. Roos, J., P. J. DiGregorio, A. V. Yeromin, K. Ohlsen, M. Lioudyno, S. Zhang, O. Safrina, J. A. Kozak, S. L. Wagner, M. D. Cahalan, et al. 2005. STIM1, an essential and conserved component of store-operated Ca^{2+} channel function. *J. Cell Biol.* 169: 435–445.
5. Liou, J., M. L. Kim, W. D. Heo, J. T. Jones, J. W. Myers, J. E. Ferrell, Jr., and T. Meyer. 2005. STIM is a Ca^{2+} sensor essential for Ca^{2+}-store-depletion-triggered Ca^{2+} influx. *Curr. Biol.* 15: 1235–1241.
6. Dziadek, M. A., and L. S. Johnstone. 2007. Biochemical properties and cellular localisation of STIM proteins. *Cell Calcium* 42: 123–132.
7. Prakriya, M., S. Feske, Y. Gwack, S. Srikanth, A. Rao, and P. G. Hogan. 2006. Orai1 is an essential pore subunit of the CRAC channel. *Nature* 443: 230–233.
8. Baba, Y., K. Hayashi, Y. Fujii, A. Mizushima, H. Watarai, M. Wakamori, T. Numaga, Y. Mori, M. Iino, M. Hikida, and T. Kurosaki. 2006. Coupling of STIM1 to store-operated Ca^{2+} entry through its constitutive and inducible movement in the endoplasmic reticulum. *Proc. Natl. Acad. Sci. USA* 103: 16704–16709.
9. Mercer, J. C., W. I. Dehaven, J. T. Smyth, B. Wedel, R. R. Boyles, G. S. Bird, and J. W. Putney, Jr. 2006. Large store-operated calcium selective currents due to co-expression of Orai1 or Orai2 with the intracellular calcium sensor, Stim1. *J. Biol. Chem.* 281: 24979–24990.
10. Akhmanova, A., and M. O. Steinmetz. 2008. Tracking the ends: a dynamic protein network controls the fate of microtubule tips. *Nat. Rev. Mol. Cell Biol.* 9: 309–322.
11. Grigoriev, I., S. M. Gouveia, B. van der Vaart, J. Demmers, J. T. Smyth, S. Honnappa, D. Splinter, M. O. Steinmetz, J. W. Putney, Jr., C. C. Hoogenraad, and A. Akhmanova. 2008. STIM1 is a MT-plus-end-tracking protein involved in remodeling of the ER. *Curr. Biol.* 18: 177–182.
12. Terasaki, M., L. B. Chen, and K. Fujiwara. 1986. Microtubules and the endoplasmic reticulum are highly interdependent structures. *J. Cell Biol.* 103: 1557–1568.
13. Oka, T., M. Hori, and H. Ozaki. 2005. Microtubule disruption suppresses allergic response through the inhibition of calcium influx in the mast cell degranulation pathway. *J. Immunol.* 174: 4584–4589.
14. Wu, S., H. Chen, M. F. Alexeyev, J. A. King, T. M. Moore, T. Stevens, and R. D. Balczon. 2007. Microtubule motors regulate ISOC activation necessary to increase endothelial cell permeability. *J. Biol. Chem.* 282: 34801–34808.
15. Smyth, J. T., W. I. DeHaven, G. S. Bird, and J. W. Putney, Jr. 2007. Role of the microtubule cytoskeleton in the function of the store-operated Ca^{2+} channel activator STIM1. *J. Cell Sci.* 120: 3762–3771.
16. Smith, A. J., J. R. Pfeiffer, J. Zhang, A. M. Martinez, G. M. Griffiths, and B. S. Wilson. 2003. Microtubule-dependent transport of secretory vesicles in RBL-2H3 cells. *Traffic* 4: 302–312.
17. Nishida, K., S. Yamasaki, Y. Ito, K. Kabu, K. Hattori, T. Tezuka, H. Nishizumi, D. Kitamura, R. Goitsuka, R. S. Geha, et al. 2005. FcεRI-mediated mast cell degranulation requires calcium-independent microtubule-dependent translocation of granules to the plasma membrane. *J. Cell Biol.* 170: 115–126.
18. Urata, C., and R. P. Siraganian. 1985. Pharmacologic modulation of the IgE or Ca^{2+} Ionophore A23187 mediated Ca^{2+} influx, phospholipase activation, and histamine release in rat basophilic leukemia cells. *Int. Arch. Allergy Immunol.* 78: 92–100.
19. Tasaka, K., M. Mio, K. Fujisawa, and I. Aoki. 1991. Role of microtubules on Ca^{2+} release from the endoplasmic reticulum and associated histamine release from rat peritoneal mast cells. *Biochem. Pharmacol.* 41: 1031–1037.
20. Martin-Verdeaux, S., I. Pombo, B. Iannascoli, M. Roa, N. Varin-Blank, J. Rivera, and U. Blank. 2003. Evidence of a role for Munc18-2 and microtubules in mast cell granule exocytosis. *J. Cell Sci.* 116: 325–334.
21. Sulimenko, V., E. Dráberová, T. Sulimenko, L. Macurek, V. Richterová, P. Dráber, and P. Dráber. 2006. Regulation of microtubule formation in activated mast cells by complexes of γ-tubulin with Fyn and Syk kinases. *J. Immunol.* 176: 7243–7253.
22. Oritani, K., and P. W. Kincade. 1996. Identification of stromal cell products that interact with pre-B cells. *J. Cell Biol.* 134: 771–782.
23. Nováková, M., E. Dráberová, W. Schürmann, G. Czihak, V. Viklický, and P. Dráber. 1996. γ-Tubulin redistribution in taxol-treated mitotic cells probed by monoclonal antibodies. *Cell Motil. Cytoskeleton* 33: 38–51.
24. Dráber, P., J. Zikán, and M. Vojtíšková. 1980. Establishment and characterization of permanent murine hybridomas secreting monoclonal anti-thy-1 antibodies. *J. Immunogenet.* 7: 455–474.

25. Mimori-Kiyosue, Y., N. Shiina, and S. Tsukita. 2000. The dynamic behavior of the APC-binding protein EB1 on the distal ends of microtubules. *Curr. Biol.* 10: 865–868.
26. Campbell, R. E., O. Tour, A. E. Palmer, P. A. Steinbach, G. S. Baird, D. A. Zacharias, and R. Y. Tsien. 2002. A monomeric red fluorescent protein. *Proc. Natl. Acad. Sci. USA* 99: 7877–7882.
27. Surviladze, Z., L. Dráberová, M. Kovářová, M. Boubelík, and P. Dráber. 2001. Differential sensitivity to acute cholesterol lowering of activation mediated via the high-affinity IgE receptor and Thy-1 glycoprotein. *Eur. J. Immunol.* 31: 1–10.
28. Dráberová, L. 1990. Cyclosporin A inhibits rat mast cell activation. *Eur. J. Immunol.* 20: 1469–1473.
29. Laemmli, U. K. 1970. Cleavage of structural proteins during the assembly of the head of bacteriophage T_4. *Nature* 227: 680–685.
30. Dráber, P., L. A. Lagunowich, E. Dráberová, V. Viklický, and I. Damjanov. 1988. Heterogeneity of tubulin epitopes in mouse fetal tissues. *Histochemistry* 89: 485–492.
31. Dráberová, E., and P. Dráber. 1993. A microtubule-interacting protein involved in coalignment of vimentin intermediate filaments with microtubules. *J. Cell Sci.* 106: 1263–1273.
32. Soile, P. 2003. *Morphological Image Analysis – Principles and Applications*. Springer Verlag, Berlin.
33. Breu, H., D. Kirkpatrick, and M. Werman. 1995. Linear time euclidean distance transform algorithms. *IEEE Trans. Pattern Anal. Mach. Intell.* 17: 529–533.
34. Zick, Y., and R. Sagi-Eisenberg. 1990. A combination of H_2O_2 and vanadate concomitantly stimulates protein tyrosine phosphorylation and polyphosphoinositide breakdown in different cell lines. *Biochemistry* 29: 10240–10245.
35. Teshima, R., H. Ikebuchi, M. Nakanishi, and J. Sawada. 1994. Stimulatory effect of pervanadate on calcium signals and histamine secretion of RBL-2H3 cells. *Biochem. J.* 302: 867–874.
36. Thastrup, O., P. J. Cullen, B. K. Drøbak, M. R. Hanley, and A. P. Dawson. 1990. Thapsigargin, a tumor promoter, discharges intracellular Ca^{2+} stores by specific inhibition of the endoplasmic reticulum Ca^{2+}-ATPase. *Proc. Natl. Acad. Sci. USA* 87: 2466–2470.
37. Paolini, R., M. H. Jouvin, and J. P. Kinet. 1991. Phosphorylation and dephosphorylation of the high-affinity receptor for immunoglobulin E immediately after receptor engagement and disengagement. *Nature* 353: 855–858.
38. Gilfillan, A. M., and J. Rivera. 2009. The tyrosine kinase network regulating mast cell activation. *Immunol. Rev.* 228: 149–169.
39. Bakowski, D., M. D. Glitsch, and A. B. Parekh. 2001. An examination of the secretion-like coupling model for the activation of the Ca^{2+} release-activated Ca^{2+} current I_{CRAC} in RBL-1 cells. *J. Physiol.* 532: 55–71.
40. Galli, S. J., M. Tsai, and A. M. Piliponsky. 2008. The development of allergic inflammation. *Nature* 454: 445–454.
41. Schwartz, M. A., M. D. Schaller, and M. H. Ginsberg. 1995. Integrins: emerging paradigms of signal transduction. *Annu. Rev. Cell Dev. Biol.* 11: 549–599.
42. Lam, V., J. Kalesnikoff, C. W. Lee, V. Hernandez-Hansen, B. S. Wilson, J. M. Oliver, and G. Krystal. 2003. IgE alone stimulates mast cell adhesion to fibronectin via pathways similar to those used by IgE + antigen but distinct from those used by Steel factor. *Blood* 102: 1405–1413.
43. Calloway, N., M. Vig, J. P. Kinet, D. Holowka, and B. Baird. 2009. Molecular clustering of STIM1 with Orai1/CRACM1 at the plasma membrane depends dynamically on depletion of Ca^{2+} stores and on electrostatic interactions. *Mol. Biol. Cell* 20: 389–399.
44. Honnappa, S., S. M. Gouveia, A. Weisbrich, F. F. Damberger, N. S. Bhavesh, H. Jawhari, I. Grigoriev, F. J. van Rijssel, R. M. Buey, A. Lawera, et al. 2009. An EB1-binding motif acts as a microtubule tip localization signal. *Cell* 138: 366–376.
45. Sampieri, A., A. Zepeda, A. Asanov, and L. Vaca. 2009. Visualizing the store-operated channel complex assembly in real time: identification of SERCA2 as a new member. *Cell Calcium* 45: 439–446.
46. Cahalan, M. D. 2009. STIMulating store-operated Ca^{2+} entry. *Nat. Cell Biol.* 11: 669–677.
47. Wu, M. M., J. Buchanan, R. M. Luik, and R. S. Lewis. 2006. Ca^{2+} store depletion causes STIM1 to accumulate in ER regions closely associated with the plasma membrane. *J. Cell Biol.* 174: 803–813.
48. Ribeiro, C. M., J. Reece, and J. W. Putney, Jr. 1997. Role of the cytoskeleton in calcium signaling in NIH 3T3 cells. An intact cytoskeleton is required for agonist-induced $[Ca^{2+}]i$ signaling, but not for capacitative calcium entry. *J. Biol. Chem.* 272: 26555–26561.
49. Hesketh, T. R., M. A. Beaven, J. Rogers, B. Burke, and G. B. Warren. 1984. Stimulated release of histamine by a rat mast cell line is inhibited during mitosis. *J. Cell Biol.* 98: 2250–2254.
50. Price, L. S., M. Langeslag, J. P. ten Klooster, P. L. Hordijk, K. Jalink, and J. G. Collard. 2003. Calcium signaling regulates translocation and activation of Rac. *J. Biol. Chem.* 278: 39413–39421.
51. Palazzo, A. F., T. A. Cook, A. S. Alberts, and G. G. Gundersen. 2001. mDia mediates Rho-regulated formation and orientation of stable microtubules. *Nat. Cell Biol.* 3: 723–729.
52. Mullins, F. M., C. Y. Park, R. E. Dolmetsch, and R. S. Lewis. 2009. STIM1 and calmodulin interact with Orai1 to induce Ca^{2+}-dependent inactivation of CRAC channels. *Proc. Natl. Acad. Sci. USA* 106: 15495–15500.
53. Srikanth, S., H. J. Jung, K. D. Kim, P. Souda, J. Whitelegge, and Y. Gwack. 2010. A novel EF-hand protein, CRACR2A, is a cytosolic Ca^{2+} sensor that stabilizes CRAC channels in T cells. *Nat. Cell Biol.* 12: 436–446.
54. Hartmann, K., B. M. Henz, S. Krüger-Krasagakes, J. Köhl, R. Burger, S. Guhl, I. Haase, U. Lippert, and T. Zuberbier. 1997. C3a and C5a stimulate chemotaxis of human mast cells. *Blood* 89: 2863–2870.
55. Hofstra, C. L., P. J. Desai, R. L. Thurmond, and W. P. Fung-Leung. 2003. Histamine H4 receptor mediates chemotaxis and calcium mobilization of mast cells. *J. Pharmacol. Exp. Ther.* 305: 1212–1221.

Changes in red

Legends to supplemental material

FIGURE S1. Correlation between formation of microtubule protrusions and degranulation in activated mast cells. Control or activated BMMCL cells were either fixed and stained for β-tubulin or used for determination of β-glucuronidase release. (A) IgE-sensitized (1 µg/ml) cells activated with different concentrations of Ag for 5 min. (B) Cells activated with different concentration of thapsigargin for 20 min. (C) IgE-sensitized cells activated with Ag (100 ng/ml) for various time intervals. (D) Cells activated with thapsigargin (2 µM) for various time. Three independent experiments were performed, each involving 500 cells and examined for the presence of microtubule protrusions. Values indicate means ± SD (n=3). Data for β-glucuronidase release represent means ± SD (n=3).

FIGURE S2. Activation of mast cells with Ag increases the number of growing microtubules in cell periphery as determined by TIRFM time-lapse imaging. (A) Time-lapse imaging of resting (a-b) and FcεRI aggregation-activated (c-d) BMMCL cells expressing EB1-GFP. Still images of EB1 (a, c) and tracks of EB1 comets over 20 sec created by maximum intensity projection of the 20 consecutive frames (b, d). Scale bar, 5 µm. (B) Histogram of microtubule growth rates in cell periphery of resting (-Ag) and Ag-activated (+Ag) cells. Total 10 different cells were tracked in 3 independent experiments. Values indicate mean ± SE, n=10 (*, $p<0.05$;**, $p<0.01$).

FIGURE S3. Degranulation and Ca^{2+} responses in cells with reduced STIM1 levels. (A-B) Changes in the degree of degranulation quantified as β-glucuronidase release. IgE-sensitized

(1 µg/ml) cells infected with empty pLKO.1 vector (Control) or cells with reduced STIM1 after infection with shRNA2 (KD2) were activated with different concentrations of DNP-albumin for 30 min (A) or thapsigargin for 20 min (B) and the release of β-glucuronidase was determined. Data in (A) and (B) represent means ± SD (n=3, both for controls and KD2). (C-D) Changes in $^{45}Ca^{2+}$ uptake. IgE-sensitized (1 µg/ml) control cells (empty pLKO.1vector) or STIM1 KD2 cells were activated for various time intervals with 100 ng/ml DNP-albumin (C) or 2 µM thapsigargin (D) in the presence of extracellular $^{45}Ca^{2+}$ (1 mM). Data in (C) and (D) represent means ± SD (n=6, both for controls and KD2). (E-F) Changes in intracellular Ca^{2+} mobilization. IgE-sensitized (1 µg/ml) control cells (empty pLKO.1vector) or STIM1 KD2 cells loaded with Fluo 3-AM were activated (arrows) by 100 ng/ml DNP-albumin (E) or 2 µM thapsigargin (F). Data in (E) and (F) represent means ± SD (n=3, both for controls and KD2). (***, $p<0.001$; in E and F the line under asterisks indicate time interval of significant differences).

Movie S1. Time-lapse imaging of EB1-GFP in quiescent cells. BMMCL cells were imaged, with 0.5 s exposure time and 1 s interval between frames, for 3 min in TIRFM.

Movie S2. Time-lapse imaging of EB1-GFP in thapsigargin activated cells. BMMCL cells were imaged, with 0.5s exposure time and 1 s interval between frames, for 3 min in TIRFM. Imaging started 13 min after addition of thapsigargin at final concentration 2 µM.

Movie S3. Time-lapse imaging of YFP-hSTIM1 in quiescent cells. BMMCL cells were imaged, with 0.5s exposure time and 1 s interval between frames, for 3 min in TIRFM.

Movie S4. Time-lapse imaging of YFP-hSTIM1 in the course of thapsigargin activation of cells. BMMCL cells were imaged, with 0.5s exposure time and 1 s interval between frames, for 3 min in TIRFM. Thapsigargin was added 30s after starting the movie.

Movie S5. Time-lapse imaging of YFP-hSTIM1 and EB3-mRFP1 in the course of nocodazole treatment of cells, folowed by thapsigargin activation. BMMCL cells were imaged, with exposure time ranging from 0.5-0.8s and 2 s interval between frames, for 3 min in TIRFM. Nocodazole and thapsigargin were added to the final concentration of 10 µM and 2 µM, respectively. Elapsed time in minutes and seconds is depicted in the upper right.

Fig. S1

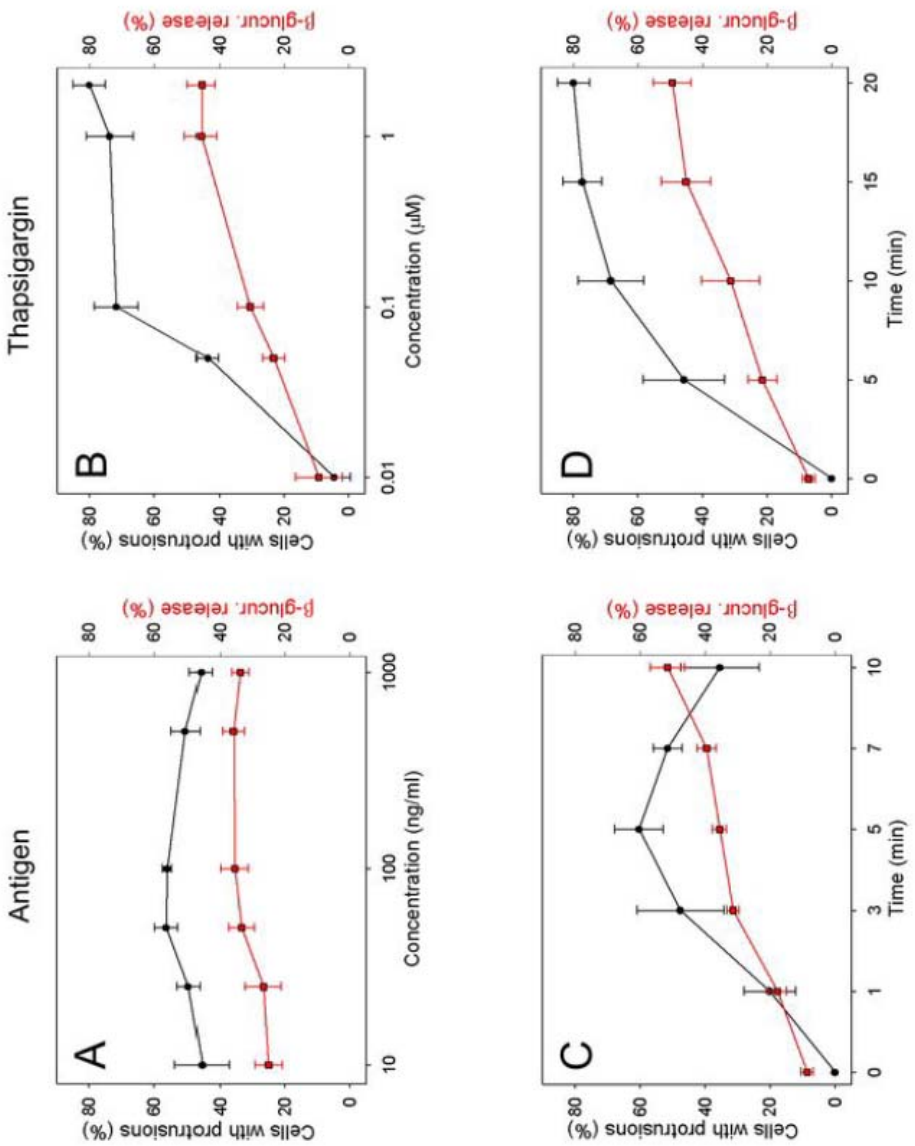
Antigen
Thapsigargin
A
B
C
D
Cells with protrusions (%)
β-glucur. release (%)
Concentration (ng/ml)
Concentration (µM)
Time (min)

Fig. S2

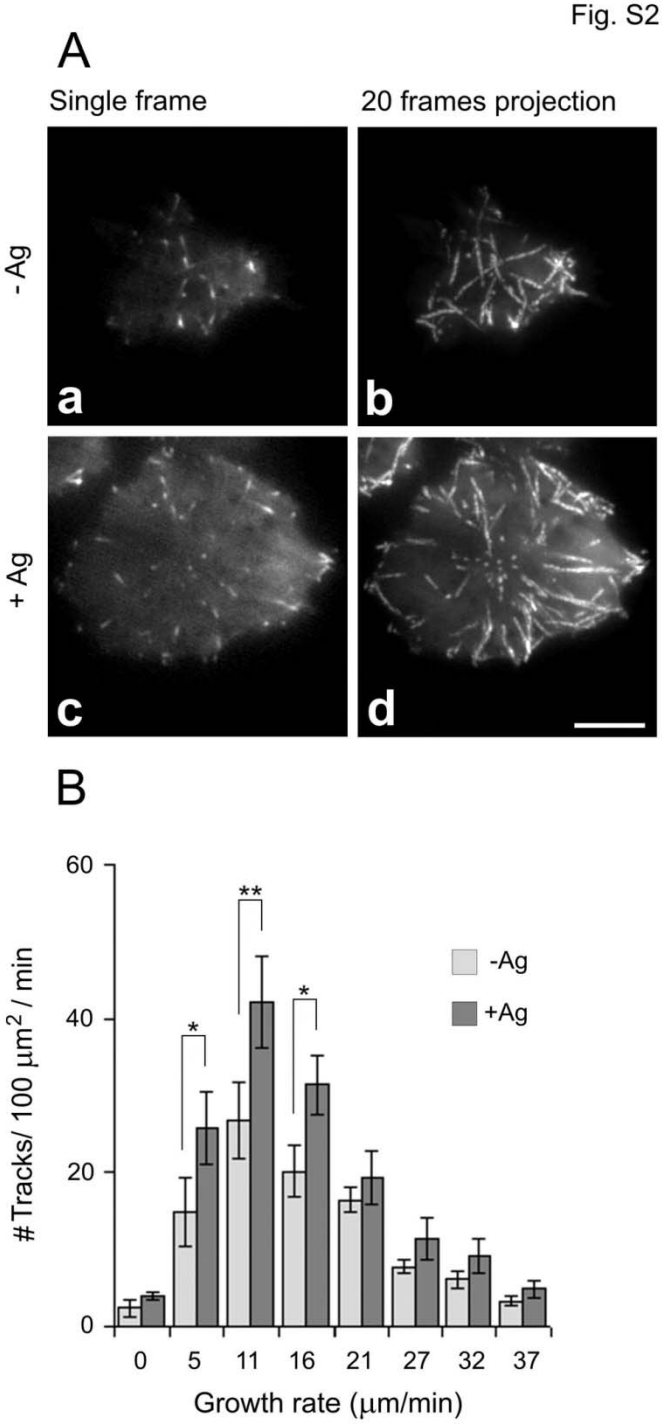
A
Single frame
20 frames projection
- Ag
+ Ag
a
b
c
d
B
Tracks/ 100 µm² / min
60
40
20
0
-Ag
+Ag
*
**
*
0
5
11
16
21
27
32
37
Growth rate (µm/min)

Fig. S3

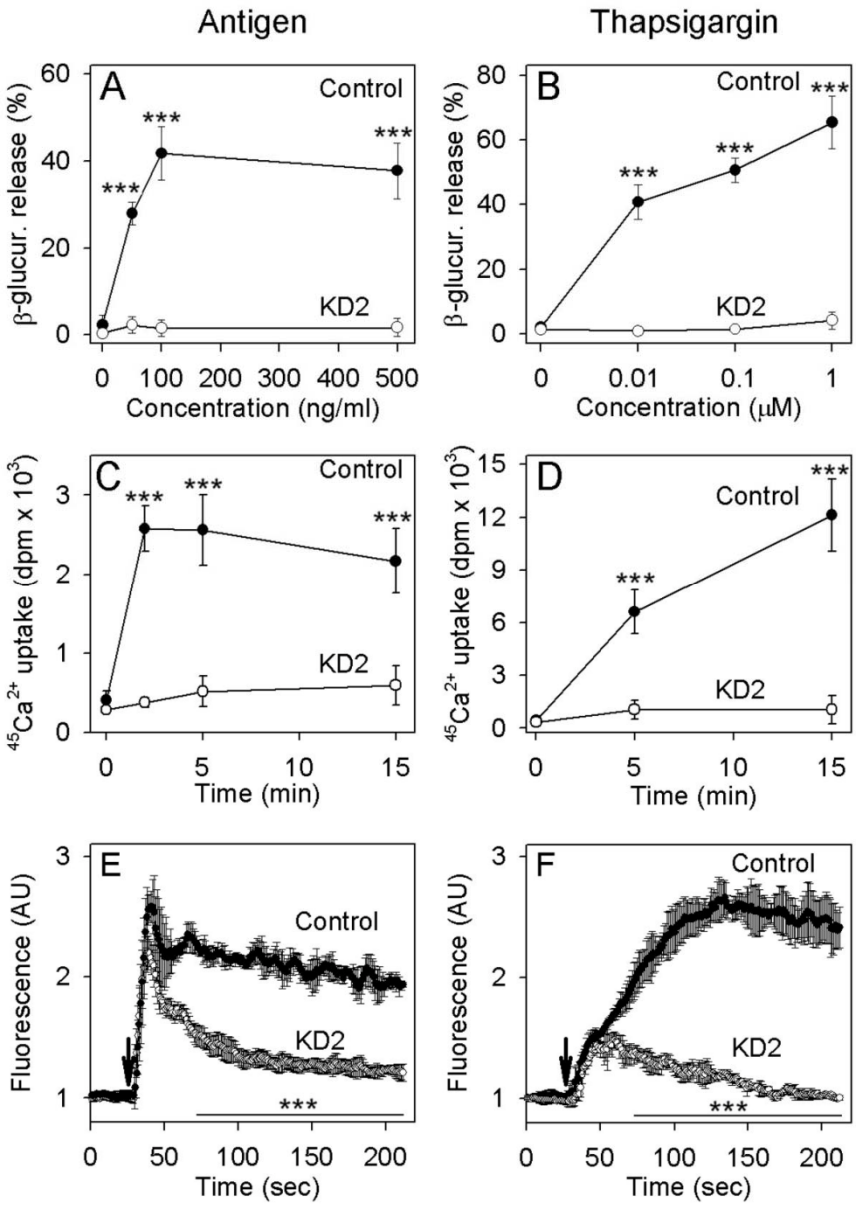
Antigen
Thapsigargin
A
B
C
D
E
F
Control
KD2
β-glucur. release (%)
Concentration (ng/ml)
Concentration (μM)
45Ca2+ uptake (dpm x 10^3)
Time (min)
Fluorescence (AU)
Time (sec)
***

1,2-propanediol-trehalose mixture as a potent quantitative real-time PCR enhancer

BMC Biotechnol. 2011 Apr 18;11:41. doi: 10.1186/1472-6750-11-41

Horáková et al. BMC Biotechnology 2011, 11:41
http://www.biomedcentral.com/1472-6750/11/41

BMC Biotechnology

METHODOLOGY ARTICLE Open Access

1,2-propanediol-trehalose mixture as a potent quantitative real-time PCR enhancer

Helena Horáková, Iva Polakovičová, Gouse M Shaik, Jiří Eitler, Viktor Bugajev, Lubica Dráberová and Petr Dráber*

Abstract

Background: Quantitative real-time PCR (qPCR) is becoming increasingly important for DNA genotyping and gene expression analysis. For continuous monitoring of the production of PCR amplicons DNA-intercalating dyes are widely used. Recently, we have introduced a new qPCR mix which showed improved amplification of medium-size genomic DNA fragments in the presence of DNA dye SYBR green I (SGI). In this study we tested whether the new PCR mix is also suitable for other DNA dyes used for qPCR and whether it can be applied for amplification of DNA fragments which are difficult to amplify.

Results: We found that several DNA dyes (SGI, SYTO-9, SYTO-13, SYTO-82, EvaGreen, LCGreen or ResoLight) exhibited optimum qPCR performance in buffers of different salt composition. Fidelity assays demonstrated that the observed differences were not caused by changes in Taq DNA polymerase induced mutation frequencies in PCR mixes of different salt composition or containing different DNA dyes. In search for a PCR mix compatible with all the DNA dyes, and suitable for efficient amplification of difficult-to-amplify DNA templates, such as those in whole blood, of medium size and/or GC-rich, we found excellent performance of a PCR mix supplemented with 1 M 1,2-propanediol and 0.2 M trehalose (PT enhancer). These two additives together decreased DNA melting temperature and efficiently neutralized PCR inhibitors present in blood samples. They also made possible more efficient amplification of GC-rich templates than betaine and other previously described additives. Furthermore, amplification in the presence of PT enhancer increased the robustness and performance of routinely used qPCRs with short amplicons.

Conclusions: The combined data indicate that PCR mixes supplemented with PT enhancer are suitable for DNA amplification in the presence of various DNA dyes and for a variety of templates which otherwise can be amplified with difficulty.

Background

Advances in the methodology of qPCR contributed significantly to a widespread use of this method for DNA genotyping, gene expression analysis and mutational scanning. Several different systems have been developed for continuous monitoring of the production of PCR amplicons and characterization of their properties. Widely used are sequence-specific probes which facilitate a highly sensitive detection of specific PCR products. However, these probes are difficult to prepare and are relatively expensive [1]. An alternative to the probe-based methods is the use of DNA-intercalating dyes which at concentrations compatible with PCR-mediated DNA amplification exhibit enhanced fluorescence after binding to double-stranded (ds)DNA. These dyes are less expensive, but they are also less specific because they bind to all dsDNAs present in PCR mixtures, including nonspecific products and primer-dimers. Although some of these unwanted DNA species can be distinguished by analysis of the melting curves of PCR amplicons, their presence reduces the sensitivity of qPCR and requires a proper adjustment of PCR conditions. Biophysical studies showed that DNA dyes bind to dsDNA by intercalation and external binding, and that these interactions could interfere with PCR [2-4]. Furthermore, it has been shown that the dyes also react with single-stranded (ss)DNA oligonucleotide primers [2] and that this binding could inhibit annealing of the

* Correspondence: petr.draber@img.cas.cz
Department of Signal Transduction, Institute of Molecular Genetics, Academy of Sciences of the Czech Republic, Vídeňská 1083, 142 20 Prague 4, Czech Republic

Horáková et al. BMC Biotechnology 2011, 11:41
http://www.biomedcentral.com/1472-6750/11/41

primers to the template during PCR [5]. This could account for some difficulties in amplifying certain DNA fragments, which are otherwise easily amplified in the absence of the dyes.

In initial studies, real-time accumulation of PCR amplicons was evaluated with ethidium bromide [6]. This dye was later substituted with SGI [7], which quickly became the most-widely used DNA dye for qPCR monitoring. Recently, several other DNA dyes have been introduced giving a strong fluorescence signal with dsDNA at concentrations not inhibiting PCR. These include YO-PRO-1 [8], BEBO [9], LCGreen [10], SYTO-9 [4,11], EvaGreen [3], SYTO-13, SYTO-82 [11] and LightCycler 480 ResoLight dye [12,13].

We have found that SGI inhibits amplification of medium-size genomic DNA fragments and that this inhibitory effect can be reduced by using a PCR mix, denoted here as mix IV, with modified salt composition [5]. In this study, we compared qPCR performance of seven DNA dyes (Table 1) in the mix IV and three other widely used PCR mixes of different salt composition. We found that amplification in the presence of SGI was optimal in mix IV, whereas all other dyes performed better in a mix marked here as mix II. To find out conditions which would allow efficient amplification of difficult-to-amplify DNA templates, such as those in whole blood and/or GC-rich and compatible with various DNA dyes, we tested various additives and their combinations. Excellent performance was found when PCR mix II was supplemented with PT enhancer. Extensive testing showed that PT enhancer-containing mix II could be used for efficient amplification of various DNA templates known to resist amplification under various routinely used conditions. The data have implications for a more rational design and routine use of qPCR assays.

Table 2 PCR mixes used and their composition

Component**	PCR mixes*			
	I	II	III	IV
Tris-HCl (mM) [pH]***	10 [8.0]	75 [8.8]	10 [8.0]	20 [8.8]
KCl (mM)	50	-	50	10
$(NH_4)_2SO_4$ (mM)	-	20	-	10
$MgSO_4$ (mM)	-	-	-	2
Triton X-100 (%)	0.1	-	0.1	0.1
Tween 20 (%)	-	0.01	-	-
$MgCl_2$ mM	2.5	2.5	2.5	-
DMSO (%)	-	-	5	-
dNTPs µM	200	200	200	200
Tac DNA pol. (U/ml)	25	25	25	25
anti-Taq mAb (nM)	22	22	22	22

* Final concentrations of the component during PCR.

** Components present at the same concentrations in all mixes include 200 µM dNTPs, Taq DNA pol. (25 U/ml) and anti-Taq mAb (22 nM). Oligonucleotide primers, DNA templates, DNA dyes and additives/enhancers were added immediately before the assay.

*** pH at 21°C.

Results

PCR with difficult-to-amplify templates

In our previous study we showed that amplification of the 864 base pairs (bp) genomic fragment of mouse Thy-1 can be achieved only in a PCR mix denoted here as mix IV [5]. In this study, we first tested whether the mix IV was also optimal for qPCR analysis with other DNA dyes. We compared amplification of Thy-1 genomic DNA fragment in mix IV and in three other widely used PCR mixes combined with seven DNA dyes. Properties of all DNA dyes and composition of all PCR mixes used are shown in Table 1 and 2, respectively. When SGI was combined with PCR mix IV, amplification was observed at all dilutions of the template DNA with reasonable regression coefficient (R^2 = 0.996 ± 0.003; mean ± SD; n = 6) and efficiency (E = 0.88 ±

Table 1 DNA dyes, their origin and properties

DNA dye	Origin	Stock concentration	Final concentration	Absorption maximum	Emission maximum
SGI	Invitrogen	10 mM in DMSO*	0.32 µM	497	520
SYTO-9	Invitrogen	5 mM in DMSO	2 µM	485	498
SYTO-13	Invitrogen	5 mM in DMSO	2 µM	488	509
SYTO 82	Invitrogen	5 mM in DMSO	2 µM	541	>560
EvaGreen	Biotium	25 mM in DMSO	1.32 µM	500	>530
LCGreen	Idaho	10 × concentrated	1×	440 470	470 520
ResoLight	Roche	20 × concentrated	1×	450 500	487

* [3]

Horáková et al. BMC Biotechnology 2011, 11:41
http://www.biomedcentral.com/1472-6750/11/41

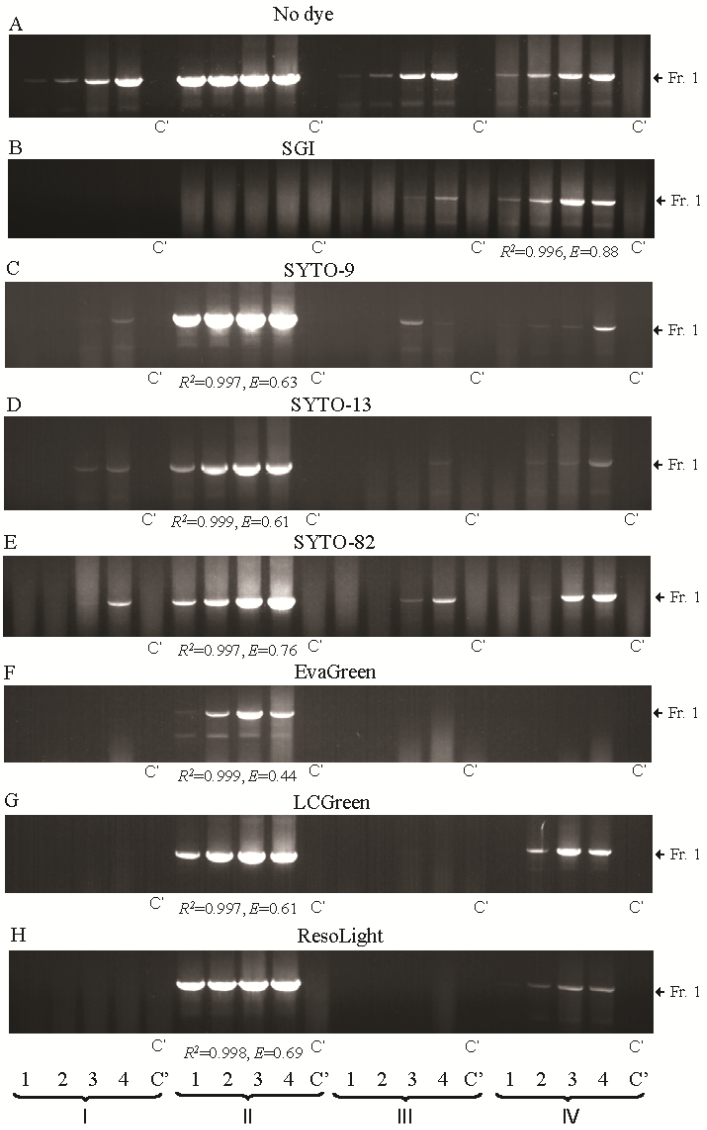

Figure 1 Amplification of genomic DNA fragments in various combinations of PCR mixes and DNA dyes. Isolated genomic DNA was diluted to contain 47 (1), 141 (2), 423 (3) 1269 (4) or none (Control; C') copies of Thy-1 gene per one μl of different PCR mixes (I - IV) supplemented without (A) or with (B - H) various DNA-binding dyes. The samples were analyzed by PCR (A) or qPCR (B - H) followed by agarose gel electrophoresis; DNA fragments were visualized by ethidium bromide staining. Migration of the specific DNA fragment (864 bp) is indicated by an arrow (Fr. 1). Regression coefficients (R^2) and efficiencies (E) were calculated from plots of Cq values versus log copy numbers, and are presented only for samples with the expected melting temperature at all template dilutions. All samples were analyzed in 3 - 7 independent experiments with similar results.

Horáková et al. BMC Biotechnology 2011, 11:41
http://www.biomedcentral.com/1472-6750/11/41

0.11). In all other mixes amplification of the fragment was either absent (mix I and II) or poor (mix III). These data were confirmed by agarose gel electrophoresis (Figure 1B). Poor amplification in PCR mixes I - III was obviously caused by the presence of SGI, since Thy-1 was reproducibly amplified in its absence (Figure 1A). Changing the Mg^{2+} concentration or optimizing the annealing temperature failed to improve the reaction in mixes I - III. It should be noted that the amount of Thy-1 amplicons in mix IV was similar regardless of the presence or absence of SGI (compare Figure 1A and 1B), indicating that the salt composition of PCR mixes has a decisive role on the inhibitory effect of SGI.

When the same fragment was amplified in SYTO-9-supplemented PCR mixes, a different profile was obtained: strong amplification (R^2 = 0.997, E = 0.63) was observed in mix II, but only week and variable amplification, as detected by melting curve analysis and gel electrophoresis, was observed in mixes I, III and IV (Figure 1C). Mix II was also optimal for other DNA dyes (SYTO-13, SYTO-82, EvaGreen, LCGreen and ResoLight; Figure 1D - H). Interestingly, inhibition of PCRs by different dyes varied in different mixes. In mix I, for example, amplification of Thy-1 DNA fragment was only observed at high concentrations of the template in the following order: SYTO-82 > SYTO-9 = SYTO-13. In mix III, some reactivity was observed with the following dyes: SYTO-82 > SGI = SYTO-9 = SYTO-13. In mix IV, Thy-1 amplification was seen in mixes supplemented with SGI > LCGreen > SYTO-82 > ResoLight > SYTO-9 = SYTO-13. In several combinations of PCR mixes and DNA dyes, complete inhibition of amplification was noted: SGI in mixes I and II, EvaGreen in mixes I, III and IV and LCGreen and ResoLight in mixes I and III. This inhibition persisted even when concentration of $MgCl_2$ was raised up to 5 mM (data not shown).

Fidelity assays

The observed difficulties with amplification of medium-size genomic DNA fragments in some PCR mixes might in part reflect an enhanced mutagenesis interfering with the synthesis of DNA fragments [14]. To find out whether salt composition of PCR mixes and the presence of DNA dyes could affect the fidelity of PCRs, we used an assay system based on streptomycin resistance of *rpsL* mutants [15]. Data presented in Table 3 show that in mix I the error rate was 3.88×10^{-7}. A similar error rate was observed in mix II and an approximately two-fold increase in mix III and IV. To prove the sensitivity of the fidelity assay, we also amplified the template using KOD polymerase in a reaction mix of undisclosed composition provided by the manufacturer of the enzyme. As expected, amplification with KOD polymerase resulted in substantially lower error rate (7.6×10^{-5}), which is in agreement with the manufacturer's data. When PCR mix II was supplemented with SYTO-9, SYTO-13, EvaGreen, LCGreen or ResoLight, no dramatic changes in mutation frequencies were observed (Table 3). These findings indicate that different mutation frequencies in different PCR mixes cannot by themselves explain the observed changes in amplification efficiency caused by various DNA dyes.

New universal PCR master mix

In an attempt to develop a universal PCR master mix compatible with all the DNA dyes and suitable for amplification of DNA templates that cannot be readily amplified due to dye interference, presence of inhibitory substances and/or secondary structure formation, we tested several additives combined with mixes I - IV and various DNA dyes. As a template we used GC-rich DNA fragment of Q8N1R6 gene (Table 4; 806 bp, 73.3% GC) in human heparinized blood which escaped

Table 3 Effect of the tested PCR mixes and selected DNA dyes on DNA polymerase fidelity

Sample	Colonies mutant/total	Template doubling[a]	Mutation frequency[b]	Error rate (× 10^{-6})[c]
Taq in mix I	362/57?9	12.5	0.063	38.8
Taq in mix II	990/16342	10.9	0.061	43.0
Taq in mix III	2760/21423	12.4	0.129	80.0
Taq in mix IV	951/8273	11.7	0.115	75.6
KOD in mix K[d]	30/25006	12.1	0.0012	0.76
Various DNA dyes in PCR mix II				
SYTO-9	318/4845	9.1	0.066	46.0
SYTO-13	640/10087	9.2	0.063	44.7
EvaGreen	307/5607	9.2	0.054	38.6
LCGreen	211/4058	9.0	0.052	35.8
ResoLight	64/1243	9.1	0.052	36.2

[a] Template doublings (d) were calculated using the equation 2^d = (amount of PCR product)/(amount of starting target).

[b] Mutation frequency = (mutant colonies)/(total colonies).

[c] Error rate = (mutation frequency)/(130 × d).

[d] PCR mix provided by KOD enzyme manufacturer

Horáková et al. BMC Biotechnology 2011, 11:41
http://www.biomedcentral.com/1472-6750/11/41

Table 4 Oligonucleotide primer sets and PCR amplicon properties

No	Gene*	Chromosome			Amplicon	Primer (5'-3')
	Name	No.	Position (Start-End)**	%GC	Fragment (bp)/name	Forward/reverse
Pr. 1	Thy-1	9	43854065-43854933	53.6	869/Fr. 1	ATGAACCCAGCCATCAGCG/GGGT4AGGACCT"G4TATAGG
Pr. 2	NTAL	5	135085842-135086225	50.8	384/Fr. 2	CTAGGGAGCTGAGTGT"CTCA/GAACGGCTAGAAC"ACACAGAG
Pr. 3	NP_660313.1	16	613645-614375	71.5	731/Fr. 3	GGTCGCCGACATCCAC"C/TGC"CCGGGAACAGAACCT
Pr. 4	Q8WZ58	11	2292033-2292813	71.7	781/Fr. 4	CCTGACCGTCCTGGCACA/CTGGCGAAATCTGCGAGTTC
Pr. 5	NP_060192.2	9	140"74905-140175662	72.4	758/Fr. 5	CCCC"CACTCAGGTCGTGTTTT/CCCTC"GAGCCCCTTTCG
Pr. 6	Q8N4X1	16	2029023-2029774	72.6	752/Fr. 6	CGG"CCATCCCCTCATCG/ACCCCTCACGCCACCAC
Pr. 7	NP_001035158.1	16	33961629-33962363	73.1	735/Fr. 7	CGGCGAACCGGAC4TCC/GGCTCGTGAGGCGGG"CT
Pr. 8	Q8N1R6	13	111267817-111268622	73.3	806/Fr. 8	GACACGGCCCTGCTCC/GGGTGTGATTGAGCGAGTTG
Pr. 9	NM_020975	10	43572323-43572724	79.1	392/Fr. 9	CCCGCACTGAGC"CCTACAC/GGACGTCGCCTTCGCCATCG

* Homo_sapiens LATESTGP database was used, except for Thy-1 and NTAL for which Mus_musculus LATESTGP database was used.
** Primer sets Pr. 3 - Pr. 9. are based on Ensembl release 56 - Sept 2009

detection under standard conditions using various commercial PCR master mixes such as iQ™ SYBR Green Supermix and LightCycler 480 SYBR Green I Master (LC 480 SGI). In pilot experiments various mixes were combined with several additives and/or procedures, which have been reported to allow amplification of GC-rich fragments and/or neutralize PCR inhibitory components present in the blood (hemoglobin, lactoferrin and immunoglobulin G [16,17]). These included 0.1 - 0.5 M trehalose (final concentration) [18], 5 - 15% dimethyl sulfoxide (DMSO) [19,20], 0.5 - 2.5 M N,N,N-trimethylglycine monohydrate (betaine) [21,22], combinations of 5 - 15% DMSO and 2.2 M betaine [23], 5 - 25 mM tetrapropylammonium chloride [5], 0.5 - 1.5 M 1,2-propanediol, 0.5 - 1.5 M ethyleneglycol [24], 50 - 150 μM 7-deaza-2'-deoxyguanosine 5'-triphosphate [25,26], PCR-enhancing coctail containing 0.3 M D-(+)-trehalose, 0.24 M L-carnitine, and 0.4% Nonidet P-40 (TCN) [27] and antibody-mediated hot start PCR [5] combined with "touchdown" procedure [28,29]. Yet, none of these additives and/or procedures improved PCR to get specific signal determined by agarose gel electrophoresis (data not shown). Interestingly, specific amplicons were observed in PCR mix II supplemented with both 1 M 1,2-propanediol and 0.2 M trehalose (mix II-PT); higher or lower concentrations of these two additives resulted in inhibition of production of the specific amplicons and/or enhanced formation of nonspecific DNA fragments (Figure 2).

Mix II-PT allowed efficient amplification of numerous gene fragments in heparin-treated whole blood, including mouse Thy-1 and NTAL (data not shown) and, as shown in Figure 3 (mix II-PT), GC-rich fragments of the human genes NP_660313.1 (Table 4; 71.5% GC, 731 bp), Q8WZ58 (71.7% GC, 781 bp), NP_060193.2 (72.4% GC, 758 bp), Q8N4X1 (72.6% GC, 752 bp), NP_001035158.1 (73.1% GC, 735 bp), and Q8N1R6 (73.3% GC, 806 bp). PT enhancer also allowed efficient amplification of 392 bp DNA fragment with 79.1% GC (Table 4; [26]) from whole blood which was resistant to amplification under standard conditions (data not shown). In its enhancing capacity mix II-PT surpassed the TCN enhancer [27], which was capable of amplifying only one of the six GC-rich templates tested (Figure 3, mix II-TCN). Similar results were obtained when blood samples were treated with other commonly used anticoagulants, 2.7 mM EDTA or 0.38% sodium citrate (data not shown).

Next we tested qPCR performance of various DNA dyes in mix II-PT during amplification of the GC-rich fragment (72.6% GC, 752 bp) of Q8N4X1 gene in whole human blood. Pilot experiments indicated that different dilutions of whole human blood in water, followed by qPCR in mix II-PT with SGI resulted in poor regression coefficients. This was probably caused by simultaneous dilution of the DNA templates and the inhibitory (e.g. hemoglobin [17]) and/or stimulatory (e.g. heparin [30]) components present in the whole blood samples. However, when human blood was diluted with mouse blood

Horáková et al. BMC Biotechnology 2011, 11:41
http://www.biomedcentral.com/1472-6750/11/41

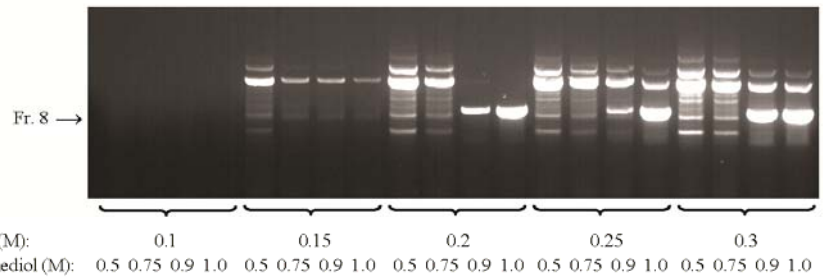

Figure 2 Amplification of medium-size GC-rich DNA fragment using whole blood as a source of the template. 806 bp fragment of human Q8N1R6 gene (73.3% GC) in heparinized human blood (2% final concentration) was amplified in PCR mix II containing various concentrations of trehalose (0.1 - 0.3 M) and 1,2-propanediol (0.5 - 1.0 M). Position of the specific product (Fr. 8) is shown by an arrow. A typical result of three independently performed experiments is shown.

to keep the concentration of human/mouse blood in PCR constant (2%), reasonable regression coefficients (R^2 = 0.986 ± 0.006; mean ± S.D.; n = 4) and efficiencies (E = 0.95 ± 0.03) were obtained. Amplification of non-specific fragments after 40 cycles of PCR was low, as determined by agarose gel electrophoresis (Figure 4, top, left). Under the same conditions other DNA dyes also gave satisfactory results in the following order (based on regression coefficients): SGI > ResoLight > SYTO-9 > LCGreen > SYTO-13 > EvaGreen (Figure 4). Thus, Mix II-PT is unique in its capability to serve as universal qPCR mix for all DNA dyes tested.

PCR mix II-PT could be used with advantage not only for amplification of DNA fragments from crude blood samples that are difficult to amplify, but also for routine qPCR analysis of cDNA fragments without time-consuming adjustment of qPCR conditions for individual primer sets. Data presented in Figure 5A show that for amplification of 138 bp fragment of actin cDNA (58% GC) mix II-PT supplemented with SGI gave comparable regression coefficients and efficiencies as the routinely used LC 480 SGI. Similar results were obtained when GAPDH cDNA fragment was analyzed (Figure 5B; 52% GC, 69 bp). However, when low abundant cDNA fragments were amplified, such as ORMDL1_Fr.a

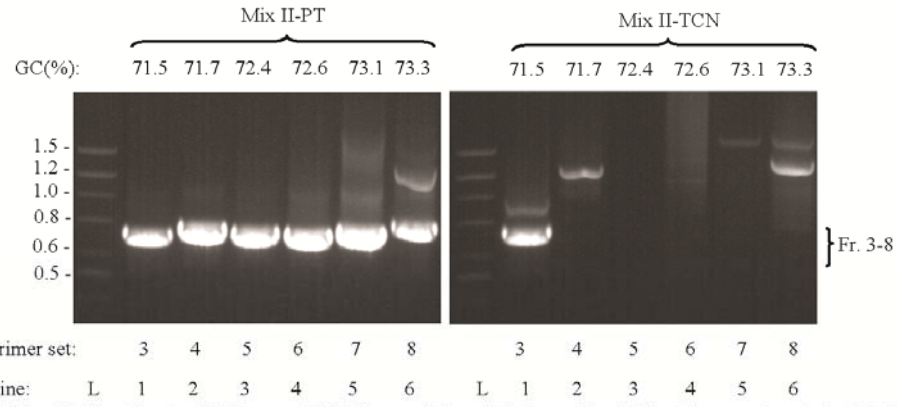

Figure 3 Amplification of various GC-rich genomic DNA fragments from whole human blood. PCR mix II was supplemented with 1 M 1,2-propanediol and 0.2 M trehalose (final concentrations; Mix II-PT) or 0.3 M trehalose, 0.24 M L-carnitine, and 0.4% Nonidet P-40 (Mix II-TCN). Various GC-rich templates from heparinized whole human blood (~100 copies of the template/μl of PCR mixture) were amplified in the two PCR mixes using primer sets specified in Table 4. Positions of the specific fragments (731-806 bp in size) are indicated on the right (Fr. 3-8). Lane L, DNA standard ladder with sizes indicated in kbp on the left. The numbers at the top indicate percentages of GCs in specific amplicons. A typical experiment of at least four performed is shown.

Horáková et al. BMC Biotechnology 2011, 11:41
http://www.biomedcentral.com/1472-6750/11/41

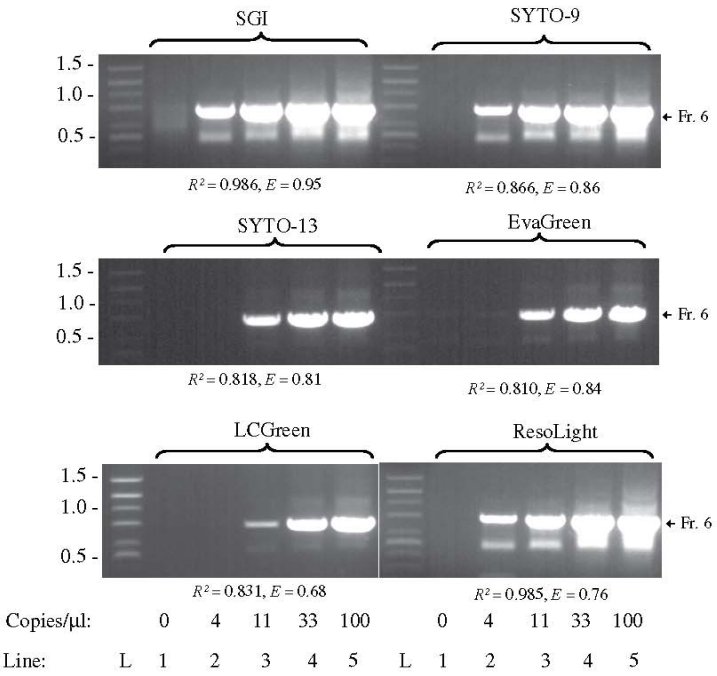

Figure 4 Amplification of GC-rich DNA fragment from whole blood in the presence of various DNA dyes. Human blood was diluted with mouse blood to yield 0, 4, 11, 33 and 100 copies of human Q8N4X1 gene per 1 µl of PCR reaction mix II supplemented with PT enhancer and various DNA dyes. Final concentration of human/mouse blood was 2% in all mixes. The samples were analyzed by qPCR followed by agarose gel electrophoresis and staining with ethidium bromide. Position of the specifically amplified DNA fragment is indicated by an arrow (Fr. 6). Lane L, DNA standard ladder with sizes indicated in kbp on the left. Regression coefficients (R^2) and efficiencies (E) were calculated from plots of Cq values versus log copy numbers. All samples were analyzed in 3-4 independent experiments with similar results.

(Figure 5C; 43% GC, 171 bp) or ORMDL1_Fr.b (Figure 5D; 47% GC, 205 bp), detectable amplification at all concentrations of template cDNA and reasonable regression coefficients and efficiencies were obtained only in mix II-PT-supplemented samples. Interestingly, addition of 1,2-propanediol and/or trehalose at various concentrations to LC 480 SGI containing chemically modified Taq DNA polymerase did not improve performance of this PCR mix, but instead had an inhibitory effect (data not shown).

Fluorescence measurements and melting temperatures

In our previous study we showed that SGI bound to ssDNA primers and suggested that the binding could at least in part contribute to the inhibitory effect of SGI in qPCR assays [5]. In further studies we evaluated whether trehalose and/or 1,2-propanediol could interfere with interaction of various DNA dyes with ssDNA, as reflected by changes in fluorescence signal. Data presented in Figure 6A indicate that interaction of various DNA dyes (at concentrations used for qPCR) with ssDNA oligonucleotide primer for tumor necrosis factor (TNF; 45.5% GC) induced fluorescence in the following order: SGI < SYTO-13 < LCGreen < SYTO-9 < EvaGreen < ResoLight. Addition of 0.2 M trehalose had little to no inhibitory effect on this fluorescence. In contrast, 1,2-propanediol significantly ($P < 0.05$; $n = 3$-5) decreased fluorescence in all DNA dyes used, except for SGI. Combination of both 1,2-propanediol and trehalose had a similar effect as 1,2-propanediol alone. When ssDNA primer No. 7, reverse (Table 4; 72.2% GC) was used, basal level of fluorescence was increased in all DNA dye-enhancer combinations and again trehalose had no significant effect on fluorescence intensity. In contrast to trehalose, 1,2-propanediol significantly ($P < 0.05$; $n = 4$) decreased fluorescence, except for SGI and ResoLight (Figure 6B).

Horáková et al. BMC Biotechnology 2011, 11:41
http://www.biomedcentral.com/1472-6750/11/41

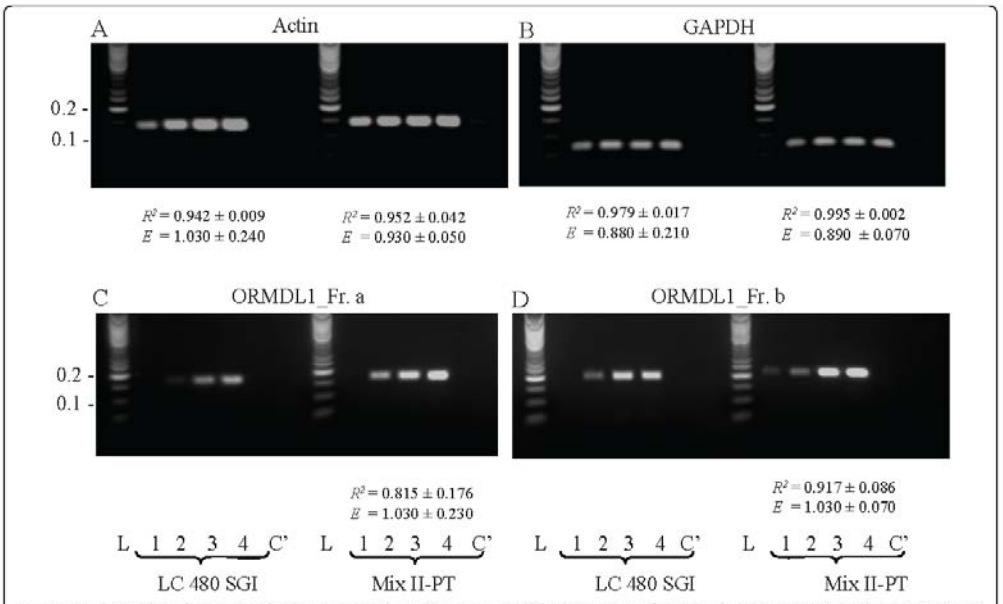

Figure 5 Enhanced performance of PCR mix II-PT in routine qPCR amplifications. cDNA from mouse bone marrow-derived mast cells was prepared, diluted 1:10^5 (1), 1:10^4 (2), 1:10^3 (3) or 1:10^2 (4) and amplified in SGI-supplemented PCR mix II-PT or LC 480 SGI using primer sets for Actin, GAPDH, ORMDL1_Fr. a or ORMDL1_Fr. b. In controls (C'), cDNA was replaced by H_2O. The samples were analyzed by qPCR followed by agarose gel electrophoresis and staining with ethidium bromide. Lane L, DNA standard ladder with sizes indicated in kbp on the left. Regression coefficients (R^2) and efficiencies (E) were calculated from the plots of Cq values versus log copy numbers and are presented only for samples with the expected melting temperature at all template dilutions. Data are presented as means ± S.D. calculated from three independent experiments performed in triplicates.

In an attempt to understand the enhancing effect of trehalose and 1,2-propanediol on qPCR performance, we also evaluated the melting temperatures of short dsDNA oligonucleotides. When dsDNA of TNF and anti-TNF (45.5% GC) was used, the melting temperature depended on DNA dye used (Figure 6C). The highest melting temperature was observed in control mix II supplemented with EvaGreen, followed by SGI > ResoLight > Syto-9 > LCGreen > Syto-13. Addition of 0.2 M trehalose decreased the melting temperature by 0.7 - 1.5°C, whereas addition of 1 M 1,2-propanediol decreased it by 4.9 - 5.9°C. When both trehalose and 1,2-propanediol were used, further decrease by 1.1 - 1.5°C was observed. Using dsDNA oligonucleotide with 72.2% GC, melting temperature was increased but a similar effect of trehalose and 1,2-propanediol was observed (Figure 6D).

Cooperative effect of 1,2-propanediol and trehalose

The above data suggested that 1,2-propanediol and trehalose have different roles in promoting DNA amplification of GC-rich DNA fragments from crude blood samples: trehalose mainly acts by neutralizing the inhibitory components present in blood, whereas 1,2-propanediol mainly acts by decreasing melting temperature. To prove this, we compared the effect of the enhancers on amplification of GC-rich fragments from whole blood or isolated DNA. As expected, efficient amplification of DNA template in whole blood, occurred only in samples supplemented with both 1,2-propanediol and trehalose (Figure 7A, line 3). In contrast, when isolated GC-rich DNA fragment was used as a template, comparable amplification was observed in samples supplemented with 1,2-propanediol alone or together with trehalose (Figure 7A, lines 6 and 7). Trehalose alone was not able to promote amplification of the DNA templates (Figure 7A, lines 1 and 5).

When PCR mix was supplemented with SGI and isolated DNA was amplified, a different picture was observed. SGI partially inhibited amplification in 1,2-propanediol-supplemented samples (Figure 7B, line 2). This inhibition was caused by SGI as indicated by no inhibition in samples containing vehicle (DMSO) instead of SGI (Figure 7B, line 6). PCR mixes supplemented with both 1,2-propanediol and trehalose exhibited an

Horáková et al. BMC Biotechnology 2011, 11:41
http://www.biomedcentral.com/1472-6750/11/41

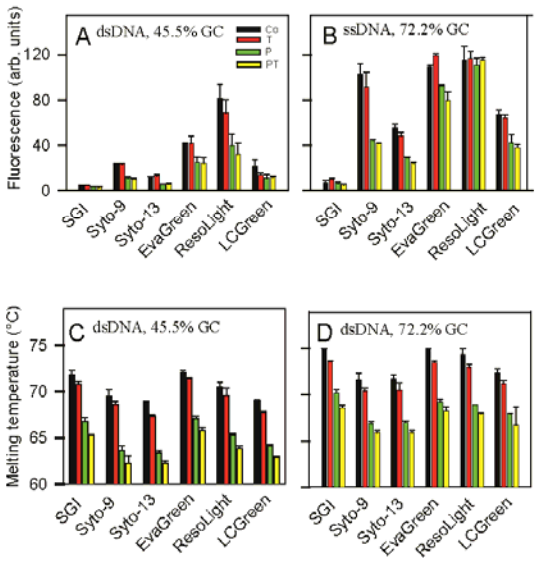

Figure 6 The effect of various DNA dyes and enhancers on ssDNA fluorescence and dsDNA melting temperature. (A) TNF-1 oligonucleotide (ssDNA, 45.5% GC; 1 μM final concentration) in PCR mix II (without dNTPs, Taq DNA polymerase and anti-Taq) was mixed with H_2O (Control; Co) or enhancers [0.2 M trehalose (T; final concentration), 1 M 1,2-propanediol (P) or both 1 M 1,2-propanediol and 0.2 M trehalose (PT)] and various DNA dyes at final concentrations as indicated in Table 1. After heating at 95°C for 2 min the samples were cooled to 50°C and fluorescence was determined using Mastercycler ep realplex. (B) Oligonucleotide primer No 7, reverse (ssDNA; 72.2% GC; 1 μM final concentration) in PCR mix II was combined with various additives and DNA dyes, and fluorescence at 50°C was determined as in A. (C) Oligonucleotide mixture of TNF-1 and anti-TNF-1 (dsDNA, 45.5% GC; 1 μM final concentration) was prepared in mix II supplemented with various additives and DNA dyes. The samples were heated to 95°C for 2 min, then cooled to 30°C and temperature-dependent changes in fluorescence were obtained during heating from 30 to 95°C (0.2°C increments) in Mastercycler ep realplex. Melting temperatures were determined from the melting curves. (D) Oligonucleotide mixture of the primer No 7, reverse, and the anti-primer 7 (dsDNA, 72.2% GC; final concentration 1 μM) was combined in mix II with additives and DNA dyes and analyzed as in C. Means ± S.D. were calculated from 3 - 5 measurements.

improved amplification in SGI-supplemented samples (Figure 7B, line 3) indicating cooperative effect of the enhancers in SGI-supplemented samples.

Next we tested the effect of trehalose and 1,2-propanediol on amplification of isolated DNA in samples supplemented with hemoglobin. Pilot experiments showed that hemoglobin completely inhibited PCR at concentrations 25 μM and higher (data not shown). Data in Figure 8A indicate that the inhibitory effect of hemoglobin (37.5 μM) was removed by addition 1,2-propanediol and trehalose together but not by trehalose or 1,2-propanediol alone.

To understand the effect of the enhancers on amplification in the presence of blood inhibitors, we analyzed melting temperatures of dsDNA. We found that hemoglobin at the inhibitory concentration (37.5 μM) significantly decreased melting temperature of short dsDNA fragments by 5.8 ± 0.6°C (mean ± S.D.; n = 4). Addition of trehalose, 1,2-propanediol or both enhancers to hemoglobin-supplemented samples further decreased Tm by 2.1 ± 1.6°C, 4.4 ± 0.6°C and 4.8 ± 0.6°C, respectively (Figure 8B). These data suggested direct or indirect interaction of hemoglobin with DNA. The direct interaction was however weak, if any, as indicated by similar mobility in agarose gel of DNA fragments alone and DNA fragments mixed with hemoglobin (37.5 μM; data not shown).

Finally, we tested whether blood inhibitors could interfere with enzymatic activity of Taq DNA polymerase as determined by incorporation of [α-^{32}P]dATP into activated salmon testes DNA. Data presented in Figure 8C indicate that blood at the inhibitory concentration (10%) significantly reduced activity of Taq DNA polymerase. Addition of trehalose significantly ($P < 0.05$) decreased the enzymatic activity of Taq DNA polymerase in control samples (- blood), but slightly increased the activity in blood-supplemented samples, leading to statistically non-significant differences between the

Horáková et al. BMC Biotechnology 2011, 11:41
http://www.biomedcentral.com/1472-6750/11/41

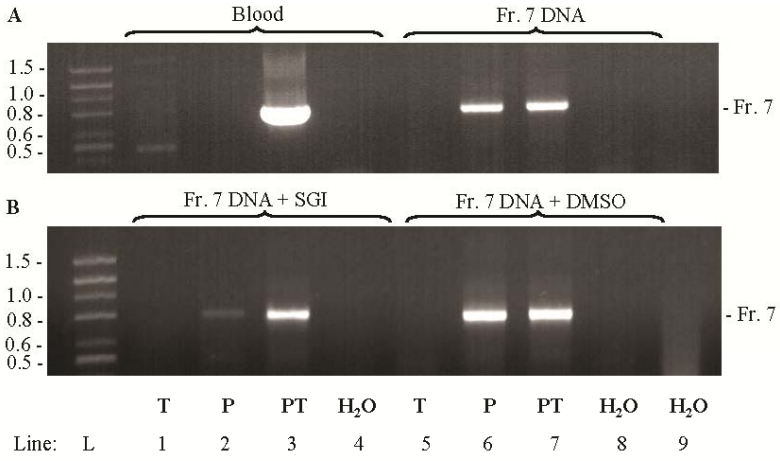

Figure 7 Cooperative effect of 1,2-propanediol and trehalose on amplification of difficult-to-amplify DNA templates. (A) DNA fragment of the human gene NP_001035158.1 (Fr. 7; 735 bp; 73.1% GC) was amplified from the whole blood (2% final) in PCR mix II supplemented with 0.2 M trehalose (T, final concentration), 1M 1,2-propanediol (P) or mixture of both (PT). Alternatively, PCR-amplified DNA (Fr. 7) was diluted in H_2O and used as a template for PCRs performed under various conditions as above. PCR mixes supplemented with H_2O instead of enhancers (line 4 and 8) and a mix without enhancers and template (line 9) served as controls. After amplification the fragments were analyzed by agarose gel electrophoresis and stained with ethidium bromide. (B) PCR amplified DNA (Fr. 7) was re-amplified and analyzed as in A, except that PCR mix II was supplemented with SGI (left) or vehicle (DMSO) alone (right). After amplification the fragments were analyzed by agarose gel electrophoresis and stained with ethidium bromide. Numbers to the left indicate migration of DNA ladder (L; in kbp). Gels from a typical experiment of at least four performed are shown.

control and blood-supplemented samples. 1,2-propanediol decreased enzymatic activity of Taq DNA polymerase in both control and blood-supplemented samples; the difference between these two groups was statistically significant. Addition of trehalose to 1,2-propanediol-supplemented control samples (PT) further significantly decreased ($P < 0.05$) the activity of Taq polymerase. In contrast, in blood-supplemented samples there was small (insignificant) increase in activity of Taq DNA polymerase in PT-containing samples compared to samples containing 1,2-propanediol alone. This led to non-significant differences between control and blood-containing samples with PT. These data indicate that trehalose has a different effect on activity of Taq polymerase in control and blood containing samples. This could explain at least in part the enhancing effect of trehalose in samples containing blood inhibitors.

Discussion

The aim of this study was to develop new qPCR mixes capable of amplifying difficult DNA templates, such as those in whole blood, of medium size and/or GC-rich, in the presence of various DNA dyes. First, we assessed the properties of seven different DNA dyes in four widely used PCR buffers differing in salt composition. Our data indicate that the performance of various DNA dyes in qPCR is differently affected by salt composition of the PCR mixes. When genomic DNA fragment of mouse Thy-1 (864 bp) was amplified, SGI completely inhibited PCR in most of the PCR mixes. The only PCR mix which allowed efficient amplification of the Thy-1 fragment in the presence of SGI was mix IV, which differed from other mixes by the presence of both KCl and $(NH_4)_2SO_4$ and the substitution of $MgSO_4$ for $MgCl_2$. This mix had pH 8.8, which also contributed to its performance; when pH of this mix was decreased to 8.0, SGI-mediated inhibition of PCR was noticed (data not shown). Besides pH, salt composition also plays a role because SGI completely inhibited amplification in PCR mix II, which has the same pH as mix IV. When other dyes were tested, amplification in mix IV was completely (EvaGreen) or partially (SYTO-9, SYTO-13, ResoLight) inhibited or remained unchanged (LCGreen and SYTO-82). In contrast to SGI, other dyes allowed amplification of the Thy-1 genomic fragment when present in PCR mix II. This mix is unique among others by containing 20 mM $(NH_4)_2SO_4$ instead of KCl, enhanced concentration of Tris-HCl (75 mM) and inclusion of Tween 20 instead of Triton X-100 (Table 2). It should be mentioned that all PCRs were run under identical cycling

Horáková et al. BMC Biotechnology 2011, 11:41
http://www.biomedcentral.com/1472-6750/11/41

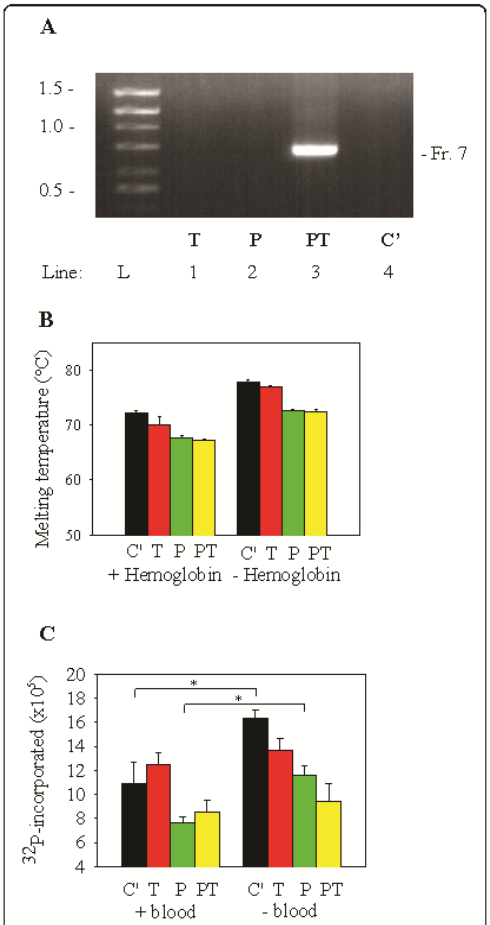

Figure 8 The effect of blood inhibitors and enhancers on PCR, melting temperature, and polymerase activity. (A) DNA fragment of NP_001035158.1 gene (Fr. 7; 735 bp; 73.1% GC) was amplified in PCR mix II supplemented with the corresponding primers, 37.5 μM hemoglobin and 0.2 M trehalose alone (T), 1 M 1,2 propanediol alone (P) or their combination (PT). PCR mix supplemented with H_2O instead of enhancers served as a control (C'). A typical experiment of four performed is shown. (B) Melting temperature of GC rich dsDNA oligonucleotide primer No 7, reverse, and the anti primer (72.2% GC; 1 μM final concentration) in the presence (+) or absence (-) of hemoglobin (37.5 μM) and various enhancers (as in A). Melting temperature was determined as in Figure 6, except that SGI was used at higher concentration (1.32 μM). (C) Enzymatic activity of Taq DNA polymerase in PCR mix II buffer supplemented with (+) or without (-) 10% blood and various enhancers (as in A). Samples supplemented with H_2O instead of enhancers (C') served as controls. Data in B and C indicate means ± S.D. (n = 4). Asterisks indicate statistically significant differences ($P < 0.05$).

conditions. Optimization of annealing temperature and cycling conditions for individual SGI-supplemented PCR mixes, however, resulted in no substantial improvement of PCR efficiency (data not shown). Neither was any improvement achieved by varying the concentration of Mg^{2+}. Since the concentrations of deoxynucleotide triphosphates (dNTPs), DNA polymerase and anti-Taq monoclonal antibody (mAb) were identical in all PCR mixes tested, it is likely that an interaction of DNA dye with ionic environment is responsible for the observed differences in qPCR performance. Both divalent and monovalent cations bind to DNA and affect its physical properties [31]. Thus, ionic environment and DNA dyes could affect DNA denaturation, annealing of oligonucleotide primers to the DNA template and/or activity of Taq DNA polymerase, including its enhanced mutation frequency which could inhibit PCR [14]. Our data indicate, however, that error rate was not dramatically affected and therefore it is unlikely that it could contribute to the observed differences in PCR mixes of different salt composition. Neither was fidelity of the Taq DNA polymerase affected by the presence of various DNA dyes.

Under more stringent conditions, such as amplification of medium-size GC-rich genomic fragments from crude blood samples, no amplification was observed in various commercial and home-made PCR mixes with or without DNA dye, and no dramatic improvement was achieved with additives and/or procedures recommended for amplification of GC-rich templates. These included supplementing PCR mixes with DMSO, betaine, trehalose, 1,2-propanediol or 7-deaza-2'-deoxyguanosine 5'-triphosphate, performing hot-start PCR under "touchdown" conditions, or with recently introduced PCR enhancing coctail containing trehalose, L-carnitin and Nonidet P-40 (Figure 3). It is likely that PCR product formation under such conditions was compromised by the presence of inhibitors present in blood (e g. hemoglobin), concurrently with inadequate strand separation due to higher GC content and/or formation of secondary structures reflecting Hoogsteen base pairing between successive guanosine bases. Furthermore, DNA templates may create intramolecular stem loops formed during initial cycles of amplification, leading to formation of hairpin structures that are resistant to amplification by Taq DNA polymerase in subsequent cycles of PCR [32].

Interestingly, strong and specific amplification was observed when PCR mix II was supplemented with both 1 M 1,2-propanediol and 0.2 M trehalose. This mix allowed efficient amplification in the presence of all DNA dyes tested, including SGI. Trehalose has been previously shown to enhance the yield of the amplified PCR products, and it has been speculated that it acts

Horáková et al. BMC Biotechnology 2011, 11:41
http://www.biomedcentral.com/1472-6750/11/41

through its thermostabilizing effect and/or lowering the template melting temperature [18,33]. However, it is unlikely that any of these two factors contributed individually to the observed effect of trehalose. In fact, the enzymatic activity of Taq DNA polymerase preincubated for 15 min at 95°C in mix II supplemented with 0.2 M trehalose (without blood inhibitors) was slightly decreased, rather than increased. Furthermore, although 0.2 M trehalose decreased melting temperature, this decrease was only marginal compared to the effect of other additives like DMSO or betaine which are routinely used as PCR enhancers.

1,2-propanediol at a final concentration 0.816 M has been recognized as an effective enhancer for amplification of medium-size GC-rich DNA sequences [24,34]. Although 1,2-propanediol surpassed 2.2 M betaine in its ability to amplify GC-rich templates [24] and decreased the melting temperature of dsDNA fragments (this study), it was unable on its own to surpass the inhibitory effect caused by the components present in the whole blood. Efficient amplification of such difficult-to-amplify templates was only achieved when 1,2-propanediol was combined with trehalose. It should be noted, that 1,2-propanediol slightly decreased enzymatic activity of Taq DNA polymerase. This inhibitory effect was however fully compensated by beneficial effects of 1,2-propanediol on PCR performance. Our finding of significant decrease of Taq DNA polymerase activity in samples supplemented with blood and even more with blood and 1,2-propanediol, and removal of this inhibitory effect after addition of trehalose suggest that trehalose acts by protecting the enzyme from negative interference of the blood inhibitors. Similarly, trehalose protected against the inhibitory effect of SGI, as indicated by enhanced amplification in the presence of both 1,2-propanediol and trehalose, compared to 1,2-propanediol alone.

In our previous study we found that SGI bound to ssDNA primers and interfered with annealing of the primers to DNA template; in this way SGI could, at least in part, contribute to its inhibitory effect on PCR [5]. In the present study we extended these tests to other DNA dyes and found that all of them bound to ssDNA oligonucleotides, as reflected by enhanced fluorescence. Importantly, for most of the dyes this binding was decreased by 1 M 1,2 propanediol. Extent of the inhibition depended on a combination of DNA dye used and GC content of the primers.

One of the PCR inhibitors present in blood is hemoglobin [17]. The inhibitory effect of hemoglobin on amplification of GC-rich DNA fragments was counteracted by addition of PT enhancer but not by 1,2-propanediol or trehalose alone. Although hemoglobin decreased melting temperature of dsDNA which was further decreased by the addition of 1,2-propanediol, it was still not sufficient for removal of its inhibitory effect. Interestingly, hemoglobin-containing samples supplemented with 1,2-propanediol or 1,2-propanediol and trehalose exhibited similar melting temperature, suggesting again that PT enhancer does not increase PCR performance solely by decreasing melting temperature.

Zhang and collaborators recently described a TCN coctail which in combination with inhibitor-resistant Taq DNA polymerase mutants enabled efficient amplification of high-GC content DNA targets directly from crude blood samples [27]. However, when wild-type Taq DNA polymerase was used for PCR with TCN, only a fraction of GC-rich DNA templates in whole blood was amplified. Under identical conditions, PCR mix supplemented with PT enhancer efficiently amplified all fragments analyzed in this study. These data indicate that PT is a superior enhancer for amplification of difficult templates when wild type Taq DNA polymerase is used. PT enhancer can be used as a universal enhancer suitable for normal targets, GC-rich targets (up to 79% GC) and/or targets in the presence of PCR inhibitors. PCR mix II supplemented with PT enhancer is suitable for DNA genotyping from whole blood without DNA extraction and is compatible with various DNA dyes. In order to get reasonable regression coefficients based on qPCR analyses of crude blood samples it is adviceable to dilute DNA templates present in human blood with e.g. mouse blood to keep the amount of the blood components in PCR constant. This will eliminate the problems with simultaneous dilution of the inhibitory (e.g. hemoglobin, immunoglobulins) and/or stimulatory (e.g. heparin) components which interfere with PCR performance, and/or recording of the fluorescence signal.

Conclusions

This study shows that a combination of 1 M 1,2-propanediol and 0.2 M trehalose represents a unique enhancer which can be combined with various DNA dyes. The enhancer can be used for amplification of various DNA templates, including those which are GC-rich and present in crude specimens, where other enhancers such as DMSO or betaine fail.

Methods

Reagents, antibodies and plasmids

The origin and properties of DNA dyes are specified in Table 1. DMSO was obtained from Fluka Chemie Gmbh (Buchs, Switzerland). Taq DNA polymerase was produced as described [5] or obtained together with buffers of various composition from several manufacturers (Fermentas, Vilnius, Lithuania; Sigma-Aldrich, Prague, Czech Republic; Promega, Madison, USA). All other

chemicals were from Sigma-Aldrich. The production of anti-Taq mAb which inhibits Taq DNA polymerase activity and is suitable for hot-start PCR has already been described [5]. The plasmid pMOL21 (4 kbp), carrying the *bla* gene for ampicillin resistance and *rpsL* gene, and *E. coli* K12 strain, MF101 [15], were obtained from Hisaji Maki (University of Tokyo, Japan).

qPCR

Most of the experiments were conducted with Mastercycler ep realplex (Eppendorf, AG, Hamburg, Germany) according to the manufacturer's instructions. Reactions were performed in 20 or 25 μl volumes in twin.tec 96 real-time PCR plates (Eppendorf) sealed with heat sealing film (Eppendorf). Amplifications of cDNAs were performed in 5 μl reaction volumes in 384-well plates sealed with LightCycler 480 sealing foil (Roche Diagnostics) using LightCycler 480 (Roche Diagnostics, Mannheim, Germany). PCR mixes of different salt composition (Table 2) were prepared according to Taq DNA polymerase manufacturer's protocols and/or literature data [5]. Oligonucleotide primers, DNA template, DNA dyes and additives/enhancers were added immediately before the assay. For comparison, we also used iQ™ SYBR Green Supermix (Bio-Rad Laboratories, Hercules, CA, USA) and LC 480 SGI (Roche Diagnostics). DNA dyes were prepared from stock solutions as recommended by manufacturers and/or previous studies [2,3] and as summarized in Table 1. Primers used for amplification of genomic DNA fragments are indicated in Table 4. For cDNA amplification, the following primers were used (forward/reverse, [accession number; fragment size, GC content]): actin, 5'-GATCTGGCACCACACCTTCT-3'/5'-GGGGTGTTGAAGGTCTCAAA-3', [NM_007393.2; 138 bp, 58% GC]; GAPDH, 5'-AACTTTGGCATTGTGGAAGG-3'/5'-ATCCACAGTCTTCTGGGTGG-3', [XM 001473623.1; 69 bp, 52% GC]; ORMDL1 Fr.a, 5'-GGATCAGGGTAGAGCAAGG-3'/5'-AGCAGAGAAGCTGTGTTTAGG-3', [NM_145517.4; 171 bp, 43% GC]; ORMDL1_Fr.b, 5'-ACTCGTGTAATGAACAGCCG-3'/5'-GCCTTGCTCTACCCTGATCC-3', [NM 145517.4; 205 bp, 47% GC]. For amplification of 864 bp genomic DNA fragment of mouse Thy-1 gene, thermal cycling consisted of 94°C/1 min | 30 × [94°C/15 s | 56°C/15 s | 72°C/1 min]. For amplification of human or mouse genomic DNA fragments from crude blood samples, the cycling conditions were: 95°C/10 min | 40 × [94°C/15 s 58°C/30 s | 72°C/1 min]. For cDNA amplification the cycling conditions were: 95°C/3 min 40 × [95°C/10 s | 60°C/20 s | 72°C/20 s]. Melting curve analysis was carried out from 50°C to 95°C with 0.2°C increments. In some experiments, DNA amplicons were size-fractionated in 1% or 2% agarose gels stained with ethidium bromide (0.5 μg/ml) and evaluated as described [35]. Quantification cycle (Cq) values [36] were determined by automated threshold analysis. PCR efficiencies (E) were determined from dilutions of DNA and calculated from the slopes of the standard curves according to the equation $E = 10^{-1/a} - 1$, where a is the slope of the corresponding standard curve.

Genomic DNA

Mouse genomic DNA was isolated from tails of C57BL/6J mice as previously described [37]. As a source of human genomic DNA, whole human blood was collected into heparin (20 U/ml), 0.38% sodium citrate or 2.7 mM EDTA, and stored in small aliquots at -70°C. All these experiments were approved by the ethical committee of the Institute of Molecular Genetics. The mass of the haploid mouse and human genome (C-value) is ~3.3 pg and ~3.5 pg, respectively [38]; this indicates that 1 ng of mouse or human genomic DNA contains approximately 303 and 286 copies of a single-copy gene. These numbers were used for generation of standard curve of Cq values from amplification plots versus log copy number.

RNA extraction and cDNA synthesis and analysis

RNA was extracted from mouse bone marrow-derived mast cells cultured under standard conditions [39] using RNeasy Mini Kit (Qiagen, Hilden, Germany). The amount of RNA was determined by spectrophotometer ND-100 (NanoDrop Technologies, Wilmington, DE). Single-stranded cDNA was synthesized by means of mouse moloney leukemia virus reverse transcriptase (Invitrogen, Carlsbad, CA, USA) according to manufacturer's instructions using 10 μg of isolated RNA and 50 ng of random hexamers per reaction.

Fluorescence measurements and melting temperature determination

PCR mix II without Taq DNA polymerase, dNTPs and anti-Taq antibody was supplemented with various additives/enhancers, DNA dyes and ssDNA oligonucleotide PCR primer TNF, 5'- TAAAACGACGGCCAGTGAATTC-3' (45.5% GC) or primer No 7, reverse (Table 4; 72.2% GC). The mixtures (25 μl) were transferred into white wells of the 96-well PCR plate, heat-sealed, and fluorescence reading was carried out on Mastercycler ep realplex (SGI filter set). The samples were heated at 95°C for 2 min, then cooled to 50°C and subjected to fluorescence reading. For determination of melting temperatures, the samples were prepared as above except that dsDNA was formed by adding oligonucleotide mixture of TNF and anti-TNF (5'-GAATTCACTGGCCGTCGTTTTA-3') or primer No 7, reverse (Table 4) and anti-primer No 7, reverse (5'-

Horáková et al. BMC Biotechnology 2011, 11:41
http://www.biomedcentral.com/1472-6750/11/41

AGACCCGCCTCACGAGCC-3'). In some experiments human hemoglobin (Sigma-Aldrich) at a final concentration 37.5 μM was also added. The samples were heated at 95°C for 2 min and then cooled to 30°C. Temperature-dependent changes in fluorescence obtained during heating from 30°C to 95°C (0.2°C increments) were determined by Mastercycler ep realplex. Melting temperatures were determined from melting curves.

DNA polymerase fidelity assay

The fidelity assay was based on streptomycin resistance of *rps*L mutants [15]. Standard PCRs (50 μl) containing mixes of different composition, as indicated in Table 2, were supplemented with 0.2 μM of each primer and 1 ng of template DNA (pMOL21 plasmid linearized with ScaI). In some experiments various DNA dyes at concentrations specified in Table 1 were also added. The PCR with KOD hot start polymerase was performed according to the manufacturer's instruction (Novagen, Darmstadt, Germany). The following primers were used: biotin-5'-AAAAACGCGTCACCAGTCACAGAAAAG-CATCTTAC-3' (forward sequence) and 5'-AAAAACGCGTCAACCAAGTCATTCTGAGAA-TAGT-3' (reverse sequence) [40]; MluI restriction sites are underlined. The standard PCR conditions were: 94°C for 2 min, followed by 25 cycles at 94°C for 15 s, 58°C for 30 s and 68°C for 5 min. The concentration of amplified DNA was determined by means of Quant-iT dsDNA HS Assay Kit (Invitrogen), and the number of template doublings was estimated. The PCR products were collected using streptavidin magnetic beads (Dynabeads M-280 Streptavidin, Invitrogen). Briefly, 100 μl aliquots of the beads were rinsed with washing solution (5 mM Tris-HCl, pH 7.5, 0.5 mM EDTA, 1 M NaCl), resuspended in 180 μl washing solution, combined with 20 μl of the PCR amplified DNA, and incubated under gentle rotation at room temperature. After 30 min, the beads were washed, resuspended in 100 μl of the corresponding enzyme mix and treated with 10 units of MluI at 37°C with gentle rotation overnight. The beads were collected using magnetic stand, and the supernatant was fractionated by electrophoresis in 0.8% agarose gel. The DNA fragment was isolated using TaKaRa Recochip (TaKaRa Biomedicals, Kyoto, Japan), precipitated in ethanol, lyophilized and dissolved in 20 μl of sterile water purified with Milli-Q Advantage A10 (Millipore, Molsheim, France). The purified DNA was self-ligated with T4 DNA ligase and transformed into MF101 competent cells. Half of the transformants were plated with ampicillin (100 μg/ml) to determine the total number of transformed cells; the remaining half on plates with ampicillin and streptomycin (100 μg/ml each) to determine the total number of *rps*L mutants. The mutation frequency was determined by dividing the total number of mutants by the total number of transformed cells. The error rate was calculated by dividing the mutation frequency by 130 (the number of amino acids that cause phenotypic changes in *rps*L), and the number of template doublings [15].

DNA polymerase activity

Activity of Taq DNA polymerase was assayed by measuring the conversion of radiolabeled dATP into acid insoluble DNA as previously described [41] with some modifications. Activated salmon testes DNA (Sigma-Aldrich) was prepared by exposing the DNA to low concentrations of pancreatic DNase [42]. Reaction mixture (100 μl) contained DNA polymerase 50 U/ml, 75 mM Tris-HCl, pH 8.8, 20 mM $(NH_4)_2SO_4$, 0.01% Tween 20, 2.5 mM $MgCl_2$, 100 μM dATP, 200 μM dGTP, 200 μM dCTP, 200 μM dTTP, activated salmon testes DNA (0.2 mg/ml), and various additives [10% (final concentration) human sodium citrate-treated blood, 0.2 M trehalose and/or 1 M 1,2-propanediol]. The samples were denatured for 15 min at 95°C then cooled to 72°C and supplemented with [α-^{32}P]dATP (14.8 kBq; 111TBq/mmol; MP Biomedicals, Irvine, CA). The mixtures were incubated for 30 min at 72°C and the reactions were then stopped by the addition of 100 μl of stop solution (150 mM sodium pyrophosphate and 100 mM EDTA, pH 8.0). DNA was precipitated by the addition of 150 μl of ice-cold 25% trichloracetic acid. After 15 min on ice, the samples were vacuum filtered on type A/E glass fiber filters (25 mm; Pall Corporation, Ann Arbor, MI) pre-wet with stop solution. Precipitated DNA retained on the disc was washed with 5 ml ice-cold 10% trichloracetic acid followed by 10 ml of ice-cold 96% ethanol. The filters were air dried and the radioactivity was measured in 10 ml scintillation fluid BetaMax ES (MP Biomedicals) in a scintillation counter with QuantaSmart software (Perkin Elmer, Waltham, MA).

Statistical analysis

Statistical analysis of intergroup differences was performed using Student's t-test.

List of abbreviations

qPCR: quantitative real time PCR; SGI: SYBR green I; PT enhancer: 1 M 1,2 propanediol and 0.2 M trehalose; ds: double-stranded; ss: single-stranded; bp: base pairs; LC 480 SGI: LightCycler 480 SYBR Green I Master; DMSO: dimethyl sulfoxide ; TCN: 0.3 M D-(+)-trehalose, 0.24 M L-carnitine, and 0.4% Nonidet P 40; TNF: tumor necrosis factor; dNTP: deoxynucleotide triphosphate; mAb: monoclonal antibody; Cq: quantification cycle; E: efficiency.

Acknowledgements

This project was supported by the Academy of Sciences of the Czech Republic, [RAN200520701, M200520901, Institutional Project AVOZ50520514] and grant 204/09/H084, 301/09/1626 and P50/11/1569 from Grant Agency of the Czech Republic. I. P. was supported by a stipend from the Ministry of Education, Youth, and Sports of the Czech Republic and Specific University

Research Project No 35779266 awarded by Charles University Prague. The authors thank Hisaji Maki for kindly providing the pMOL21 plasmid and MF101 competent cells, and Lukáš Kocanda and Hanka Mrázová for skilled technical assistance.

Authors' contributions

HH carried out experiments with PT enhancers. IP performed DNA polymerase fidelity assays and wrote the corresponding part of the manuscript. GMS carried out the experiments presented in Figure 1. JE performed the experiments presented in Figure 5. VB conceived the experiments with cDNA analysis and wrote the corresponding part. LD and PD conceived the study and wrote the manuscript. All authors read and approved the final manuscript.

Competing interests

The authors declare that they have no competing interests.

Received: 4 December 2010 Accepted: 18 April 2011
Published: 18 April 2011

References

1. Bustin SA: *A-Z of Quantitative PCR* International University Line. La Jolla, California; 2004.
2. Zipper H, Brunner H, Bernhagen J, Vitzthum F: **Investigations on DNA intercalation and surface binding by SYBR Green I, its structure determination and methodological implications.** *Nucleic Acids Res* 2004, **32(12)**:e103.
3. Mao F, Leung WY, Xin X: **Characterization of EvaGreen and the implication of its physicochemical properties for qPCR applications.** *BMC Biotechnol* 2007, **7**:76.
4. Monis PT, Giglio S, Saint CP: **Comparison of SYTO9 and SYBR Green I for real-time polymerase chain reaction and investigation of the effect of dye concentration on amplification and DNA melting curve analysis.** *Anal Biochem* 2005, **340(1)**:24-34.
5. Shaik GM, Draberova L, Draber P, Boubelik M, Draber P: **Tetraalkylammonium derivatives as real-time PCR enhancers and stabilizers of the qPCR mixtures containing SYBR Green I.** *Nucleic Acids Res* 2008, **36(15)**:e93.
6. Higuchi R, Dollinger G, Walsh PS, Griffith R: **Simultaneous amplification and detection of specific DNA sequences.** *Biotechnology (N Y)* 1992, **10(4)**:413-7.
7. Wittwer CT, Herrmann MG, Moss AA, Rasmussen RP: **Continuous fluorescence monitoring of rapid cycle DNA amplification.** *BioTechniques* 1997, **22(1)**:130-8.
8. Ishiguro T, Saitoh J, Yawata H, Yamagishi H, Iwasaki S, Mitoma Y: **Homogeneous quantitative assay of hepatitis C virus RNA by polymerase chain reaction in the presence of a fluorescent intercalater.** *Anal Biochem* 1995, **229(2)**:207-13.
9. Bengtsson M, Karlsson HJ, Westman G, Kubista M: **A new minor groove binding asymmetric cyanine reporter dye for real time PCR.** *Nucleic Acids Res* 2003, **31(8)**:e45.
10. Wittwer CT, Reed GH, Gundry CN, Vandersteen JG, Pryor RJ: **High-resolution genotyping by amplicon melting analysis using LCGreen.** *Clin Chem* 2003, **49(6)**:853-60.
11. Gudnason H, Dufva M, Bang DD, Wolff A: **Comparison of multiple DNA dyes for real-time PCR: effects of dye concentration and sequence composition on DNA amplification and melting temperature.** *Nucleic Acids Res* 2007, **35(19)**:e127.
12. Takano EA, Mitchell G, Fox SB, Dobrovic A: **Rapid detection of carriers with BRCA1 and BRCA2 mutations using high resolution melting analysis.** *BMC Cancer* 2008, **8**:59.
13. Mackay JF, Wright CD, Bonfiglioli RG: **A new approach to varietal identification in plants by microsatellite high resolution melting analysis: application to the verification of grapevine and olive cultivars.** *Plant Methods* 2008, **4**:8.
14. Barnes WM: **PCR amplification of up to 35 kb DNA with high fidelity and high yield from λ bacteriophage templates.** *Proc Natl Acad Sci USA* 1994, **91(6)**:2216-20.
15. Fujii S, Akiyama M, Aoki K, Sugaya Y, Higuchi K, Hiraoka M, Miki Y, Saitoh N, Yoshiyama K, Ihara K, Seki M, Ohtsubo E, Maki H: **DNA replication errors produced by the replicative apparatus of Escherichia coli.** *J Mol Biol* 1999, **289(4)**:835-50.
16. Al-Soud WA, Jönsson LJ, Rådström P: **Identification and characterization of immunoglobulin G in blood as a major inhibitor of diagnostic PCR.** *J Clin Microbiol* 2000, **38(1)**:345-50.
17. Al-Soud WA, Rådström P: **Purification and characterization of PCR-inhibitory components in blood cells.** *J Clin Microbiol* 2001, **39(2)**:485-93.
18. Spiess AN, Mueller N, Ivell R: **Trehalose is a potent PCR enhancer: lowering of DNA melting temperature and thermal stabilization of Taq polymerase by the disaccharide trehalose.** *Clin Chem* 2004, **50(7)**:1256-9.
19. Sidhu MK, Liao MJ, Rashidbaigi A: **Dimethyl sulfoxide improves RNA amplification.** *BioTechniques* 1996, **21(1)**:44-7.
20. Jung M, Muche JM, Lukowsky A, Jung K, Loening SA: **Dimethyl sulfoxide as additive in ready-to-use reaction mixtures for real-time polymerase chain reaction analysis with SYBR Green I dye.** *Anal Biochem* 2001, **289(2)**:292-5.
21. Weissensteiner T, Lanchbury JS: **Strategy for controlling preferential amplification and avoiding false negatives in PCR typing.** *BioTechniques* 1996, **21(6)**:1102-8.
22. Henke W, Herdel K, Jung K, Schnorr D, Loening SA: **Betaine improves the PCR amplification of GC-rich DNA sequences.** *Nucleic Acids Res* 1997, **25(19)**:3957-8.
23. Baskaran N, Kandpal RP, Bhargava AK, Glynn MW, Bale A, Weissman SM: **Uniform amplification of a mixture of deoxyribonucleic acids with varying GC content.** *Genome Res* 1996, **6(7)**:633-8.
24. Zhang Z, Yang X, Meng L, Liu F, Shen C, Yang W: **Enhanced amplification of GC-rich DNA with two organic reagents.** *BioTechniques* 2009, **47(3)**:775-9.
25. Motz M, Paabo S, Kilger C: **Improved cycle sequencing of GC-rich templates by a combination of nucleotide analogs.** *BioTechniques* 2000, **29(2)**:268-70.
26. Musso M, Bocciardi R, Parodi S, Ravazzolo R, Ceccherini I: **Betaine, dimethyl sulfoxide, and 7-deaza-dGTP, a powerful mixture for amplification of GC-rich DNA sequences.** *J Mol Diagn* 2006, **8(5)**:544-50.
27. Zhang Z, Kermekchiev MB, Barnes WM: **Direct DNA amplification from crude clinical samples using a PCR enhancer cocktail and novel mutants of taq.** *J Mol Diagn* 2010, **12(2)**:152-61.
28. Don RH, Cox PT, Wainwright BJ, Baker K, Mattick JS: **'Touchdown' PCR to circumvent spurious priming during gene amplification.** *Nucleic Acids Res* 1991, **19(14)**:4008.
29. Hubé F, Reverdiau P, Iochmann S, Gruel Y: **Improved PCR method for amplification of GC-rich DNA sequences.** *Mol Biotechnol* 2005, **31(1)**:81-4.
30. Kermekchiev MB, Kirilova LI, Vail EE, Barnes WM: **Mutants of Taq DNA polymerase resistant to PCR inhibitors allow DNA amplification from whole blood and crude soil samples.** *Nucleic Acids Res* 2009, **37(5)**:e40.
31. Owczarzy R, Moreira BG, You Y, Behlke MA, Walder JA: **Predicting stability of DNA duplexes in solutions containing magnesium and monovalent cations.** *Biochemistry* 2008, **47(19)**:5336-53.
32. McDowell DG, Burns NA, Parkes HC: **Localised sequence regions possessing high melting temperatures prevent the amplification of a DNA mimic in competitive PCR.** *Nucleic Acids Res* 1998, **26(14)**:3340-7.
33. Carninci P, Nishiyama Y, Westover A, Itoh M, Nagaoka S, Sasaki N, Okazaki Y, Muramatsu M, Hayashizaki Y: **Thermostabilization and thermoactivation of thermolabile enzymes by trehalose and its application for the synthesis of full length cDNA.** *Proc Natl Acad Sci USA* 1998, **95(2)**:520-4.
34. Chakrabarti R, Schutt CE: **Chemical PCR: Composition for enhancing polynucleotide amplification reactions.** *US patent 7772383* 2004.
35. Kovárová M, Dráber P: **New specificity and yield enhancer of polymerase chain reactions.** *Nucleic Acids Res* 2000, **28(13)**:e70.
36. Bustin SA, Benes V, Garson JA, Hellemans J, Huggett J, Kubista M, Mueller R, Nolan T, Pfaffl MW, Shipley GL, Vandesompele J, Wittwer CT: **The MIQE guidelines: minimum information for publication of quantitative real-time PCR experiments.** *Clin Chem* 2009, **55(4)**:611-22.
37. Wolff R, Gemmill R: **Purifying and Analyzing Genomic DNA.** In *Genome Analysis. A Laboratory Manual.* Edited by: Birren B, Green ED, Klapholz S, Myers RM, Roskams J. Cold Spring Harbor, New York, NY, Cold Spring Harbor Laboratory Press; 1997:1-81.
38. Gregory TR: **Animal Genome Size Database.** 2010 [http://www.genomesize.com].
39. Volná P, Lebduška P, Dráberová L, Šímová S, Heneberg P, Boubelík M, Bugajev V, Malissen B, Wilson BS, Hořejší V, Malissen M, Dráber P: **Negative**

Regulation of Mast Cell Signaling and Function by the Adaptor LAB/NTAL. *J Exp Med* 2004, **200(8)**:1001-13.
40. Lackovich KK, Lee JE, Chang P, Rashtchian A: **Measuring the fidelity of Platinum Pfx DNA polymerase.** *Focus* 2001, **23**:6-7.
41. Scalice ER, Sharkey DJ, Daiss JL: **Monodonal antibodies prepared against the DNA polymerase from Thermus aquaticus are potent inhibitors of enzyme activity.** *J Immunol Methods* 1994, **172(2)**:147-63.
42. Aposhian HV, Komberg A: **Enzymatic synthesis of deoxyribonucleic acid. IX. The polymerase formed after T2 bacteriophage infection of Escherichia coli: a new enzyme.** *J Biol Chem* 1962, **237(2)**:519-25.

doi:10.1186/1472-6750-11-41
Cite this article as: Horáková *et al.*: 1,2-propanediol-trehalose mixture as a potent quantitative real-time PCR enhancer. *BMC Biotechnology* 2011 11:41.

Real-time PCR-based genotyping from whole blood using Taq DNA polymerase and a buffer supplemented with 1,2-propanediol and trehalose

J. Immunol. Meth. (submitted)

Benchmarks

Real-time PCR-based genotyping from whole blood using Taq DNA polymerase and a buffer supplemented with 1,2-propanediol and trehalose

Lukas Kocanda[1], Petr Matousek[2], Petr Wagner[2], Pavol Utekal[1], Viktor Bugajev[1] and Petr Draber[1]

[1] Department of Signal Transduction, Institute of Molecular Genetics, Academy of Sciences of the Czech Republic, Videnska 1083, 14220 Prague 4, Czech Republic

[2] Department of Clinical Biochemistry, Regional Hospital Liberec, Husova 10, 46063 Liberec 1, Czech Republic

Correspondence to: Petr Draber, Department of Signal Transduction, Institute of Molecular Genetics, Academy of Sciences of the Czech Republic, Videnska 1083, 14220 Prague 4, Czech Republic, Email: draberpe@img.cas.cz

Keywords: real-time PCR; unseparated blood; 1,2-propanediol; trehalose; Taq DNA polymerase, SYBR green I

Word count for abstract: 74

Word count for the body of manuscript (excluding title page, acknowledgements, competing interests statement, references, tablets and table and figure legends: 994.

ABSTRACT

Amplification of DNA templates from whole blood with Taq DNA polymerase still remains a difficult task worldwide. Using a real-time PCR setup and a buffer supplemented with 1M 1,2-propanediol, 0.2 M trehalose and SYBR green I we show a reliable technique of genotyping in mice and detection of single-nucleotide polymorphisms/mutations in humans. Elimination of DNA extraction and use of common Taq DNA polymerase and DNA dye bring about substantial savings in labor and cost.

Quantitative real-time PCR (qPCR) has dramatically improved the genotyping and detection of single-nucleotide polymorphisms/mutations. Preparation of samples and presence of PCR inhibitors remain the bottleneck often complicating PCR-based diagnostic tests. These problems, accentuated in assays based on templates from whole blood, have in part been solved by modifications of PCR cycling conditions (1), employment of new generations of heat resistant DNA polymerases (2) or Taq DNA polymerase mutants (3). We described a new qPCR master mix containing, among others, the commonly used Taq DNA polymerase and a reaction buffer supplemented with 1 M 1,2-propanediol, 0.2 M trehalose and SYBR green I. This mix, referred to as PT-SYBR master mix, facilitated amplification of GC-rich and long DNA templates (4). Here we show that the PT-SYBR master mix is convinient even for qPCR genotyping from murine or human whole blood, allowing substantial savings in labor and cost and reducing the volume of blood needed.

Blood from mice was obtained by submandibular bleeding using Goldenrod animal lancet (5 mm, MEDIpoint, Mineola, USA) as described (5); heparin at a final concentration 10 U/ml was used as anticoagulant. Human peripheral blood was collected

into BD Vacutainer K3E/EDTA (BD Diagnostic). Blood was used either immediately or after storage at -20°C for several months. PCRs were performed in LightCycler 480 multiwell plates 96, white, sealed with LightCycler 480 sealing foil (Roche Diagnostics, Mannheim, Germany). Final concentrations for 25 µl PT-SYBR master mixes were as follows: 75 mM Tris-HCl, pH 8.8, 20 mM $(NH_4)_2SO_4$, 2.5 mM $MgCl_2$, 0.01 % Tween 20, 200 µM dNTPs, 25 U/ml Taq DNA polymerase, 22 nM anti-Taq monoclonal antibody (6), 0.2 M trehalose, 1 M 1,2-propandiol, 0.33 µM SYBR green I [concentration determined as described (7)], optimized concentrations of the corresponding oligonucleotide primers (Table 1) and 1 µl of whole blood diluted 1:8 in 0.9% NaCl. qPCR cycling was performed using Light Cycler 480 Real-time PCR instrument (Roche Diagnostics) with a program of denaturation at 95°C for 10 min, followed by 35 cycles of 94°C for 20 s, 54 – 60°C (depending on the primer set used) for 30 s and 72°C for 60 s; final extension step was at 72°C for 7 min.

In an initial set of experiments we intended to confirm the non-T cell activation linker (NTAL) genotype of mouse strains (8) previously characterized by genotyping by means of DNA isolated from mouse tail by standard procedures (9). Blood was obtained from mice of wild-type (WT) $NTAL^{+/+}$ genotype (Fig. 1 A), $NTAL^{-/-}$ knockout (KO) homozygotes (Fig. 1B) or heterozygotes (HZ) $NTAL^{-/-}$ (Fig. 1C). Diluted blood samples were directly added to PT-SYBR master mixes containing selected primer pairs and analyzed by qPCR. All samples showed the expected amplifications determined by fluorescence of SYBR green I (Fig. 1A-C, left). The samples were next analyzed by agarose gel electrophoresis and again only the expected bands were observed in all cases (Fig. 1A-C, right). In further experiments we found that routinely performed genotyping for linker for activation of T cell, phosphoprotein associated with glycosphingolipid-

enriched microdomains and 4.1R protein from the whole blood was similarly simplified by using whole blood and PT-SYBR master mix (not shown).

Next we tested samples of human whole blood for a point mutation in the coagulation Factor V gene (G to A at position 1691), which makes the mutant Factor V (called Factor V Leiden, FVL) resistant to activated protein C, a risk factor in venous thrombosis (10). In total we analyzed 40 samples which had been previously characterized by qPCR using DNA isolated from blood leucocytes as FVL WT (1691G, Fig. 2A), FVL homozygote mutant (1691A, Fig. 2B) and FVL HZ (1691G/A, Fig. 2C). We found in all cases that mixing of human blood samples with PT-SYBR master mix followed by qPCR gave the expected results manifested by enhanced SYBR green I fluorescence (Fig. 2A-C; left) or PCR amplified fragments mobility in agarose gels (Fig. 2A-C; right). Alike, we clearly identified WT and point mutations in Factor II prothrombin [G to A at position 20210 (11)] directly from unseparated human blood analyzed as above (not shown).

Proper and reliable amplification of DNA templates in samples from whole blood was dependent on the presence of 0.2 M trehalose and 1 M 1,2-propanediol (final concentrations) in the PCR mix; no reliable amplification was observed in the absence of these enhancers (data not shown). Trehalose has previously been found to be a potent enhancer of PCR, effective by decreasing DNA melting temperature, enhancing thermal stability, and protecting the enzymatic activity of Taq DNA polymerase from negative interferences with blood inhibitors (3, 4, 12) . On the other hand, 1,2-propanediol is an effective enhancer of amplification of GC-rich templates (13) and decreases the melting temperature of double stranded DNA fragments (4). When 1,2-propanediol and trehalose are used as enhancers together, a potent PCR mix is formed (PT mix) suitable for a

variety of applications. Supplementation of the PT mix with SYBR green I produces a reagent, which is suitable for qPCR genotyping directly from whole blood without DNA isolation. On the other hand addition of cresol red at a final concentration of 0.2 mM, which does not inhibit PCR (14) and is compatible with PT mixes permits an easy transfer of the amplicons after PCR into gel without the necessity to add loading buffer (not shown). PT master mix thus offers a useful alternative for some expensive commercial products intended to amplify PCR in the presence of blood inhibitors; at the same time, it provides a platform for efficient amplification of GC-rich templates.

Acknowledgments

This work was supported in part by project TA01010436 of the Technology Agency of the Czech Republic, project FR-TI3/067 of the Ministry of Industry and Trade of the Czech Republic, and Institutional support RVO 68378050.

Competing interests

The authors declare no competing interests.

115

116 **References**

117

118 1. **Mercier, B., C. Gaucher, O. Feugeas, and C. Mazurier**. 1990. Direct PCR from
119 whole blood, without DNA extraction. Nucleic Acids Res. *18*:5908.

120 2. **Panaccio, M. and A. Lew**. 1991. PCR based diagnosis in the presence of 8% (v/v)
121 blood. Nucleic Acids Res. *19*:1151.

122 3. **Zhang, Z., M.B. Kermekchiev, and W.M. Barnes**. 2010. Direct DNA
123 amplification from crude clinical samples using a PCR enhancer cocktail and novel
124 mutants of taq. J. Mol. Diagn. *12*:152-161.

125 4. **Horakova, H., I. Polakovicova, G.M. Shaik, J. Eitler, V. Bugajev, L.**
126 **Draberova, and P. Draber**. 2011. 1,2-propanediol-trehalose mixture as a potent
127 quantitative real-time PCR enhancer. BMC. Biotechnol. *11*:41.

128 5. **Golde, W.T., P. Gollobin, and L.L. Rodriguez**. 2005. A rapid, simple, and
129 humane method for submandibular bleeding of mice using a lancet. Lab Anim (NY)
130 *34*:39-43.

131 6. **Shaik, G.M., L. Draberova, P. Draber, M. Boubelik, and P. Draber**. 2008.
132 Tetraalkylammonium derivatives as real-time PCR enhancers and stabilizers of the
133 qPCR mixtures containing SYBR Green I. Nucleic Acids Res. *36*:e93.

134 7. **Mao, F., W.Y. Leung, and X. Xin**. 2007. Characterization of EvaGreen and the
135 implication of its physicochemical properties for qPCR applications. BMC.
136 Biotechnol. *7*:76.

8. **Volna, P., P. Lebduska, L. Draberova, S. Simova, P. Heneberg, M. Boubelik, V. Bugajev, B. Malissen, et al.** 2004. Negative Regulation of Mast Cell Signaling and Function by the Adaptor LAB/NTAL. J. Exp. Med. *200*:1001-1013.

9. **Wolff, R. and R. Gemmill**. 1997. Pyrifying and Analyzing Genomic DNA, p. 1-81. In B. Birren, E.D. Green, S. Klapholz, R.M. Myers, and J. Roskams (Eds.), Genome Analysis: A Laboratory Manual. Cold Spring Harbor Laboratory Press, Cold Spring Harbor, New York, NY.

10. **Corral, J., J.A. Iniesta, R. Gonzalez-Conejero, and V. Vicente**. 1996. Detection of factor V Leiden from a drop of blood by PCR-SSCP. Thromb. Haemost. *76*:735-737.

11. **Dahlback, B.** 2008. Advances in understanding pathogenic mechanisms of thrombophilic disorders. Blood *112*:19-27.

12. **Spiess, A.-N., N. Muellr, and R. Ivell**. 2004. Trehalose is a potent PCR enhancer: lowering of DNA melting temperature and thermal stabilization of Taq polymerase by the disaccharide trehalose. Clin. Chem. *50*:1256-1259.

13. **Zhang, Z., X. Yang, L. Meng, F. Liu, C. Shen, and W. Yang**. 2009. Enhanced amplification of GC-rich DNA with two organic reagents. BioTechniques *47*:775-779.

14. **Hodges, E., S.M. Boddy, S. Thomas, and J.L. Smith**. 1997. Modification of IgH PCR clonal analysis by the addition of sucrose and cresol red directly to PCR reaction mixes. Mol. Pathol. *50*:164-166.

158 15. **Endler, G., P.A. Kyrle, S. Eichinger, M. Exner, and C. Mannhalter**. 2001.
159 Multiplexed mutagenically separated PCR: simultaneous single-tube detection of
160 the factor V R506Q (G1691A), the prothrombin G20210A, and the
161 methylenetetrahydrofolate reductase A223V (C677T) variants. Clin. Chem. *47*:333-
162 335.

163

164

Table 1. Oligonucleotide primers used in PT-SYBR master mixes

Gene name (Reference)	Primer	Amplicon length (bp)*	Primer sequence (5'->3')
NTAL (8)			
	Sense		CTACGGAGCTGAGTGTTCTCA
	Antisense - WT	383	GAACGGCTAGAACTACACAGAG
	Antisense - KO	450	GAGAGGAGGATAAAGTGGACCTC
FVL (15)			
	Sense		CGCAGGAACAACACCATGAT
	Antisense - 1691G	233	AACAAGGACAAAATACCTGTATTCATC
	Antisense - 1691A	246	GTCTGTCTGTCTCTTCAAGGACAAAATACCTGTATTCTTT

* Sense primers are combined with antisense primers to get the amplicons of given length.

181

182 **Figure legends**

183

184 **Figure 1. Mouse genotyping from whole blood using PT-SYBR master mix.** Blood
185 was collected from NTAL$^{+/+}$ (WT; A), NTAL$^{-/-}$ (KO, B) or NTAL$^{-/-}$ (HZ, C) mice and
186 added directly into PT-SYBR master mixes containing the primer sets for NTAL WT or
187 NTAL KO genotyping. Panels shown on the left indicate fluorescence signal plotted as a
188 function of cell cycle. After PCR, the samples were analyzed by 1% agarose gel
189 electrophoresis and ethidium bromide staining. Mobility of the selected amplicons and
190 their sizes are indicated by arrows. Numbers in square brackets indicate the number of
191 samples examined in each group.

192

193 **Figure 2. Identification of FVL point mutations in whole blood using PT-SYBR**
194 **master mix.** Blood was collected from donors with WT FVL (A), FVL mutant (MUT; B)
195 or FVL HZ (C) and added directly into PT-SYBR master mixes containing the primer
196 sets for FVL genotyping. Panels shown on the left indicate fluorescence signal plotted as
197 a function of cell cycle. After PCR, the samples were analyzed by 2% agarose gel
198 electrophoresis and ethidium bromide staining. Mobility of selected amplicons and their
199 sizes are indicated by arrows. Numbers in square brackets indicate the number of samples
200 examined in each group.

Fig. 1
Click here to download Figures (separate file for each figure): Figure 1.ppt

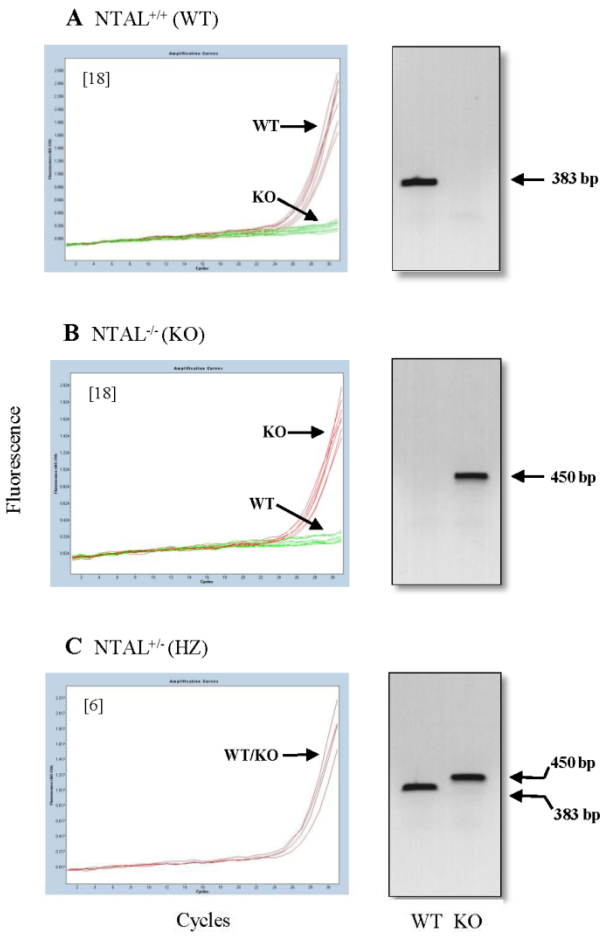

Figure 1
Kocanda et al.

Figure 2
Click here to download Figures (separate file for each figure): Figure 2 PPT97.ppt

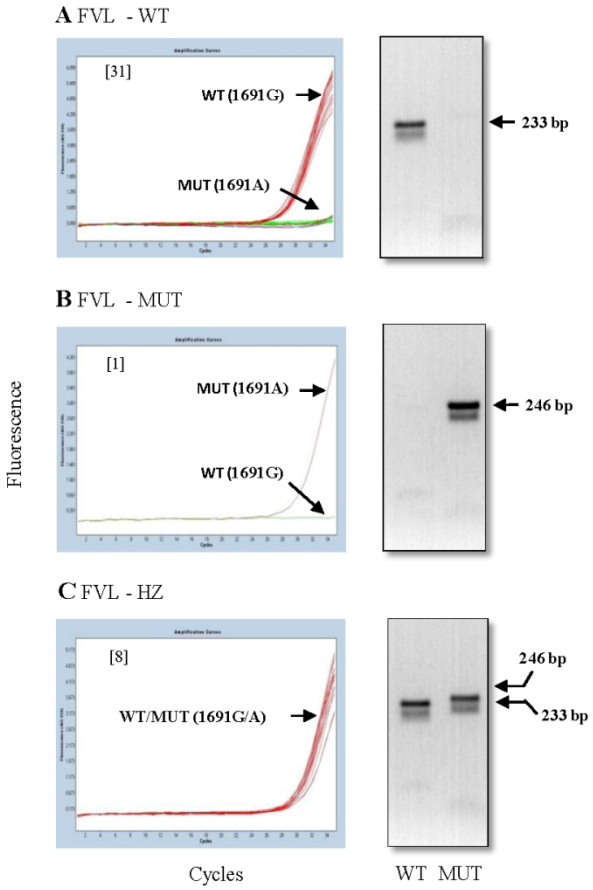

Figure 2
Kocanda et al.

GENERAL DISCUSSION

Although the role of FcεRI in IgE-associated acquired immune responses is well known, the exact molecular mechanism of initiation and termination of the FcεRI signaling is still elusive. Obviously, understanding of these events has a therapeutic significance in treatment of life threating IgE-mediated responses such as anaphylaxis. It is widely accepted that Src kinase family Lyn functions as the central molecule responsible for both processes initiation and termination of the FcεRI signaling. Especially the role of Lyn in FcεRI desensitization can be at first sight surprising but the importance of a tight regulation of proinflammatory mediators release may explain the ambiguous role of this kinase in the regulation of mast cell signaling at the very beginning [199]. The kinetics of FcεRI-mediated degranulation is characterized by dose-dependent bell-shaped curve when sub-optimal concentration of antigen exhibits not fully developed response whereas supra-optimal concentrations of antigen has an inhibitory effect on degranulation (Figure 5) [200]. The canonical ITAMs of FcRβ subunits serve as the amplifiers of the FcεRI signaling whereas the non-canonical ITAM is involved in the suppression of IgE-mediated responses [105;201]. Xiao et al. showed that stimulation of the FcεRI with monomeric IgE, IgE plus anti-IgE, or IgE plus low valency antigen positively regulated degranulation. However, when FcεRI signaling was triggered with high concentration of multivalent antigen Lyn functioned as a negative regulator. The association of Lyn with FcRβ was markedly increased when activated with high concentration of multivalent antigen and subsequent phosphorylation of FcRβ was enhanced. Negative regulatory molecules SHP-1 and SHIP have been found to be associated with FcRβ even in quiescent cells. These phosphatases were phosphorylated by Lyn and their subsequent association with FcRβ was increased in cells stimulated with high concentration of the multivalent antigen [124]. Thus, massive stimulus suppresses the FcεRI signaling via increased association of SHP-1 and/or SHIP with the FcεRI aggregates. Indeed, it has been shown that $Lyn^{-/-}$ BMMCs activated with high concentrations of multivalent antigens exhibited saturation of the response but not dose-dependent bell-shaped curve-dependent inhibition of the response (Figure 5) [120].

Signaling molecules specific for mast cells are very limited, if any. Therefore, new molecular targets are still searched for treatment of allergic disorders On the other hand it has been shown that allergy can be also treated via desensitization of FcεRI signaling using inhibitors of Syk or PI3K activity [202]. This let us to evaluate current models explaining the initial stages of FcεRI.

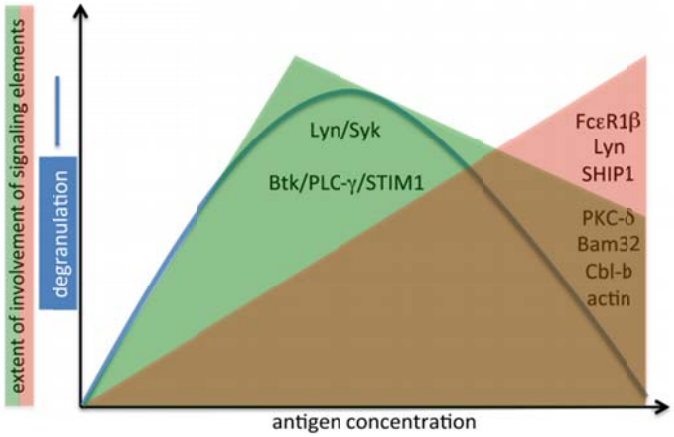

Figure 5. Effect of antigen concentration on the extent of FcεRI-mediated degranulation. The bell-shaped curve-dependent inhibition of the response is characteristic for signaling via FcεRI (blue curve). A sub-optimal dose of multivalent antigen results in only weak downstream signaling and induction of effector functions whereas an optimal concentration of antigen causes maximal activation of antigen-triggered signaling pathways and effector functions, including calcium signaling initiated by activation of PLCγ and subsequent STIM1-dependent opening of CRAC channels (green triangle). Activation of mast cells with supra-optimal concentrations of multivalent antigen induces only weak signaling and execution of effector functions. Lyn in this case plays a negative role by phosphorylating non-canonical ITAM motif of FcRβ and SHIP is subsequently recruited to FcεRI (magenta triangle). Proteins in brown area promote suppression of signaling (Huber, 2013).

The transphosphorylation model assumes that FcεRI in quiescent cells is non-covalently associated through its non-phosphorylated β subunit with Lyn kinase [114;203;204] which is unable to phosphorylate its carrier receptor, despite the fact that Lyn kinase in quiescent mast cells is enzymatically active and its activity is not further enhanced after FcεRI triggering [205]. Aggregation of the IgE–FcεRI complexes with multivalent antigen initiates Lyn-dependent phosphorylation of the neighboring receptors within the aggregate [109]. This process is known as transphosphorylation and was suggested to play a role in the signal transduction in several other systems [206]. However, some data are in conflict with this hypothesis. For example, aggregated FcεRI becomes tyrosine phosphorylated even in the absence of β subunit [104]. Furthermore, chimeric receptors containing only the FcRγ cytoplasmic tail become tyrosine phosphorylated upon their aggregation [207]. Alternative models had been therefore proposed.

The model based on lipid raft membrane microdomains presumes that in resting cells FcεRI is physically separated from active Lyn residing in lipid raft domains and after aggregation, the FcεRI is translocated into these domains and is phosphorylated there by Lyn [208]. Decreased detergent solubility was observed not just in extensively aggregated FcεRI, but even upon FcεRI dimerization, although the activation was delayed and more sustained [209]. The lipid raft hypothesis is in part based on studies presuming that DRM correspond to lipid rafts, an assumption which is probably incorrect [117]. However, recent studies based on advanced microscopy methods revealed that membrane

domains in quiescent cells are highly dynamic and small in size (less than 10 nm). They can transiently coalesce after ligand-induced aggregation of membrane proteins and form larger domains [210]. In antigen-stimulated mast cells, transient association of IgE-FcεRI in specialized cholesterol-rich domains within ~4 nm proximity, peaking at 5 min after receptor aggregation has been described [211]. It remains to be determined whether these changes reflect either an association of FcεRI with cholesterol-enriched lipid rafts possessing sequestered Lyn, or rather changes leading to removal of aggregated FcεRI. In fact, experiments with N-palmitoylation-site deficient Lyn show that anchor of the Lyn to the plasma membrane but not to DRMs is important for proper tyrosine phosphorylation of the FcεRI [116]. Thus, lipid raft localization of Lyn is not sufficient for its interaction with aggregated FcεRI and initiation of phosphorylation occurs outside the lipid rafts.

The PTK–PTP interplay model was coined to explain some conflicting experimental data which were inconsistent with lipid raft model. PTK-PTP interplay model is based on the fact that the extent of phosphorylation of the immunoreceptors and other substrates depends not only on enzymatic activity of the PTKs, but, at least partly, also on the activity of PTPs. Initially, the model was elaborated in studies of immunoreceptor signaling in B cells. Reth and co-workers showed that the B cell receptor forms a complex with PTKs and PTPs; this complex is indispensable for reactive oxygen species (ROS)-induced phosphorylation [212]. One possible way of regulation of the PTP activity is reversible oxidation of Cys residue in a conserved signature motif (I/V)HCxxGxxR(S/T) in the catalytic domain of some of the PTPs at physiological pH (pKa <6.0). ROS are produced under physiological conditions by the activity of specialized enzymes such as nicotinamide adenine dinucleotide phosphate oxidase [213]. It has been shown that ROS encompassing superoxide or hydrogen peroxide are known inhibitors of PTPs and are capable of initiating early FcεRI-induced signaling events in mast cells. Despite a growing list of confirmed PTPs present in mast cells, their contribution to cell signaling regulation is still poorly understood [153;214]. Strong oxidants like pervanadate (a mixture of vanadate and H_2O_2) irreversibly inactivated PTPs by the formation of Cys-sulphonic acid residues [215]. It has been shown that solubilization of the cells with detergents destroys preformed signaling assemblies containing PTKs, PTPs, and their substrates because most of PTK substrates are not phosphorylated if pervanadate is added to cell lysates instead of intact cells [212]. Exposure of mast cells to pervanadate leads to activation events which resemble those induced by physiological activators [216;217]. Moreover, association of FcεRI with DRMs and enhanced receptor clustering are not required for receptor phosphorylation in cells stimulated with pervanadate or H_2O_2 [216]. Using a monoclonal antibody (oxPTP) recognizing oxidized Cys residue in catalytic domain of PTPs, enzymatically inactive PTPs were detectable in a time- and dose-dependent manner in mast cells activated with pervanadate, H_2O_2 or antigen [216].

In our study we extended current knowledge of topography of signaling molecules involved in FcεRI signaling. We have found that TRAPs, LAT and NTAL, are increasingly colocalized with oxidized PTPs in antigen and pervanadate activated cells [218]. Nevertheless, oxidized phosphatases have not been found in DRMs [216]. Similarly, Syk was detected in FcεRI clusters on plasma

membrane sheets isolated from activated mast cells [204], in spite of the fact that only FcεRI, was associated with DRMs [219]. Moreover, experiments with disaggregated FcεRI clusters showed that the rate of their dephosphorylation was the same as that of other proteins [219]. These data indicate that proteins in DRMs are not protected from phosphatase activity and that even typical DRMs proteins could be phosphorylated as proposed by the PTK–PTP interplay model.

Recently, the association of BCR with voltage-gated proton channel HVCN1 was shown to be important for ROS production in B cells. HVCN1-deficient B cells exhibited reduce ROS production and subsequent attenuation of BCR signaling via impaired BCR-dependent oxidation of the SHP-1 [220]. The role of ROS in FcεRI regulation under physiological conditions is, however, questionable [213;221]. Therefore, we also considered an alternative explanation how PTPs could be involved in FcεRI activation and we came to a model of antigen-induced conformational changes in aggregated FcεRI. According to this model, the expected changes in microenvironment of FcεRI may impair the access of PTPs to their substrates. Conformational changes upon activation in the BCR and TCR have already been described [222;223]. It is possible that the expected change in topography of FcεRI could lead to a shift in access of PTK and PTP to FcεRI, in favor of PTK, and thus enhance phosphorylation of FcεRI after mast cells triggering. The association of FcεRI with SHP-1, SHP-2 and SHIP-1 has been found in resting cells [124;216;224]. It should be mentioned that SHIP-1 is constitutively active and regulated mainly by phosphorylation-mediated translocation to the plasma membrane [199]. BMMCs lacking SHIP-1 exhibit massive degranulation even when IgE alone was bound to FcεRI. Thus, the interaction of FcRβ with SHIP-1 in non-activated cells may set a treshold for mast cells degranulation [225]. These data imply that the addition of IgE alone to the mast cells stimulates multiple cascades, which are prevented from progressing to degranulation by SHIP-1 [225]. Indeed, Carroll-Portillo et al. showed that FcεRI cross-linking is not an obligatory step in triggering mast cell signaling and suggest that dense populations of mobile receptors are capable of initiating low-level degranulation upon ligand recognition [78].

These models are still incomplete, because other factors play a role in the early FcεRI signaling. Surprisingly, mast cells with low expression of Fyn, Hck and Fgr exhibit significant changes in FcεRI signaling [122;127;128]. Fgr is important for phosphorylation of FcRγ and Syk. Mice with decreased levels of Fgr exhibit impaired passive cutaneous anaphylaxis [128]. Moreover Hck seems to be upstream of Lyn signaling [127]. Thus, it is possible that other kinases from Src kinase family are involved at the very beginning of the FcεRI signaling. The PTK-PTP interplay model fits to this situation as well. On the other hand BMMCs isolated from mice with targeted disruption of the GPI biosynthesis gene *PigA* lack expression of GPI-APs. These cells exhibit reduced degranulation and knock-out mice are resistant to passive cutaneous anaphylaxis. Interestingly, BMMCs deficient in GPI-APs exhibit impaired association of FcRβ and FcRγ with FcRα after mast cells activation with antigen. Association of active Lyn in resting cells with FcεRI was enhanced whereas in activated cells was decreased. These data imply that some GPI-AP competes with Lyn for association with FcεRI in quiescent cells. Interestingly, phosphorylation of FcRβ upon FcεRI aggregation was normal but

phosphorylation of FcRγ was impaired [226]. Thus, so far not yet identified GPI-APs seem to be responsible for stabilization of aggregated FcεRI complex and increased association of active Lyn with resting FcεRI. An important factor involved in early signaling is calcium. Basal phosphorylation detected in lysates of quiescent B cells as well as phosphorylation pattern of activated B cells is dependent on cytosolic Ca^{2+} levels. The basal levels of calcium and Ca^{2+} released from the ER stores were sufficient for initiation of BCR signaling. Surprisingly, BCR signaling in the absence of free Ca^{2+} (EDTA or BABTA treatment) exhibit impaired phosphorylation of Lyn and ZAP70 after BCR triggering [227].

It has been mentioned in introduction that STIM1 is a sensor of Ca^{2+} levels in ER and that it is responsible for I_{CRAC} and SOCE. The SOCE occurs almost immediately after mast cells activation with antigen or thapsigargin [190]. It takes seconds from initial FcεRI phosphorylation mediated by Src family kinase Lyn to initiate formation of LAT-dependent docking sites for PLCγ which yields IP3 and DAG. IP3 diffuses through the cytosol to bind to IP3R and thus fastly depletes the ER Ca^{2+} stores. The dynamics of STIM1 translocation to the ER/plasma membrane junctions was studied in Jurkat T cells upon TCR cross-linking. Accumulation of STIM1 near the plasma membrane begins in seconds after FcεRI triggering and precedes the I_{CRAC} [228]. Complexes of STIM1 with CRAC channel component Orai1 are involved in TCR-dependent immunological synapse [187]. As was mentioned in introduction STIM1 is the essential regulator of CRAC channels. Upon depletion of Ca^{2+} ER stores, STIM1 physically interacts with Orai1 channels. This direct interaction can be dynamically traced *in vivo* using flow cytometry based FRET after store depletion mediated by cells treatment with thapsigargin. The data presented in Figure 6 indicate that STIM1-EYFP increasingly interacts with Orai1-ECFP after the ER stores depletion with thapsigargin.

STIM1 in quiescent cells colocalizes with the microtubule filaments [195] and dynamically moves in microtubule-dependent manner [194]. The direct association of STIM1 with microtubule +TIP protein EB1 explains the comet-like movement of STIM1 [196]. In our study we focused on the dynamic of microtubules in mast cells and the role of STIM1 in microtubule reorganization after cells activation with different stimuli as well as on the role of microtubules in STIM1 translocation into the subplasmalemmal region. This cross-talk between STIM1 and microtubules is taking place at multiple levels (direct interaction with EB1 and calcium signaling) and thus the question whether microtubules affect STIM1 translocation to the ER/plasma membrane junctions and conversely whether STIM1 influences microtubules dynamics in resting cells via interaction with EB1 or in activated cells via calcium mobilization, is of importance.

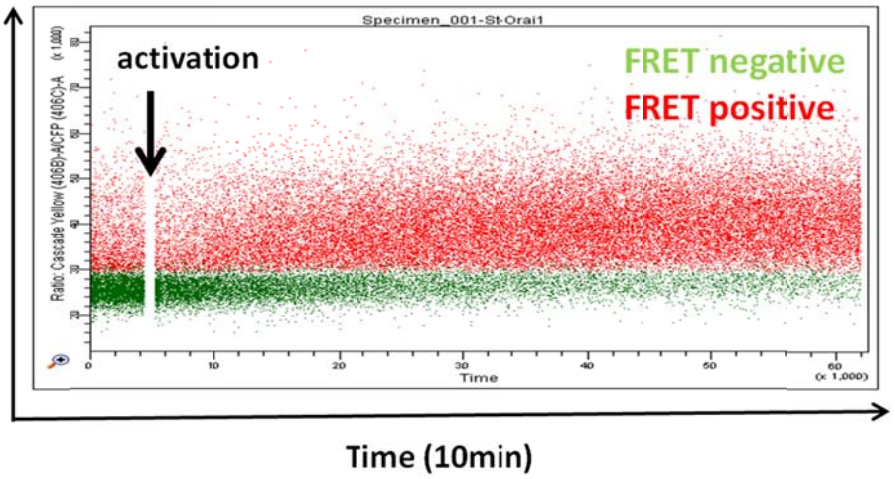

Figure 6. Kinetics of interaction between Ora1-ECFP and STIM1-EYFP in activated cells. Interaction between Orai1 and STIM1 was measured by flow cytometry based FRET in living cells after activation induced by 1 μM thapsigagin (arrow).For the experiments, HEK293 cells expressing STIM1-EYFP and Orai1-ECFP were used. The "basal" gate was ~20% positive for cells with FRET (red dots); 5 min after activation with 1 μM thapsigargin, the FRET was detected in ~70% of cells. The cells without the FRET signal are shown as green dots whereas the cells in FRET gate are marked as red dots. This profile indicates strong interaction of the proteins in the ER-plasma membrane junctions upon cells activation.

We described unknown phenotype of BMMCs that is characterized by formation of microtubule protrusions upon cells activation via FcεRI, pervanadate or thapsigargin. Interestingly, this phenotype is observed in BMMCs attached to fibronectin-coated slides resembling thus more closely the natural conditions in tissue where mast cells are congregated. It has been shown that compared with resting cells, FcεRI- or pervanadate-induced activation of BMMCs attached to poly-L-lysine-coated coverslips resulted in more intense staining of microtubules. However, no obvious microtubule protrusions were detected [229]. Similarly, activation and fixation of BMMCs in suspension followed by attachment to glass slides by cytospin intensified the tubulin immunostaining, but microtubule protrusions were not reported [126]. Thus, a new co-stimulatory signaling mediated by integrins towards microtubule reorganization was described. The microtubule protrusions in cells activated by FcεRI aggregation were most prominent ~5 min after cross-linking and Src family inhibitor PP2 inhibited their formation. This phenotype was restricted to BMMC and BMMC line but it has been tested only on a limited number of cell lines. Using a new algorithm we were able to analyze the dynamics of microtubules in a cell periphery. This dynamics was determined by total internal reflection fluorescence microscopy time-laps imaging of EB1-enhanced green fluorescent protein (EGFP). Using this algorithm we showed that thapsigargin- or antigen-mediated activation increases the numbers of growing microtubules in cell periphery and also the growth rate of microtubules. There was direct correlation between formation of microtubule protrusions and degranulation in activated mast cells [190].

We have prepared STIM1 knock-downs in BMMCs to evaluate the role of STIM1 in these processes. BMMCs with reduced STIM1 levels exhibited impaired degranulation, calcium mobilization nad calcium uptake after antigen or thapsigargin activation. These data corroborated and extended the results of Baba et al. [188] obtained on fetal liver-derived mast cells. It has been reported that calcium is dispensable for microtubule formation, but essential for F-actin disassembly in BMMCs [126]. In

contrast to these data, our observation indicate, that reorganization of microtubules in BMMCs with reduced STIM1 levels was impaired. It has been shown that both Ca^{2+} and STIM1 expression in BMMCs are indispensable for formation of microtubule protrusions. Moreover, the microtubule dynamic in the cell periphery of activated BMMCs with STIM1 knock-downs was impaired but the dynamic of EB1 movement in resting cells was without significant changes. It implies that STIM1-dependent Ca^{2+} levels in cytosol after activation are important for microtubules reorganization but in quiescent cells the comet-like interaction of EB1 with STIM1 alone does not change the dynamics of microtubules polymerization. We were capable of reverting the formation of microtubule protrusions and calcium mobilization in the activated cells with reduced STIM1 levels nucleofected with mCherry-hSTIM1 and EYFP-hSTIM1, respectively [190].

STIM1 puncta are formed several seconds before the opening of calcium channels [228], and one could expect that microtubules are involved in this process. However, our data demonstrate that although microtubule disruption by nocodazole abolished the comet-like movement of STIM1, it had no effect on puncta formation in activated cells. This finding is in line with our observation that the uptake of extracellular Ca^{2+} was only partially inhibited in nocodazole-pretreated and thapsigargin-activated BMMCs. This suggests that STIM1 aggregation beneath the plasma membrane and subsequent opening of CRAC channels does not require intact microtubules in activated mast cells. Previous studies often reported discordant effects of nocodazole treatment on SOCE or I_{CRAC} (see chapter STIM1 in Introduction). It appears that different factors, including cell type, treatment protocol and the way of Ca^{2+} depletion might modify the results of the experiments. It is also possible that microtubules play a supporting role in SOCE signaling by optimizing the location of ER containing STIM1 before cell activation [195]. The presence of aggregated STIM1 in protrusion could help to organize CRAC channels [230] and open locally these channels to cause SOCE. Our finding that BMMCs with STIM1 knock-down exhibited defective chemotaxis toward antigen supports previous data on the role of Ca^{2+} in chemotaxis [231;232]. Based on these data we proposed that microtubule protrusions might be involved in sensing external chemotactic gradients of antigen or other signals reaching mast cells at inflammatory sites. Recently, it was found that mast cells are capable of surmounting blood vessels to capture serum IgE with extended processes [34]. The direct contact with endothelial cells is required, thus the interaction with integrins is expected and the protrusions that we observed *in vitro* can be the non-directional response of mast cells to ubiquitous stimuli which *in vivo* may be important for IgE capturing from blood stream. Interestingly, although the migration of mast cells towards antigen was impaired, cells spread normally when compared to control cells in the presence of antigen (Figure 7 A and B). Spreading of cells reflects the reorganization of actin filaments. Moreover, STIM1 knock-downs cells were capable of spreading when activated with antigen and thapsigargin, in contrast to control cells, but not after activation with thapsigargin alone (Figure 7B). These data suggest that sustained levels of calcium inhibit spreading of BMMCs but the FcεRI-mediated signaling is important for cells to spread. These data are in accord with our previous observation that NTAL-deficient BMMCs exhibit increased calcium signaling [132] and spreading [233] but migration of these cells toward antigen was enhanced [233].

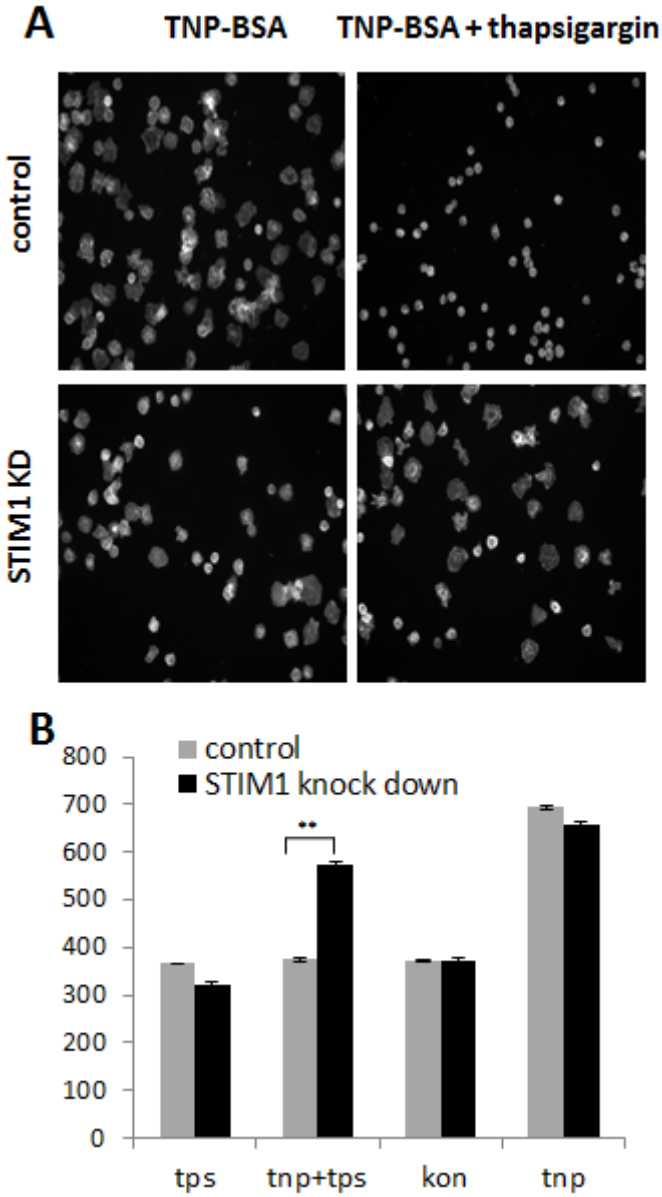

Figure 7. Negative regulation of cell spreading by STIM1 in antigen and thapsigargin activated cells. (A) IgE-sensitized BMMC were attached to fibronectin-coated glass surface and then stimulated with antigen (TNP-BSA), thapsigargin or antigen plus thapsigargin (only cells activated with antigen alone or together with thapsigargin are shown). After 30min, cells were fixed and stained for F-actin. (B) Cell area was determined and normalized to nonactivated cells. Means and SE were calculated from two independent experiments. Significance of differences between control BMMCs and STIM1 knock-down (KD) BMMCs cells is shown ($p<0.01$; Student's t-test).

Cell membranes serve as the docking sites for many signaling events. It is obvious that some of the proteins residing in the membranes can serve as sensors transferring the signal between distinc compartments. IgE-FcεRI complex and STIM1 sense the antigen and Ca^{2+}, respectively. Although their function is distinct, both of them require to be phosphorylated and both of them show changes in membrane topography after cell triggering. Interestingly, the initiation of signaling termination of FcεRI

or STIM1 aggregates-dependent signaling is mediated by the associated sensor (Lyn) or sensing object (calcium). It has been shown that refilling of ER with Ca^{2+} is not sufficient for dis-aggregation of STIM1 [234] but some proteins, probably CRACR2A and SARAF are involved in this process (see Introduction).

The peak of STIM1 phosphorylation occur 2.5 s after platelets treatment with thapsigargin; thus, STIM1 is probably associated in resting cells with other molecule/s [174]. ERK1/2 were identified as kinases phosporylating STIM1 and thus important for SOCE [175]. Association of STIM1 with the liquid ordered lipid domains initiates redistribution of Orai1 from the liquid disordered regions of the plasma membrane to lipid ordered domains [186]. Our preliminary data suggest that incubation of mast cells with 2-bromo-palmitate reduces calcium mobilization. 2-bromo-palmitate blocks proteins palmitoylation and thus the association of some proteins with lipid ordered domains can be disrupted. In this connection the inhibition of SOCE after mast cells treatment with 2-bromo-palmitate is of importance. Therefore we established the flow cytometry based FRET to detect the changes between EYFP-STIM1 and ECFP-Orai1 in living cells. As the process of STIM1 aggregation can be influenced by reduced early signaling we will measure this event also in cells expressing EYFP-STIM1 and ECFP-STIM1. Until now, this system is working in HEK 293 cells and we plan measure flow cytometry based FRET during FcεRI signaling in mast cells or basophiles.

Currently, we are engaged also in the research of a complex organizing metabolism of AA (membrane-associated proteins in eicosanoid and glutathione signaling). This multimolecular complex recruits 5-LO in calcium dependent manner and according to our results is also involved in unfolded protein response in mast cells.

CONCLUSIONS

1. **We evaluated current models explaining the initial stages of FcεRI. We found that the best model explaining various experimental findings fulfils PTK-PTP interplay model. We propose that shift in balance in favor of PTKs could be the signal leading to initial phosphorylation of the FcεRI. This model is supported by our findings of the presence of irreversibly oxidized, and therefore inactivated, PTPs in the vicinity of FcεRI complexes.**

2. **We found that activated mast cells attached to fibronectin-coated slides form microtubule protrusions after activation with different stimuli. STIM1 was essential for formation of the protrusions and mast cells migration towards antigen. Moreover, in activated BMMCs with STIM1 knock-down the changes in microtubule dynamics were prevented.**

   2.1 We used a 29-aa oligopeptide which corresponded to the C-terminal part of STIM1 (conjugated to protein carrier) for immunization of mice and rabbits. From immunized rabbits we obtained polyclonal antibodies and from immunized mice we generated two hybridoma clones which produced highly specific monoclonal antibodies against STIM1. All of these antibodies were usefull for immunoprecipitation and immunoblotting. We used the antibodies for quantification of STIM1 in BMMCs with STIM1 knock-downs by immunoblotting. Antibody produced by one of the hybridoma clones is at present commercially avaliable from Exbio Praha, a.s.

   2.2 hSTIM1 complementary DNA was cloned into the mammalian expression vector coding mCherry so that sequence 1-23 aa corresponding to the SP of hSTIM1 was placed at the beginning of mCherry and the remaning part of hSTIM1 was cloned on the C-terminus of mCherry. The construct was used in STIM1 rescue experiments.

   2.3 Cells with reduced STIM1 expression were prepared by transduction of BMMCs with lentivirus vectors bearing STIM1 specific shRNAs; control cells were transduced with empty vector. The efficiency of knock-downs was tested at the protein level by immunobloting. Subsequently, cells with STIM1 knock-down were used to evaluate hypothesis that STIM1 is crucial for activation-induced changes in microtubule dynamics.

   2.4 BMMCs with STIM1 knock-down exhibited impaired degranulation, calcium mobilization and other markers of mast cells activation. These changes could not be explained by reduced expression of FcεRI as determined by flow cytometry.

2.5 We have found that in activated cells there was close correlation between the formation of microtubule protrusions and degranulation as measured by β-glucuronidase release.

2.6 Cells with STIM1 knock-down were nucleofected with human EYFP-hSTIM1 or mCherry-hSTIM1. Detailed analysis showed that in the transfectants the phenotype was reverted as refected by restauration of microtubule protrusions formation and enhanced calcium mobilization after FcεRI trigering. The data indicate that formation of microtubule protrusions is dependent on the presence and activity of STIM1.

2.7 Induction of microtubule depolymerization by nocodazole decreased mast cell degranulation but $^{45}Ca^{2+}$ uptake was only slightly reduced. These data corroborate the microscopic observation that microtubules are not essential for initial STIM1 aggregation.

3 In search for a new universal PCR master mix suitable for amplification of DNA fragments from whole blood and/or GC-rich templates, we modified PCR mixture by inclusion 1 M 1,2-propanediol and 0.2 M trehalose. We found that the additives allowed amplification of GC-rich DNA fragments and amplification in the presence of PCR inhibitors such as hemoglobin.

REFERENCES

[1] Beaven MA (2009) Our perception of the mast cell from Paul Ehrlich to now. *Eur. J. Immunol.*, **39,** 11-25.

[2] Kirshenbaum AS, Kessler SW, Goff JP, & Metcalfe DD (1991) Demonstration of the origin of human mast-cells from CD34+ bone-marrow progenitor cells. *J. Immunol.*, **146,** 1410-1415.

[3] Chen CC, Grimbaldeston MA, Tsai M, Weissman IL, & Galli SJ (2005) Identification of mast cell progenitors in adult mice. *Proc. Natl. Acad. Sci. U. S. A*, **102,** 11408-11413.

[4] Arinobu Y, Iwasaki H, Gurish MF, Mizuno S, Shigematsu H, Ozawa H, Tenen DG, Austen KF, & Akashi K (2005) Developmental checkpoints of the basophil/mast cell lineages in adult murine hematopoiesis. *Proc. Natl. Acad. Sci. U. S. A*, **102,** 18105-18110.

[5] Stevens RL & Adachi R (2007) Protease-proteoglycan complexes of mouse and human mast cells and importance of their beta-tryptase-heparin complexes in inflammation and innate immunity. *Immunol. Rev.*, **217,** 155-167.

[6] Razin E (1982) Generation of leukotriene C4 from a subclass of mast cells differentiated in vitro from mouse bone marrow. *Proc. Natl. Acad. Sci. U. S. A*, **78,** 2559-2561.

[7] Lewis RA, Soter NA, Diamond PT, Austen KF, Oates JA, & Roberts LJ (1982) Prostaglandin D2 generation after activation of rat and human mast cells with anti-IgE. *J. Immunol.*, **129,** 1627-1631.

[8] Sredni B, Friedman MM, Bland CE, & Metcalfe DD (1983) Ultrastructural, biochemical, and functional characteristics of histamine-containing cells cloned from mouse bone marrow: tentative identification as mucosal mast cells. *J. Immunol.*, **131,** 915-922.

[9] Miller HR, Wright SH, Knight PA, & Thornton EM (1999) A novel function for transforming growth factor-β1: upregulation of the expression and the IgE-independent extracellular release of a mucosal mast cell granule-specific β-chymase, mouse mast cell protease-1. *Blood*, **93,** 3473-3486.

[10] Cavalcante MCM, Allodi S, Valente AP, Straus AH, Takahashi HK, Mourao PAS, & Pavao MSG (2000) Occurrence of heparin in the invertebrate Styela plicata (Tunicata) is restricted to cell layers facing the outside environment - An ancient role in defense? *J. Biol. Chem.*, **275,** 36189-36196.

[11] Blott EJ & Griffiths GM (2002) Secretory lysosomes. *Nat. Rev. Mol. Cell Biol.*, **3,** 122-131.

[12] Raposo G, Tenza D, Mecheri S, Peronet R, Bonnerot C, & Desaymard C (1997) Accumulation of major histocompatibility complex class II molecules in mast cell secretory granules and their release upon degranulation. *Mol. Biol. Cell*, **8,** 2631-2645.

[13] Puri N & Roche PA (2008) Mast cells possess distinct secretory granule subsets whose exocytosis is regulated by different SNARE isoforms. *Proc. Natl. Acad. Sci. U. S. A*, **105,** 2580-2585.

[14] Sotelo JR & Porter KR (1959) An electron microscope study of the rat ovum. *J. Biophys. Biochem. Cytol.*, **5,** 327-342.

[15] Perrigoue JG, Saenz SA, Siracusa MC, Allenspach EJ, Taylor BC, Giacomin PR, Nair MG, Du Y, Zaph C, van RN, Comeau MR, Pearce EJ, Laufer TM, & Artis D (2009) MHC class II-dependent basophil-CD4+ T cell interactions promote T(H)2 cytokine-dependent immunity. *Nat. Immunol.*, **10,** 697-705.

[16] Sokol CL, Chu NQ, Yu S, Nish SA, Laufer TM, & Medzhitov R (2009) Basophils function as antigen-presenting cells for an allergen-induced T helper type 2 response. *Nat. Immunol.*, **10,** 713-720.

[17] Yoshimoto T, Yasuda K, Tanaka H, Nakahira M, Imai Y, Fujimori Y, & Nakanishi K (2009) Basophils contribute to T(H)2-IgE responses in vivo via IL-4 production and presentation of peptide-MHC class II complexes to CD4+ T cells. *Nat. Immunol.*, **10,** 706-712.

[18] Gaudenzio N, Espagnolle N, Mars LT, Liblau R, Valitutti S, & Espinosa E (2009) Cell-cell cooperation at the T helper cell/mast cell immunological synapse. *Blood*, **114,** 4979-4988.

[19] Carroll-Portillo A, Surviladze Z, Cambi A, Lidke DS, & Wilson BS (2012) Mast cell synapses and exosomes: membrane contacts for information exchange. *Front Immunol.*, **3,** 46.

[20] Valadi H, Ekstrom K, Bossios A, Sjostrand M, Lee JJ, & Lotvall JO (2007) Exosome-mediated transfer of mRNAs and microRNAs is a novel mechanism of genetic exchange between cells. *Nat. Cell Biol.*, **9,** 654-U72.

[21] Eldh M, Ekstrom K, Valadi H, Sjostrand M, Olsson B, Jernas M, & Lotvall J (2010) Exosomes communicate protective messages during oxidative stress; possible role of exosomal shuttle RNA. *PLoS. One.*, **5,** e15353.

[22] Kunder CA, St John AL, Li G, Leong KW, Berwin B, Staats HF, & Abraham SN (2009) Mast cell-derived particles deliver peripheral signals to remote lymph nodes. *J. Exp. Med.*, **206,** 2455-2467.

[23] Abraham SN & St John AL (2010) Mast cell-orchestrated immunity to pathogens. *Nat. Rev. Immunol.*, **10,** 440-452.

[24] Cho KJ, Seo JM, & Kim JH (2011) Bioactive lipoxygenase metabolites stimulation of NADPH oxidases and reactive oxygen species. *Molecules and Cells*, **32,** 1-5.

[25] Mandal AK, Jones PB, Bair AM, Christmas P, Miller D, Yamin TT, Wisniewski D, Menke J, Evans JF, Hyman BT, Bacskai B, Chen M, Lee DM, Nikolic B, & Soberman RJ (2008) The nuclear membrane organization of leukotriene synthesis. *Proc. Natl. Acad. Sci. U. S. A*, **105,** 20434-20439.

[26] Galli SJ, Kalesnikoff J, Grimbaldeston MA, Piliponsky AM, Williams CM, & Tsai M (2005) Mast cells as "tunable" effector and immunoregulatory cells: recent advances. *Annu. Rev. Immunol.*, **23,** 749-786.

[27] Smrž D, Dráberová L, & Dráber P (2007) Non-apoptotic phosphatidylserine externalization induced by engagement of glycosylphosphatidylinositol-anchored proteins. *J. Biol. Chem.*, **282,** 10487-10497.

[28] Yoshikawa H, Nakajima Y, & Tasaka K (2000) Enhanced expression of Fas-associated death domain-like IL-1-converting enzyme (FLICE)-inhibitory protein induces resistance to Fas-mediated apoptosis in activated mast cells. *J. Immunol.*, **165,** 6262-6269.

[29] Xiang Z, Ahmed AA, Moller C, Nakayama K, Hatakeyama S, & Nilsson G (2001) Essential role of the prosurvival bcl-2 homologue A1 in mast cell survival after allergic activation. *J. Exp. Med.*, **194,** 1561-1569.

[30] Xiang Z, Moller C, & Nilsson G (2006) IgE-receptor activation induces survival and Bfl-1 expression in human mast cells but not basophils. *Allergy*, **61,** 1040-1046.

[31] Ekoff M, Strasser A, & Nilsson G (2007) FcεRI aggregation promotes survival of connective tissue-like mast cells but not mucosal-like mast cells. *J. Immunol.*, **178,** 4177-4183.

[32] Michaloudi H, Grivas I, Batzios C, Chiotelli M, & Papadopoulos GC (2003) Parallel development of blood vessels and mast cells in the lateral geniculate nuclei. *Brain Res. Dev. Brain Res.*, **140,** 269-276.

[33] Sayed BA, Christy AL, Walker ME, & Brown MA (2010) Meningeal mast cells affect early T cell central nervous system infiltration and blood-brain barrier integrity through TNF: a role for neutrophil recruitment? *J. Immunol.*, **184,** 6891-6900.

[34] Cheng LE, Hartmann K, Roers A, Krummel MF, & Locksley RM (2013) Perivascular mast cells dynamically probe cutaneous blood vessels to capture immunoglobulin E. *Immunity.*, **38,** 166-175.

[35] Abraham SN & St John AL (2010) Mast cell-orchestrated immunity to pathogens. *Nat. Rev. Immunol.*, **10,** 440-452.

[36] Matzinger P (2007) Friendly and dangerous signals: is the tissue in control? *Nat. Immunol.*, **8,** 11-13.

[37] Akahoshi M, Song CH, Piliponsky AM, Metz M, Guzzetta A, Abrink M, Schlenner SM, Feyerabend TB, Rodewald HR, Pejler G, Tsai M, & Galli SJ (2011) Mast cell chymase reduces the toxicity of Gila monster venom, scorpion venom, and vasoactive intestinal polypeptide in mice. *J. Clin. Invest*, **121,** 4180-4191.

[38] Metz M, Piliponsky AM, Chen CC, Lammel V, Abrink M, Pejler G, Tsai M, & Galli SJ (2006) Mast cells can enhance resistance to snake and honeybee venoms. *Science*, **313,** 526-530.

[39] Kunder CA, St John AL, & Abraham- SN (2011) Mast cell modulation of the vascular and lymphatic endothelium. *Blood*, **118,** 5383-5393.

[40] Soter NA, Lewis RA, Corey EJ, & Austen KF (1983) Local-Effects of Synthetic Leukotrienes (Ltc4, Ltd4, Lte4, and Ltb4) in Human-Skin. *Journal of Investigative Dermatology*, **80,** 115-119.

[41] Datta YH, Romano M, Jacobson BC, Golan DE, Serhan CN, & Ewenstein BM (1995) Peptido-Leukotrienes Are Potent Agonists of Von-Willebrand-Factor Secretion and P-Selectin Surface Expression in Human Umbilical Vein Endothelial-Cells. *Circulation*, **92,** 3304-3311.

[42] van Mourik JA, de Wit TR, & Voorberg J (2002) Biogenesis and exocytosis of

Weibel-Palade bodies. *Histochemistry and Cell Biology*, **117,** 113-122.

[43] Miki I, Kusano A, Ohta S, Hanai N, Otoshi M, Masaki S, Sato S, & Ohmori K (1996) Histamine enhanced the TNF-α-induced expression of E-selectin and ICAM-1 on vascular endothelial cells. *Cell. Immunol.*, **171,** 285-288.

[44] Shelburne CP, Nakano H, St John AL, Chan C, McLachlan JB, Gunn MD, Staats HF, & Abraham SN (2009) Mast Cells Augment Adaptive Immunity by Orchestrating Dendritic Cell Trafficking through Infected Tissues. *Cell Host & Microbe*, **6,** 331-342.

[45] Dahlen SE, Hedqvist P, Hammarstrom S, & Samuelsson B (1980) Leukotrienes Are Potent Constrictors of Human Bronchi. *Nature*, **288,** 484-486.

[46] Hanna CJ, Bach MK, Pare PD, & Schellenberg RR (1981) Slow-Reacting Substances (Leukotrienes) Contract Human Airway and Pulmonary Vascular Smooth-Muscle Invitro. *Nature*, **290,** 343-344.

[47] Cyphert JM, Kovarova M, Allen IC, Hartney JM, Murphy DL, Wess J, & Koller BH (2009) Cooperation between Mast Cells and Neurons Is Essential for Antigen-Mediated Bronchoconstriction. *J. Immunol.*, **182,** 7430-7439.

[48] Kasugai T, Tei H, Okada M, Hirota S, Morimoto M, Yamada M, Nakama A, Arizono N, & Kitamura Y (1995) Infection with Nippostrongylus-Brasiliensis Induces Invasion of Mast-Cell Precursors from Peripheral-Blood to Small-Intestine. *Blood*, **85,** 1334-1340.

[49] Ohnmacht C & Voehringer D (2010) Basophils Protect against Reinfection with Hookworms Independently of Mast Cells and Memory Th2 Cells. *J. Immunol.*, **184,** 344-350.

[50] Wada T, Ishiwata K, Koseki H, Ishikura T, Ugajin T, Ohnuma N, Obata K, Ishikawa R, Yoshikawa S, Mukai K, Kawano Y, Minegishi Y, Yokozeki H, Watanabe N, & Karasuyama H (2010) Selective ablation of basophils in mice reveals their nonredundant role in acquired immunity against ticks. *Journal of Clinical Investigation*, **120,** 2867-2875.

[51] Furuta T, Kikuchi T, Iwakura Y, & Watanabe N (2006) Protective roles of mast cells and mast cell-derived TNF in murine malaria. *J. Immunol.*, **177,** 3294-3302.

[52] Knight PA, Wright SH, Lawrence CE, Paterson YYW, & Miller HRP (2000) Delayed expulsion of the nematode Trichinella spiralis in mice lacking the mucosal mast cell-specific granule chymase, mouse mast cell protease-1. *J. Exp. Med.*, **192,** 1849-1856.

[53] Maurer M, Kostka SL, Siebenhaar F, Moelle K, Metz M, Knop J, & von Stebut E (2006) Skin mast cells control T cell-dependent host defense in Leishmania major infections. *Faseb Journal*, **20,** 2460-2467.

[54] Kambayashi T, Allenspach EJ, Chang JT, Zou T, Shoag JE, Reiner SL, Caton AJ, & Koretzky GA (2009) Inducible MHC Class II Expression by Mast Cells Supports Effector and Regulatory T Cell Activation. *J. Immunol.*, **182,** 4686-4695.

[55] von Kockritz-Blickwede M, Goldmann O, Thulin P, Heinemann K, Norrby-Teglund A, Rohde M, & Medina E (2008) Phagocytosis-independent antimicrobial activity of mast cells by means of extracellular trap formation. *Blood*, **111,** 3070-3080.

[56] Papayannopoulos V, Metzler KD, Hakkim A, & Zychlinsky A (2010) Neutrophil elastase and myeloperoxidase regulate the formation of neutrophil extracellular traps. *J. Cell Biol.*, **191,** 677-691.

[57] Malaviya R, Ross EA, MacGregor JI, Ikeda T, Little JR, Jakschik BA, & Abraham SN (1994) Mast cell phagocytosis of FimH-expressing enterobacteria. *J. Immunol.*, **152,** 1907-1914.

[58] Arock M, Ross E, Lai-Kuen R, Averlant G, Gao ZM, & Abraham SN (1998) Phagocytic and tumor necrosis factor α response of human mast cells following exposure to Gram-negative and Gram-positive bacteria. *Infection and Immunity*, **66,** 6030-6034.

[59] Abel J, Goldmann O, Ziegler C, Holtje C, Smeltzer MS, Cheung AL, Bruhn D, Rohde M, & Medina E (2011) Staphylococcus aureus Evades the Extracellular Antimicrobial Activity of Mast Cells by Promoting Its Own Uptake. *Journal of Innate Immunity*, **3,** 495-507.

[60] Echtenacher B, Mannel DN, & Hultner L (1996) Critical protective role of mast cells in a model of acute septic peritonitis. *Nature*, **381,** 75-77.

[61] Malaviya R, Ikeda T, Ross E, & Abraham SN (1996) Mast cell modulation of neutrophil influx and bacterial clearance at sites of infection through TNF- α. *Nature*, **381,** 77-80.

[62] Malaviya R & Abraham SN (2000) Role of mast cell leukotrienes in neutrophil recruitment and bacterial clearance in infectious peritonitis. *Journal of Leukocyte Biology*, **67,** 841-846.

[63] Huang CF, Friend DS, Qiu WT, Wong GW, Morales G, Hunt J, & Stevens RL (1998) Induction of a selective and persistent extravasation of neutrophils into the peritoneal cavity by tryptase mouse mast cell protease 6. *J. Immunol.*, **160,** 1910-1919.

[64] Sutherland RE, Olsen JS, McKinstry A, Villalta SA, & Wolters PJ (2008) Mast cell IL-6 improves survival from Klebsiella pneumonia and sepsis by enhancing neutrophil killing. *J. Immunol.*, **181,** 5598-5605.

[65] Di Nardo A, Vitiello A, & Gallo RL (2003) Cutting edge: Mast cell antimicrobial activity is mediated by expression of cathelicidin antimicrobial peptide. *J. Immunol.*, **170,** 2274-2278.

[66] St John AL, Rathore APS, Yap H, Ng ML, Metcalfe DD, Vasudevan SG, & Abraham SN (2011) Immune surveillance by mast cells during dengue infection promotes natural killer (NK) and NKT-cell recruitment and viral clearance. *Proc. Natl. Acad. Sci. U. S. A*, **108,** 9190-9195.

[67] Gabriel BW & Justus DE (1979) Quantitation of Immediate and Delayed-Hypersensitivity Responses in Trichinella-Infected Mice - Correlation with Worm Expulsion. *Int. Arch. Allergy Immunol.*, **60,** 275-285.

[68] Matossian RM, Salti I, & Stephan E (1977) Variation in Serum Immunoglobulin Levels in Acute Trichinosis. *Journal of Helminthology*, **51,** 1-4.

[69] Gurish MF, Bryce PJ, Tao H, Kisselgof AB, Thornton EM, Miller HR, Friend DS, & Oettgen HC (2004) IgE enhances parasite clearance and regulates mast cell responses in mice infected with Trichinella spiralis. *J. Immunol.*, **172,** 1139-1145.

[70] Mukai K, Matsuoka K, Taya C, Suzuki H, Yokozeki H, Nishioka K, Hirokawa K, Etori M, Yamashita M, Kubota T, Minegishi Y, Yonekawa H, & Karasuyama H (2005) Basophils play a critical role in the development of IgE-mediated chronic allergic inflammation independently of T cells and mast cells. *Immunity*, **23,** 191-202.

[71] Galli SJ, Tsai M, & Piliponsky AM (2008) The development of allergic inflammation. *Nature*, **454,** 445-454.

[72] Grimbaldeston MA, Metz M, Yu M, Tsai M, & Galli SJ (2006) Effector and potential immunoregulatory roles of mast cells in IgE-associated acquired immune responses. *Current Opinion in Immunology*, **18,** 751-760.

[73] Feyerabend TB, Weiser A, Tietz A, Stassen M, Harris N, Kopf M, Radermacher P, Moller P, Benoist C, Mathis D, Fehling HJ, & Rodewald HR (2011) Cre-Mediated Cell Ablation Contests Mast Cell Contribution in Models of Antibody- and T Cell-Mediated Autoimmunity. *Immunity*, **35,** 832-844.

[74] Nigrovic PA, Binstadt BA, Monach PA, Johnsen A, Gurish M, Iwakura Y, Benoist C, Mathis D, & Lee DM (2007) Mast cells contribute to initiation of autoantibody-mediated arthritis via IL-1. *Proc. Natl. Acad. Sci. U. S. A*, **104,** 2325-2330.

[75] Carlson T, Kroenke M, Rao P, Lane TE, & Segal B (2008) The Th17-ELR+ CXC chemokine pathway is essential for the development of central nervous system autoimmune disease. *J. Exp. Med.*, **205,** 811-823.

[76] Zhou JS, Xing W, Friend DS, Austen KF, & Katz HR (2007) Mast cell deficiency in Kit(W-sh) mice does not impair antibody-mediated arthritis. *J. Exp. Med.*, **204,** 2797-2802.

[77] Piconese S, Costanza M, Musio S, Tripodo C, Poliani PL, Gri G, Burocchi A, Pittoni P, Gorzanelli A, Colombo MP, & Pedotti R (2011) Exacerbated experimental autoimmune encephalomyelitis in mast-cell-deficient Kit(W-sh/W-sh) mice. *Laboratory Investigation*, **91,** 627-641.

[78] Carroll-Portillo A, Spendier K, Pfeiffer J, Griffiths G, Li HT, Lidke KA, Oliver JM, Lidke DS, Thomas JL, Wilson BS, & Timlin JA (2010) Formation of a Mast Cell Synapse: Fc epsilon RI Membrane Dynamics upon Binding Mobile or Immobilized Ligands on Surfaces. *J. Immunol.*, **184,** 1328-1338.

[79] Bhattacharyya SP, Drucker I, Reshef T, Kirshenbaum AS, Metcalfe DD, & Mekori YA (1998) Activated T lymphocytes induce degranulation and cytokine production by human mast cells following cell-to-cell contact. *Journal of Leukocyte Biology*, **63,** 337-341.

[80] Inamura N, Mekori YA, Bhattacharyya SP, Bianchine PJ, & Metcalfe DD (1998) Induction and enhancement of Fc epsilon RI-dependent mast cell degranulation following coculture with activated T cells: Dependency on ICAM-1- and leukocyte function-associated antigen (LFA)-1-mediated heterotypic aggregation. *J. Immunol.*, **160,** 4026-4033.

[81] Caron G, Delneste Y, Roelandts E, Duez C, Herbault N, Magistrelli G, Bonnefoy JY, Pestel J, & Jeannin P (2001) Histamine induces CD86 expression and chemokine production by human immature dendritic cells. *J. Immunol.*, **166,** 6000-6006.

[82] Ren SR, Xu LB, Wu ZY, Du J, Gao MH, & Qu CF (2010) Exogenous dendritic cell homing to draining lymph nodes can be boosted by mast cell degranulation. *Cell. Immunol.*, **263,** 204-211.

[83] Dudeck A, Dudeck J, Scholten J, Petzold A, Surianarayanan S, Kohler A, Peschke K, Vohringer D, Waskow C, Krieg T, Muller W, Waisman A, Hartmann K, Gunzer M, & Roers A (2011) Mast Cells Are Key Promoters of Contact Allergy that Mediate the Adjuvant Effects of Haptens. *Immunity*, **34,** 973-984.

[84] Otsuka A, Kubo M, Honda T, Egawa G, Nakajima S, Tanizaki H, Kim B, Matsuoka S, Watanabe T, Nakae S, Miyachi Y, & Kabashima K (2011) Requirement of Interaction between Mast Cells and Skin Dendritic Cells to Establish Contact Hypersensitivity. *Plos One*, **6**.

[85] Mazzoni A, Siraganian RP, Leifer CA, & Segal DM (2006) Dendritic cell modulation by mast cells controls the Th1/Th2 balance in responding T cells. *J. Immunol.*, **177,** 3577-3581.

[86] Kitawaki T, Kadowaki N, Sugimoto N, Kambe N, Hori T, Miyachi Y, Nakahata T, & Uchiyama T (2006) IgE-activated mast cells in combination with pro-inflammatory factors induce T(h)2-promoting dendritic cells. *International immunology*, **18,** 1789-1799.

[87] Dudeck A, Suender CA, Kostka SL, von Stebut E, & Maurer M (2011) Mast cells promote Th1 and Th17 responses by modulating dendritic cell maturation and function. *Eur. J. Immunol.*, **41,** 1883-1893.

[88] Skokos D, Botros HG, Demeure C, Morin J, Peronet R, Birkenmeier G, Boudaly S, & Mecheri S (2003) Mast cell-derived exosomes induce phenotypic and functional maturation of dendritic cells and elicit specific immune responses in vivo. *J. Immunol.*, **170,** 3037-3045.

[89] Skokos D, Le Panse S, Villa I, Rousselle JC, Peronet R, David B, Namane A, & Mecheri S (2001) Mast cell-dependent B and T lymphocyte activation is mediated by the secretion of immunologically active exosomes. *J. Immunol.*, **166,** 868-876.

[90] Shefler I, Salamon P, Reshef T, Mor A, & Mekori YA (2010) T Cell-Induced Mast Cell Activation: A Role for Microparticles Released from Activated T Cells. *J. Immunol.*, **185,** 4206-4212.

[91] Vincent-Schneider H, Thery C, Mazzeo D, Tenza D, Raposo G, & Bonnerot C (2001) Secretory granules of mast cells accumulate mature and immature MHC class II molecules. *J. Cell Sci.*, **114,** 323-334.

[92] Blank U, Ra C, Miller L, White K, Metzger H, & Kinet J-P (1989) Complete structure and expression in transfected cells of high affinity IgE receptor. *Nature*, **337,** 187-189.

[93] Garman SC, Kinet JP, & Jardetzky TS (1998) Crystal structure of the human high-affinity IgE receptor. *Cell*, **95,** 951-961.

[94] Gounni AS (2006) The high-affinity IgE receptor (Fc epsilon RI): a critical regulator of airway smooth muscle cells? *American Journal of Physiology-Lung Cellular and Molecular Physiology*, **291,** L312-L321.

[95] Kinet JP (1999) The high-affinity IgE receptor (FcεRI): from physiology to pathology. *Annu. Rev. Immunol.*, **17,** 931-972.

[96] Kraft S & Kinet JP (2007) New developments in FcepsilonRI regulation, function and inhibition. *Nat. Rev. Immunol.*, **7,** 365-378.

[97] van der Kleij H, Charles N, Karimi K, Mao YK, Foster J, Janssen L, Yang PC, Kunze W, Rivera J, & Bienenstock J (2010) Evidence for neuronal expression of functional Fc (ε and γ) receptors. *Journal of Allergy and Clinical Immunology*, **125,** 757-760.

[98] Letourneur O, Sechi S, Willettebrown J, Robertson MW, & Kinet JP (1995) Glycosylation of Human Truncated Fc-E ε -Ri α-Chain Is Necessary for Efficient Folding in the Endoplasmic-Reticulum. *J. Biol. Chem.*, **270,** 8249-8256.

[99] Garman SC, Wurzburg BA, Tarchevskaya SS, Kinet JP, & Jardetzky TS (2000) Structure of the Fc fragment of human IgE bound to its high-affinity receptor Fc epsilon RI alpha. *Nature*, **406,** 259-266.

[100] McDonnell JM, Calvert R, Beavil RL, Beavil AJ, Henry AJ, Sutton BJ, Gould HJ, & Cowburn D (2001) The structure of the IgE Cε2 domain and its role in stabilizing the complex with its high-affinity receptor FcεRl α. *Nature Structural Biology*, **8,** 437-441.

[101] Miller L, Blank U, Metzger H, & Kinet J-P (1989) Expression of high-affinity binding of human immunoglobulin E by transfected cells. *Science*, **244,** 334-337.

[102] Dombrowicz D, Quatannens B, Papin JP, Capron A, & Capron M (2000) Expression of a functional FcεRI on rat eosinophils and macrophages. *J. Immunol.*, **165,** 1266-1271.

[103] Letourneur F, Hennecke S, Demolliere C, & Cosson P (1995) Steric Masking of A Dilysine Endoplasmic-Reticulum Retention Motif During Assembly of the Human High-Affinity Receptor for Immunoglobulin-e. *J. Cell Biol.*, **129,** 971-978.

[104] Lin S, Cicala C, Scharenberg AM, & Kinet JP (1996) The FcεRIβ subunit functions as an amplifier of FcεRIγ-mediated cell activation signals. *Cell*, **85,** 985-995.

[105] On M, Billingsley JM, Jouvin MH, & Kinet JP (2004) Molecular dissection of the FcR β signaling amplifier. *J. Biol. Chem.*, **279,** 45782-45790.

[106] Sakurai D, Yamasaki S, Arase K, Park SY, Arase H, Konno A, & Saito T (2004) FcεRI γ-ITAM is differentially required for mast cell function in vivo. *J. Immunol.*, **172,** 2374-2381.

[107] Furuichi K, Rivera J, & Isersky C (1985) The Receptor for Immunoglobulin-e on Rat Basophilic Leukemia-Cells - Effect of Ligand-Binding on Receptor Expression. *Proc. Natl. Acad. Sci. U. S. A*, **82,** 1522-1525.

[108] Yamaguchi M, Lantz CS, Oettgen HC, Katona IM, Fleming T, Miyajima I, Kinet JP, & Galli SJ (1997) IgE enhances mouse mast cell FcεRI expression in vitro and in vivo: evidence for a novel amplification mechanism in IgE-dependent reactions. *J. Exp. Med.*, **185,** 663-672.

[109] Pribluda VS, Pribluda C, & Metzger H (1994) Transphosphorylation as the mechanism by which the high-affinity receptor for IgE is phosphorylated upon aggregation. *Proc. Natl. Acad. Sci. USA*, **91,** 11246-11250.

[110] Shiue L, Green J, Green OM, Karas JL, Morgenstern JP, Ram MK, Taylor MK, Zoller MJ, Zydowsky LD, Bolen JB, & Brugge JS (1995) Interaction of p72syk with the gamma and beta subunits of the high-affinity receptor for immunoglobulin E, Fc epsilon RI. *Mol. Cell Biol.*, **15,** 272-281.

[111] Okada M (2012) Regulation of the Src Family Kinases by Csk. *International Journal of Biological Sciences*, **8,** 1385-1397.

[112] Okada M, Nada S, Yamanashi Y, Yamamoto T, & Nakagawa H (1991) CSK: a protein-tyrosine kinase involved in regulation of src family kinases. *J. Biol. Chem.*, **266,** 24249-24252.

[113] Yi TL, Bolen JB, & Ihle JN (1991) Hematopoietic-Cells Express 2 Forms of Lyn Kinase Differing by 21 Amino-Acids in the Amino Terminus. *Molecular and Cellular Biology*, **11,** 2391-2398.

[114] Yamashita T, Mao S-Y, & Metzger H (1994) Aggregation of the high-affinity IgE receptor and enhanced activity of $p53/p56^{lyn}$ protein-tyrosine kinase. *Proc. Natl. Acad. Sci. USA*, **91,** 11251-11255.

[115] Avarez-Errico D, Yamashita Y, Suzuki R, Odom S, Furumoto Y, Yamashita T, & Rivera J (2010) Functional Analysis of Lyn Kinase A and B Isoforms Reveals Redundant and Distinct Roles in Fc epsilon RI-Dependent Mast Cell Activation. *J. Immunol.*, **184,** 5000-5008.

[116] Kovářová M, Tolar P, Arudchandran R, Dráberová L, Rivera J, & Dráber P (2001) Structure-function analysis of Lyn kinase association with lipid rafts and initiation of early signaling events after Fcε receptor I aggregation. *Mol. Cell Biol.*, **21,** 8318-8328.

[117] Brown DA (2006) Lipid rafts, detergent-resistant membranes, and raft targeting signals. *Physiology. (Bethesda.)*, **21,** 430-439.

[118] Kawakami Y, Kitaura J, Satterthwaite AB, Kato RM, Asai K, Hartman SE, Maeda-Yamamoto M, Lowell CA, Rawlings DJ, Witte ON, & Kawakami T (2000) Redundant and opposing functions of two tyrosine kinases, Btk and Lyn, in mast cell activation. *J. Immunol.*, **165,** 1210-1219.

[119] Nishizumi H & Yamamoto T (1997) Impaired tyrosine phosphorylation and Ca^{2+} mobilization, but not degranulation, in lyn-deficient bone marrow-derived mast cells. *J. Immunol.*, **158,** 2350-2355.

[120] Hernandez-Hansen V, Smith AJ, Surviladze Z, Chigaev A, Mazel T, Kalesnikoff J, Lowell CA, Krystal G, Sklar LA, Wilson BS, & Oliver JM (2004) Dysregulated FcεRI signaling and altered Fyn and SHIP activities in Lyn-deficient mast cells. *J. Immunol.*, **173,** 100-112.

[121] Odom S, Gomez G, Kovarova M, Furumoto Y, Ryan JJ, Wright HV, Gonzalez-Espinosa C, Hibbs ML, Harder KW, & Rivera J (2004) Negative regulation of immunoglobulin E-dependent allergic responses by Lyn kinase. *J. Exp. Med.*, **199,** 1491-1502.

[122] Parravicini V, Gadina M, Kovarova M, Odom S, Gonzalez-Espinosa C, Furumoto Y, Saitoh S, Samelson LE, O'Shea JJ, & Rivera J (2002) Fyn kinase initiates complementary signals required for IgE-dependent mast cell degranulation. *Nat. Immunol.*, **3,** 741-748.

[123] Yamashita Y, Charles N, Furumoto Y, Odom S, Yamashita T, Gilfillan AM, Constant S, Bower MA, Ryan JJ, & Rivera J (2007) Cutting edge: genetic variation influences FcεRI-induced mast cell activation and allergic responses. *J. Immunol.*, **179,** 740-743.

[124] Xiao WB, Nishimoto H, Hong H, Kitaura J, Nunomura S, Maeda-Yamamoto M,

Kawakami Y, Lowell CA, Ra CS, & Kawakami T (2005) Positive and negative regulation of mast cell activation by Lyn via the Fc epsilon RI. *J. Immunol.*, **175,** 6885-6892.

[125] Yu M, Lowell CA, Neel BG, & Gu HH (2006) Scaffolding adapter Grb2-associated binder 2 requires Syk to transmit signals from Fc epsilon RI. *J. Immunol.*, **176,** 2421-2429.

[126] Nishida K, Yamasaki S, Ito Y, Kabu K, Hattori K, Tezuka T, Nishizumi H, Kitamura D, Goitsuka R, Geha RS, Yamamoto T, Yagi T, & Hirano T (2005) FcεRI-mediated mast cell degranulation requires calcium-independent microtubule-dependent translocation of granules to the plasma membrane. *J. Cell Biol.*, **170,** 115-126.

[127] Hong H, Kitaura J, Xiao WB, Hořejši V, Ra CS, Lowell CA, Kawakami Y, & Kawakami T (2007) The Src family kinase Hck regulates mast cell activation by suppressing an inhibitory Src family kinase Lyn. *Blood*, **110,** 2511-2519.

[128] Lee JH, Kim JW, Kim DK, Kim HS, Park HJ, Park DK, Kim AR, Kim B, Beaven MA, Park KL, Kim YM, & Choi WS (2011) The Src Family Kinase Fgr Is Critical for Activation of Mast Cells and IgE-Mediated Anaphylaxis in Mice. *J. Immunol.*, **187,** 1807-1815.

[129] Eiseman E & Bolen JB (1992) Engagement of the high-affinity IgE receptor activates *src* protein-related tyrosine kinases. *Nature*, **355,** 78-80.

[130] Dráber P, Hálová I, Levi-Schaffer F, & Dráberová L (2011) Transmembrane adaptor proteins in the high-affinity IgE receptor signaling. *Front Immunol.*, **2,** 95.

[131] Brdička T, Pavlistová D, Leo A, Bruyns E, Kořínek V, Angelisová P, Scherer J, Shevchenko A, Hilgert I, Černý J, Drbal K, Kuramitsu Y, Kornacker B, Hořejší V, & Schraven B (2000) Phosphoprotein associated with glycosphingolipid-enriched microdomains (PAG), a novel ubiquitously expressed transmembrane adaptor protein, binds the protein tyrosine kinase csk and is involved in regulation of T cell activation. *J. Exp. Med.*, **191,** 1591-1604.

[132] Volná P, Lebduška P, Dráberová L, Šímová S, Heneberg P, Boubelík M, Bugajev V, Malissen B, Wilson BS, Hořejši V, Malissen M, & Dráber P (2004) Negative Regulation of Mast Cell Signaling and Function by the Adaptor LAB/NTAL. *J. Exp. Med.*, **200,** 1001-1013.

[133] Wilson BS, Pfeiffer JR, & Oliver JM (2002) FcεRI signaling observed from the inside of the mast cell membrane. *Mol. Immunol.*, **38,** 1259-1268.

[134] Saitoh S, Arudchandran R, Manetz TS, Zhang W, Sommers CL, Love PE, Rivera J, & Samelson LE (2000) LAT is essential for FcεRI-mediated mast cell activation. *Immunity.*, **12,** 525-535.

[135] Malbec O, Malissen M, Isnardi I, Lesourne R, Mura AM, Fridman WH, Malissen B, & Daeron M (2004) Linker for activation of T cells integrates positive and negative signaling in mast cells. *J. Immunol.*, **173,** 5086-5094.

[136] Zhu M, Liu Y, Koonpaew S, Granillo O, & Zhang W (2004) Positive and negative regulation of FceRI-mediated signaling by adaptor protein LAB/NTAL. *J. Exp. Med.*, **200,** 991-1000.

[137] Tkaczyk C, Hořejší V, Shoko I, Dráber P, Samelson LE, Satterthwaite AB, Nahm DH, Metcalfe DD, & Gilfillan AM (2004) NTAL phosphorylation is a pivotal link between the signaling cascades leading to human mast cell degranulation following kit activation and FcεRI aggregation. *Blood*, **104,** 207-214.

[138] Dráberová L, Shaik GM, Volná P, Heneberg P, Tůmová M, Lebduška P, Korb J, & Dráber P (2007) Regulation of Ca^{2+} signaling in mast cells by tyrosine-phosphorylated and unphosphorylated non-T cell activation linker. *J. Immunol.*, **179,** 5169-5180.

[139] Kawabuchi M, Satomi Y, Takao T, Shimonishi Y, Nada S, Nagai K, Tarakhovsky A, & Okada M (2000) Transmembrane phosphoprotein Cbp regulates the activities of Src-family tyrosine kinases. *Nature*, **404,** 999-1003.

[140] Ohtake H, Ichikawa N, Okada M, & Yamashita T (2002) Cutting Edge: Transmembrane phosphoprotein Csk-binding protein/phosphoprotein associated with glycosphingolipid-enriched microdomains as a negative feedback regulator of mast cell signaling through the FcεRI. *J. Immunol.*, **168,** 2087-2090.

[141] Gilfillan AM & Rivera J (2009) The tyrosine kinase network regulating mast cell activation. *Immunol. Rev.*, **228,** 149-169.

[142] Bolotina VM & Csutora P (2005) CIF and other mysteries of the store-operated Ca^{2+}-entry pathway. *Trends Biochem. Sci.*, **30,** 378-387.

[143] Ma HT & Beaven MA (2009) Regulation of Ca^{2+} Signaling with Particular Focus on Mast Cells. *Critical Reviews in Immunology*, **29,** 155-186.

[144] Liou J, Kim ML, Do HW, Jones JT, Myers JW, Ferrell JE, Jr., & Meyer T (2005) STIM is a Ca^{2+} sensor essential for Ca^{2+}-store-depletion-triggered Ca^{2+} influx. *Curr. Biol.*, **15,** 1235-1241.

[145] Roos J, DiGregorio PJ, Yeromin AV, Ohlsen K, Lioudyno M, Zhang S, Safrina O, Kozak JA, Wagner SL, Cahalan MD, Velicelebi G, & Stauderman KA (2005) STIM1, an essential and conserved component of store-operated Ca^{2+} channel function. *J. Cell Biol.*, **169,** 435-445.

[146] Williams RT, Manji SSM, Parker NJ, Hancock MS, Van Stekelenburg L, Eid JP, Senior PV, Kazenwadel JS, Shandala T, Saint R, Smith PJ, & Dziadek MA (2001) Identification and characterization of the STIM (stromal interaction molecule) gene family: coding for a novel class of transmembrane proteins. *Biochemical Journal*, **357,** 673-685.

[147] Zhang SL, Yu Y, Roos J, Kozak JA, Deerinck TJ, Ellisman MH, Stauderman KA, & Cahalan MD (2005) STIM1 is a Ca^{2+} sensor that activates CRAC channels and migrates from the Ca^{2+} store to the plasma membrane. *Nature*, **437,** 902-905.

[148] Hauser CT & Tsien RY (2007) A hexahistidine-Zn^{2+}-dye label reveals STIM1 surface exposure. *Proc. Natl. Acad. Sci. U. S. A*, **104,** 3693-3697.

[149] Jardin I, Lopez JJ, Redondo PC, Salido GM, & Rosado JA (2009) Store-operated Ca^{2+} entry is sensitive to the extracellular Ca^{2+} concentration through plasma membrane STIM1. *Biochimica et Biophysica Acta-Molecular Cell Research*, **1793,** 1614-1622.

[150] Luik RM, Wu MM, Buchanan J, & Lewis RS (2006) The elementary unit of store-operated Ca^{2+} entry: local activation of CRAC channels by STIM1 at ER-plasma membrane junctions. *J. Cell Biol.*, **174,** 815-825.

[151] Feske S, Gwack Y, Prakriya M, Srikanth S, Puppel SH, Tanasa B, Hogan PG, Lewis RS, Daly M, & Rao A (2006) A mutation in Orai1 causes immune deficiency by abrogating CRAC channel function. *Nature*, **441,** 179-185.

[152] Vig M, Peinelt C, Beck A, Koomoa DL, Rabah D, Koblan-Huberson M, Kraft S, Turner H, Fleig A, Penner R, & Kinet JP (2006) CRACM1 is a plasma membrane protein essential for store-operated Ca^{2+} entry. *Science*, **312,** 1220-1223.

[153] Zhang SL, Yeromin AV, Zhang XH, Yu Y, Safrina O, Penna A, Roos J, Stauderman KA, & Cahalan MD (2006) Genome-wide RNAi screen of $Ca^{(2+)}$ influx identifies genes that regulate $Ca^{(2+)}$ release-activated $Ca^{(2+)}$ channel activity. *Proc. Natl. Acad. Sci. U. S. A*, **103,** 9357-9362.

[154] Vig M, Beck A, Billingsley JM, Lis A, Parvez S, Peinelt C, Koomoa DL, Soboloff J, Gill DL, Fleig A, Kinet JP, & Penner R (2006) CRACM1 multimers form the ion-selective pore of the CRAC channel. *Current Biology*, **16,** 2073-2079.

[155] Mercer JC, Dehaven WI, Smyth JT, Wedel B, Boyles RR, Bird GS, & Putney JW, Jr. (2006) Large store-operated calcium selective currents due to co-expression of Orai1 or Orai2 with the intracellular calcium sensor, Stim1. *J. Biol. Chem.*, **281,** 24979-24990.

[156] Gwack Y, Srikanth S, Feske S, Cruz-Guilloty F, Oh-hora M, Neems DS, Hogan PG, & Rao A (2007) Biochemical and functional characterization of Orai proteins. *J. Biol. Chem.*, **282,** 16232-16243.

[157] Demuro A, Penna A, Safrina O, Yeromin AV, Amcheslavsky A, Cahalan MD, & Parker I (2011) Subunit stoichiometry of human Orai1 and Orai3 channels in closed and open states. *Proc. Natl. Acad. Sci. U. S. A*, **108,** 17832-17837.

[158] Yeromin AV, Zhang SYL, Jiang WH, Yu Y, Safrina O, & Cahalan MD (2006) Molecular identification of the CRAC channel by altered ion selectivity in a mutant of Orai. *Nature*, **443,** 226-229.

[159] Muik M, Fahrner M, Schindl R, Stathopulos P, Frischauf I, Derler I, Plenk P, Lackner B, Groschner K, Ikura M, & Romanin C (2011) STIM1 couples to ORAI1 via an intramolecular transition into an extended conformation. *EMBO J.*, **30,** 1678-1689.

[160] Navarro-Borelly L, Somasundaram A, Yamashita M, Ren D, Miller RJ, & Prakriya M (2008) STIM1-Orai1 interactions and Orai1 conformational changes revealed by live-cell FRET microscopy. *Journal of Physiology-London*, **586,** 5383-5401.

[161] Park CY, Hoover PJ, Mullins FM, Bachhawat P, Covington ED, Raunser S, Walz T, Garcia KC, Dolmetsch RE, & Lewis RS (2009) STIM1 clusters and activates CRAC channels via direct binding of a cytosolic domain to Orai1. *Cell*, **136,** 876-890.

[162] Yuan JP, Zeng W, Dorwart MR, Choi YJ, Worley PF, & Muallem S (2009) SOAR and the polybasic STIM1 domains gate and regulate Orai channels. *Nat. Cell Biol.*, **11,** 337-343.

[163] Yang X, Jin H, Cai XY, Li SW, & Shen YQ (2012) Structural and mechanistic

insights into the activation of Stromal interaction molecule 1 (STIM1). *Proc. Natl. Acad. Sci. U. S. A*, **109,** 5657-5662.

[164] Brandman O, Liou J, Park WS, & Meyer T (2007) STIM2 is a feedback regulator that stabilizes basal cytosolic and endoplasmic reticulum Ca^{2+} levels. *Cell*, **131,** 1327-1339.

[165] Srikanth S, Jung HJ, Kim KD, Souda P, Whitelegge J, & Gwack Y (2010) A novel EF-hand protein, CRACR2A, is a cytosolic Ca^{2+} sensor that stabilizes CRAC channels in T cells. *Nat. Cell Biol.*, **12,** 436-446.

[166] Zeiger W, Ito D, Swetlik C, Oh-hora M, Villereal ML, & Thinakaran G (2011) Stanniocalcin 2 Is a Negative Modulator of Store-Operated Calcium Entry. *Molecular and Cellular Biology*, **31,** 3710-3722.

[167] Mullins FM, Park CY, Dolmetsch RE, & Lewis RS (2009) STIM1 and calmodulin interact with Orai1 to induce Ca^{2+}-dependent inactivation of CRAC channels. *Proc. Natl. Acad. Sci. U. S. A*, **106,** 15495-15500.

[168] Fujii Y, Shiota M, Ohkawa Y, Baba A, Wanibuchi H, Kinashi T, Kurosaki T, & Baba Y (2012) Surf4 modulates STIM1-dependent calcium entry. *Biochemical and Biophysical Research Communications*, **422,** 615-620.

[169] Palty R, Raveh A, Kaminsky I, Meller R, & Reuveny E (2012) SARAF inactivates the store operated calcium entry machinery to prevent excess calcium refilling. *Cell*, **149,** 425-438.

[170] Srikanth S, Jew M, Kim KD, Yee MK, Abramson J, & Gwack Y (2012) Junctate is a Ca^{2+}-sensing structural component of Orai1 and stromal interaction molecule 1 (STIM1). *Proc. Natl. Acad. Sci. U. S. A*, **109,** 8682-8687.

[171] Stamboulian S, Moutin MJ, Treves S, Pochon N, Grunwald D, Zorzato F, De WM, Ronjat M, & Arnoult C (2005) Junctate, an inositol 1,4,5-triphosphate receptor associated protein, is present in rodent sperm and binds TRPC2 and TRPC5 but not TRPC1 channels. *Dev. Biol.*, **286,** 326-337.

[172] Tian G, Tepikin AV, Tengholm A, & Gylfe E (2012) cAMP Induces Stromal Interaction Molecule 1 (STIM1) Puncta but neither Orai1 Protein Clustering nor Store-operated Ca^{2+} Entry (SOCE) in Islet Cells. *J. Biol. Chem.*, **287,** 9862-9872.

[173] Chung SC, Limnander A, Kurosaki T, Weiss A, & Korenbrot JI (2007) Coupling Ca^{2+} store release to lcrac channel activation in B lymphocytes requires the activity of Lyn and Syk kinases. *J. Cell Biol.*, **177,** 317-328.

[174] Lopez E, Jardin I, Berna-Erro A, Bermejo N, Salido GM, Sage SO, Rosado JA, & Redondo PC (2012) STIM1 tyrosine-phosphorylation is required for STIM1-Orai1 association in human platelets. *Cellular Signalling*, **24,** 1315-1322.

[175] Pozo-Guisado E, Campbell DG, Deak M, Alvarez-Barrientos A, Morrice NA, Alvarez IS, Alessi DR, & Martin-Romero FJ (2010) Phosphorylation of STIM1 at ERK1/2 target sites modulates store-operated calcium entry. *J. Cell Sci.*, **123,** 3084-3093.

[176] Smyth JT, Petranka JG, Boyles RR, Dehaven WI, Fukushima M, Johnson KL, Williams JG, & Putney JW (2009) Phosphorylation of STIM1 underlies suppression of store-operated calcium entry during mitosis. *Nat. Cell Biol.*, **11,** 1465-U190.

[177] Yu F, Sun L, & Machaca K (2009) Orai1 internalization and STIM1 clustering inhibition modulate SOCE inactivation during meiosis. *Proc. Natl. Acad. Sci. U. S. A*, **106,** 17401-17406.

[178] Smyth JT, Dehaven WI, Bird GS, & Putney JW, Jr. (2008) Ca^{2+}-store-dependent and -independent reversal of Stim1 localization and function. *J. Cell Sci*, **121,** 762-772.

[179] Kawasaki T, Ueyama T, Lange I, Feske S, & Saito N (2010) Protein Kinase C-induced Phosphorylation of Orai1 Regulates the Intracellular Ca^{2+} Level via the Store-operated Ca^{2+} Channel. *J. Biol. Chem.*, **285,** 25720-25730.

[180] Yuan JP, Zeng W, Huang GN, Worley PF, & Muallem S (2007) STIM1 heteromultimerizes TRPC channels to determine their function as store-operated channels. *Nat. Cell Biol.*, **9,** 636-645.

[181] Ong HL, Cheng KT, Liu X, Bandyopadhyay BC, Paria BC, Soboloff J, Pani B, Gwack Y, Srikanth S, Singh BB, Gill DL, & Ambudkar IS (2007) Dynamic assembly of TRPC1-STIM1-Orai1 ternary complex is involved in store-operated calcium influx. Evidence for similarities in store-operated and calcium release-activated calcium channel components. *J. Biol. Chem.*, **282,** 9105-9116.

[182] Lee KP, Yuan JP, Hong JH, So I, Worley PF, & Muallem S (2010) An endoplasmic reticulum/plasma membrane junction: STIM1/Orai1/TRPCs. *FEBS Letters*, **584,** 2022-2027.

[183] Park CY, Shcheglovitov A, & Dolmetsch R (2010) The CRAC Channel Activator STIM1 Binds and Inhibits L-Type Voltage-

Gated Calcium Channels. *Science*, **330,** 101-105.

[184] Mignen O, Thompson JL, & Shuttleworth TJ (2007) STIM1 regulates Ca^{2+} entry via arachidonate-regulated Ca^{2+}-selective (ARC) channels without store depletion or translocation to the plasma membrane. *J. Physiol*, **579,** 703-715.

[185] Walsh CM, Chvanov M, Haynes LP, Petersen OH, Tepikin AV, & Burgoyne RD (2010) Role of phosphoinositides in STIM1 dynamics and store-operated calcium entry. *Biochemical Journal*, **425,** 159-168.

[186] Calloway N, Owens T, Corwith K, Rodgers W, Holowka D, & Baird B (2011) Stimulated association of STIM1 and Orai1 is regulated by the balance of PtdIns(4,5)P(2) between distinct membrane pools. *J. Cell Sci.*, **124,** 2602-2610.

[187] Lioudyno MI, Kozak JA, Penna A, Safrina O, Zhang SL, Sen D, Roos J, Stauderman KA, & Cahalan MD (2008) Orai1 and STIM1 move to the immunological synapse and are up-regulated during T cell activation. *Proc. Natl. Acad. Sci. U. S. A*, **105,** 2011-2016.

[188] Baba Y, Nishida K, Fujii Y, Hirano T, Hikida M, & Kurosaki T (2008) Essential function for the calcium sensor STIM1 in mast cell activation and anaphylactic responses. *Nat. Immunol.*, **9,** 81-88.

[189] Vig M, Dehaven WI, Bird GS, Billingsley JM, Wang H, Rao PE, Hutchings AB, Jouvin MH, Putney JW, & Kinet JP (2008) Defective mast cell effector functions in mice lacking the CRACM1 pore subunit of store-operated calcium release-activated calcium channels. *Nat. Immunol.*, **9,** 89-96.

[190] Hájková Z, Bugajev V, Dráberová E, Vinopal S, Dráberová L, Janaček J, Dráber P, & Dráber P (2011) STIM1-directed reorganization of microtubules in activated mast cells. *J. Immunol.*, **186,** 913-923.

[191] Rosado JA, Redondo PC, Sage SO, Pariente JA, & Salido GM (2005) Store-operated Ca^{2+} entry: Vesicle fusion or reversible trafficking and de novo conformational coupling? *Journal of Cellular Physiology*, **205,** 262-269.

[192] Oka T, Hori M, & Ozaki H (2005) Microtubule disruption suppresses allergic response through the inhibition of calcium influx in the mast cell degranulation pathway. *J. Immunol.*, **174,** 4584-4589.

[193] Darbellay B, Arnaudeau S, Bader CR, Konig S, & Bernheim L (2011) STIM1L is a new actin-binding splice variant involved in fast repetitive Ca^{2+} release. *J. Cell Biol.*, **194,** 335-346.

[194] Baba Y, Hayashit K, Fujii Y, Mizushima A, Watarai H, Wakamori M, Numaga T, Mori Y, Iino M, Hikida M, & Kurosaki T (2006) Coupling of STIM1 to store-operated Ca^{2+} entry through its constitutive and inducible movement in the endoplasmic reticulum. *Proc. Natl. Acad. Sci. U. S. A*, **103,** 16704-16709.

[195] Smyth JT, Dehaven WI, Bird GS, & Putney JW (2007) Role of the microtubule cytoskeleton in the function of the store-operated Ca^{2+} channel activator STIM1. *J. Cell Sci.*, **120,** 3762-3771.

[196] Grigoriev I, Gouveia SM, van d, V, Demmers J, Smyth JT, Honnappa S, Splinter D, Steinmetz MO, Putney JW, Jr., Hoogenraad CC, & Akhmanova A (2008) STIM1 is a MT-plus-end-tracking protein involved in remodeling of the ER. *Curr. Biol.*, **18,** 177-182.

[197] Honnappa S, Gouveia SM, Weisbrich A, Damberger FF, Bhavesh NS, Jawhari H, Grigoriev I, van Rijssel FJA, Buey RM, Lawera A, Jelesarov I, Winkler FK, Wuthrich K, Akhmanova A, & Steinmetz MO (2009) An EB1-Binding Motif Acts as a Microtubule Tip Localization Signal. *Cell*, **138,** 366-376.

[198] Banning C, Votteler J, Hoffmann D, Koppensteiner H, Warmer M, Reimer R, Kirchhoff F, Schubert U, Hauber J, & Schindler M (2010) A Flow Cytometry-Based FRET Assay to Identify and Analyse Protein-Protein Interactions in Living Cells. *Plos One*, **5**.

[199] MacGlashan DW (2009) Self-Termination/Anergic Mechanisms in Human Basophils and Mast Cells. *International Archives of Allergy and Immunology*, **150,** 109-121.

[200] Huber M (2013) Activation/Inhibition of mast cells by supra-optimal antigen concentrations. *Cell Communication and Signaling*, **11**.

[201] Furumoto Y, Nunomura S, Terada T, Rivera J, & Ra C (2004) The Fc epsilon RI beta immunoreceptor tyrosine-based activation motif exerts inhibitory control on MAPK and I kappa B kinase phosphorylation and mast cell cytokine production. *J. Biol. Chem.*, **279,** 49177-49187.

[202] MacGlashan D & Undem BJ (2008) Inducing an anergic state in mast cells and basophils without secretion. *Journal of Allergy and Clinical Immunology*, **121,** 1500-1506.

[203] Larson DR, Gosse JA, Holowka DA, Baird BA, & Webb WW (2005) Temporally resolved interactions between antigen-

stimulated IgE receptors and Lyn kinase on living cells. *J. Cell Biol.*, **171,** 527-536.

[204] Wilson BS, Pfeiffer JR, & Oliver JM (2000) Observing FcεRI signaling from the inside of the mast cell membrane. *J. Cell Biol.*, **149,** 1131-1142.

[205] Tolar P, Dráberová L, Tolarová H, & Dráber P (2004) Positive and negative regulation of Fcε receptor I-mediated signaling events by Lyn kinase C-terminal tyrosine phosphorylation. *Eur. J. Immunol.*, **34,** 1136-1145.

[206] Tamir I & Cambier JC (1998) Antigen receptor signaling: integration of protein tyrosine kinase functions. *Oncogene*, **17,** 1353-1364.

[207] Eiseman E & Bolen JB (1992) Signal transduction by the cytoplasmic domains of Fc epsilon RI-gamma and TCR-zeta in rat basophilic leukemia cells. *J. Biol. Chem.*, **267,** 21027-21032.

[208] Field KA, Holowka D, & Baird B (1997) Compartmentalized activation of the high affinity immunoglobulin E receptor within membrane domains. *J. Biol. Chem.*, **272,** 4276-4280.

[209] Dráberová L, Lebduška P, Hálová I, Tolar P, Stokrová J, Tolarová H, Korb J, & Dráber P (2004) Signaling assemblies formed in mast cells activated via Fcepsilon receptor I dimers. *Eur. J. Immunol.*, **34,** 2209-2219.

[210] Kusumi A & Suzuki K (2005) Toward understanding the dynamics of membrane-raft-based molecular interactions. *Biochim. Biophys. Acta*, **1746,** 234-251.

[211] Davey AM, Krise KM, Sheets ED, & Heikal AA (2008) Molecular perspective of antigen-mediated mast cell signaling. *J. Biol. Chem.*, **283,** 7117-7127.

[212] Wienands J, Larbolette O, & Reth M (1996) Evidence for a preformed transducer complex organized by the B cell antigen receptor. *Proc. Natl. Acad. Sci. USA*, **93,** 7865-7870.

[213] Suzuki Y, Yoshimaru T, Matsui T, Inoue T, Niide O, Nunomura S, & Ra C (2003) FcεRI signaling of mast cells activates intracellular production of hydrogen peroxide: role in the regulation of calcium signals. *J. Immunol.*, **171,** 6119-6127.

[214] Heneberg P & Dráber P (2002) Nonreceptor protein tyrosine and lipid phosphatases in type I Fcε receptor-mediated activation of mast cells and basophils. *Int. Arch. Allergy Immunol.*, **128,** 253-263.

[215] Barrett WC, DeGnore JP, Konig S, Fales HM, Keng YF, Zhang ZY, Yim MB, & Chock PB (1999) Regulation of PTP1B via glutathionylation of the active site cysteine 215. *Biochemistry*, **38,** 6699-6705.

[216] Heneberg P, Dráberová L, Bambousková M, Pompach P, & Dráber P (2010) Down-regulation of protein tyrosine phosphatases activates an immune receptor in the absence of its translocation into lipid rafts. *J. Biol. Chem.*, **285,** 12787-12802.

[217] Teshima R, Ikebuchi H, Nakanishi M, & Sawada J (1994) Stimulatory effect of pervanadate on calcium signals and histamine secretion of RBL-2H3 cells. *Biochem. J.*, **302 (Pt 3),** 867-874.

[218] Bugajev V, Bambousková M, Dráberová L, & Dráber P (2010) What precedes the initial tyrosine phosphorylation of the high affinity IgE receptor in antigen-activated mast cell? *FEBS Letters*, **584,** 4949-4955.

[219] Peirce M & Metzger H (2000) Detergent-resistant microdomains offer no refuge for proteins phosphorylated by the IgE receptor. *J. Biol. Chem.*, **275,** 34976-34982.

[220] Capasso M, Bhamrah MK, Henley T, Boyd RS, Langlais C, Cain K, Dinsdale D, Pulford K, Khan M, Musset B, Cherny VV, Morgan D, Gascoyne RD, Vigorito E, DeCoursey TE, MacLennan ICM, & Dyer MJS (2010) HVCN1 modulates BCR signal strength via regulation of BCR-dependent generation of reactive oxygen species. *Nat. Immunol.*, **11,** 265-U12.

[221] Swindle EJ, Hunt JA, & Coleman JW (2002) A comparison of reactive oxygen species generation by rat peritoneal macrophages and mast cells using the highly sensitive real-time chemiluminescent probe pholasin: inhibition of antigen-induced mast cell degranulation by macrophage-derived hydrogen peroxide. *J. Immunol.*, **169,** 5866-5873.

[222] Gil D, Schamel WW, Montoya M, Sanchez-Madrid F, & Alarcon B (2002) Recruitment of Nck by CD3 epsilon reveals a ligand-induced conformational change essential for T cell receptor signaling and synapse formation. *Cell*, **109,** 901-912.

[223] Tolar P, Hanna J, Krueger PD, & Pierce SK (2009) The constant region of the membrane immunoglobulin mediates B cell-receptor clustering and signaling in response to membrane antigens. *Immunity.*, **30,** 44-55.

[224] Kimura T, Zhang J, Sagawa K, Sakaguchi K, Appella E, & Siraganian RP (1997) Syk-independent tyrosine phosphorylation and association of the protein tyrosine phosphatases SHP-1 and SHP-2 with the high affinity IgE receptor. *J. Immunol.*, **159,** 4426-4434.

[225] Huber M, Helgason CD, Damen JE, Liu L, Humphries RK, & Krystal G (1998) The src homology 2-containing inositol phosphatase (SHIP) is the gatekeeper of mast cell degranulation. *Proc. Natl. Acad. Sci USA*, **95,** 11330-11335.

[226] Hazenbos WLW, Wu P, Eastham-Anderson J, Kinoshita T, & Brown EJ (2011) Impaired Fc epsilon RI stability, signaling, and effector functions in murine mast cells lacking glycosylphosphatidylinositol-anchored proteins. *Blood*, **118,** 4377-4383.

[227] Lyubchenko T, Nielsen JP, Miller SM, Liubchenko GA, & Holers VM (2009) Role of initial protein phosphorylation events and localized release-activated calcium influx in B cell antigen receptor signaling. *Journal of Leukocyte Biology*, **85,** 298-309.

[228] Wu MM, Buchanan J, Luik RM, & Lewis RS (2006) Ca^{2+} store depletion causes STIM1 to accumulate in ER regions closely associated with the plasma membrane. *J. Cell Biol.*, **174,** 803-813.

[229] Sulimenko V, Dráberová E, Sulimenko T, Macurek L, Richterova V, Dráber P, & Dráber P (2006) Regulation of microtubule formation in activated mast cells by complexes of gamma-tubulin with Fyn and Syk kinases. *J. Immunol.*, **176,** 7243-7253.

[230] Cahalan MD (2009) STIMulating store-operated Ca^{2+} entry. *Nat. Cell Biol.*, **11,** 669-677.

[231] Hofstra CL, Desai PJ, Thurmond RL, & Fung-Leung WP (2003) Histamine H-4 receptor mediates chemotaxis and calcium mobilization of mast cells. *Journal of Pharmacology and Experimental Therapeutics*, **305,** 1212-1221.

[232] Hartmann K, Henz BM, KrugerKrasagakes S, Kohl J, Burger R, Guhl S, Haase I, Lippert U, & Zuberbier T (1997) C3a and C5a stimulate chemotaxis of human mast cells. *Blood*, **89,** 2863-2870.

[233] Tumova M, Koffer A, Simicek M, Draberova L, & Draber P (2010) The transmembrane adaptor protein NTAL signals to mast cell cytoskeleton via the small GTPase Rho. *Eur. J. Immunol.*, **40,** 3235-3245.

[234] Shen WW, Frieden M, & Demaurex N (2011) Local Cytosolic Ca^{2+} Elevations Are Required for Stromal Interaction Molecule 1 (STIM1) De-oligomerization and Termination of Store-operated Ca^{2+} Entry. *J. Biol. Chem.*, **286,** 36448-36459.